HYDROGEOCHEMISTRY AND MICROBIAL GEOCHEMISTRY OF DIFFERENT DEPTH AQUIFER SEDIMENTS FROM MATLAB BANGLADESH: RELATION TO ARSENIC CONTAMINATION IN GROUNDWATERS

By

MD. GOLAM KIBRIA

B.Sc. (Hons.), University of Dhaka, 2009

A THESIS

Submitted in partial fulfillment of the requirements for the degree

MASTER OF SCIENCE

Department of Geology
College of Arts and Sciences

KANSAS STATE UNIVERSITY
Manhattan, Kansas

Summer, 2014

Approved by:

Major Professor
Dr. Saugata Datta

Abstract

The incidence of high arsenic (As) and other oxyanions (e.g. Mn) has been examined in a ~410km^2 areas within the Bengal Delta between North and South Matlab, Bangladesh. The aim of this study was to examine the role of sediment geochemistry, coupled with microbial community studies and their relations with different colors and grain sizes of sediments, in determining evolved groundwater hydrochemistry within the aquifers in Matlab. Groundwaters are Ca–Mg–HCO_3^- types in shallow aquifers, Mg-HCO_3^- in the intermediate depths and Na-K-Cl rich in the deeper aquifers. Dissolved As concentration is high (~781µg/l) associated with shallow grey and dark grey sediments, whereas light grey sediments at intermediate depths contain lower As (<10 µg/l). Dissolved Fe_T on other hand in both sediment types (light grey and grey) shows good correlation with dissolved SO_4^{2-}. In plots of $\delta^{18}O$ vs δD, intermediate and deeper depth aquifer waters plot on the arrays for LMWL and GMWL, which indicates the principal recharge mechanism is likely to be from local precipitation within the shallow aquifers. Only the high As groundwaters deflect from the LMWL, indicating that recharge might be a mixture of precipitation and surficial discharges / infiltrations for these waters. Bulk extraction of sediments showed that grey and dark grey sediments from shallow depths have higher As concentrations (~31 mg/kg) and light grey sediments have comparatively less (~11mg/kg). Sequential extractions for sediment fractionations showed that most of the As was bound to amorphous and poorly crystalline hydrous oxides of Fe and Al phases. Synchrotron-aided bulk-XANES studies conducted on sediments revealed As and S speciation in the core samples at different depths indicating the occurrences of hotspots of As distributed randomly in light grey and grey sediments. As^{3+} is the dominant species in Matlab sediments. More than 101 bacterial families were identified among the eight sediment samples from the South Matlab core and out of them fewer than six families comprised more than ~80% of total bacterial families. Our results indicate significant relationships between bacterial community structure, grain size fractionation, dissolved As concentration and sediment C, Mn, and Fe concentrations for these samples. Groundwater abstracted from these light grey sediments, in contrast to reduced greyish to dark greyish sediments, contain significantly lower amounts of dissolved As and can be a source of safe water for the future. Our work demonstrates that intermediate depth light grey sediments have geochemical and microbial features conducive with safe drinking water for the future.

Table of Contents

List of Figures

List of Tables

Acknowledgements

It would not have been possible to write this thesis without the help and support of the kind people around me, to only some of whom it is possible to give particular mention here. My parents, brothers, sister and friends back in Bangladesh have given me their unequivocal support throughout, as always, for which my mere expression of thanks likewise does not suffice.

This thesis would not have been possible without the help, support and patience of all my committee members Dr. Saugata Datta, Dr. Pamela Kempton, Dr. Ganga Hettiarachchi, Dr. Matthew Kirk and Dr. Sam, not to mention their advice and unsurpassed knowledge that helped me pull through. The good advice, support of Dr. Matthew Kirk has been invaluable on academic level, for which I am extremely grateful. I am very much indebted to Dr. Ganga Hettiarachchi for the many valuable discussions that helped me understand my research and execute my experiments in the best possible way.

I would like to acknowledge the financial, academic support of Kansas State University for providing me necessary financial support throughout my studies. I would also like to thank Paul and Deana Strunk for providing me scholarship for two consecutive years, which helped me immensely. Immense thanks to NASA for providing financial support for my field work in Bangladesh. Special thanks to Professor George Clark, Dept of Geology for support in every way possible. I am also want to thanks GSA for their graduate student research fund.

I would like to thank Prof. Prosun Bhattacharya and Mohammed Hossain from KTH Royal Institute of Technology, Sweden and SASMIT project and Professor Kazi Matin Ahmed (University of Dhaka) for providing me field support and shear research knowledge during the thesis time.

I would like to thank Dr. Phillip Defoe, Madhubhashini Buddhika Galkaduwa and Ranju Karna, who are as good friends, were always willing to help and give their best suggestions, encouragement, practical and scientific advice. It would have been a lonely lab without them.

Special thanks to Musabbir Ahmed Khan Musa (B.S Senior student at the University of Dhaka) and Awlad Bhai (field driver) for immense support throughout the field work.

I would like to thank Brookhaven National Lab, NSLS facilities and scientists especially Dr. Paul Northrup, Dr. Ryan Tappero and Dr.Kaumudi Pandya for providing me beamtime for synchrotron x-ray studies during the years.

Many friends, fellow graduate students Shovon Barua, MS Sankar, Dr. Shyamal Talukder, Haydory Ahmed, Harshad Kulkarni and Brent who helped me stay sane through these two academic years.

Last but not the least I would like to thank my major professor Dr. Saugata Datta for his insightful comments and constructive criticisms at different stages of my research which were thought provoking and they helped me focus my ideas. I also thank him for holding me to a high research standard and forcing strict validations for each research result. For any errors or inadequacies that may remain in this work, of course, the responsibility is entirely my own.

Chapter 1 - Introduction

All over the world people rely on groundwater as a major source of drinking water. The level of concentrated geogenic and anthropogenic trace elements, such as arsenic in groundwater can lead to various detrimental health problems for the consuming population, which generally develop over a long time. Arsenic (As) in aquifer water has affected roughly 100 million people in Bangladesh and West Bengal (Bhattacharya et al., 1997; BGS, 2001; Ahmed et al., 2003; Ahmed et al., 2004; Hoque et al., 2014), and one of the most affected area within Bangladesh (i.e., South and North Matlab) has produced groundwaters with As concentration as high as 769 µg/L (South Matlab, piezometer nest-16, @16 m depth). In the late 1980s, river and pond waters were the main source of drinking waters in this region (Bengal Basin) and was harmfully polluted by presence of various strains of pathogens. With the help of funding from UNICEF (United Nations International Children's Emergency Fund), the Bangladeshi and Indian Governments started exploring and promoting groundwater as an alternative source for drinking water in this region, and for this purpose they installed approximately 4 million tubewells within Bangladesh and India (West Bengal). Unfortunately, this project is thought to be a cause of one of the worst environmental problems (As toxicity) in the Bengal delta (which covers part of Bangladesh and West Bengal) (Caldwell *et al.*, 2003, Polizzotto *et al.*, 2008). Being a class I carcinogen, elevated levels of As in drinking water can cause various dermal lesions, such as hyperpigmentation-hyperkeratosis and melanosis, generating toperipheral neuropathy, skin cancer, bladder and lung cancers and peripheral vascular disease in the consuming population (Zaloga et al., 1985, Yoshida *et al.*, 2004, Kocar *et al.*, 2008, Pierce et al., 2012). The WHO (World Health Organization) guideline value for As in drinking water is 10µg/L (WHO, 2011). Manganese (Mn) is a neurotoxin and toxicity is particularly adverse for newborns and children (Wasserman et al., 2006, Montes et al., 2008). Consuming high amounts of Mn can cause various birth defects, impaired fertility in males and involuntary muscular movements (Ono et al., 2002; Yazbeck et al., 2006; Wasserman et al., 2006; Buschmann et al., 2007). WHO guideline value for Mn was 0.4 mg/l prior to June 2011, but in the 4th edition of WHO's guidelines for drinking water quality there is no guideline value (MCL) for Mn because none of the adverse health effects are associated with the usual Mn levels in the drinking waters.

Arsenic geochemistry and Microbial interaction

Arsenic is the 3rd member of the 'V-A' group of the periodic table and 47th in abundance of the 90 naturally occurring elements (Plant et al., 2003). The atomic number is 33 and atomic mass is 74.9216 g/mol. Arsenic exists in +3 and +5 oxidation sates, +3 (arsenite, As^{+3}) and +5 (arsenate, As^{+5}) oxidation states are the most common. Concentration of As in most natural water is 1-2 µg/L (WHO, 2011). The ore minerals of As are arsenopyrite (FeAsS), realgar (As_4S_4) and orpiment (As_2S_3) (Smedley and Kinniburgh, 2002). The native form of As^{+5} occurs in soils and sediments as $H_xAsO_4^{x-3}$, which can get adsorbed onto a wide range of minerals, such as iron and aluminum hydroxides and aluminosilicate minerals (Ying et al., 2012). As^{+3} occurs as natural H_3AsO_3 species in non-sulfidic environments and prefer to be adsorbed onto iron hydroxides, iron oxides, iron-oxyhydroxides (Gupta and Chen, 1978; Raven et al., 1998; Dixit and Hering, 2003; Herbel and Fendorf, 2006; seddiqueet al., 2008; Ying et al., 2012). As^{+3} usually forms weak complexes and upon the change in chemical conditions the bonds break and As^{+3} goes into solution (Tufano and Fendorf, 2008).

Arsenic speciation in groundwater is control by Eh and pH conditions. $H_3AsO_3^0$ exists under reducing conditions (Eh <100mV and pH 6 to 7.5) (Smedley and Kinniburgh, 2002; Mukherjee et al., 2009). When Eh is less than 250mV, As complexes with sulfide species (HS^-, S^{2-}, and H_2S) to form the mineral orpiment, As_2S_3. Arsenic exhibits very slow redox transformations and so both As^{3+} and As^{5+} occur in natural conditions (Smedley and Kinniburgh, 2002; Mukherjee et al., 2009). The redox conditions greatly affect the ratio of As^{3+} to As^{5+} in groundwater and in strongly reducing (Fe^{3+} reducing and sulphate reducing) conditions As^{3+} species dominate over As^{5+} (Smedley and Kinniburgh, 2002). Under reducing acidic conditions arsenic-bearing minerals (orpiment & realgar) and other sulphidic minerals that co-precipitate with As, can precipitate from the solution (Mason and berry, 1978; Cullen and Reimer, 1989; Smedley& Kinniburgh, 2002). It is expected that, if there is high concentration of free sulphides in water, then the As concentration will be much less (Moor et al., 1988; Smedley& Kinniburgh, 2002.

Ratio of As(III)/As(V) can vary considerably (Mukherjee et al., 2009b), depending on the abundance of organic carbon and microbial activities (Smedley and Kinniburgh, 2002). At circumneutral pH, As(III) exists as H_3AsO_3, an uncharged molecule, so its mobility is enhanced, whereas an As(V) anion is more likely to sorb strongly onto mineral surfaces.

Arsenic is unique among other oxyanion-forming elements in that its mobilization can be controlled by both oxidizing and reducing conditions at pH values typical of most groundwaters (pH 6.5 to 8.5) (Smedley and Kinniburgh, 2002). The solubility of most trace metal cations at near-neutral pH is limited by precipitation as, or coprecipitation with, an oxide, hydroxide, carbonate or phosphate mineral, or by their strong adsorption to hydrous metal oxides, clays, and organic matters. Arsenate is different in that it tends to be less strongly sorbed as pH increases (Dzombak and Morel, 1990). The oxidation state of As influences many of its properties, such as adsorption to soil minerals, solubility in soil, and toxicity to plants and animals.

Arsenic can be removed from groundwater by several natural processes. In the presence of organic matter, Fe (II) and sulfides can precipitate (or co-precipitate with As) to form pyrite, onto which As(III) can sorb strongly via inner-sphere complexation (Bostick and Fendorf, 2003). Sorption of As(V) on clay minerals is a pH-driven process. The degree of sorption of As(V) depends on clay mineralogy, surface area, surface charge and availability of sorption sites. The maximum amount of sorption of As(III) (and similar elements) on clay minerals occurs at pH 7.5-9.5 (Clauer and Chaudhuri, 1995; Lin and Puls, 2000). Arsenic mobility in groundwater can also be affected by presence of carbonate phases (e.g. As(III) can be associated in the calcite lattice or surface adsorbed at high pH) (Mukherjee et al., 2009b).

Dissolved organic matter (DOM) is a major component of natural waters and composed of a complex mixture of humic acids, fulvic acids, low molecular weight organic acids, carbohydrates and various bacterial derived proteins (Her et al., 2003). DOC form water soluble complexes with trace metals like As and Mn and it is very significant in their mobility and transport. Fulvic acids in particular show strong metal binding capacity and thus increasing metal solubility in natural water systems (McKnight et al.,1992; Anawar et al., 2003; Mladenov et al., 2008; Sharma et al., 2010; Reza et al., 2010). Fe and As reducing bacteria use DOC as an energy source (electron donor) and oxidize it, reducing Fe^{3+} to Fe^{2+} or As^{5+} to $As^{3+.}$ The reductive dissolution of FeOOH minerals causes As to go into solution. The humic substances in DOM have quinone moieties that act as electron shuttle (Scott et al., 1998) to accelerate Fe reduction (Lovely et al., 1996). Humic substances readily form complexes with Fe and form ternary complexes with Fe and As to keep As in solution. They can also compete with As for sorption sites (competitive sorption) (Lu et al., 1991; Mukhopadhyay and Sanyal, 2004. Warwick et al., 2005; Luo et al., 2006; Mikutta, and Kretzschmar, 2011; Liu et al., 2011) Laboratory

experiments by Lovely et al. (1996) have shown that the DOM act as an electron shuttle between iron reducing bacteria and iron oxides and thus enhance iron reduction. Microbes in the water use DOC as the major source for their growth (Miettimen et al., 1999; Harvey and Swartz, 2002). DOC increases the solubility of iron oxides and can release adsorbed As onto the waters (Weber et al., 2006). Total nitrogen (TN) is another component in natural waters. It consists of all the available nitrogen species (NO_3^-, NO_2^-, NH_4^+) present in water. Amount of dissolved organic nitrogen (DON) can be calculated by subtracting the concentration of all the inorganic nitrogen species in the water from the TN content (Burdige and Zheng,1998; Burdige, 2000).

Natural organic matter in sediments enhances the release of sediment-bound arsenic into the pore water (Wang and Mulligan, 2006; McArthur et al., 2004; Acharyya et al., 1999). Organic matter in sediments can have various sources. The DOM in lacustrine and riverine environments can be derived from various decomposed photosynthetic higher plants and micro-flora (Wetzel, 1992). Deltaic sediments account for roughly 45% of the global carbon burial and receive organic matter from both autochthonous and allochthonous sources (Hedges and Keil, 1995; Gordon and Goni, 2003).

Most of the microbial ecology studies of arsenic-rich sediments have focused on sediments collected from Holocene aquifers (Acharyya et al., 2000; Ravenscroft et al., 2005; Zheng et al., 2005). The use of waters from deeper Pleistocene aquifers (well switching) may represent a viable strategy for limiting arsenic uptake by at risk populations, as shown in Bengal (van Geen et al., 2003; Polya and Charlet, 2009; Burgess et al., 2010). Recent studies have suggested that biogeochemical mobilisation of As (III) may occur to a lesser extent in Pleistocene sediments (Sutton et al., 2009; Al Lawati et al., 2012). Another study showed that the addition of arsenate respiring *Shewanella* species to Pleistocene sediments is necessary to trigger the release of As(III) (Dhar et al., 2011).

Mn in Groundwater

Mn is the first member of group VIIIB in the periodic table, with an atomic number of 25 and atomic mass 54.94 g/mol. It is the 12th most abundant element in the earth's crust. There are three possible oxidation states of manganese in soil, namely Mn(II), Mn(III) and Mn(IV) (Gabriela et al., 2011). Among them most common are Mn^{3+} and Mn^{4+} (Pinsino et al., 2012). Most common Mn minerals are braunite ($Mn^{2+}Mn^{3+}{}_6$)(SiO_{12}), psilomelane ($Ba,H_2O)_2Mn_5O_{10}$),

pyrolusite (MnO_2) and rhodochrosite ($MnCO_3$). Under natural pH and redox conditions Mn is release into water in only low concentrations, due to the low solubility of the most stable oxidation state Mn^{4+}(Björkvald et al., 2008). Oxidation of Mn is pH dependent and it is very slow under acidic conditions (Stumm & Morgan, 1996). The levels of manganese in groundwater from natural leaching processes can vary widely depending upon the types of minerals present at the aquifer. Mn is present in soil as a result of mineral weathering and atmospheric deposition, originating from both natural and anthropogenic sources. The divalent ion is the only form that is stable in soil solutions, while Mn(III) and Mn(IV) are only stable in the solid phase of soil (McBride,1994). Mn mobility in soil is extremely sensitive to soil conditions such as acidity, wetness, organic matter content and biological activity (Gabriela et al., 2011). H_2MnO_2 or $Mn(OH)_2$ (manganese hydroxides) in alluvial sediments are examples of aquagene mineral formations or alluvial manganese mineralization (Silaev et al., 2000).

Wells with suboxic conditions (Eh~200) and low As concentrations (<50 µg/L) typically have higher Mn concentrations (1-2 mg/l). Research specifies that MnO_2 is reduced and Mn^{2+} is free to the aqueous phase. The Eh values are generally insufficiently low to entirely reduce sediment-bound ironhydroxides; they therefore tend to offer strong binding sites for As and phosphate. The absence of nitrate or low nitrate concentrations in most of the wells supports the hypothesis of MnO_2 conditions (Buschmann et al., 2007). Mn concentration shows a weak positive correlation with Eh. High levels of Mn have an impact on flora, fauna and human beings. Due to elevated level of Mn crop production is very limited in some region (almost 30% of the world's total land area suffered by high level of Mn) (Alam et al., 2006). In flora, symptoms such as chlorosis (phytooxidation of chlorophyll) and necrosis due to accumulation of phenolic compounds are observed. It has also been shown that maternal environmental exposure to Mn is associated with a reduced activity of the newborn's erythrocyte Ca-pump (Yazbeck et al., 2006). Moreover, Mn in drinking water is associated with neurotoxic effects in children, such as diminished intellectual function (Wasserman et al., 2006). Accordingly, high Mn concentrations in irrigation and drinking water are hazardous for plants and human beings.

Global Scale Arsenic Pollution

Arsenic affected sedimentary aquifers occur across the world and in all continents. As pollution in drinking waters (As concentration >10 µg/L) can be caused by geogenic or

anthropogenic causes. The geogenic causes are mainly dependent on the proximity of As mineralized zones to the aquifers. The As from the mineralized zones can leach into the aquifer system and thus contaminate them, for example Canada (British Columbia; sulphide mineral deposits); Germany (Northern Bavaria; sulphide mineralization) Smedley & Kinniburgh, 2002. Arsenic-rich sediments in aquifer systems can also lead to geogenic As contamination, for example: Bengal Basin encompassing Bangladesh and West Bengal part of India (Holocene aquifer sediments derived from Himalaya is enriched in shallow depth aquifers), USA (Tulare basin, California; Nevada; Idaho; South Dakota), China, Taiwan and Mongolia (aquifer sediments enriched in arsenic) (Smedley& Kinniburgh, 2002). Volcanic ash could be a source of As contamination in Northern Chile and Mexico (Smedley& Kinniburgh, 2002).

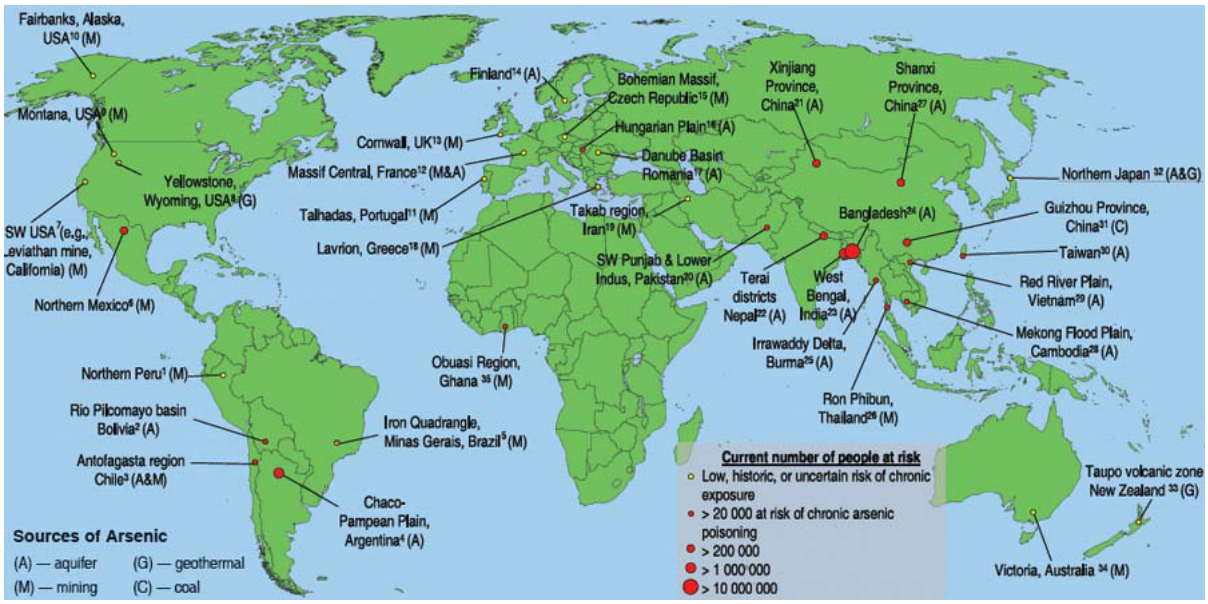

Figure 1.1 Map showing locations of As-contaminated areas around the world (Gorelick and Jones 2008). Highest number of people exposed to elevated As concentrations in drinking water supplies are in Bangladesh and West Bengal, India.

Mining activities can affect natural systems and thus contaminate the aquifers and examples exist in USA (Fairbanks, Alaska); Canada (Moira lake, Ontario); Brazil and Thailand. Geothermal systems can also cause geogenic As contamination and known examples include New Zealand, Japan, Russia, USA, Chile and France (Smedley & Kinniburgh, 2002). The first report on As contamination in drinking water was from Argentina in the year 1917 and the main cause of the contamination there was volcanic ash deposits and thermal springs (Mukherjee et al., 2006). In Australia As contamination is reported due to the leaching of arsenic from As-

enriched country rocks and other anthropogenic activities like mining and extensive use of pesticides for agriculture (Mukherjee et al., 2006). The global distribution of As contaminated aquifers are depicted in the map (**Figure 1.1**).

Global Scale Manganese Pollution

Mn is widely distributed in soils, sediments, waters and other biological systems (Gabriela et al., 2011; Pinsino et al., 2012). Mn is an essential element for humans, but high doses can lead to various fatal diseases. Mn, being an emerging contaminant, its distribution and affected population across the world is not yet completely known. More studies are being done in various parts of Bengal basin (BGS, 2001; Neal et al., 2009; Biswas et al., 2011; Sankar et al., 2012, McArthur et al., 2012; Sankar et al., 2013) to understand its natural occurrence. Lundy and Soule (2012) reported naturally occurring Mn in Minnesota groundwaters, USA; Björkvald et al. (2008) reported natural Mn contamination in the snow melt driven boreal streams of Sweden. Nduka et al. (2008) reported anthropogenic Mn contamination in the Niger delta, Nigeria; Homoncik et al., (2010) reported natural Mn contamination in Scottish groundwaters. Excessive Mn in water can result in having metallic taste in water, can cause stains on clothes and dishes, reduced water pressure in pipes due to the formation of Mn-oxide coating inside the pipe wall (Sly et al., 1990).

As and Mn contamination in the Bengal Basin

The current study explores the causes of As and Mn contamination in parts of the Bengal Basin (South and North Matlab, Bangladesh) groundwaters. The arsenic problem in Bengal delta plain has been referred to as the greatest natural mass poisoning in human history (Bhattacharya et al., 1997; Nickson et al., 1998; Smith et al., 2000; McArthur et al., 2001; Dowling et al., 2002; Paul., 2004; Ravenscroft et al., 2005; Routh et al., 2005; Harvey et al., 2006; Acharyya and Shah, 2007; Datta et al., 2011). Elevated levels of Manganese (Mn) are another upcoming issue in the groundwaters of this region (McArthur et al., 2012; Biswas et al., 2012). The mechanism of As mobilization from Bengal Basin sediments to local groundwaters is complicated and poorly understood. However the common consensus is that the organic matter within the aquifer sediments drives dissimilatory iron reduction reaction and thus release As to the groundwaters (McArthur et al., 2001& 2004, Dowling et al., 2002; Van green et al., 2002; 2006 & 2008). Bengal Basin covers most part of Bangladesh and West Bengal India and is composed of

Quaternary alluvial sediments. Most part of Bangladesh and seven districts in West Bengal are affected by arsenic contamination. Most of the As contaminated aquifers are at a depth range of 60 m (shallow depth) (McArthur et al., 2001 & 2004; Dowling et al., 2002; Harvey et al., 2002 & 2006). Many people in these areas are affected by arsenicosis in the form of various skin lesions.

Major Quaternary sediments in this areas are classified as either older sediments or Dupitila formation (Pleistocene age) and younger alluvium (Holocene age). Aquifers present in older alluvium or Dupitila formation are devoid of As however some causes enriched in Mn. The source(s) of As in Bengal Basin sediments have been described by various authors. Nickson et al. (2000) argued that, as the Bengal Basin formed in the foreland basin of the Himalayan mountain chain and contains sediments derived from the Himalayas, the source of the As could be Himalayan rocks.

Weathering of As minerals releases As-containing iron oxy-hydroxide minerals. These iron oxy-hydroxides can form grain coatings in the sediments. With time various geochemical processes can lead to the dissociation of Fe-oxyhydroxide grain coatings and thus release As into the groundwater containing them (Nickson et al., 2000; McArthur et al., 2001; BGS,2001; Dowling et al., 2002; Ravenscroft et al., 2005; Datta et al., 2011; Dhar et al., 2011 references there in). McArthur et al., 2012 explained that microbial metabolism of organic carbon in sediments could cause the reduction of Mn oxides and Fe oxy-hydroxides and thus releasing Mn and As into the water along with other trace elements.

Regional Geology of Bengal Basin

Ganges-Brahmaputra-Meghna (GBM) Basin is an important part of the Himalayan foreland formed as the result of India-Asia collision. Flexural subsidence of the Indian lithosphere created the Ganges Plain foreland basin at late Quaternary time (Singh, 2004, Sinha et al., 2005). The basin is composed of Quaternary sediments deposited by major meandering rivers like Ganges- Brahmaputra-Meghna and hence the name of GBM delta (Morgan and McIntyre 1959; Mukherjee et al., 2008; Hoque et al., 2011; McArthur et al., 2011). The basin is bounded in the north by the Himalayan mountain ranges and in the south by the Precambrian, Peninsular Indian craton. It extends to the Bay of Bengal to the south, forming the great Bengal fan. Choronostratigraphically the basin holds two major types of sedimentary units; the older Pleistocene unit and the younger Holocene unit (Morgan and McIntyre 1959; Mukherjee et al.,

2008; Datta et al., 2011; McArthur et al., 2008 & 2011). During the Last Glacial Maximum (~20 ka before present) when sea level was substantially lower, the current highlands in the basin (i.e., current paleointerfluvial areas) were exposed and a thin layer of paleosol developed (McArthur et al., 2008). However, the low-lying areas (current paleochannels) were devoid of such deposits (McArthur et al., 2008; Hoque et al., 2011). The lowstand of sea level during the last glacial maximum caused deep erosion in paleochannels by the paleorivers. Later the interfluvial areas were deeply weathered by high rainfall during the warmer climatic regime and developed a widespread paleosol of impermeable clay that is found widely today across the Bengal Basin.

Geomorphologically, the Bengal Basin comprises of lowland river floodplains and delta plains, and is surrounded by the Tertiary hills of various origins (Goodbred and Kuehl, 2000). Within the basin, the Madhupur and Barind Tracts, and the Lalmai hills comprise the Pleistocene inliers composed of highly mottled, deeply weathered and oxidized clays (Morgan and McIntire, 1959). Three major rivers, Ganges, Brahmaputra and Meghna drain through the basin to the Bay of Bengal in the south, where sediment is transported further south of the basin by turbidity currents to the Bengal deep-sea fan, the largest submarine fan in the world (Curray and Moore, 1971; Goodbred and Kuehl, 2000). Although much of the delta remains buried, marginal uplift has exposed stratigraphic sequences representing most of its depositional history. Sediment deposition in the Bengal Basin has taken place in a variety of environments (Uddin and Lundberg, 1999; Goodbred and Kuehl, 2000) ranging from predominant fluvial (channels, floodplains, natural levees, back swamps, oxbow lakes) and paralic (e.g., mangrove forests, tidal flats, distributary channels, beaches), and a few deep marine (trench slope, deep-sea fan). Many deposits can be categorized as mixed as a result of changes in regional tectonics, climate change and sea-level oscillations (Goodbred and Kuehl, 2000; Uddin and Lundberg, 2004; Shamsudduha and Uddin, 2007). Several studies have suggested that the sea level rose to a maximum of about 3.0–3.5 m relative to present-day sea level during the Holocene high system Tracts and encroached on most of the southern parts of the Bengal Basin (Islam and Tooley, 1999; Woodroffe and Horton, 2005). The depositional environments thus migrated back and forth between the Pleistocene inliers and the position of the present-day shoreline, leaving behind their characteristic sedimentary features, now buried beneath the recent sedimentary cover.

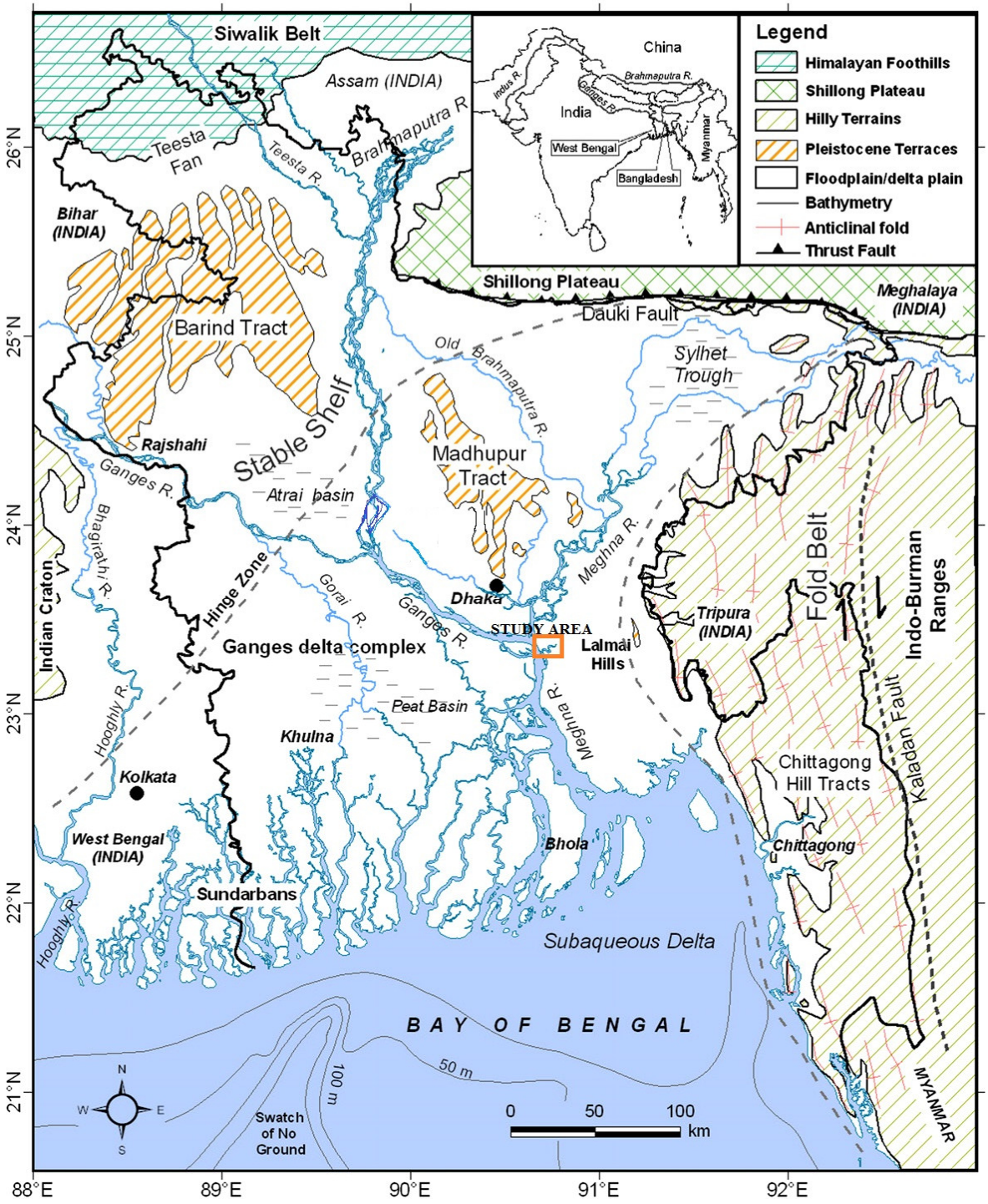

Figure 1.2 Regional geology of Bengal Basin and the study area-Matlab, Bangladesh (modified from Uddin et al., 2011)

Local geology of South and North Matlab

The occurrence, movement and storage of groundwater are governed by the lithology, geological structure, thickness and the depth of occurrence of different geological formations along with the tectonic activities prevailing in the area. An understanding of landscape and its formation is essential for the demarcation of catchments boundaries, assessment of surface and subsurface water resources and planning of water development projects for irrigation development. Moreover, the design and development of water wells depend on the hydrogeological conditions. Hence the important of geology, in assessing hydrogeology of an area, cannot be over-emphasized.

Bangladesh is located at the head of the Bay of Bengal and occupies most of the Bengal Basin that is the largest sedimentary basin of the world. The sediments, mostly alluvial, are transported by the Ganges, Brahmaputra and Meghna river systems that converge in this great delta complex, forming the Bengal delta plain. Bangladesh can be divided int three major physiographic units: the Tertiary hills, the Pleistocene uplands represented by the Barind and Madhupur Tracts and the Holocene alluvial lowlands. Out of these three units, the Bengle Delta Plain(BDP) includes the Pleistocene uplands and the Holocene lowlands (Umitso 1993). The Quaternary period is an important period for understanding the As-related geology of the basin. The period extends from approximately 2 Ma to the Present. The Quaternary sediments are dominantly composed of sand, silts and clays and provide good aquifers. The Quaternary period could be divided into two major epochs; the Pleistocene and the Holocene. The former extends two million years to ten thousand years ago and the latter from ten thousand years ago to the present day. The climate of the Quaternary period was significantly different from today, including glaciations and water fluctuations with levels of 130 m below the water levels of today. During the Holocene period heavy flooding eroded much of the former sediment deposits, leaving only two major Pleistocene regions; the Barind Tracts in north-west and the Madhupur Tracts north of Dhaka. Weathering and oxidations created reddish-brown secondary clays and iron oxides of the Pleistocene sediment. Since then, the valleys have been filled with fresh alluvium of mainly greyish color, labelled Holocene sediments. These Holocene sediments were deposited under reducing conditions and contain large amounts of organic matter (Pasupuleti, 2005).

Thick alluvial deposits of recent age cover the floodplains of the study area. The thickness of the alluvium gradually increases westward from Lalmai Hills east of Matlab Upazila. The Pleistocene Madhupur Clay crops out at the hilltops of Lalmai east of the area, which unconformably overlies the Plio-Pleistocene DupiTila Formation (Pasupuleti, 2005).

Tectonic processes have played an important role in the development of these delta systems. The Bengal Basin is situated at the triple junction of the Tibetian, Indian and Burmese Continental plates and it formed after the separation of the Indian plate from the southern continent of Gondwana (Carry & Moore, 1974). The separation started during the late Cretaceous and initially marine sediments were deposited within the basin floor (miogeosynclinal wedge). During Eocene time the Indian plate collided with the Burmese plate, which caused the deposition of sediment eroded from the uplifted Indo-Burman hill range. The Indian plate then further collided with the Tibetian and Burmese plates during Miocene times, causing a huge sediment influx into the basin from south of the Himalayas and western part of the Indo-Burman hill range.

During the Pliocene large-scale movement along the Dauki fault caused upliftment of the Shillong plateau and the subsidence of the Garo-Rajmahal gap. This tectonic activity resulted in the formation of the north-south trending Tripura-Chittagong folded belt (Alam, 1989).

The area is covered by a sequence of deltaic deposits of Quaternary age. Exploratory drillhole data of the Ground Water Circle (GWC) of the Bangladesh Water Development Board (BWDB) and Department of Public Health Engineering (DPHE) provide stratigraphic information on the water-bearing aquifers. In the context of the present study, concerning the hydrogeology of the water-bearing sediments the focus is given on the presentation of the Mio-Pliocene and Quaternary stratigraphy of the area.

Morton (1979), based on Landsat imagery studies, delineated the Quaternary deltaic arcs in Bangladesh. Much of the present-day delta-building activity is within the Meghna estuary, whereas the early Meghna delta lies in the Sundarban.

The Dupitila Formation includes a sand and silt member of Pleistocene age, representing a fluvial meandering product. The Madhupur Clay can be divided into a lower sandy and an upper clay unit. The Madhupur Clay overlies unconformably the Dupitila formation. After the deposition of this unit, tectonic activity raised the Lalmai Hills, which have been eroded, and dissected giving rise to fragmentary terraces. Consequently a topographical unconformity had

been formed. As a consequence, the drainage system changed, resulting in the deposition of the Chandina Deltaic Plain deposit, the Chandina Formation, a sequence of grey silt, clayey silt and clay with high percentage of illite and kaolinite.

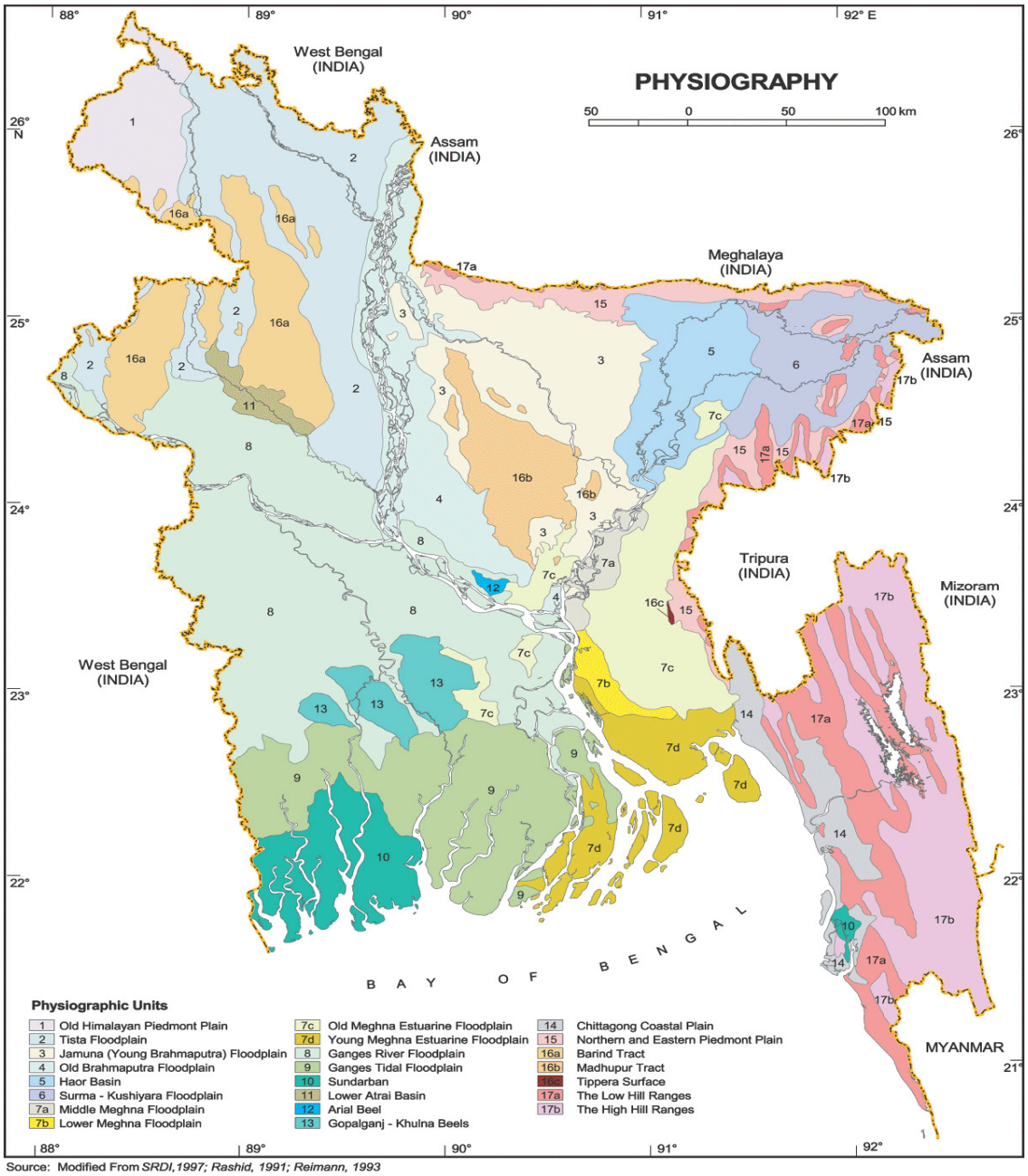

Source: Modified From *SRDI,1997; Rashid, 1991; Reimann, 1993*

Figure 1.3 Physiographic map of Bangladesh (after Rashid,1991; Reimann,1993; and modified from SRDI, 1997)

Based on available borehole data, the study area and the adjoining area can be divided into four hydrostratigrphic units. These units, in order of depth, are the upper aquitard, the upper aquifer, the lower aquitard and the lower aquifer. These units are described later. The stratigraphic status of these units is not known. However, the upper aquitard is assumed to be the flood plain deposits of Holocene age. The upper aquifer is assigned to the Chandina Formation (Bakr, 1976). By correlating stratigraphic information of the study area and adjoining areas the following stratigraphic column of the study area has been developed.

The surface geologic map of the study area presented in Figure 1.3 is based on the geological map published by the Geological Survey of Bangladesh and the hydrostratigraphic succession of the study area is shown in Table-1.l.

The lithostratigraphic units are, listed youngest to oldest :

1. Meghna Flood plain Deposits
2. Chandina Deltaic Plain
3. Madhupur Clay Formation
4. DupiTila Formation

Age	Group/series	Formation	Thickness (m)	Systematic lithology
Holocene		Meghna river flood plain deposits	No data available	Alluvial sand and silt
Holocene		Surma-Kushiara flood plain deposits	No data available	
Late Pleistocene-Holocene		Chandina formation	No data available	Upper sandy sequence, lower silty sequence
Lower Pleistocene		Madhupur Clay	No data available	Red-Brown silty clay(residuum)
Upper Miocene To Lower Pleistocene		Dupitila	749	Grey, fine to coarse sandstone with thick layers of grey to bluish grey, soft plastic and sticky clay.
Middle to upper Miocene	Tipam	Girujan clay	170	Bluish grey, softsticky and mildly calcareous sand.
		Tipam Sandstone	340	Grey, fine to very fine,poorly consolidated sandstone with a thick bluish grey shale.
Lower to Middle Miocene	Surma	Bokabil 3	50	Bluish grey, soft and plastic shale
		Bokabil 2	400	Grey, fine to very fine, poorly consolidated micaceous sandstone with trace shalealternation.
		Bokabil 1	652	Thick bedded, bluish grey well laminated sand and shale alternation.
		Upper Bhuban	865	Thick bedded, light grey well consolidated, mildly calcareous sand separated by bluish grey, well-laminated shale.
		Middle Bhuban	160+	Alternation of light grey, fine, well to moderately consolidated and mildly calcareous sandstone and dark clay, dard compact and massive clay stone.

Table-1.1 Stratigraphic successions of the study and adjoining areas (Khan 1999)

Chapter 2 - Background

The presence of elevated As (>10 μg/L) in groundwaters was first reported from West Bengal, India in early 1980s (Saha, 1984). In the subsequent years, similar enrichment was also reported from the aquifers of Bangladesh (Dhar et al., 1997; Roy Chowdhury et al., 1999). Since the first reporting of As in groundwater, significant progress have been made in the context of its source characterization, identification of mobilization and immobilization processes, spatial and vertical distributions, etc. (Bhattacharya et al., 1997; Nickson et al., 1998; BGS and DPHE, 1999, 2001; Harvey et al., 2002; van Geen et al., 2003; Islam et al., 2004; Ravenscroft et al., 2005; Polizzotto et al., 2008; Nath et al., 2009; Polya and Charlet, 2009; Mukherjee et al., 2011; Datta et al., 2009 & 2011; Biswas et al., 2012). The geogenic nature of groundwater As and its mobilisation primarily from iron-oxyhydroxide minerals through the reductive dissolution process mediated by microbial metabolism of organic carbon (OC) has been widely accepted by the global scientific community (Bhattacharya et al. 1997; Nickson et al. 1998; BGS and DPHE 2001; Harvey et al. 2002; Islam et al. 2004; McArthur et al. 2004; Saunders et al. 2005; Zheng et al. 2005; Shamsudduha et al. 2008). Controversy over the source and nature of the organic carbon remains. Several hypotheses proposed over the last decade postulate that organic carbon derives from buried peat deposits (McArthur et al. 2001), carbon-enriched recharge from surface-water (Harvey et al. 2002), co-deposition of plant materials with sediments over geologic time (BGS and DPHE 2001; Meharg et al. 2006), or recharge water from ponds (Neumann et al. 2010). Since the distribution of observed groundwater As in Bangladesh and other Asian Mega-Deltas cannot be entirely explained by the variation of solid-phase As in aquifer sediments (Neumann et al. 2010), the type and sources of organic carbon which drive the microbial reductions remain critical in explaining the variation in groundwater As concentrations.

Groundwater flow plays an important role in the transportation and distribution of As and its evolution in alluvial aquifers (Fendorf et al., 2010; Hoque, 2010). Groundwater flow systems in the Bengal Basin of Bangladesh and other Asian lowland river basins and deltas all feature highly seasonal characteristics (i.e., high amplitude in annual groundwater levels) due to monsoonal climate and similar hydrogeological conditions (Harvey et al. 2002; Benner et al. 2008; Larsen et al. 2008). Shallow (<50 m below ground level) groundwater flow systems are highly dynamic, reflecting transient, intra-annual patterns of recharge and discharge (Fendorf et

al. 2010). Unlike other Asian mega-deltas, groundwater-fed irrigation to sustain dry-season hybrid rice (Boro) cultivation is substantial in the Ganges-Brahmaputra-Meghna (GBM) Delta of Bangladesh. Intensive irrigation and return flow from agricultural fields modify regional and local flow patterns (MPO 1987; WARPO 2000; Ravenscroft et al. 2005; Harvey et al. 2006; Mukherjee et al. 2007; Michael and Voss 2008; Michael and Voss 2009a).

A range of contrasting hypotheses has been proposed to establish causal links between groundwater recharge and As mobilisation in the Bengal Basin (Figure 2.1; Table 2.1 provides a summary). Based on geochemical observations and hydrogeological conditions at localised study sites in Bangladesh, a series of hypotheses has been proposed which assert that irrigation-induced recent recharge triggered groundwater As mobilisation by drawing organic carbon from agricultural fields (Harvey et al. 2002; Harvey et al. 2006). Specifically, intensive irrigation is thought to induce mixing of young, organic carbon-enriched groundwater with older groundwater at depths where As concentrations are the highest (Klump et al. 2006); recent recharge from ponds carries reactive organic carbon into shallow aquifers facilitated by intensive irrigation pumping and mobilise groundwater As (Neumann et al. 2010).

Datta et al. (2009), however, investigated the fate of As during groundwater discharge and found that high As concentrations in sediment result from As-rich groundwater discharging to the Meghna River (Bangladesh) through a more oxidizing environment. Here a significant portion of dissolved As sorbs to Fe-bearing minerals (i.e. biotite, hornblende, goethite, magnetite, vivianite and clays (chlorite, illite, smectite)), forming a natural reactive barrier (NRB). The NRB, when recycling and reworking of its sediments occurs in an active fluvial-deltaic environment such as the GBM Delta, can provide a potential source of As to further contaminate the groundwater. Results presented by Datta et al (2009) suggest that there is a systematic process that is driven by seasonally active hydrogeological and biogeochemical interactions between discharging anoxic groundwater and more oxic river water.

It has also been proposed (BGS and DPHE 2001; McArthur et al. 2004; Ravenscroft et al. 2005; Stute et al. 2007; van Geen et al. 2008) that recharge flushes the aquifer which subsequently depletes mobilisable As content over time. Recent groundwater-fed irrigation has induced more recharge to shallow aquifers and, therefore, flushed out As from aquifer's sediments and water in areas of greater groundwater recharge. The assumptions central to these hypotheses have never been tested at the basin or national scale beyond the localised study areas.

It is also unknown whether recharge or groundwater-fed irrigation can explain the national-scale variability in observed As concentrations in shallow aquifers.

Sequential extractions of sediments from the Chapai-Nawabganj District of northwestern Bangladesh by Reza et al. (2010) revealed that fine-grained Mn and Fe hydroxides and organic matter are the major leachable solids carrying arsenic. Statistical analyses from this work clearly show that As is tightly associated with Fe and Mn in sediments, but As is better correlated with Mn in groundwater. This may be due to reductive dissolution of MnOOH and FeOOH, where possible precipitation of dissolved Fe as siderite under reducing conditions may account for the poor correlation between Fe and As in solution (Reza et al., 2010). Mukherjee et al. (2008) compared hydrogeochemistry in the western and eastern margins of the Bengal Basin and concluded that presence of As in groundwater in different parts of the basin cannot be explained simply by mobilization mechanisms, rather it may be a function of retention (and potential re-mobilzation) mechanisms. This study also indicated that simultaneous redox processes occur at different depths, suggesting an environment with overlapping redox zones.

Deeper waters from Pleistocene aquifers are relatively As free, and 3H dating (along with small amounts of O2) of some groundwaters revealed recent contact with the atmosphere, i.e. young groundwater (Zheng et al., 2004). Isotopic signatures of deep groundwater closely reflect those of meteoric water (Lawson et al., 2008). However, widespread irrigation pumping of the deep aquifer in the Bengal Basin may eliminate deep groundwater as an As-free resource within a few decades (Burgess et al., 2010).

NO	**Hypothesis**	**Mechanism for As mobilisation**	**Hydrodynamic Components**	**Geological control**	**References**
H1	Young carbon hypothesis	Ponds and irrigation return-flows provide organic carbon for Fe-oxyhydroxides reduction and mobilisation of As at shallow depths	Irrigation enhances recharge (induced) by lowering groundwater levels and creating vertical hydraulic gradients in shallow aquifers	Geologically independent	Harvey et al. (2002; 2006) Datta et al. (2011)
H2	Groundwater mixing hypothesis	Pumping for intensive irrigation causes convergent groundwater flow and promotes mixing between shallow, younger and deeper, older groundwaters	Changes in hydraulics due to irrigation causes As mobilisation. Irrigation increases the rate of groundwater renewal by pumping large water volumes	Geologically independent	Klump et al. (2006)
H3	Aquifer flushing hypothesis	Irrigation induces recharge and thereby reduces the residence times of shallow groundwater. At shallow depths (<20 m bgl), As positively correlate with groundwater residence times	As concentrations at shallow depths are controlled by aquifer flushing rates. Increased irrigation results in a reduction of As concentrations in shallow aquifers. Areas of low recharge have high As concentrations	Geologically independent	McArthur et al. (2004); Stute et al. (2007); van Geen et al. (2008)
H4	As-peat hypothesis	Peat provides the organic carbon to drive the microbial reduction of Feoxyhydroxides. Spatial distributions of As do not correlate with areas of intensive abstractions for irrigation	No direct indication of hydrodynamics control. Higher As concentrations negatively correlate with dry-season water levels and also with groundwater-fed irrigation trends. Less irrigated areas have higher As concentrations	Geologically dependent	Ravenscroft et al. (2001; 2005); McArthur et al. (2004)
H5	As-OC codeposition hypothesis	As was codeposited with organic carbon in the aquifer sediments. Areas of higher abstraction for irrigation have lower As concentrations in groundwater	No direct indication of Hydrodynamics control. As concentrations are highest where irrigation is lowest. In other words, low-As concentrations are associated with areas of declining groundwater levels due to irrigation	Geologically dependent	Meharg et al. (2006)

Table 2.1 Proposed hypotheses on the mobilization of groundwater As in shallow aquifers in Bangladesh. Assumed processes or mechanism(s) associated with each of these hypotheses are summarized above. References for each hypothesis are also listed. (adapted from Shamsudduha et al., 2011)

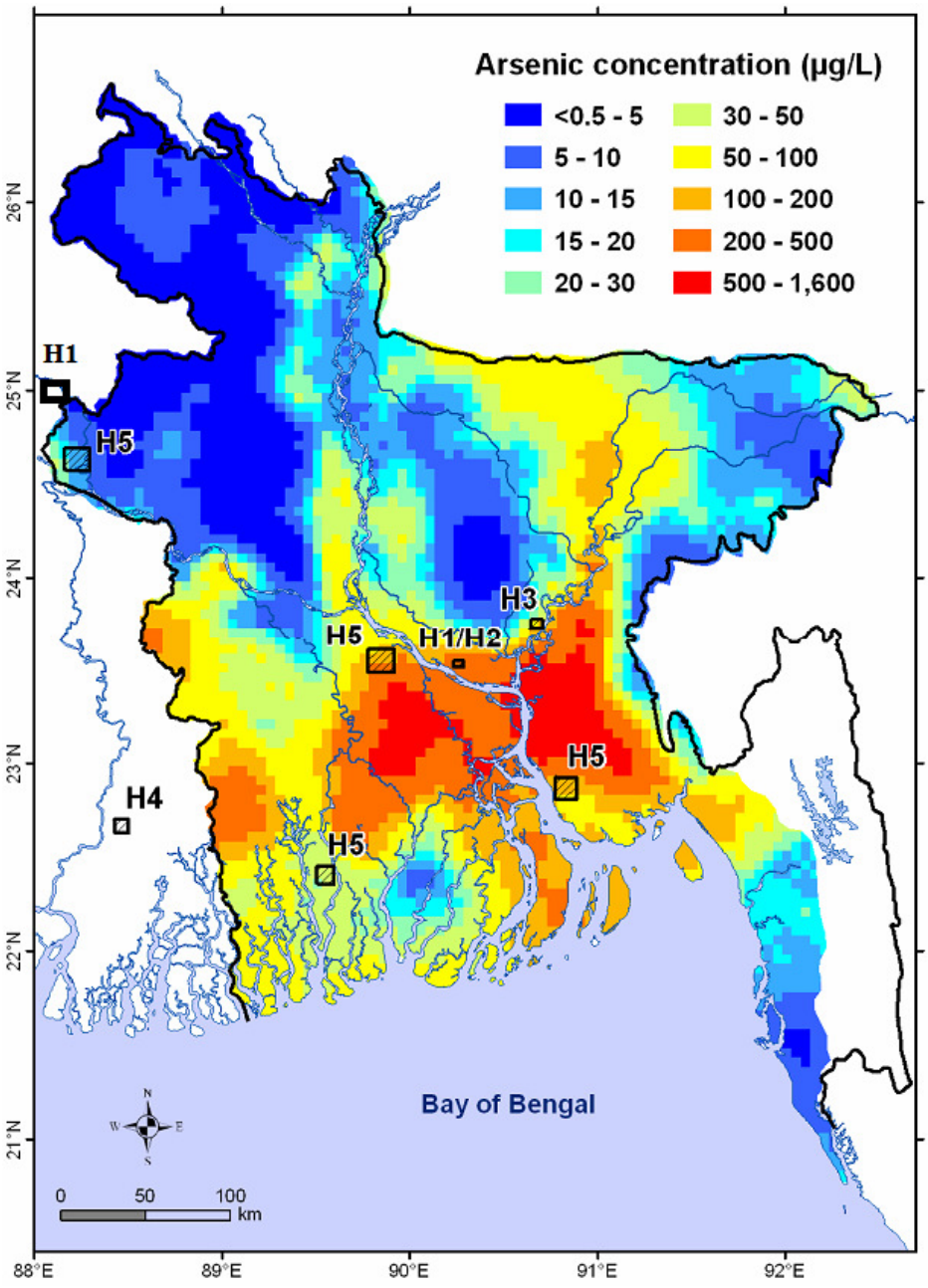

Figure 2.1 Spatial distribution of groundwater As concentrations in shallow (<50 mbgl) aquifers in Bangladesh. The gridded map of As concentrations was created by interpolating 2410 data points using ordinary kriging method with a fitted variogram model. Locations for the study sites associated with various As mobilisation hypotheses are shown on the map. Keys: H-1, H-2, H-3, H-4 and H-5 (see table 2.1) (adapted from Shamsudduha et al., 2011)

Background of Present Research

People living in the villages do not prefer alternate drinking water sources other than tubewell located within their premises. The use of tubewell water for domestic purpose is deeply embedded within the daily life of the villagers (Johnston et al., 2010). Thus tubewell switching and deep tubewell installation gained gradual popularity and thus effectively reduced the number of As exposed population (Ahmed et al., 2006). However, the installation of deep tubewells requires advanced drilling technologies, which increases the installation cost (500–1200 USD) several times more than a shallow tubewell installation (depth within 70 m, cost 50–120 USD) (Hug et al., 2011). Rural villagers cannot afford the cost to install household deep-tubewells. Instead, they either need to depend on the community tubewells, which are also fewer in numbers, or on the deep tubewells installed by wealthier people in the community. Additionally villagers are also reluctant to collect drinking waters from tubewells owned by someone else, a powerful social burden to access safe drinking water by means of tubewells switching and deep tubewell installation (Johnston et al., 2010). Consequently 54% of the exposed populations in Bangladesh still have no other options except to drink As-contaminated water (Ahmed et al., 2006). Thus, to prioritize sustainable As mitigation management and achieve the United Nations (UN) Millennium Development Goals (MDGs) of reducing the proportion of population having no/very little access to sustainable safe drinking water worldwide by 2015 (Target 7C), it is imperative to delineate safe aquifer(s) within shallow depth (or at the most intermediate depths), which can be targeted by locally available cheap drilling technology. Few recent studies have investigated the ongoing indigenous drilling practices by local drillers in the rural Bengal and attempted to correlate aquifer sediment color with the occurrence of As in groundwater (van Geen et al., 2002, 2003; Jakariya et al., 2007; von Brömssen et al., 2007, 2008; Pal and Mukherjee, 2008, 2009; Bundschuh et al., 2010, Biswas et al.2012; McArthur et al, 2011, Sankar et al., 214; Hossain et al., 2014). Based on the studies in Bangladesh it is reported that grey and dark grey sand aquifers are mostly contaminated with dissolved As (>10 μg/L), whereas brown and light grey sand aquifers may be safe (<10 μg/L) (e.g. von Brömssen et al., 2007; Hossain etal; 2014). The underlying reason for the occurrence of contrasting dissolved As in groundwater of these two aquifers has been hypothesized as follows. Being sub-aerially oxidized during temporal sea level regression period (Umitsu, 1993), the redox potential of the brown and light grey sediment is quite high, but does not reach the stage of Fe-oxy-hydroxide reduction (von

Brömssen et al., 2007, 2008), which prevails in the grey and dark grey sediments. It is the latter that causes high As groundwater (Bhattacharya et al., 1997; Nickson et al., 1998). Consequently the light grey and brown sediments within shallow depth has been suggested to be targeted for safe drinking water supply in Bangladesh (von Brömssen et al., 2007; Bundschuh et al., 2010; Hossain et al, 2014). However, so far no attempt has been made to geochemically validate the redox status of these two aquifers, which is important for assessing the long term sustainability of light grey and brown sediment aquifer for safe drinking water supply. In order to explore the groundwater evolution and validate redox status within grey, dark grey, light grey and brown sediment, the present study has undertaken a detailed sediment geochemistry, sediment microbial community and hydrogeochemical investigation of groundwaters from intermediate well depths (<125 m).

Identification of low-arsenic aquifers using the color method was first explored at Matlab by Von Bromssen et al. (2007). Based on the sediment colour at the screen depths, 40 domestic shallow tubewells were selected for water sampling for von's research work. Four colours were used to describe the sediments: black, white, off-white (buff) and red. Von Bromssen found that the groundwater was anoxic and the As concentrations ranged from less than 5.2 to 355 μg/L. Water derived from the black sediment was characterized by relatively higher concentrations of dissolved NH_4^+, DOC, Fe, P, As and by low Mn and SO_4^{2-} concentrations. The off-white and red sediments had high concentration of Mn and low NH_4^+, DOC, Fe, P and As concentrations. The water abstracted from the black sediments indicated the most reducing environment, followed by white, off-white and red, respectively. Three boreholes verified the driller's perception of the subsurface lithologic conditions. Most tubewells were installed to a depth of about 60 m. The chemical characteristics of the groundwater correlate well with the colour of the aquifer sands. The redox conditions follow a trend from very reducing conditions for black (as described by the drillers) sediments with increasing redox potential in sequence through white, off-white to red sediments. Von Bromssen(2007) states that reductive dissolution of Fe(III)-oxyhydroxides under strongly reducing conditions of the Holocene black to grey sediments is the cause for mobilisation of As in Matlab Upazila.

Jakaria et al (2007) did research on social impact of arsenic testing using field test kits. Their study showed that field test kits offer the only practical tool for most people, given limitations on time and financial resources available for screening and assessment of the As

contaminated tubewells; they are also the most practical for monitoring than laboratory measurement. They compared field test kit and laboratory measurements by AAS (as "goldstandard" for As in water) of 12,532 tubewells in Matlab Upazila in Bangladesh. Their results showed that the field kit correctly determined the status of 91% of the As levels compared to the Bangladesh Drinking Water Standard (BDWS) of 50 µg/L, and 87% of the WHO guideline value of 10 µg/L. Cross-checking of the field test kit results, both by Field Supervisor and by the laboratory analyses, revealed considerable discrepancies in the correct screening mainly at As concentration ranges of 10–24.9 µg/L and 50–99.9 µg/L,. These concentration levels are critical from a public health point of view.

Von Bromssen et al (2008) worked on geochemical characterization of shallow aquifer sediment. Their research showed that groundwater abstracted from oxidised reddish sediments, in contrast to greyish reducing sediments, contains significantly lower amount of dissolved arsenic and can be a source of safe water. In order to study the sustainability of that mitigation option, they described the lithofacies and genesis of the sediments within 60 m depth and established a relationship between aqueous and solid phase geochemistry. They found that oxalate-extractable Fe and Mn contents are higher in the reduced unit than in the oxidised unit, where Fe and Mn are present in more crystalline mineral phases. Equilibrium modeling of saturation indices suggests that the concentrations of dissolved Fe, Mn and PO_4^{3-} in groundwater are influenced by secondary mineral phases in addition to redox processes. Simulating As^{III} adsorption on hydroferric oxides using the Diffuse Layer Model and analytical data gave realistic concentrations of dissolved and adsorbed As^{III} for the reducing aquifer and that the presence of high PO_4^{3-}-tot in combination with reductive dissolution results in the high-As groundwater. The study confirmed high mobility of As in reducing aquifers with typically dark colour of sediments found in previous studies and thus validates the approach for location of wells used by local drillers based on sediment colour. Groundwaters in the contaminated reducing aquifers were characterised by high concentrations of PO_4^{3-}-tot, NH_4^+, DOC, Fe and low SO_4^{2-},whereas the targeted oxidised low-As aquifers are characterised by high Mn, low NH_4^+, DOC, Fe, and PO_4^{3-}. Analysis of dediment chemistry from the high-and low-As aquifers showed that Fe_{total} and Mn_{total} correlated well for both the high- and the low-As unit. The Fe_{Ox}/Mn_{Ox} (oxalate extraction) were distinctively higher for the reducing high-As unit, indicating that amorphous Fe oxides and hydroxides are more inclined to weathering and oxidation than amorphous Mn oxides and

hydroxides. Their geochemical modeling also showed that the concentrations of Fe, Mn and PO_4^{3-} in the groundwater were influenced by the formation of secondary minerals in addition to redox processes. Simulation of As^{3+} adsorption within the reducing aquifer unit system showed that As^{III} was largely influenced by the amount of Eh, pH and by competing ion(s).

Robinson et al. (2011) study focuses on the adsorption behaviour of shallow oxidized sediments from Matlab Region, Bangladesh, and their capacity to attenuate As if cross-contamination of the oxidized aquifers occurs. Robinson's work sediment extractions indicate a relatively low amount of As in the oxidized sediments, below 2.5 mg kg^{-1}, batch isotherm experiments show that the sediments have a high capacity to adsorb As. Simulations using a surface complexation model that considers adsorption to amorphous Fe(III) oxide minerals only, under-predict the experimental isotherms. Their rsearch suggests that a large proportion of the adsorption sites in the oxidized sediments may be associated with crystalline Fe(III) oxides, Mn(IV) and Al(III) oxides, and clay minerals. Batch isotherm and column experiments demonstrated the oxidized sediments in Matlab Region have a high capacity to absorb As. Robinson's suggests targeting these sediments for installation of tube-wells may be a simple sustainable solution for delivering As-safe drinking water to the rural communities in areas where oxidized sediments exist at shallow depth.

Researchers have also targeted different types of health impacts of arsenic in Matlab, Bangladesh. Rahman et al (2006) assessed the prevalence of arsenic exposure through drinking water and skin lesions, and their variation by geographical area, age, sex, and socioeconomic conditions. The result showed sex, age, and socioeconomic differentials in both exposure and skin lesions. Findings clearly showed the urgency of effective arsenic mitigation activities. Rahman et al (2007) evaluated the effect of arsenic exposure on fetal and infant survival in a cohort of 29,134 pregnancies identified by the health and demographic surveillance system in Matlab, Bangladesh, in 1991–2000. Drinking tube-well water with more than 50 µg/l of arsenic per liter during pregnancy significantly increased the risks of fetal loss (relative risk = 1.14, 95% confidence interval: 1.04, 1.25) and infant death (relative risk = 1.17, 95% confidence interval: 1.03, 1.32). There was a significant dose response of arsenic exposure to risk of infant death ($p = 0.02$). Vahter et al. (2011) assessed the exposure of pregnant women to arsenic in Matlab, Bangladesh, by measuring concentrations of arsenic in urine. There was a considerable variation in urinary concentrations of arsenic (total range 1-1,470 µg/L, adjusted to specific gravity 1.012

g/mL), with an overall median concentration of 80 μg/L (25th and 75th percentiles were 37 and 208 μg/L respectively). Arsenic exposure was about the same in early pregnancy and late pregnancy, this research results indicating that the foetuses were exposed during the entire intrauterine life. Arsenic is a potent toxicant and carcinogen, and there is reason to believe that the developing child is particularly sensitive.

This present thesis work is based on SASMIT (Sustainable Arsenic Mitigation Project-funded by Swedish International Development Agency) research combined with implementation project. SASMIT is an action research project which has developed to be a community-based strategy for installation of safe drinking water wells in arsenic affected regions of Bangladesh. The installations are optimised on the basis of hydrogeological suitability and the demand for safe water among the underserved segments of the society. The approach can be scaled up for improving safe water access in other arsenic affected regions of Matlab, Bangladesh. Undoubtedly ground-water exploitation will increase for the purpose of drinking both in rural and urban areas of Bangladesh and if local drillers could target safe aquifers, it would be a very viable option for arsenic mitigation as the practice of using tubewells is deep-rooted in the minds of rural peoples. The awareness of local drillers to elevated As concentrations in tubewell water at shallow depths has made them change their practice of installation of tubewells. Using the visual color attributes of the shallow sediments (< 50 m) and content of dissolved Fe, which in general are associated with high As concentrations, the local drillers presently install community tubewells at depths targeting off-white or red/brownish sediments. The drillers' perception and local knowledge of the sediments are often commendable and there is a good potential for capacity building of the local drillers to target safe aquifers. Involving the local drillers in this process would enhance their awareness and knowledge, which will help them target safe aquifers on a country-wide scale and thereby reduce the exposure to As through drinking water. In Bangladesh approximately 90% of the wells are installed privately, where the local drillers play the key role in the process of making decision on well installations. Considering drillers as the driving force, their perception of the nature of the aquifers (layers) in terms of sediment colour and depth is taken as a key consideration during private tubewell installation.

SASMIT project research introduce that for local drillers for installing shallow tubewells in reddish brown sediment with low concentrations of As with average and median values lower than the WHO drinking water guideline (10 μg/L). The levels of As in the off-white sediments

were also similar, however, targeting off-white sands could be limited due to uncertainty of proper identification of colour, specifically when day-light is a factor. Elevated Mn in both red and off-white sands is a constraint for installation of safe tubewells. Grey and dark grey colored sediments at shallow depths are rare and apparently less important for well installations. The SASMIT project installed most of the shallow wells (> 90%) in black sands (grey and dark grey) where As concentration was high (for monitoring As concentration in this color depth) , with an average of 235 µg/L and therefore installation of wells in shallow black sand aquifers must be avoided.

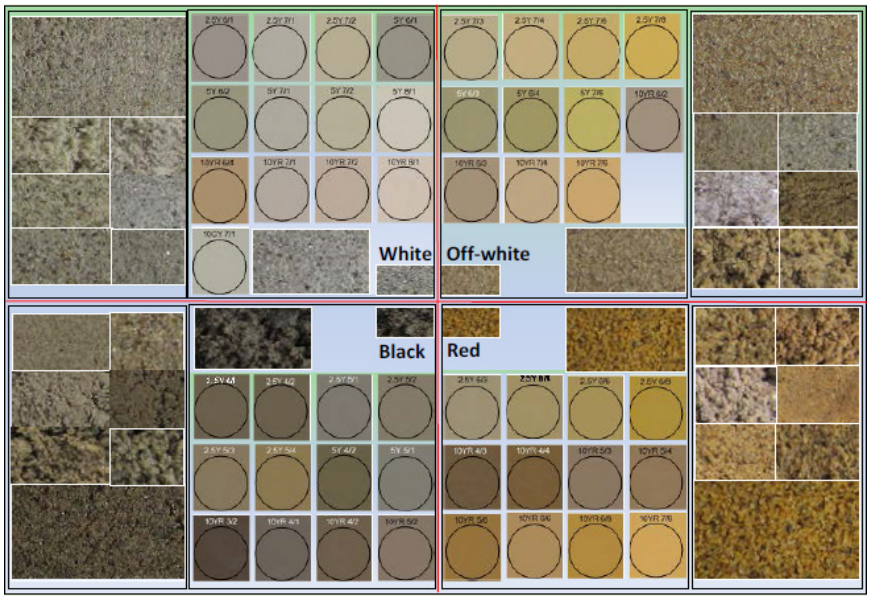

Figure 2.2 A simplified colour tool for the identification of low arsenic aquifers at shallow depth (from SASMIT colour guide) (Hossein et al. 2014)

There is a distinct relationship of sediment colour and corresponding As concentrations in water. Based on these findings a simple colour based tool for targeting shallow aquifers for the installation of arsenic safe community tubewells has been developed by SASMIT for the local drillers (**Figure 2.2**). The low As wells installed in red colour sediments comply with the drinking water standards for As, although concentrations of Mn in many of these wells are above national drinking water standards. However, As warrants highest attentions as its health effects are more serious than those on Mn. Based on the comprehensive hydrogeological investigation by SASMIT, a strategy was developed to target the intermediate deep aquifer to avoid the risk for both As and Mn. This aquifer was found to be low in both As and Mn and the SASMIT

project successfully installed 268 tubewells during the project period. Among the tubewells installed, 96 % were found to be As-safe according to Bangladesh Department of Water and Sanitation (BDWS). These newly explored intermediate depth aquifers could be a potential source for As- and Mn-safe water supply at a reasonable cost. Replication trials in neighbouring upazilas validated the wider applicability of the tubewell strategy of As mitigation.

Figure 2.3 Piezometer Nest in North Matlab (Nest- 9)

Realtion of present thesis and SASMIT project

Based on the SASMITpiezometer database we have acquired two drill-core samples in Matlab area; one from South Matlab (Daksin Nayergoan, N23.36834 E90.76748) and another from North Matlab (Hapania, N23.48756 E90.66227) (**Figures 4.1 c & d red color**). Both boreholes were drilled within close proximity to an already exisitng piezometer nest. In this case piezometer nests 5 and 7 (according to earlier studies done by SASMIT project) were selected. We collected undisturbed core samples from variuos depths, both within aquifers and aquitards. From the North Matlab site, the following depth samples were collected: 15m, 26m, 55m, 75m,

88m and 108m. From the South Matlab site the following depth samples were collected: 10m, 28m, 47m, 65m, 83m, 96m, 103m and 117m.

Figure 2.4 Sketch of typical piezometer nest installed in Matlab by SASMIT project (2009-2010)

Chapter 3 - Objectives

The focus of this research project is to demonstrate the mineralogical and geochemical differences between differently colored aquifer sediments in Matlab area [this work was planned as an extension of an already completed and executed SASMIT project in collaboration with KTH (Royal Institute of Technology), Sweden and University of Dhaka]. Our work encompasses analyses of sediment core samples from shallow and intermediate depth aquifers in order to understand the relationship between sediment color and associated water chemistries. The idea was to compare the geochemistry and mineralogy of aquifer sediments with hydrochemistry, stable isotope geochemistry (O,H) of groundwaters and then connecting that to microbial community in sediment samples within contrasting groundwater As-bearing environments within an area (~410 km^2) of Matlab in Bangladesh. The wider impact of this research project is to develop a community-based initiative for sustainable As mitigation by developing a sediment color based tool for the local drillers for prioritizing the hydrogeological and geochemical investigations of the sediments and waters. The key objectives of this current study are summarized below.

(a) Understanding the role of geochemical and mineralogical parameters that control the geochemistry of arsenic in the red/brown and light grey sediments; in particular, understanding why light grey sediments produce low As and Mn free water; and what processes lead to dark grey sediments producing high As bearing water

(b) Understanding the role of biogeochemical reactions that contribute to the explanation for why light grey and reddish sediments correlate strongly with As-free water while dark grey sediments correlate with As polluted waters in Matlab and elsewhere in the Bengal Delta

(c) Understanding the release mechanism for As from these sediments by studying the speciation of As and Fe in associated porewaters, groundwaters (HPLC-HR-ICPMS) and mineralogical and sedimentological analyses of sediment cores by thin section petrography, SEM-EDX, characterization of sediment speciation by synchrotron studies, total extractions and sequential extraction for As, Mn and Fe from sediments.

(d) Understanding the type of associations of microbial communities in the sediments to delineate levels of microbial controls on the As release mechanisms from these particular sediments (via detailed microbial community analyses in the sediment core samples

Chapter 4 - Methods and Materials

Study Area Description

The study was conducted in North and South Matlab Upazilas in Chandpur district, Bangladesh, approximately 60 Km southeast of Dhaka near the confluence of the Padma and Meghna Rivers (Fig. 1). It has an area about 408 sq.km. Our research area is within 3 km east of the Meghna and this area is naturally flooded each year during the monsoon (May-July). The sediments are represented by Holocene alluvial silt deposited by the Meghna and its tributary Gumti (local name Dhonagoda) rivers. These Holocene sediments are expected to be moderately deep here as the Meghna River dissected the delta during the latest glacial maximum (Umitsu, 1987, 1993; Goodbred et al., 2003., Hasan et al, 2008). The North Matlab area lies within an embankment that prevents the area from the natural flooding. The study area is situated in a triangular-shaped tract known as Chandina Deltaic plain, which is bounded by the Meghna River to the west, Lalmai Hills in the east and old Meghna estuary at its south. The dominant topographical feature is represented by a vast expanse of deltaic plain and old Meghna estuarine flood plain deposit. It is generally a plain land, occurring at a slightly higher elevation than the adjacent flood plains. It is typically flat and intermittently flooded. The terrain slopes westward to the main channel of the Meghna River. The average elevation of the area is 4 meters in the western side and 5 meters in the eastern side. This unit is referred to as Tipperah surface by Morgan and McIntyre (1959). Older Alluvial surface by Old Meghna Estuarine Surface by Brammer (1971) and Umitsu (1985) (**Figure-2.2**). The unit is made up of silt, silty loam, silty clay, and greyish clay and has been named as the Chandina Formation. The sediments resemble those of the Recent Meghna Flood Plain but are more compact, decomposed and oxidized. Radiocarbon dating of samples of the Old Meghna estuarine deposits ranges from 3000 years BP to 1800 years BP (Brammer, 1969).

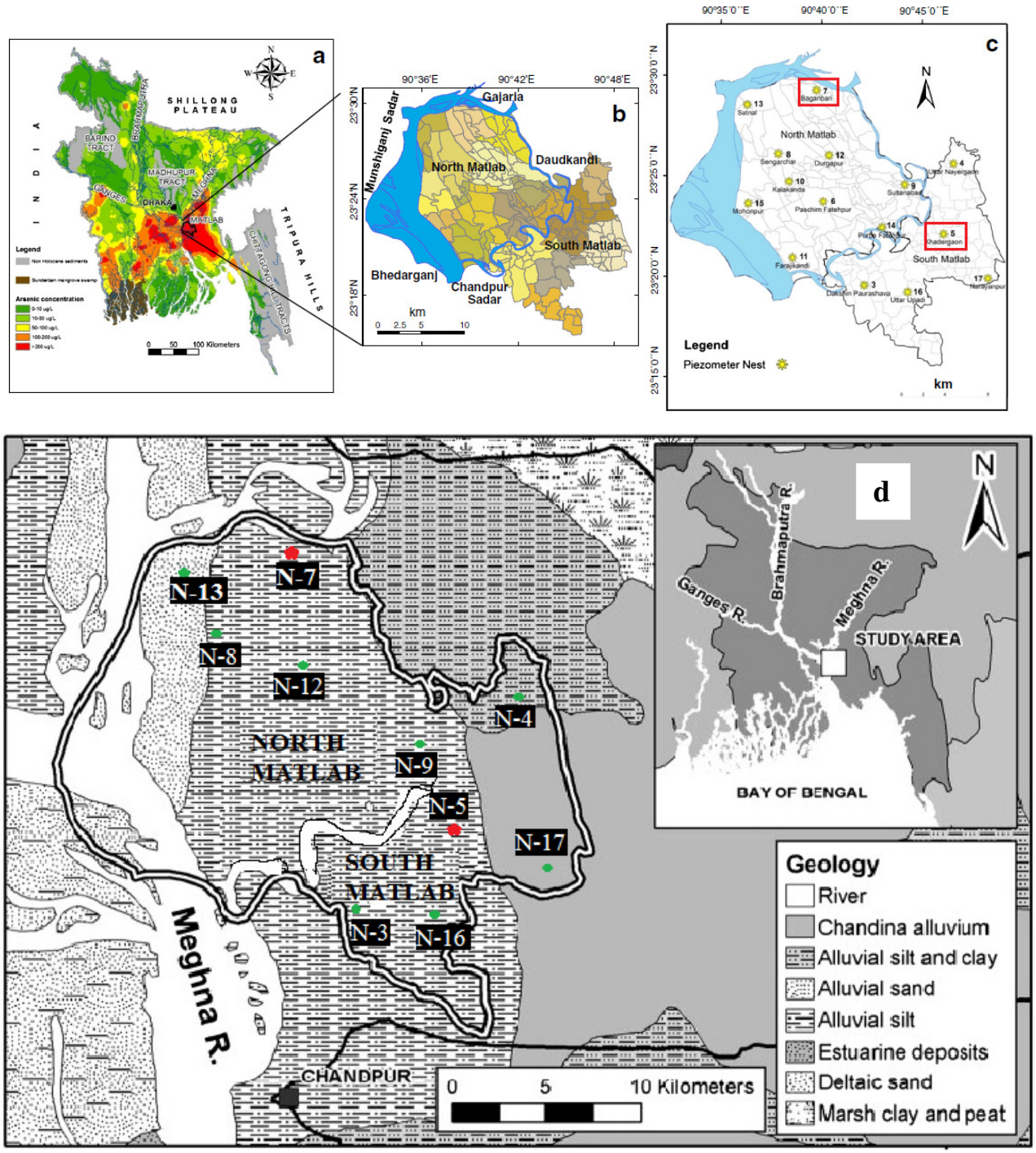

Figure 4.1 Map of Bangladesh (a) with the location of the study area and (b) sites of drill coresand installed piezometer nests (c) (after Hossain et al. 2014). (d) Surficial geology map of North and South Matlab (after Von Bromssen et al 2008)

The area is drained by a network of streams and khal (canals). Meghna river is the main river flowing through the Upazila along the western side of the Upazila that separates many chars (uplands) from the main land of the Upazila. Meghna River also forms the Upazila boundary at the north-western side of the Upazila. Dhanagoda is the second big river flowing through this Upazila. It is located in the central part of the Upazila and flowing from north-east to south-west direction and seperated North Upazila from South Matlab. The Dhanagoda river has a meandering pattern and is a distributary of the Meghna river. Meghna river has some tributaries that drain water from the land and emerge into the Meghna river. The Dhanagoda river has numerous tributaries which are interconnected to form a semi-rectangular drainage pattern. Khals (canals) are more common features in the area. Most of the khals are along the roadsides. Khals were developed both in natural and artificial processes. Many of these khals were developed by man for agricultural purpose.

The regional study area experiences three major climatic seasons, e.g., a hot summer (March–May), followed by monsoon or rainy season (June–October) and a moderate winter season (November–February) like other parts of Bangladesh. The temperature gradually rises from 10°-12°C in winter to a maximum of about 36°C in summer. The average annual rainfall in and around the study area is over 2,500 mm (according to Bangladesh Meteorology Department) and about 95% of its total rainfall is received during May to October (wet period); the remaining 5% of the rainfall is received during November to April (dry period) (Hasan, 2008)

Sample Collection

Water Sampling

During the field trips (January 2013), groundwaters from tubewells (**Figure 4.2**) (shallow aquifer < 60 m, intermediate aquifer 60 to120 m and deep aquifer > 120 m) were collected from South and North Matlab. Tubewell waters (n=62) were collected from wells ranging in depth from 8.5 to 226 m. We collected groundwaters from a nest of 10 pizometers, which were installed by SASMIT all over the South and North Matlab (**as pointed out in Figure 4.1**). Well waters were collected only after a minimum of 5-10 minutes of pumping to purge the well casing several times (van Geen et al., 2003).

Before heading to the field sites, each sample bottle was pre-washed following a specific protocol. Each bottle was rinsed three times with tap water, rinsed three times with de-ionized

water, soaked in RBS (detergent) overnight, rinsed three times again with de-ionized water, soaked in an acid bath (10% Trace Metal grade HCl) overnight, rinsed with de-ionized water three times, and air-dried on KimWipes. DIC vials were pretreated with an $HgCl_2$ (Acros Organics, Mercury (II) Chloride, 99.5%; Fisherbrand® Cat. No. 7487-94-7) solution and heated on a hot plate (Corning Remote Hotplate;~95°C) in the lab (KSU-Geology) so as to form a thin white precipitate covering of $HgCl_2$ on the inside bottom of the vial to remove organic carbon from the sample (Zheng et al., 2005).

Figure 4.2 Example of a handpumped well which was used for drawinging water from aquifers.

Most samples were collected in duplicate, and some in triplicate after rinsing the bottles three times with the water to be collected—one in a white Fisherbrand® 500 ml Nalgene® high-density polyethylene narrow-mouth bottle (Cat. No. 12-100-317) (unfiltered, unacidified) and the other (sometimes 2 each) in an amber 125 ml Nalgene® high-density polyethylene narrow-mouth bottles (Cat. No.02-923-5c) (one unfiltered, unacidified; one filtered with 0.2% ultrapure

nitric acid 250µl, acidified to prevent precipitation of dissolved iron as well as adsorption of trace metals onto the container surface [Tareq et al., 2003]). Flat top closure 50 ml centrifuge tubes (Fisherbrand® cat no. 06-443-19) used for unfiltered, unacidified samples to preservation. 250 ml Boston round narrow mouth clear glass bottle (Fisherbrand® cat no.05-719-163) unfiltered, unacidified sample collected for oxygen and hydrogen isotope studies. 250 ml narrow mouth amber glass Boston round glass bottle (Fisherbrand® cat no.02-911-928) unfiltered, acidified sample collected for preservation purpose. 20 ml glass vials water sealed with a rubber stopper and crimp top (National Scientific® Vials cat no. C4020-20, rubber stopper cat no. C4020-34, Crimp top cat no. C4020-5A used for collecting unfiltered and unacidified DIC samples.

Filtering was done using disposable plastic syringes (25 ml) pushing the water through a 0.45 µm polypropylene filter (Whatman syringe filter, 25 mm GD/X Disposable Filter Device, PP Filter Membrane with Polypropylene Housing, Cat. No. 6878-2504 into respective sample bottles. Each sample bottle was labeled with the type of sample (i.e. tubewell (TW), sample number (Nest=N, piezometer depth), location (village), and date. Coordinates were taken at each sampling location with hand-held GPS (Garmin eTrex Vista HCx). Sample ID, coordinates and other relevant information (i.e. well depth, date of well installation, owners name, number of members in household, symptoms of arsenic poisoning, etc) were recorded manually in field notebooks.

Rhizons for Sampling Pore Waters

We used rhizons sampler for collecting in-situ pore water from our sediment cores. These rhizon samplers extract small volumes of pore water from core sediments, in an easy, non-destructive way. It can be used for sampling waters from unsaturated soils as well as from saturated zones. The pore size of the porous part is 0.12 - 0.18 µm, so no need to filtering these samples before analyzing. Rhizons samplers are made of inert polymer with no ion exchange properties. It has also small diameter and low dead volume. Rhizons are easy to handle and once installed for an experiments, it's easy to use. It consists of two parts: a porous part of 8 mm with an outer diameter of 1 mm, and PEEK tubing with a connector fit to a syringe (**Figure 4.3**). The yield of MicroRhizons is up to 2-5 ml. (Seeberg-Elverfeldt et al., 2005; Dickens et al., 2007; Shotbolt et al., 2010)

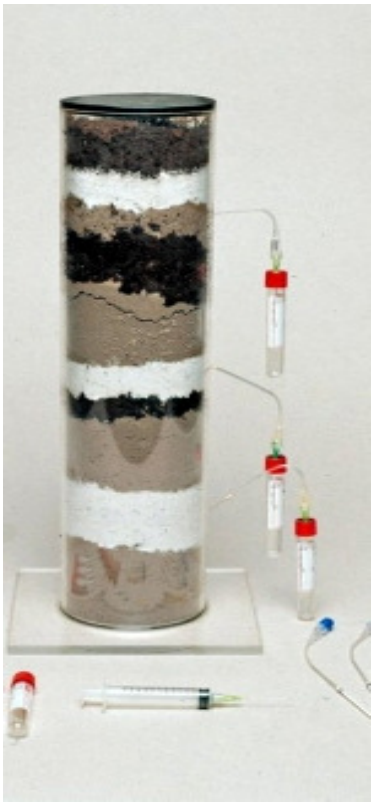

Figure 4.3 Rhizons samplers for collecting in-situ pore water from core sediments (http://www.rhizosphere.com)

Sediment Sampling

Core Sediment Sampling

Subsurface sediments were collected from shallow (2 to < 60 m) and intermediate (60 to < 110m) depth from South (N 23.36834 and E 90.76748) and North Matlab (N 23.48756 and E 90.66227) via rotary wash boring drilling methods (**Figures 4.3 & 4.4**) with split spoon samplers for undisturbed samples (**Figure 4.5**). These two drilling locations were closest to previously installed monitoring well Nest-7 (North Matlab) and Nest-5 (South Matlab) in 2009. From each location we collected samples from different depths.

From the South Matlab nest we collected core from 10, 27, 46, 64, 81, 95, 100, 112 m and from North Matlab 14, 26, 55, 75, 86, 104 m. In this method, water is pumped through a string of hollow boring rods and is released under pressure through narrow holes in a chisel attached to the lower end of the rods (**Figure 4.3**). The soil is loosened and broken up by the water jets and the up and down movement of the chisel. There is also provision for the manual rotation of the

chisel by means of a tiller attached to the boring rods above the surface. The soil particles are washed to the surface between the rods and the side of the borehole and are allowed to settle out in a sump. The rig consists of a derrick, a winch and a water pump. The winch carries a light steel cable which passes through the sheaf of the derrick and is attached to the top of the boring rods.

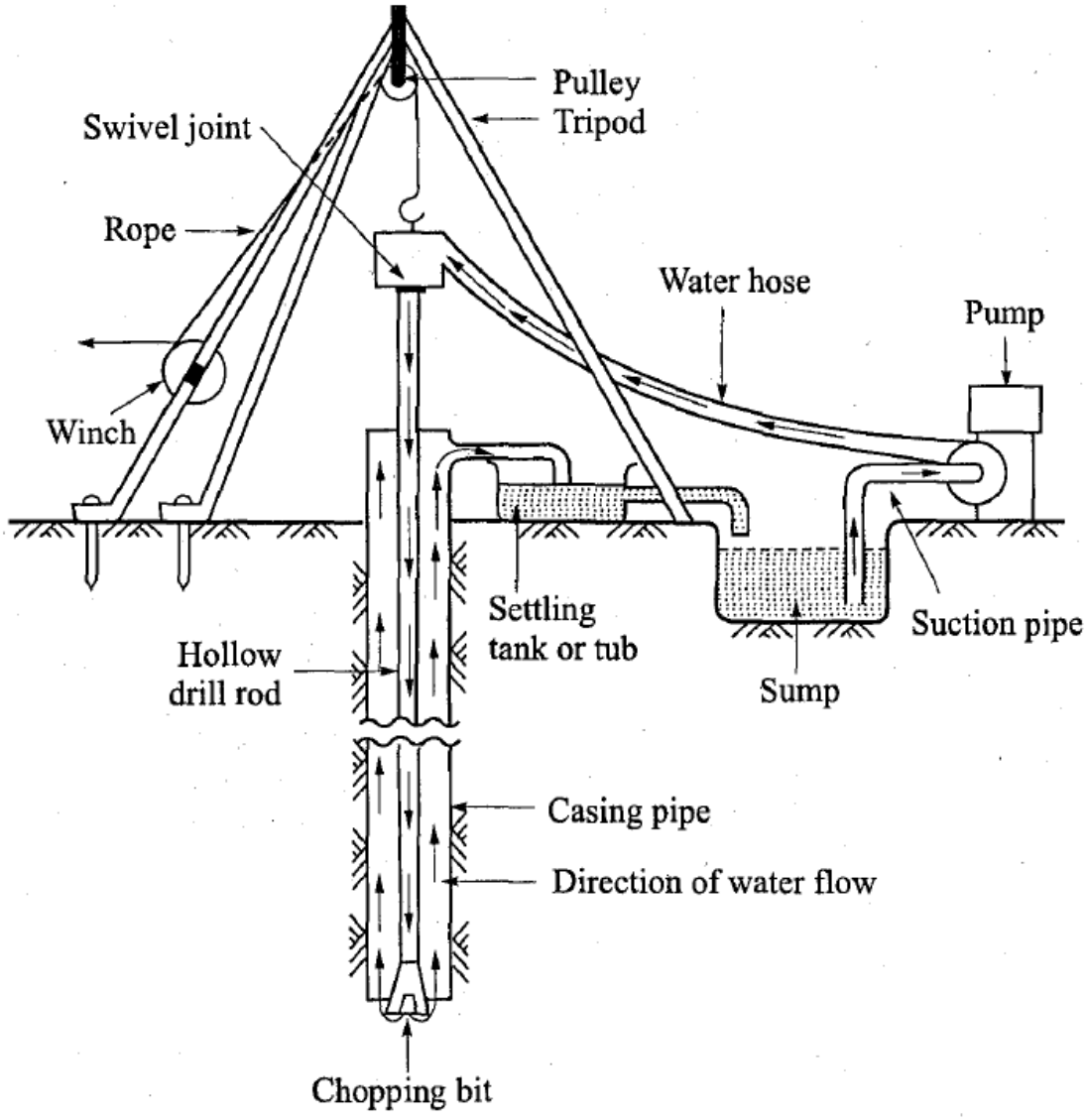

Figure 4.4 Sketch of a rotary wash boring method implemented in the field for collecting sediment cores at two nests, one in North Matlab, one in South Matlab.

The string of rods is raised and dropped by means of the winch unit, producing the chopping action of the chisel. The borehole is generally cased but the method can be used in uncased holes.

Figure 4.5 Rotary wash boring in North Matlab site (Nest 7)

Drilling fluid may be used as an alternative to water in the method, eliminating the need for casing. However, a change in the feel of the boring tool can sometimes be detected, and there may be a change in the color of the water rising to the surface, when the boundaries between different strata are reached. When we reached our targeted zone we pull out the whole pipe and use the split spoon sampler for collecting the undisturbed samples. After joining the split spoon sampler with sample tubes we hold down our borehole pipe carried out below the bottom of the hole and take the undisturbed samples using STP hammer. Before placing sediment core liners in the coring device we rinsed the liners with 100% ethanol in order to reduce contamination. An advantage of the method is that the soil immediately below the hole remains relatively undisturbed.

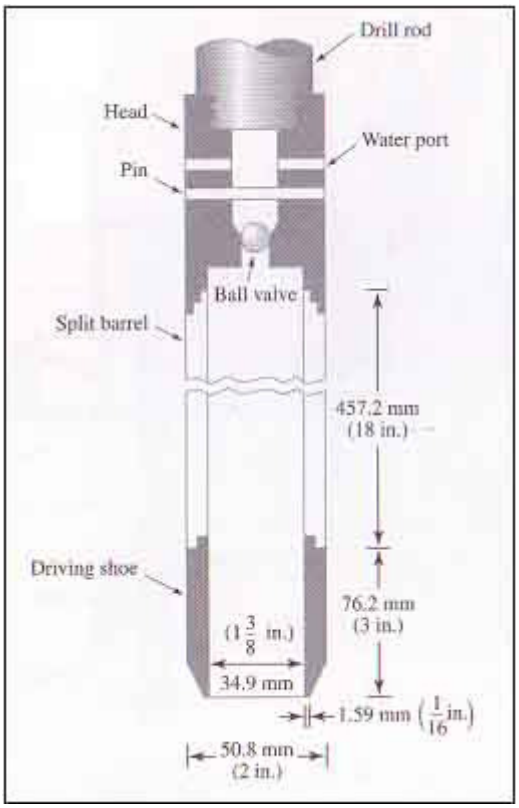

Figure 4.6 Sketch of a split-spoon sampler

Split-spoon sampler

Split-spoon samplers (**Figure 4.5**) were used to collect undisturbed samples. It consists of a tube which is split longitudinally into two halves: a shoe and a sampler head incorporating air-release holes are screwed onto the ends. The two halves of the tube can be separated when the shoe and head are detached to allow the sample to be removed. The internal and external diameters are 35 and 50 mm, respectively, the area ratio being approximately 100%, with the result that there is considerable disturbance of the sample. This sampler is used mainly in unconsolidated sediments, being the tool specified in the standard penetration test (SPT).

Wash sediment was collected at regular depth intervals (usually~3 m) and undisturbed sediment samples were collected from targeted depth aquifers and aquitards and we documented all noticeable changes in lithology (i.e. grain size, color, etc) in each borehole. Vinyl gloves (Fisherbrand® powder-fFree, lLatex-free, vinyl exam gloves; Cat. No. 19-041-190C) were worn when collecting each sample and transferring sediment either directly from the pipe (more consolidated sediments, i.e. silt, clay) or from a small, clean pale that captured the loose sediments as they discharged from the top of the drilling pipe. Samples were immediately placed

in an O_2-impermeable Remel® Bag (Mitsubishi Gas Company, Remel®, Cat No. 2019-11-02), along with an O_2 absorber pouch (Mitsubishi Gas Company, AnaeroPouch® Anaero; Cat. No. 23-246-379). The bag was immediately flushed with N_2 gas (to prevent oxidation of anaerobic sediments) in the field and sealed. Duct tape was added to some sample bags for extra security in providing a proper seal. Sample bags were labeled according to locations (as water samples were) along with a sample number, depth (in feet), and the date of collection. They were stored as cool as possible while in the field within a coller and nearby refrigerator. Core samples were used for several different types of analysis, including petrographic analyses (thin sections), scanning electron microscopy (SEM) with energy dispersive x-ray spectrum (EDX), Fe(II), total Fe and phosphate, total digestion, sequential extractions and synchrotron X-ray studies.

Grain Size Analyses

In-situ sediments were used for grain size analyses in this study. These sediment samples were collected from depths between 10 to 112 m from South Matlab and North Matlab to their difference in grain szes. For this experiment a modification of the USGS East Coast Sediment Analyses Procedure protocol was used (Poppe et al., 2000, Legg et al., 2012). Sediments were freeze-dried for 48–72 hours and then oven-dried at 60˚C for 48h. In order to disaggregate the sediments (for finer sediment samples), samples were suspended in deionised water for 24h. Then wet samples were passed serially through 1 to <0.002 mm sieves calculated to exact size percentages. Sediment fractions were re-dried and weighed and grain size distributions were reported (**Appendix-Table: 2**) as percentages. For grain size analyses the following classification was used: coarse sand (between 1.0 to 0.5 mm in diameter), medium sand (between 0.5 to 0.25 mm in diameter), fine sand (between 0.25 to 0.125 mm in diameter), very fine sand (between 0.125 to 0.063 mm in diameter) and silty clay (less than 0.063 mm in diameter and smaller) (Wentworth et al, 1922; Krumbein et al, 1937).

Microbial Sediment Sampling From Core Sediment Samples

Before placing sediment core liners in the coring device we rinsed the liners with 100% ethanol in order to reduce contamination. After collecting the cores, we always removed the top and bottom of each core with an ethanol-sterilized saw to take away sample that had contact with drilling fluids. After that we placed the undisturbed samples in air tight Mylar bags with oxygen-absorbing packets and placed them on ice for roughly 6 hour in the field; subsequently the cores

were kept at −80˚C once returned to the lab. For our experimental work we opened each sediment core within a N_2 glove box chamber with a sterilized dermal tool, positioned the sediment in a sterile bag, and then homogenized the sediment by hand from the 14 different depth samples (eight and six depths at two sites).

Figure 4.7 Microbial sediment sample collection method in the field after recovery of a core; a) separating the split spoon sampler from drill pipe; b) & c) taking fresh sediment samples for microbial testing in a sterile BD centrifuge tube; d) sample liner before separating from split spoon sampler.

Disturbed sediment samples were collected for every 3 m, or more often if characteristics of the sediment changed in between undisturbed sampling. Washed sediments were collected in a bucket and allowed to settle before being transferred on a white plastic sheet. Later, the sediment samples were allowed to drain (but not dry), before putting them into plastic bags. Oxidation of sediments did not change the colour of the sediments. Each of the sediment samples was described on the basis of texture and colour by the local driller in field and later visual inspection

of the sediments was carried out and compared with the Munsell standard soil colour chart for colour classification. At the time of sieving, we did not observe plant roots or invertebrates such as worms.

Sample Transport

All samples (water and sediment) were shipped via DHL to Kansas State University (KSU), Manhattan, Kansas, USA, immediately after returning from the field. Upon receipt of the sample shipments, samples were stored in refrigerators (core samples in freezer) in KSU-Geology Department until further analyses were performed in the lab.

Analyses

Field Analyses

METTLER TOLEDO SevenGo^{TM} for water parameters

In the field in January 2013, temperature (°C), total dissolved solids (TDS) (mg/l), conductivity (µS/cm), salinity (ppt) and resistivity (Ω cm) were measured using METTLER TOLEDO SG3-FK2-SevenGoTM (Mettler Toledo SevenGo^{TM} Conductivity Meter SG3 with MT InLab® 731 Conductivity Sensor (cat. no. 51344120). pH was measured using OAKTON® (Model WD-35801-00 pH 5 Acorn series). The water quality measurements were done for only 10 nests out of 19 nests all over South and North Matlab piezometers (n=53). While collecting the water parameters, the tube wells were pumped for 10-15 minutes into a bucket. Then after this pumping the bucket was emptied and the pumping was continued. During this time all the above mentioned parameters were measured. During the measurement the pumping was continued until the instruments were stabilized in their numbers or values.

Field test kits for water chemistry

A total of ninefield test kits were used to measure *in situ* water chemistry at the place of collection. In the field water chemistry was measured for all water samples (n=53). While collecting the sample a small field laboratory was set up near the tubewell to measure arsenic (As), manganese (Mn), nitrate (NO_3^-), sulfate (SO_4^{2-}), phosphate (PO_4^{3-}) and alkalinity. Arsenic concentration was measured using two different HACH test kits. One was for aarsenic in low concentration range (0-500 µg/L As) test kit (HACH, Cat. No: 2800000). It's operation

procedure as follows. Fill 50ml water to be tested in to the reaction bottle (Cat no.28002-00) after that add one reagent#1 powder pillow (Cat no. 27978-99) to the bottle containing 50 ml water sample. Swirl to mix until the power dissolve. Then add reagent #2 powder pillow (Cat no: 27977-99) to the bottle containing sample and swirl to mix. At this point solution could be cloudy. After adding reagent #2 wait for 3 minutes. After waiting time is over add reagent #3 powder pillow (Cat. No. 27979-99) to the same bottle and swirl to mix until the reagent power dissolve. Wait for 2 minutes and swirl again. After this procedure add a scoop,~2gm (plastic scoop, Cat no: 27998-00) of reagent #4 (Cat. no: 454-29) to the sample and swirl to mix until the reagent is dissolved. In the mean time insert a test strip (Cat. No. 28001-00) to the bottle cap pad so that it covers the small opening and then close the flap and press to secure. Then add reagent#5 (Cat. no: 27981-99) powder pillow to the same bottle containing sample. Immediately after this attach the cap containing test strip to the reaction bottle and swirl to mix. While swirling makes sure that the bottle is not shaken or invert or never allow the sample to get in to the test strip. Then bottle is kept for 30-35 minutes for reaction time. Within this 30-35 minutes of reaction time swirl 2 times. Once the reaction time is over then remove the test strip and immediately compare the developed color to the chart on the test strip bottle. Compare the color code in shade and read the concentration of As in µg/l. After the test is complete the wash thoroughly the reaction bottle and the cap with water then wash 3 times with distilled water. Then wipe bottle and the cap with chemwipes and preserve the test strip inside a plastic bag.

The second test was for arsenic in higher concentration, EZ arsenic high range (0-500 µg/L & 0-4000 µg/L As) test kit (HACH, Cat No:2822800). It was used as follows. Insert a test strip to the cap of the reaction bottle(cat no. 4934800) in such a way that the test strip completely covers the small opening. Then close the flap of the cap and secure. Fill the reaction bottle (cat no. 2800200) to the 50ml line. Then add reagent #1 (Cat no.28229-99) and reagent #2 (Cat. no.28230-99) to the sample in the reaction bottle. Immediately after this step attach the cap containing the test strip to the reaction bottle. Swirl gently for 60 seconds. Then keep the bottle for 20minuits for the reaction to take place and swirl twice in between the reaction time. Once the reaction time is over then remove the test strip and immediately compare the developed color to the chart on the test strip bottle and compare the color code in shade and read the concentration of As in µg/l. After the test is complete the wash thoroughly the reaction bottle and

the cap with water then wash 3 times with distilled water. Then wipe bottle and the cap with chemwipes and preserve the test strip inside a plastic bag.

(0-4000µg/l As test): Insert a test strip to the cap of the reaction bottle (Cat no. 4934800) in such a way that the test strip completely covers the small opening. Then close the flap of the cap and secure. Fill the reaction bottle (Cat no. 2800200) with 9.6ml of water to be analyzed. Then add reagent #1 (Cat no. 28229-99) and reagent #2 (Cat. no. 28230-99) to the sample inside the reaction bottle. Immediately after this step attach the cap containing the test strip to the reaction bottle. Swirl gently for 60 seconds. Then keep the bottle for 20minuits for the reaction to take place and swirl twice in between the reaction time. Once the reaction time is over then remove the test strip and immediately compare the developed color to the chart on the test strip bottle and compare the color code (0-4000µg/l color code) in shade and read the concentration of As in µg/l. After the test is complete the wash thoroughly the reaction bottle and the cap with water then wash 3 times with distilled water. Then wipe bottle and the cap with chemwipes and preserve the test strip inside a plastic bag.

2. HACH® Manganese Test kit (Model MN-5, Cat. No: 1467-00): Mn test kit was used to find out Mn concentration in field. First fill the water sample to be analyzed in to the sample mixing bottle (Cat. no:493-06) add the contents of the buffer powder pillow for Manganese, periodate method (Cat. no. 983-99) to the mixing bottle containing sample. Then add contents of sodium periodate power pillow for manganese (Cat.no. 984-99) to the mixing bottle. Swirl to mix and then keep the sample undisturbed for two minutes for the color development. If manganese is present then a pink color will develop. During this time fix the color comparator (Cat. no. 1732-00) by inserting lengthwise viewing adapter (Cat. no. 24122-00) inside the color comparator. Place the colors disc for manganese (Cat. no. 1739-00) in the proper slot inside the comparator and then close the color comparator. After two minutes of waiting period transfer 15ml of this sample to the color viewing tube (Cat. no. 1730-00). Place this color viewing tube containing the prepared sample to the comparator opening labeled “prepared sample" or in to top right opening. Then fill another color viewing tube (Cat. no. 1730-00) with same unprepared sample and insert it to the left opening labeled "clear sample". Hold the comparator with the tube tops pointing to a light source and then view and compare both samples through two small opening in the comparator. During this process make sure that sample will not spill. Rotate the color disc for manganese until there is a color match between the two samples. Once the match is done read the

concentration of manganese (mg/l) through the scale window. Once the experiment is done wash the tubes and bottles properly with water. Then wash again properly with distilled water. Then rinse the bottles and tubes with distilled water at least 3 times and then wipe with chemwipes. Store the prepared sample in the waste collection bottle.

3. Nitrate CHEMetrics® test kit (Cat.No. K-6909D): CHEMetrics nitrate test kit was used to find the nitrate concentration of groundwater samples in the field and the details of the test kit procedure is represented in the **Appendix-A**

4. HACH® Sulfate Test kit (Model SF-1, Cat.No: 2251-00): Sulfate concentration of ground waters were measured using HACH sulfate test kit and the details of test kit procedure is represented in the **Appendix-A**

5. HACH® Orthophosphate Test kit (Model PO-19, Cat.No: 2251-00): There are 3 different types of tests for Phosphate (PO_4^{3-}) they are a). Low range phosphate concentration (0-1mg/L) test procedure. b . Mid range phosphate concentration (0-5 mg/L) test procedure c). High range phosphate concentration (0-50 mg/l) test procedure. Spectrophotometer test for phosphate concentration was conducted to determine the concentration of phosphate. Then based on concentration of phosphate measured from spectrophotometer, the test kit procedure was decided (low, mid or high range) to reconfirm the concentration. The details of test kit procedure for low range mid range and high range phosphate concentration is represented in the **Appendix-A.**

6. HACH® Alkalinity test kit (Model AL-DT; Cat. No. 20637-00) Phenolphthalein and Total Alkalinity Method 8203 was used to measure alkalinity of the groundwater samples in this area. The detailed procedure to use the test kit is represented in **Appendixp-A**.

Figure 4.8 Testing for different field parameters using test kits after setting up a small working lab in the field site

Some of the parameters were measured using field kits were rechecked and confirmed by analyzing the same sample using the spectrophotometers. Parameters re-measured were iron (Fe_T), ferrous ion (Fe^{2+}) and ammonia (NH_3-N).

1. HACH® Iron total FerroVer method for powder pillow(method:10249): The analyses was indicated by filling 10mL of sample to be analyzed to the HACH DR 2800 spectrophotometer cell. The 2 drops of EDTA solution (Cat. no. 2241926) was added to the cell containing sample and swirled to mix. Then sample was inserted to the cell holder of the DR 2800 spectrophotometer and zero the instrument and read the display and it will show 0mg/l. After that the cell containing the sample was removed from the cell holder and contents of one FerroVer iron reagent powder pillow (Cat. no. 2105769) was added to the sample cell. Then the instrument timer was set for 3 minute reaction time. If iron is present then an orange color will appear. When the timer expires the sample was inserted to the cell holder of DR 2800 and read the concentration of iron total in mg/l.

2. Fe^{2+} concentration of Matlab waters samples were analyzed using spectrophotometer (HACH®, DR 2800). The test started by making a blank by filling the sample cuvette (cell) with fresh water sample to be analyzed. Then the sample was prepared by snapping the tip of the AccuVac® ampoule (Cat. no.2514025) inside a beaker containing the sample to be analyzed. The ampoule was kept inside the beaker until it filled up completely with sample. Then ampoule was capped and mixed the contents well. The instrument timer was set for 3 minutes reaction period. The blank was inserted inside the cell holder of DR 2800 closed the shutter. Before inserting the

blank make sure that the cells are wiped to dry. Zero the instrument then display will show 0.00mg/l Fe^{2+} . Then ampoule was inserted into the cell holder after wiping it to dry and close the shutter. Read the result for Fe^{2+} mg/l .

3. HACH®Salicylate Method for measuring Ammonia (NH_3-N) (method: 8155): 10ml of sample to be tested was filled to a spectrophotometer cell and contents of one Ammonia salicylate powder pillow (Cat. no. 2653299) was added to it. Prepare a blank by filling other cell with 10mL deionized water and then contents of one Ammonia salicylate powder pillow were added to it. Both cells were capped and shock to dissolve the contents. The instrument timer was set for 15 minutes reaction period. Green color will develop if ammonia-nitrogen is present. Once the timer was expired, wipe the cell containing blank and inserted to the cell holder. Zero the instrument and read the concentration of the blank from displayer and it will show 0mg/l . Then wipe the cell with processed sample and inserted it in to the sample holder. Read the concentration of NH_3-N in mg/l.

Sediment characteristics

Observations of general physical characteristics of sediment samples (e.g. sediment color (wet), grain size(s) (general feel in hand, e.g. sandy, silty, clayey, etc.), depths of sediments, visible mineral content [with aid of hand lens], presence or absence of visible plant/organic matter, etc.) were made in the field at time of collection and recorded in a field notebook and sometimes on the sample bag itself. We took each samples wet and dry photograph for comparing there color in wet and dry condition.

Lab Analyses

Water Analyses

Cations in water samples

Concentrations of cations in water samples (n=33) were analyzed by HR ICP-MS (High Resolution Inductively Coupled Plasma Mass Spectrometry) at Actlabs®, Canada. Expected concentration of various elements in the samples were studied from various available literature and on the basis of this all the above defined standards we suggested to prepared. The standards were prepared in such a way that the concentration of the samples to be measured will fall almost

in the middle of the best fit line (standard curve) created for each element with a good cluster. The 6 mL of samples were taken from preacidified with 0.2% ultrapure HNO_3 and filtered 125 ml amber plastic bottles (explained during sample collection) in to 30 ml centrifuge tubes and shipped to Actlab Canada. They calibrated the instrument after analyzing every 10 samples for better accuracy and samples were analyzed for Ca, Mg, Na, K, Fe, As, Mn and many other element in µg/L. A duplicate and triplicate of the sample run after every tenth sample to recheck the accuracy of the analyses.

Anions in waters

Anions in water samples were analyzed by ion chromatograph (Dionex,ICS-1000 ion chromatography system) in the soil chemistry lab in the department of Agronomy at Kansas State University. Water from a total of 33 tube wells was analyzed. After every 10th sample a duplicate and triplicate of the sample run to check the accuracy of the analyses. Standards were prepared for Cl^-, Br^-, NO_3^-, PO_4^{3-}, SO_4^{2-}, F^- and NO_2^- and were analyzed for Matlab waters. Five standards were prepared using 0.2 µm filtered de-ionized distilled water and stock standard solutions of 1000 mg/l. The standards for each element were made for the following (in mg/l): Cl- [5, 10, 50, 100, 500]; Br- [0.5, 1, 2, 5,10]; F- [0.1, 0.2, 0.4, 0.8,1.0]; NO2- [0.1, 0.2, 0.4, 0.8, 1.0]; NO3- [1.0, 2.5, 5, 15, 25]; PO43- [0.5, 5, 10, 25, 50];SO42- [5, 10, 40, 60, 100]. Samples were prepared by filtering through 0.2 µm filters (Cat. No. 09-927-26C), and approximately 2.5 ml of sample was added to IC vials which were then loaded into the autosampler. The five standards, along with a blank, were run for calibration of the machine. Then the 50 water samples were analyzed for their respective anion concentrations.

Alkalinity (bicarbonate) was measured for the same 53 water samples by HACH® Alkalinity Test Kit (~5 weeks after collection in the field and in the field) using same method as described above in Field Analyses section.

Dissolved Organic Carbon and Total Nitrogen Measurements

A total of 53 tube wells were analyzed for dissolved organic carbon (DOC) and total nitrogen (TN) in water samples. The fresh samples were taken from 500ml amber plastic bottles. The sample preparation starts with preheating the Fisherbrand® Binder-free, borosilicate glass fiber filters have 0.7µm pore size (Cat. no. 09-804-142H) to 400°C for 4 hrs in a muffle furnace. After 4 hrs switch off the furnace and allow cooling for some time (45 minutes) to avoid

breakage of the fibers. Then the fibers were taken out of the furnace and allowed to cool inside a glass desiccator for a day. Then glass fiber filters were fixed inside the Fisherbrand® filter holder (Cat. no. 09-753-2). Then with the help of a Thermo scientific® syringe 20 mL (cat. no. 03-377-24) 60 mL of water sample to be analyzed was taken and pushed through the syringe opening in filter holder containing the glass fiber filter. Then the filtered samples were collected pre washed 50 mL centrifuge tube. 50 mL sample is latter acidified to a pH < 3 with 12.1 molar HCl (assay 37.4%) hydrochloric acid Fisherbrand® (lot. no. 983618). The 50 mL acidified samples were used for DOC and TN analyses in TOC-L SHIMADZU®, Total Organic Carbon analyzer at Civil engineering Department, at Kansas State University.

A total of 53 samples were loaded to sample holder disc of TOC-L SHIMADZU, Total Organic Carbon analyzer along with distilled water in between the samples. The samples are taken in the TOC sample glass vials. Vials are preheated by packing inside aluminum foil at 450°C for 4 hrs in a muffle furnace to remove organic carbon if present in it. To cross check the result 3 repeat samples were also loaded along with the samples. While analyzing water samples in TOC-L SHIMADZU, Total Organic Carbon analyzer following configuration was maintained. Number of injections per sample was 5. Out of 5 results the best 4 were used and averaged to calculate the final result. 50µL samples are used per injections. After each samples 2 wash steps were carried to flush out the system. The standard deviation maximum method set up was 1. Spurge gas flow was 80 mL and spurge time set up was 1.30 minutes.

Stable Isotopes of water samples

Stable isotope values of δ^2H and $\delta^{18}O$ for samples from 50 tube wells were measured using Cavity Ringdown spectrometer (Picarro® G1301) at the Stable Isotope Mass Spectrometry Lab in the Department of Biology at Kansas State University. The precision of the Picarro® G1301 was ~50 ppm. The samples for oxygen isotopes were collected in 250ml Boston round narrow mouth clear glass bottles. Before collecting the waters samples these bottles were washed with the same water with 3 times and the rinsed 2 times. Then water samples were collected to the top leaving no space for air in the bottle. Then capped the bottle and sealed with back tape. In the lab 5 mL of samples were filtered through 0.45µm filter (Whatman® cat. no.6784-2504) to Piccaro® vials. From these vials approximately 2 µg of sample was injected into the Picarro water analyzer for determination of δ^2H and $\delta^{18}O$. Inside the instrument the

injected water sample was converted to vapor and carried by a N_2 carrier stream to the analyzer where the relative abundance of heavy and light isotopes was measured. There was a slight memory effect between samples as water molecules from one injection adhere on the surface of the analyzers internal plumbing unit. In order to avoid such memory effect per sample a total of 6 injections were made and out of that 6 injections, the first 3 were removed from the analyses and the last three were averaged (as recommended in the Picarro® instrument user's manual). The average value represents a 'raw' data point that is then corrected to three secondary standards (Evian bottled water [$\delta D = -78.07‰$ and $\delta^{18}O = -10.01‰$], KSU de-ionized water [$\delta D = -40.72‰$ and $\delta^{18}O = -5.30‰$], and KSU de-ionized enriched water [$\delta D = -8.36‰$ and $\delta^{18}O = 4.03‰$]) that are analyzed along with each batch of samples. The standards have been calibrated to National Institute of Standards and Technology (NIST) accepted standards (Greenland Ice Sheet Precipitation (GISP: $\delta D = -189.5‰$ and $\delta^{18}O = -24.78‰$), Standard Light Arctic Precipitation (SLAP: $\delta D = -428.0‰$ and $\delta^{18}O = -55.5‰$), and Vienna Standard Mean Ocean Water (VSMOW: $\delta D = 0‰$ and $\delta^{18}O = 0‰$)) (Coplen, 1994). The $\delta^{2}H$ and $\delta^{18}O$ values of the standards span the entire range of expected isotope values for the samples submitted. In order for correction of drift in the analyzer during a batch of samples, a working standard of known isotope ratios was analyzed every four samples. Finally, the raw isotope data was corrected to the three standards analyzed with the measured water samples.

Sediment Analyses

Sediment characteristics

A small representative subsample was taken from each core and each depth from North and South Matlab and allowed to air dry on paper plates in the lab in N_2 glove box. After drying, similar observations of general physical characteristics of sediment samples (e.g. sediment color (dry) and grain size(s) [for creation of a litholog with sediment colors and grain size(s)], visible plant/organic matter, mineral content, etc.) made in the field were done in the lab.

Grain Size Analyses

We used undisturbed sediment samples collected at South Matlab and North Matlab from depths between10 and 112 m to investigate grain size. We used a modification of the USGS East Coast Sediment Analyses Procedures protocol for these analyses (Poppe et al., 2000, Legg et al.,

2012). Sediments were freeze-dried for 48–72 h and then oven-dried at 60˚C for 48h. In order to disaggregate the sediment (for finer sediment samples), we suspended samples in distilled water for 24h. Then we passed each wet subsamples serially through 1 to <0.002 mm sieves. Sediment fractions we re-dried and weighed and grain size distributions were reported (**Appdix-Table: 2**) as percentage coarse sand (between 1.0 to 0.5 mm in diameter), medium sand (between 0.5 to 0.25 mm in diameter), fine sand (between 0.25 to 0.125 mm in diameter, very fine sand (between 0.125 to 0.063 mm in diameter) and silty clay (less than 0.063 mm in diameter and smaller) (Wentworth et al, 1922; Krumbein et al, 1937).

Thin Section Petrography of Sediments

Fourteen different depth sediment samples collected from two cores at the field were placed in 20 ml HDPE scintillation vials (Wheaton; Cat. No. 0334172) and shipped to Spectrum Petrographics in Vancouver, Washington (http://www.petrography.com/), to have thin sections (9.14 cm x 5.33 cm) made from the loose sediments. Epoxy was injected into the loose sediments, and once solidified; the hardened mass was glued to the glass thin section. The mass was then cut relatively thin and ground to a thickness of 30 μm and polished.

Once samples were returned from Spectrum Petrographics, each thin section was carefully analyzed with a polarizing light petrographic microscope (Leica DM EP Microscope) with objectives of 4x, 10x, and 40x (all 3 Leica Hi Plan), and oculars with 10x magnification (Model No. 13581008) at Geology Department, Kansas State University. During analyses of each slide, apparent textures/color variations were noted, major minerals and accessory minerals and their relative abundance within the sample were identified, along with any other noticeable/unique features, especially the textures. Mineralogy was determined by both plane-polarized light and cross-polarized light. Some key features used to identify minerals were relief, color, pleochroism, interference colors, birefringence, extinction angles, presence/absence of cleavage, and mineral shape/habit. Photomicrographs were taken with a camera (SPOT Insight QE, Model # 4.2) attached to Nikon Eclipse E-600 POL polarizing light microscope. SPOT Advanced Software was used for digital photo capture.

Scanning Electron Microscopy with Energy Dispersive X-Rays of sediments

Sediment samples from South Matlab core (depth of samples are 10m, 28m, 45m, 64m, 80m, 95, 100m, and 110m) were run for SEM (Hitachi S-3500N). Each sample was mounted on a separate

aluminum SEM stub with a carbon coating. The sample was then coated with a conductive material (0.1% Au-Pd) to prevent accumulation of surface charging, which can occur when electron beams from the SEM are bombarding the sample and are not allowed to escape from the surface via a conductive path. If there is no such path, the image formed by the SEM will be very poor. Each sample was carefully scanned, aiming to delineate specific conspicuous'grains (any grain with an appearance different than the majority of surrounding grains) for analyses. When a grain of interest was observed, x-ray microanalyses (EDS) were done at several points on the grain. This technique generated a spectrum in which the peaks corresponded to specific x-ray lines and the elements could be identified. The peaks were obtained as a result of the three basic components of the EDS at work. An x-ray detector detects and converts x-rays into electronic signals. Then a pulse processor measures the electronic signals to determine the energy of each x-ray detected. Finally, an analyzer interprets and displays the x-ray data. Several main elements of interest were As, Ca, P, Mg, K, Fe, Mn, Cr, Cu, and S. X-ray spectra were used as a 1st-order interpretation of the mineral being analyzed.

Total digestion of Sediment Samples

Total digestion was done for both 2 core sediments samples. We took 14 sediment samples; 3 duplicates, 3 triplicates and 1 standard reference material (Montana II-www.nist.gov/srm) were digested by reflux tube (following the procedure described in Zarcinas et al., 1996) and analyzed over ICP-OES at the Department of Agronomy at Kansas State University. The methods and the detailed procedures are described in **Appendix-B.**

Sequential extraction of Core Sediments

A 6-step method of He et al., 2010 was the most relevant method of sequrntial extraction and therefore was used for this study to find out the concentrations of As, Mn and Fe at various soil fractions. Aquifer samples from each location were selected for the study. A total of 14 samples, 3 duplicates, 2 triplicate and one standard reference material (Montana II 2711, www.nist.gov/srm ; national institute of standards and technology US department of commerce NIST) were used for the experiment. Sample preparation started by measuring of ~1 g subsamples of the wet samples being placed in previously weighed (to 0.001 g precision) plastic 50 mL centrifuge tubes in a N_2 glove box for a few days for drying. We used 6 steps which are accordingly: step-1 non-specifically sorbed As, Mn and Fe, step-2 specifically sorbed as, Mn and

Fe, Step-3 concentration of as, Mn and Fe present in amorphous and poorly crystalline hydrous oxides of Fe and Al, step-4 well crystalline hydrous oxides of Fe and Al.(e.g. goethite, hematite), step-5: organic matter phase and step-6 Residual phases excluding silicates. The methods and the deatiled procedures are described in **Appendix-B.**

Synchrotron studies of Aquifer Sediments (XANES and EXAFS)

We conducted our synchrotron studies at Brookhaven National Laboratory's National synchrotron light source lab (NSLS). X-ray absorption near edge structures (XANES) and X-ray absorption fine structures (EXAFS) were conducted by X-ray absorption spectroscopy (XAS). XAS studies were conducted for South and North Matlab aquifer sediment samples to speciate As ($As^{3+}$and As^{5+}), Fe (Fe^{2+} and Fe^{3+}) and sulfur (SO_4^{2-} and S^{2-}). XANES was used to find the various As and sulfur species (oxidation states) in sediments. EXAFS were used to find the local molecular structure of a particular element in question within the sample. Sulfur is very good redox sensitive element and by studying the various sulfur species in aquifer sediments will give insight about the redox condition of the aquifer. Three separate beam lines were used and they were X27A (energy range:4.5-32 keV); X 15 B (energy range:1.2-8 keV) and X11A (energy range:4.5-40 keV). X27A and X11A were used for As speciation and X15B was used for sulfur speciation. The sample prepared for X15B beam line is shown is Figure 8. The samples for the beam line were selected based on total digestion data of aquifer samples. Those samples with high As concentration were selected for study. Before the analyses, all the samples were dried inside a nitrogen glove bag in a nitrogen environment to avoid oxidation. Later these samples were transferred to 50 mL centrifuge tubes and flushed with nitrogen to keep the sample environment inert. For all 14 samples, As, S and Fe spectra were collected X11A, X15B and X11B, respectively. (Detail in **Appendix- 3**)

Microbial community analysis

DNA was extracted from undisturbed sediment samples using the Mo Bio PowerSoil™ DNA isolation kit following the manufacturer's directed protocol (Mo Bio Laboratories, Inc., Carlsbad, CA, USA). For extracting DNA of microbes from the sediment this detailed Protocol used. (Detail in **Appendix – C**)

DNA extracts were used to amplify 16S rRNA genes using bacterial (Primers 27F and 519R were used for Bacteria: 27F = AGRGTTTGATCMTGGCTCAG 519R =

GTNTTACNGCGGCKGCTG and 349F and 806R for Archaea: 349F = GYGCASCAGKCGMGAAW 806R = GGACTACVSGGGTATCTAAT). The Molecular Research LP (MR DNA) genomics facility performed the 454 pyrosequencing of our 16S rRNA gene amplification. For microbial community analyses did a quick phylogenetic analysis for diversity calculations, mostly I did clean up the data (i.e., denoise and trim), define operational taxonomic units (OTUs), and perform a taxonomic analysis (i.e., assign taxonomy to each OTU) using Mothur (mothur v.1.33.3) (Schloss et al., 2009) against a high quality reference alignment selected from the SILVA based bacterial 16S rRNA gene data base(DeSantis et al.,2006). The community richness of Bacteria and Archaea in the sediment was estimated using mothur (Schloss et al., 2009). 16S rRNA gene sequences were clustered into operational taxonomic units (OTUs) based on an average nucleotide similarity at fixed cutoff 0.03. Sequences with an average nucleotide similarity of 97% were binned together into a single OTU.

Chapter 5 - Results

Sediment Characterization

In our study area, there were mainly two different types of sediment color: grey to dark grey color sediments and light grey color. Other studies in this area encountered reddish brown colored sediment which wasn't encountered in any of the wells studied here. Most of the shallow aquifers from 5 to 80 m were grey to dark grey colored silt and clay sized and very fine to fine grain sand, all across Matlab. Quartz and feldspars with a substantial content of micas dominated these sediments. SASMIT annual report (2011) showed layers of red-brown sediments that are mainly the result of oxidation of the Fe-rich minerals present in them; these sediments occur predominantly in South Matlab. This reddish brown layer is common at 60 to 80m depth relatively high content of biotite and other dark-coloured ferromagnesian and opaque minerals is responsible for the dark grey and greyish color of the sediments we have studied. A black to grey unit extended from the surface down to a depth of 37 to 56 m and indicated a general fining upward cycle that presumably represents fluvial sediments of Holocene age (Goodbred et al., 2003). The boundary between the units could be identified by the change in sediment colours as well as by the presence of a 2 to 6 m clayey layer. This clay has been exposed to be drained and remains under oxidising conditions; it may serve as an impervious barrier in this system. Below the clay, a yellowish-grey to reddish brown sandy unit was encountered (by other researcher, related with some nests water chemistry) and the sediment from this unit had a relatively lower abundance of biotite and lower occurrence of Fe(III)-oxyhydroxides as coatings on quartz, feldspars and other mineral grains. These mineralogical differencegive the sediment its reddish brown colour. This lower unit was more heterogeneous in texture and colour. Visual inspection of the yellowish-grey to reddish-brown aquifer indicated that these sediments were exposed to sub-aerial weathering and oxidation when sea level in the Bengal delta plain (BDP) was significantly lowers (Umitsu, 1987, 1993; McArthur et al., 2004; van Geen et al., 2004). Unfortunately in our present study, neither core-1 in North Matlab and nor core-2 in South Matlab penetrated reddish brown sedimentary layers. In the intermediate depth aquifers, depths of 100 to 115 m, the sediment was medium to coarse grained and light grey in color. This light grey sediment contained high amounts of quartz but few accessory minerals. Based on the sediment variations described above, the stratigraphy can be logically divided into three

operationally-defined depths: shallow - < 60 m; intermediate - 60 to 115m; and deep - > 120 m. Due to the high cost of collectingsediment from the deeper layers, it was not possible to collect sediments from these depths as part of this study. Different colored sediment are shown in the below pictures.

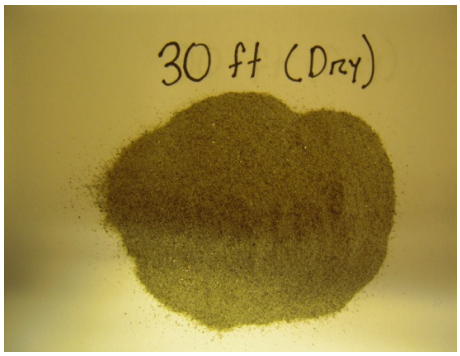

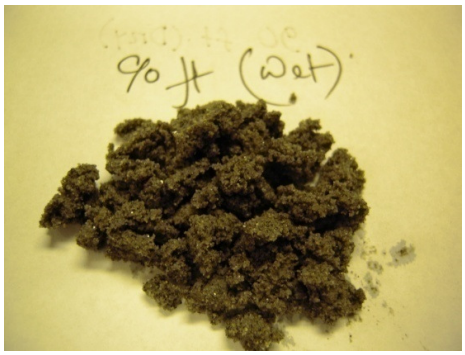

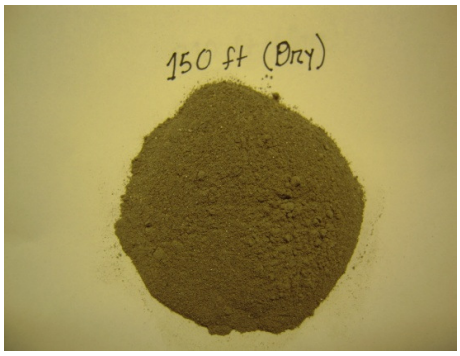

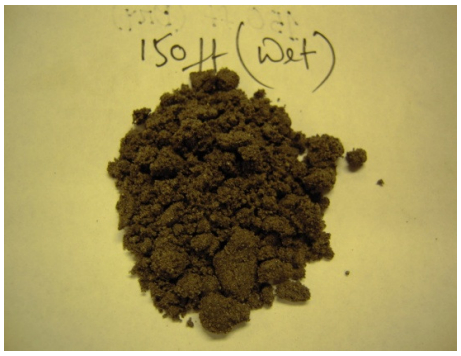

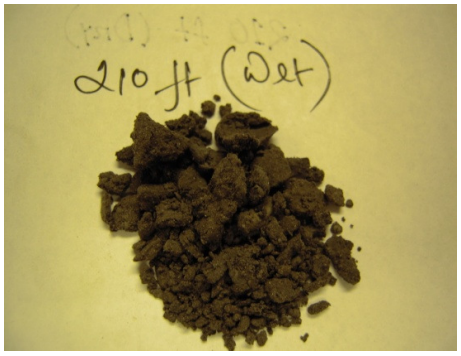

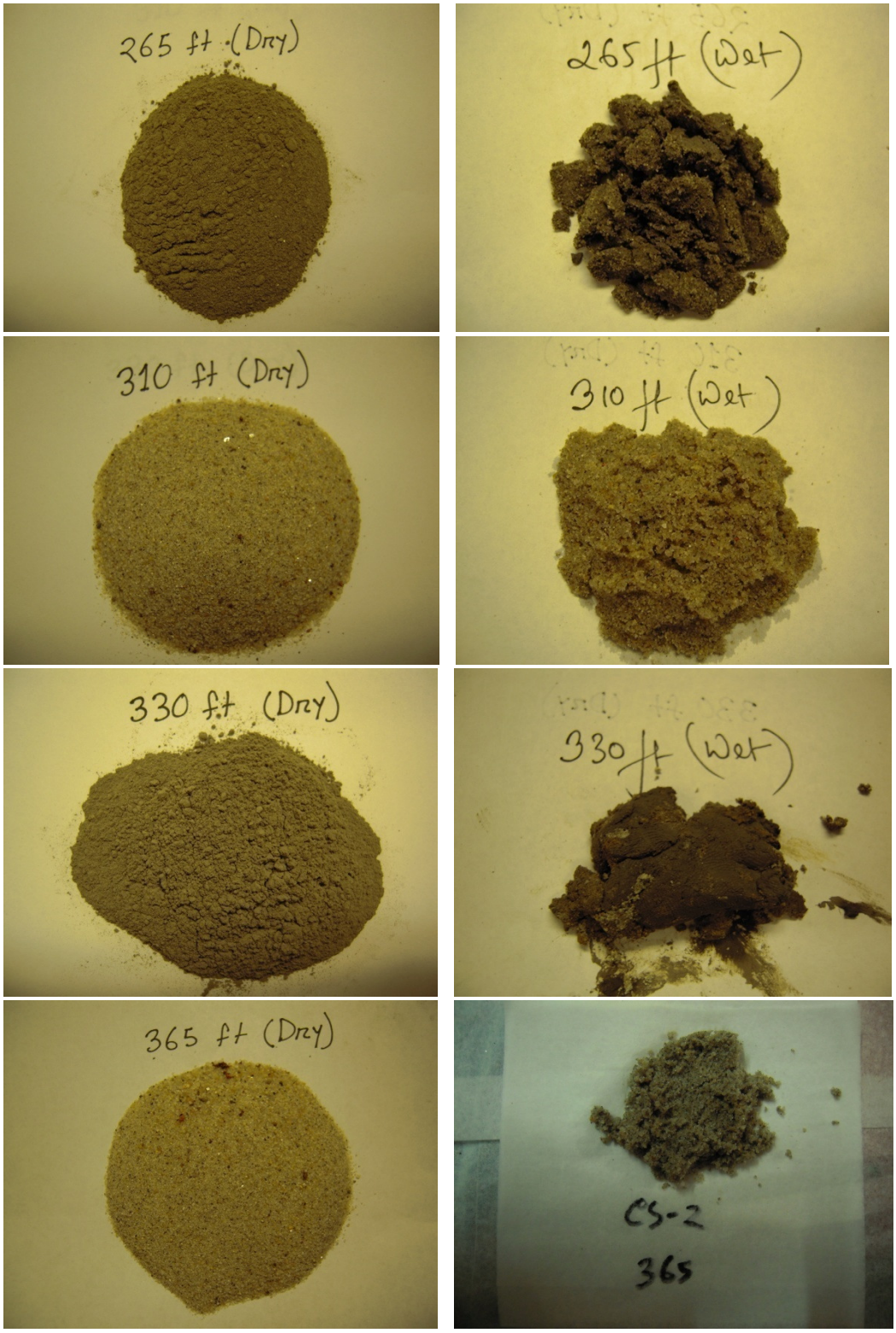

Figure 5.1 Colors of wet and dry sediments described with depth, from Core-2, South Matlab (N 23.36834 and E 90.76748)

Mineralogy and Chemistry of Sediment Cores

Petrographic Analyses

Thin section petrography made from undisturbed sediments revealed several distinctions between grey, dark grey and light grey color sediments, as well as changes in texture and mineralogy with depth. Mineralogy of sediments in both cores and for all color variations depends on composition and grain size. Shallow depth sediments are predominantly composed of quartz (40-65%) and feldspar (15-25%), followed by micas (biotite and muscovite, 10-20%) and other minerals(percentage estimate visually). The intermediate depth samples, which are light grey in color, have more quartz (80-90%) and feldspar (5-10%) along with accessory minerals(<2%). Modes were obtained via visual estimations of thin sections and then averaged for all samples from the same unit/depth. Textures and the presence and proportions of micas, may be some amphiboles and carbonates and other accessory minerals were the major minerals among the sediments.

Grey and dark grey colored sediments: The textures of sediments varied with depth, while relative proportions of angular to sub-angular quartz (40-65%) and feldspars (15-25%) remained fairly constant throughout the entire core. Abundance of mostly lath-shaped and highly weathered biotite and muscovite was more prominent in the shallower depths (10-15%) and decreased in intermediate depths (5-10%).

At shallow depths, the sediments are predominantly comprised of fine to very fine grained materials with clay agglomerates containing angular grains of quartz (~50%) and feldspar (~25%), which had a sieve-like texture. A fine-grained matrix surrounds small, fragmented quartz and feldspar grains and small weathered semi-lath-shaped micas. Some grains have Fe-oxide coatings (**Figures 5.1 C and D**). Fe-mottling was present among some of the Fe-rich clay agglomerates. Within the matrix of these agglomerates, biotite (~6-8%) and muscovite (~12-14%) were observed, along with some carbonates, amphiboles, zircon and chlorite.

Light grey sediments: Sediments from intermediate depths are generally coarse-grained, but are interspersed with some fine-grained materials. Core sediments include mostly Fe-stained/coated quartz or fresh quartz (80%) with some weathered feldspar and micas (~10-20%) and Fe-oxides, with only a few accessory minerals (abundeance <2-3%).

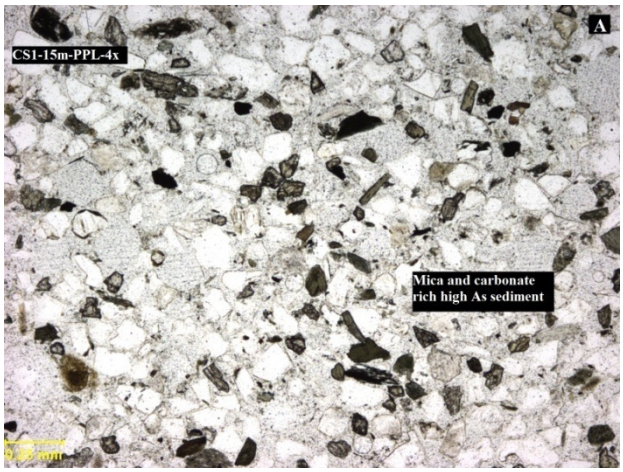

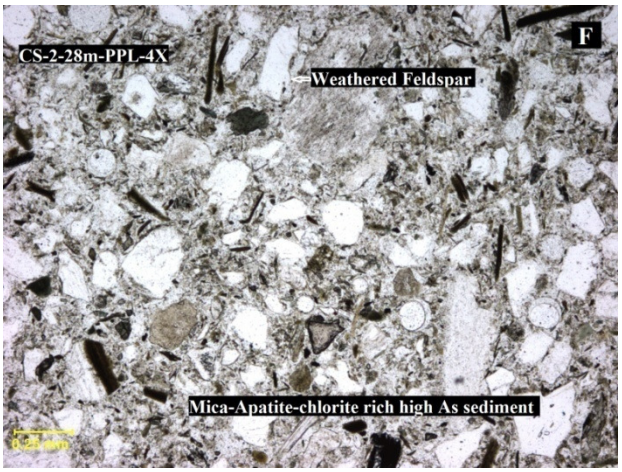

A. CS1-15m-fine sand(grey color) **F. CS2-28m-fine sand(grey color)**

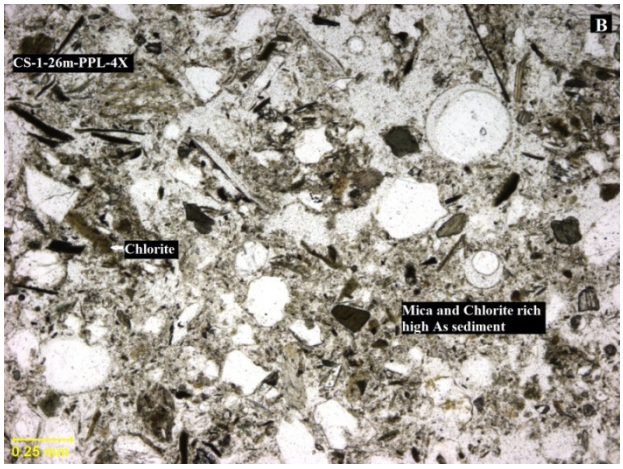

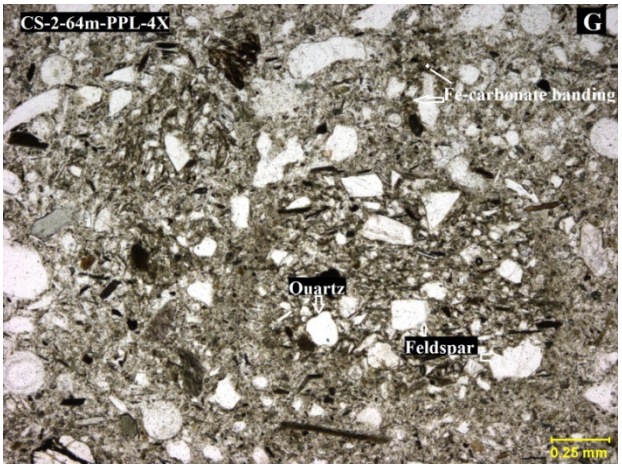

B. CS1-26m-fine sand (dark grey color) **G. CS2-64m-clay and silt(dark grey color)**

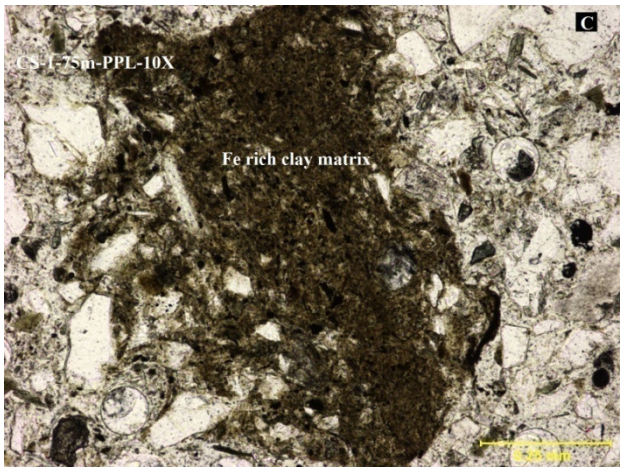

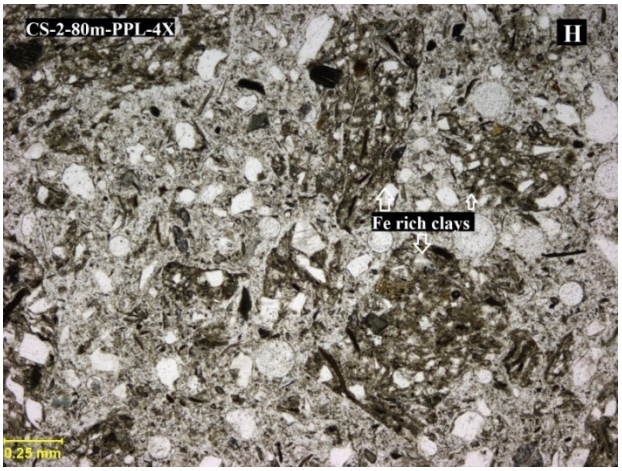

C. CS1-75m-clay and silt (dark grey color) **H. CS2-80m-clay and silt(dark grey color)**

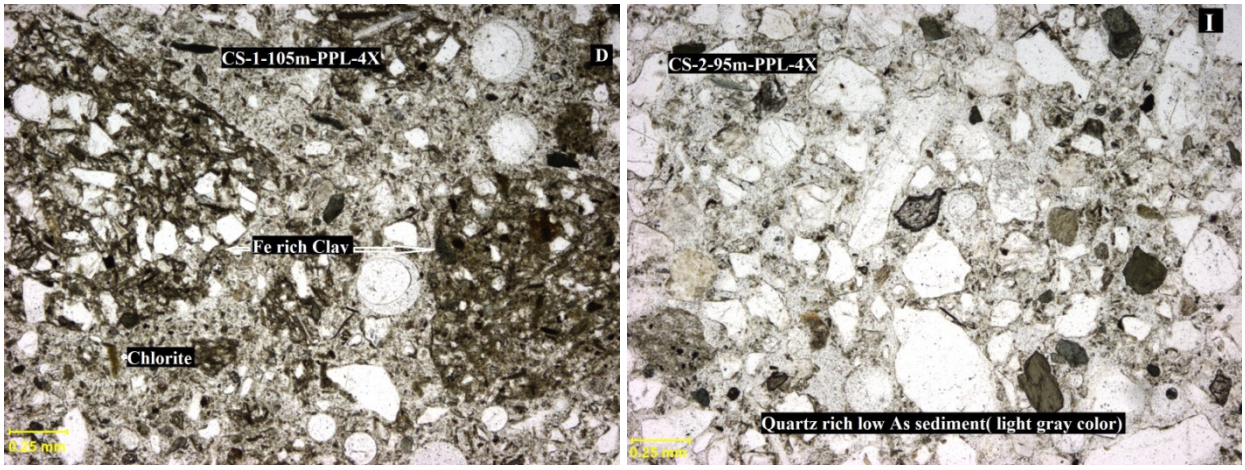

D. CS1-105m-silt and clay (dark grey) I. CS2-95m-medium to coarse sand(light grey color)

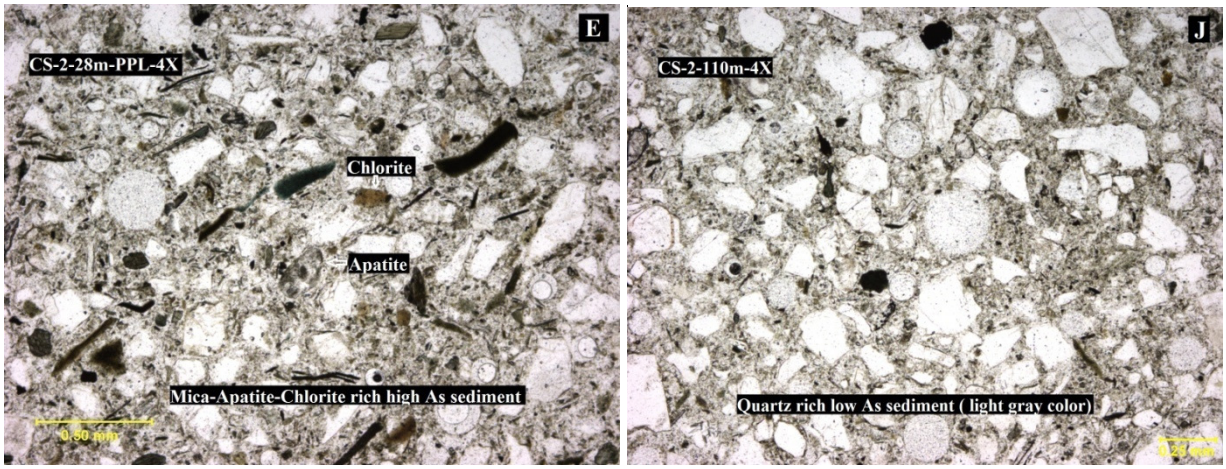

E. CS2-28m-fine sand (grey color) J.CS2-110m-medium to coarse sand (light grey color)

Figure 5.2 Photomicrographs for North (A,B,C,D) and South Matlab (E,F,G,H,I,J) cores showing dominant textures and mineralogy of sediments with their depth and color variations.

One of the more significant variations in texture/mineralogy with depth observed in this core is the abundance occurrence of Fe-oxide blobs (**Figures 5.2 I and J**). Their colors vary from light brown to black, which gives the sediments their overall brownish-orange color.

Grain Size Analyses of the Sediment Cores

Grain size analyses used the classification scheme of Wentworth et al (1922) and Krumbein et al (1937): coarse sand (between 1.0 to 0.5 mm in diameter), medium sand (between 0.5 to 0.25 mm), fine sand (between 0.25 to 0.125 mm), very fine sand (between 0.125 to 0.063 mm) and silty clay (less than 0.063 mm in diameter and small.

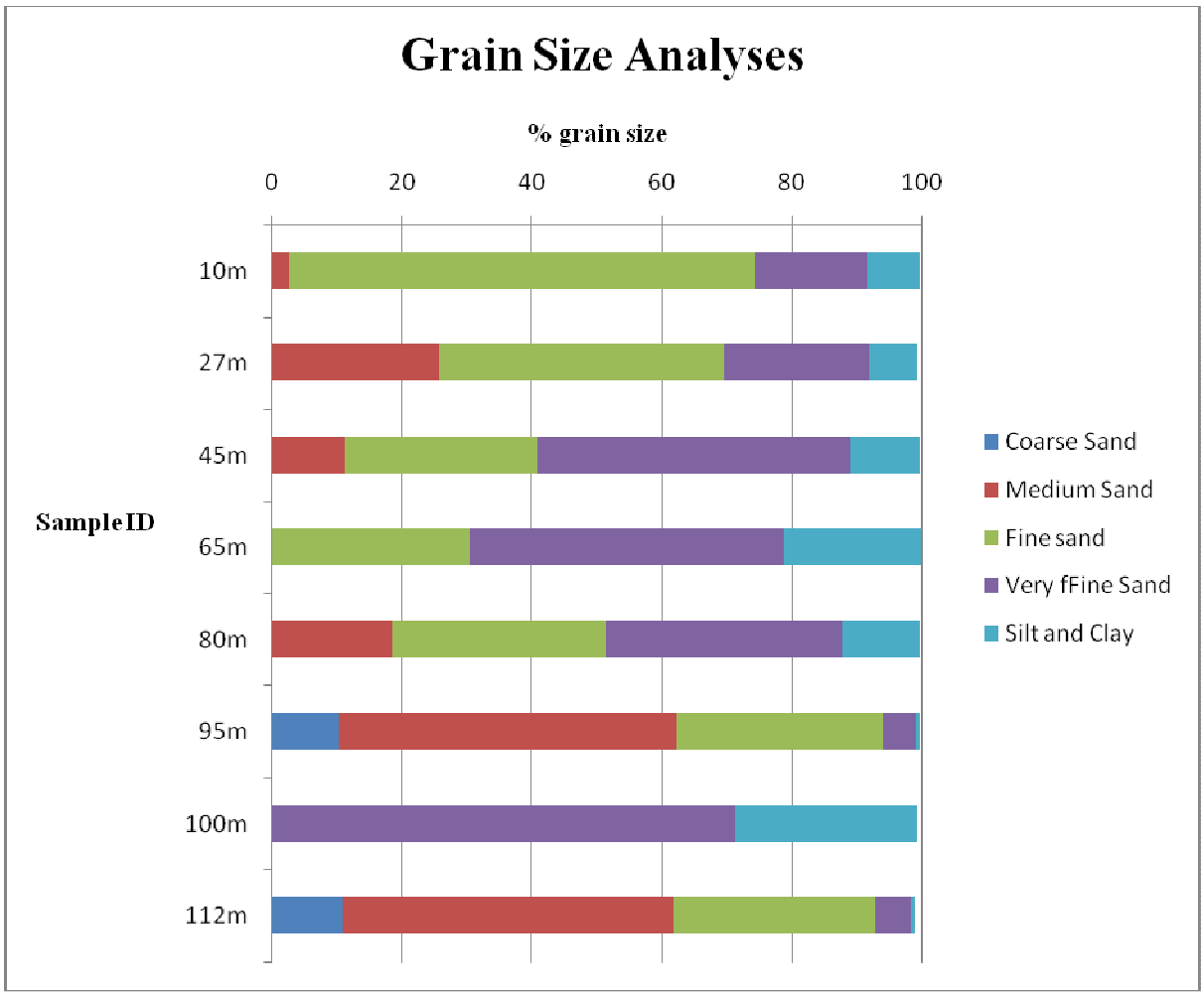

Figure 5.3 Grain size analyses of sediment core -2 (South Matlab).

Grain size analyses show the distribution of different sizes of grains throughout the core. At 10 m depth, the sediments consist of more than 90% fine to very fine sand size particles. At 27m depth, medium, fine and very fine grained sand particles occur in similar proportions. At 45m and 65m depth, fine to very fine sand, silt and clay predominate (95% and 100%, respectively). The sediments at 80m depth consist of four different size particles ranging from medium to fine, very fine and silt-clay. These sediments tend to be light grey in color, which are also the sediments that tend to produce As-free water. It is worth noting that these sediments are composed of more then 60% coarse and medium size sand grains, with the remainder of the sediment consisting of fine to very fine grained sand. Samples from a depth of 100m consist of very fine sand, silt and clay (**Figure 5.3**).

This result showed relation with grey, dark grey and light grey sediment. At 10 and 27 m the sediments are grey and consist of nearly 75% fine and very fine sand. At depths of 45, 65, 80 and 100m they are grey and consist of more than 55% silt and clay particles. The light grey sediments from 95 and 112m consist of more than 60% medium and coarse sand (**Appendix-2**). This link between color and sediment mineralogy and texture is important for understanding the behavior of As and Mn (discussed below).

Scanning Electron Microscope Study with Energy Dispersive X-ray Analysis of the Sediments

Six solid phase whole sediments from shallow to intermediate depth aquifers from South Matlab were analyzed by scanning electron microscopy coupled with an energy-dispersive X-ray analysis system in order to acquire combined textural and compositional information (EDX). . The SEM analyses enabled characterization of (a). arsenic and other elemental concentrations associated with those fractions and (b).the relationship between As ad other elements. A total 6 aquifer sediment samples were analyzed. They were all (core-2 samples from South Matlab) (core sample depth were 10m, 28m, 45, 64m, 80m and 95m). .

Kaolinite was the major clay minerals that were easily detected. In Matlab, the total Mg content in clays increases with depth from shallow to intermediate depth within the core (**Appendix-3**). Clays or fine-grained micas rich in Fe, K, and Mg are observed in the deeper aquifer sediments. Chromium (Cr) and titanium (Ti) were detected in the deepest part of the core, along with Fe, C, Al and Si. Most grains from both South and North Matlab analyzed for elemental compositions were alumino-silicates containing minor amounts of Fe and K. Matlab sediments are predominantly made up of angular quartz and feldspars. Only few percentage (0 - 0.43%)of As was detected in most of the grains analyzed by SEM. The highest percentage detected was 0.43wt% of As in kaolinite grain (possibly due the fact that kaolinite was bound together with Fe oxyhydroxides or Fe coatings). SEM photomicrographs (**Figure 5.5**) and the concentration of As content in those SEM were represented in the corresponding table beside (**Appendix-3**). For some of the analyses, spectra showing elemental proportions were also taken. The detection limit of EDS is 0.01%.

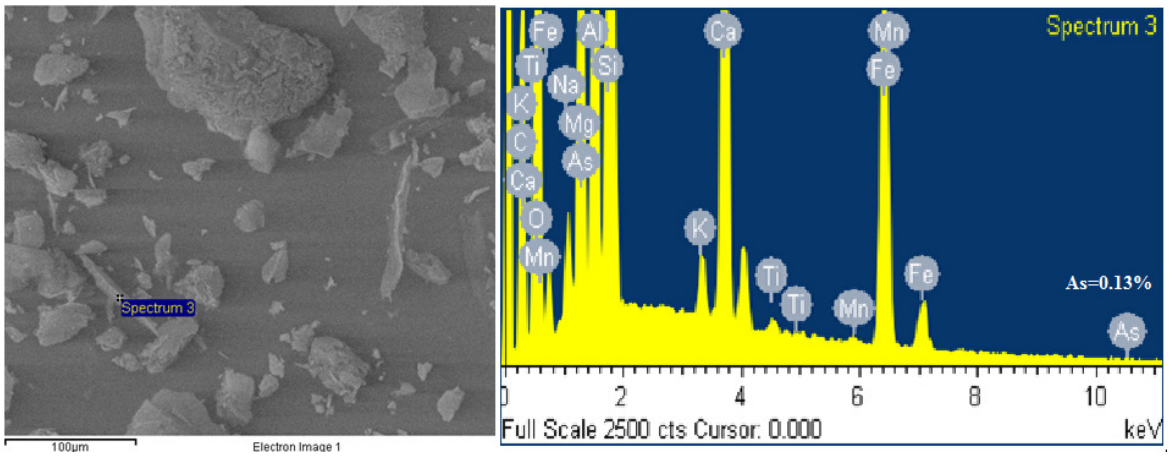

Figure 5.4 SEM micrograph with EDX of spot A as spectrac 3 for CS-2-30 (10m) grey colored fine sand sample.

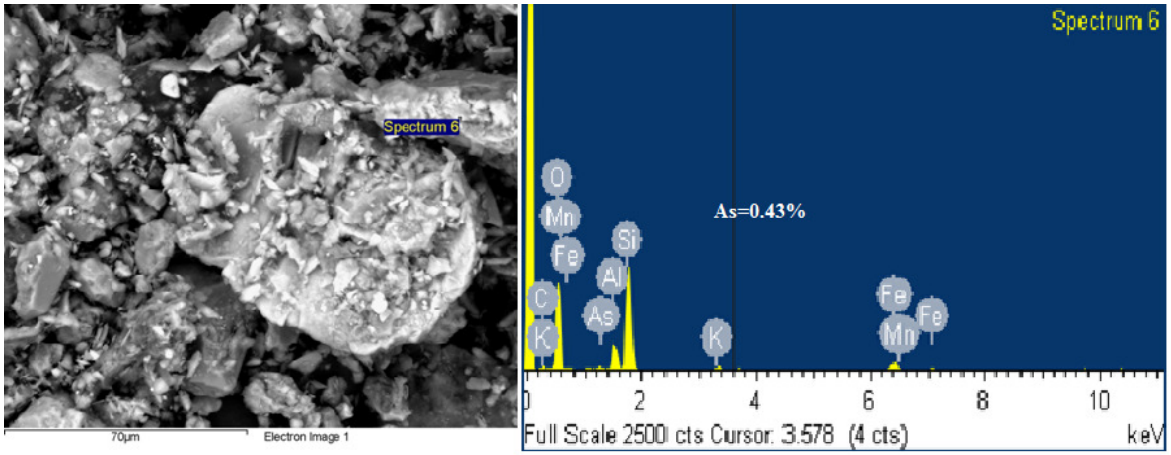

Figure 5.5 SEM micrograph with EDX of spot A as spectrac 6 for CS2-265 (64m) dark grey colored silty clay sample.

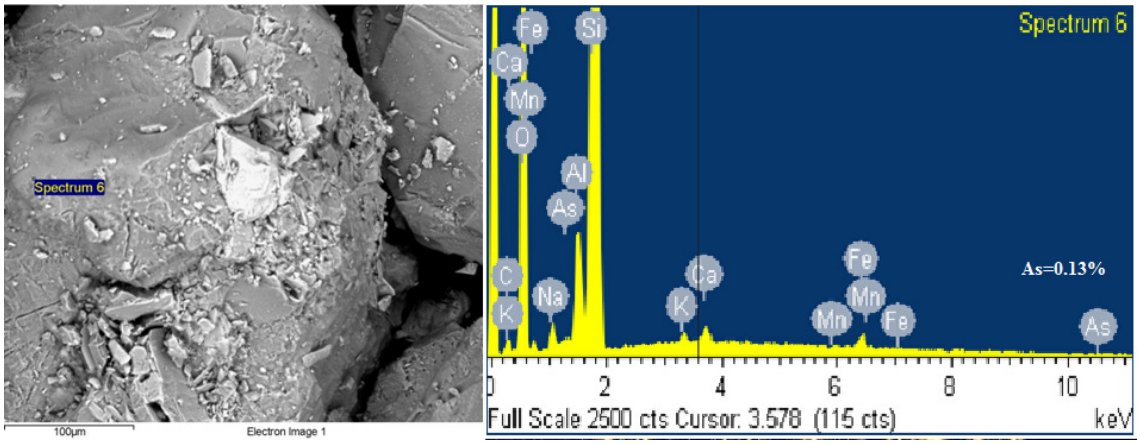

Figure 5.6 SEM micrograph with EDX of spot A as spectrac 6 for CS2-310 (95m) light grey colored medium sand sample.

Synchrotron studies of aquifer sediments (XANES data on selected samples)

Aquifer sediments from South and North Matlab were analyzed using three separate beam lines, X11A, X11B and X15B. A total of nine samples (six from North Matlab Core-1 and three from South Matlab Core-2) were analyzed using the X11A beam line: for solid-state As speciation.Standards that were run were As(III)oxide, As(V)oxide, realgar and orpiment. The accuracy of XANES data fiting procedure depends on data quality and how well the reference standards represent the component in the sample spectra. Since we used a limited number of standard spectra, the best-fit compostions may not give the true compostion. Nevertherless, the results can be used to describe approximate concentartions of As^{3+} and As^{5+} in the samples.

The nine samples included six from North Matlab depth accordingly 14m (45ft), 25m (85ft), 42m (140ft), 73m (240ft), 85m (280ft), 104m (340ft) and three from South Matlab depth accordingly 10m (30ft), 27ft (90ft) and 65m (210ft).

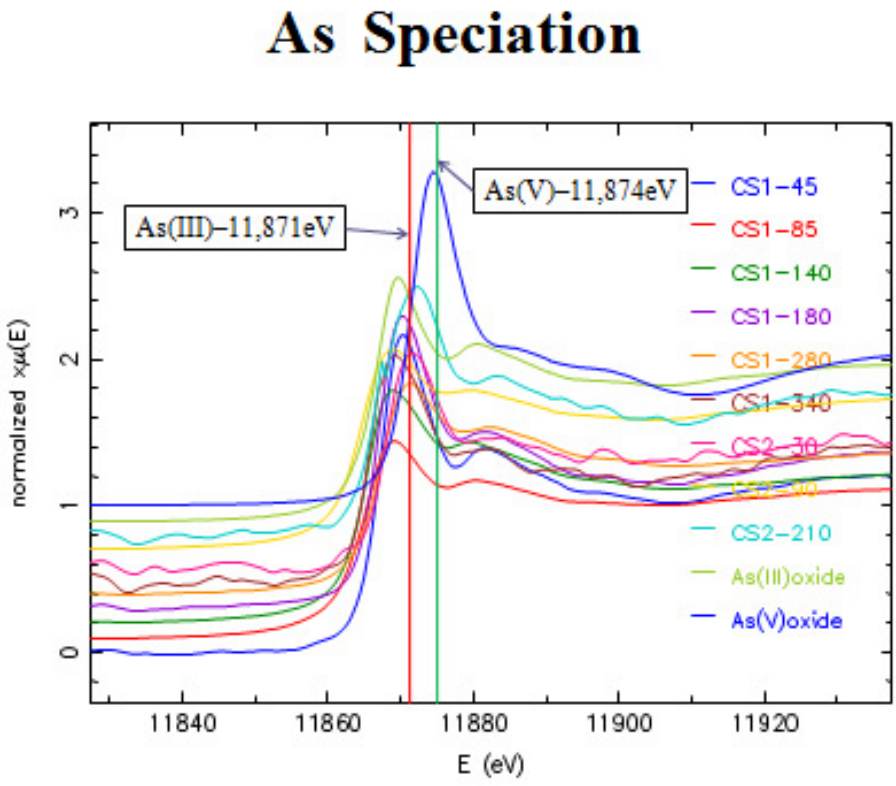

Figure 5.7 Sediment bulk XANES spectra for North Matlab (CS-1) and South Matlab (CS-2) as examined via X11A beam. The peak (white line) covers both 11871 eV for $As^{3+}$and 11874 eV for As^{5+}. X axis represents the energy level (eV) and Y axis represents the normalized peak values.

Two standards used for this wrok were As (III) oxide and As (V) oxide. The XANES peaks for the samples were compared with the standards peaks; 11871eV for As^{3+} and 11874 eV for As^{5+} (Polizzotto et al., 2006). Shallow sediments from North Matlab (CS-1-45 (14m), which was a grey colored sediment showed a sharp peak for As^{5+}. The remaining samples from both South and North Matlab showed As speciation as As^{3+}. This suggests most of the samples contain As^{3+}. We were not bale to get useable As spectra for light grey color sediments from South Matlab, which incidentally contain low As contaminated water (<10 µg/l). For the light grey samples the results showed a broad peak covering both 11871eV and 11874eV values. This might indicate coexistence of both As3+ and As5+ at these depths (**Figure 5.7**).

Sulfur speciation was done using X15B beam line. Eight samples were analyzed for this study, but only two samples gave us peaks for sulfide and sulfate. The results showed that major sulfur species present in the sediments were sulfide (S^{2-}) and sulfate (SO_4^{2-}) represented by the peak value 2472eV and 2482 eV (Prietzel et al., 2006).

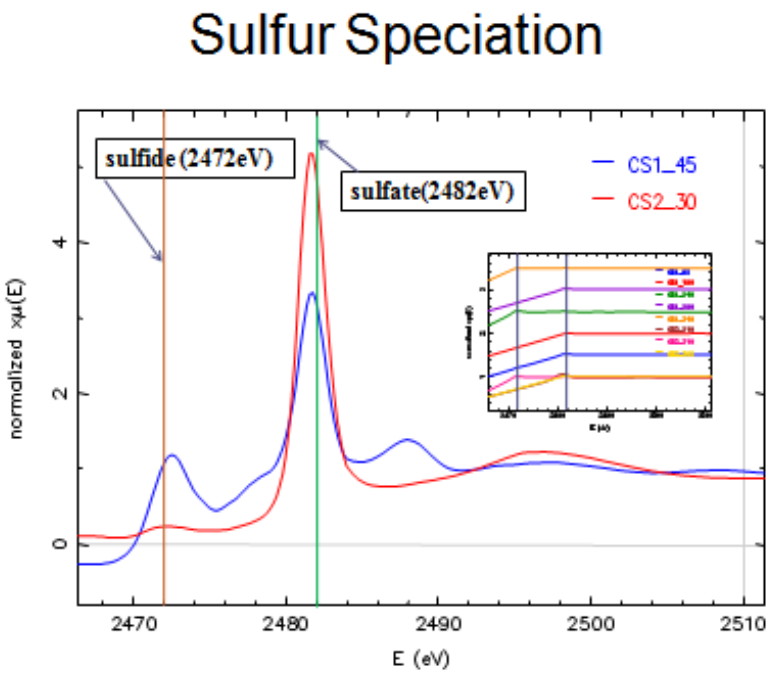

Figure 5.8 XANES spectra for South and North Matlab sediments as examined by X15B beam. The white line values are 2472 eV (S^{2-}) for sulfide and 2482 eV (SO_4^{2-}) for sulfate. X axis represents the energy level (eV) and Y axis represents the normalized peak values.

Mainly shallow depth sediment, with higher bulk As concentrations from both cores showed better As white lines. Sedimnt samples from North Matlab CS-1-45 (14m depth) showed peaks for both sulfide and sulfate. Whereas sediment samples from South Matlab CS-2-30 (10m depth) showed only white lines for sulfate. None of the other samples produced definitive peaks for interpreting the sulfur speciation (**Figure 5.8**).

Samples were run for Fe and Mn speciation at X11B beamline. Due to some technical problems, samples did not good enough spectra for interpretation.

Total Extractable As, Mn & Fe from sediment cores (Aqua Regia Digestion)

Total digestion of sediments by aqua regia (Zarcinas et al. 1996, Reza et al., 2010) from North Matlab and South Matlab cores are presented as different plots for As, Mn and Fe. Arsenic in Matlab sediments showed variations with depth. Arsenic concentrations of shallow depth sediments were ~31mg/kg, but decreased to 13 mg/kg in the intermediate depth sediments at North Matlab Core-1. In South Matlab (Core-2) As concentration in shallow depth was 30 mg/kg and it decresased to 13 mg/kg at intermediate sediments. (**Data appendix-4**)

In North Matlab (Core-1) the maximum As concentration is observed in grey colored very fine sand to clay-silt size sediments at shallow depth and the concentrations were 31 mg/kg at 14m depth. At all other depths (26m, 43m, 73m, 85m and 104m) As concentrations in the sediments were within 13 to 16 mg/kg. Al of the sediments in this core are grey colored (**Figure 5.9 A**).

In South Matlab (core-2) the maximum As concentration, 30 mg/kgm was observed at 9m depth where the sediments are gray colored very fine sand and clay. Below that depth, As concentration decreases in concentration and color changes from grey to light grey 8-12mg/kg. It was second highest in the 64m depth where As concentration in sediment was 27mg/kg which was a dark grey color sdiment. In all other grey sediments As concentration was within 15 to 22 mg/kg. In the light grey colored and medium sand sediment As concentration were 13mg/kg and 12 mg/kg at 95m and 111m depth respectively (**Figure 5.9A**).

The Mn and Fe(t) concentration in North Matlab (core-1) also changes with depth and lithologies. The concentration ranges for FeT and Mn in grey colored very fine to clay and silt sediment (85-104 m, intermediate depth) are 20792-21546 mg/kg and 611-830 mg/kg

respectively. In the other shallower depth Fe(t) was within 11650 to 18219mg/kg and Mn was within 513 to 123mg/kg) (**Figures 5.9B and 5.9C**).

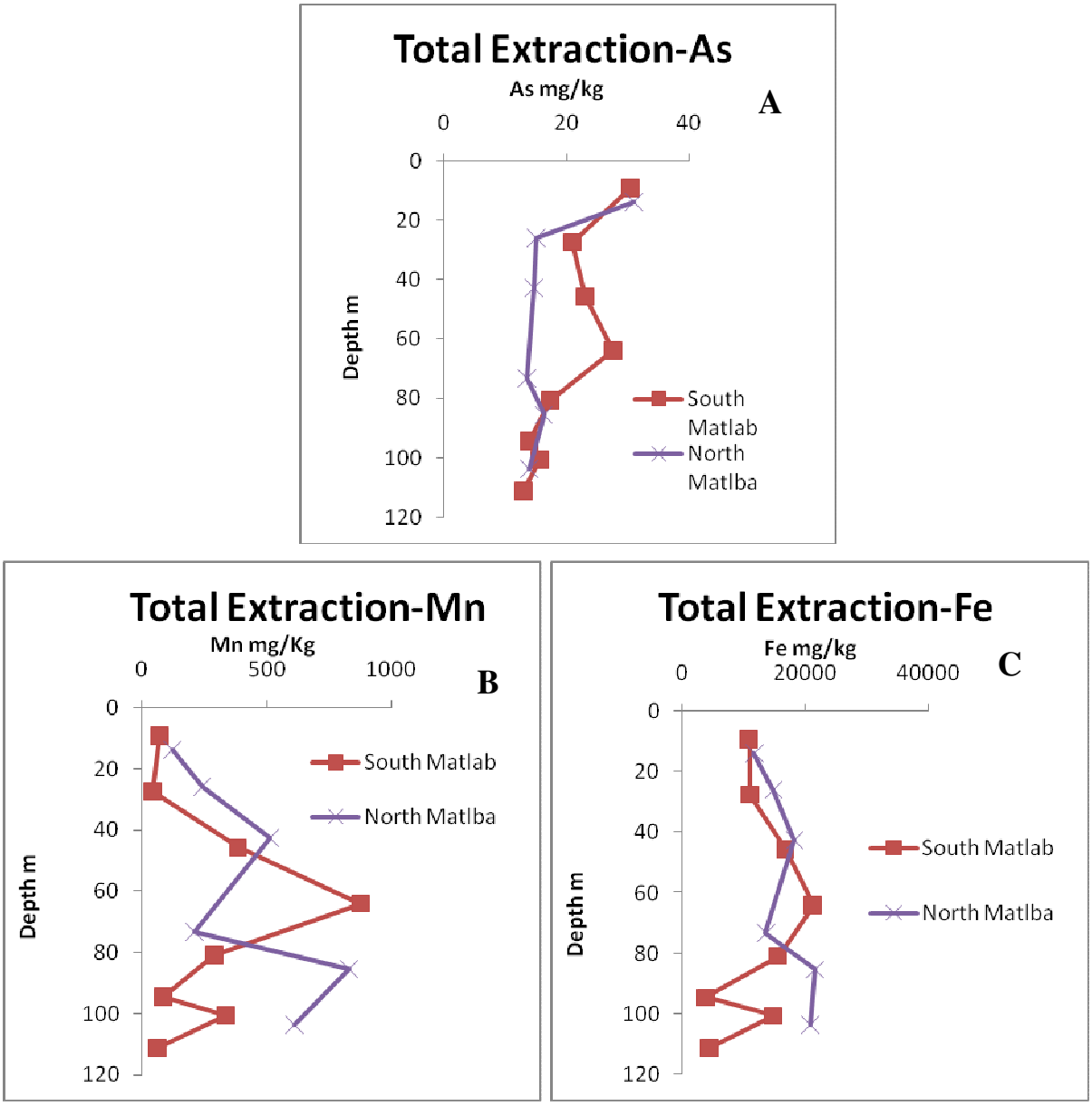

Figure 5.9 Depth-wise distribution (A) As (B) Mn and (C)Fe $_T$ concentration variation in the sediment cores determined by total extractions (aqua regia). Results from both sites are represented by different colors.

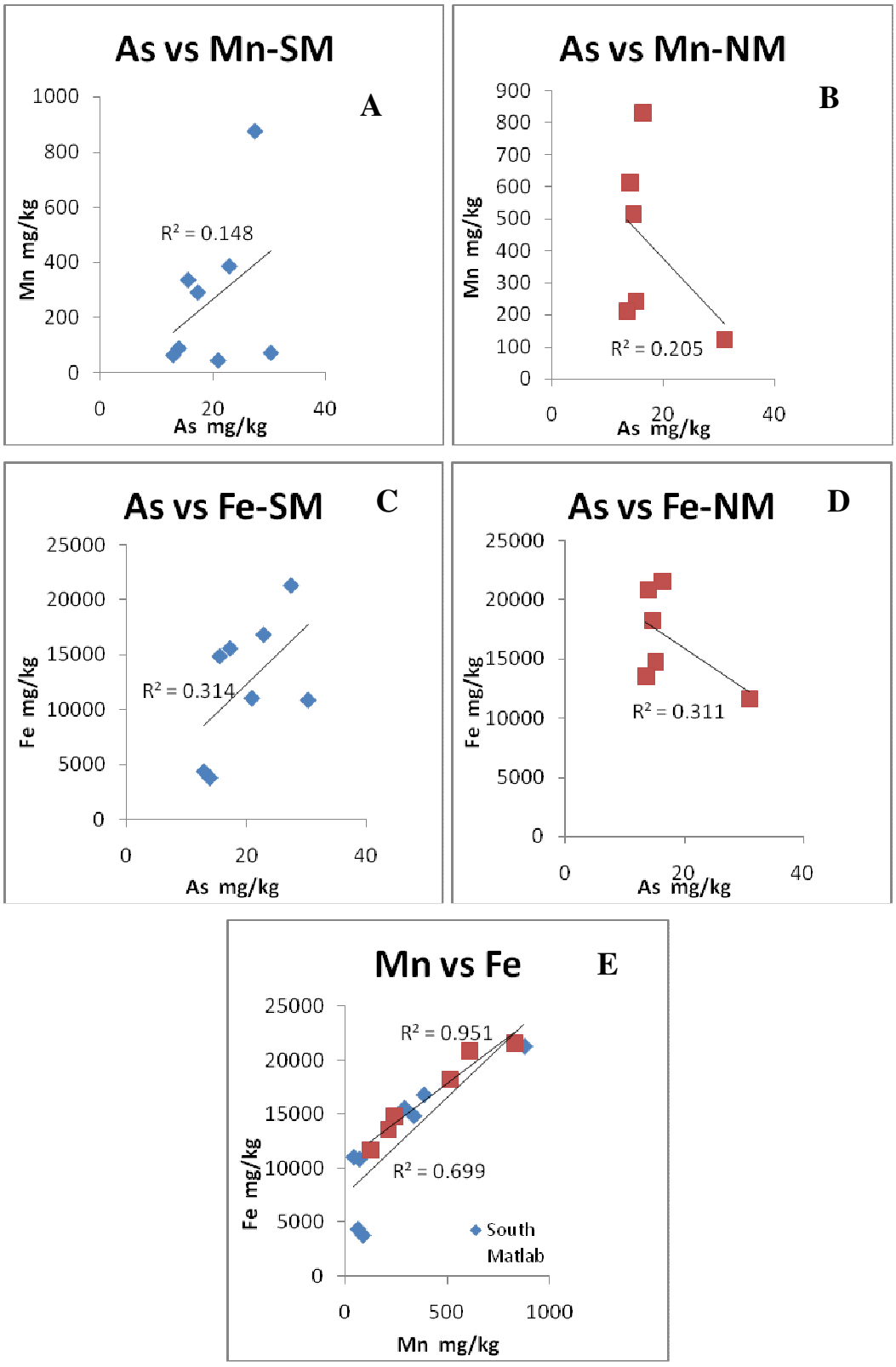

Figure 5.10 Correlation (linear) plots for As and Mn vs. Fe $_T$ for South and North Matlab sites. The correlation coefficients are stated as r^2 values.

The Mn and Fe(t) concentrations in South Matlab (core-2) change with depth and lithology. The concentration ranges for FeT and Mn in grey colored very fine to clay and silt sediment (46-81 m and 101m) are 14871-21308 mg/kg and 290-876 mg/kg, respectively. At shallower depths Fe(t) was within 10878 to 11051mg/kg and Mn was within 44.01 to 71.41mg/kg). At depths of 95m and 111m,the sediments have much lower Mn and FeT concentrations, with Mn ranging from 63.65 to 87.97 mg/kg and FeT from 3815 to 4384mg/kg (**Figures 5.9B and 5.9C**).

In the study area concentrations of As, Mn and FeT showed change with lithology. In both South Matlab and North Matlab, the FeT concentration shows positive linear correlation with As and Mn content. The r^2 values for Mn vs. FeT for South and north Matlab As were 0.699 and 0.951 (**Figures 5.10 A & B**). The r^2 values for As vs. FeT for South and North Matlab areas are 0.314 and 0.311 respectively (**Figures 5.10 C & D**). The r^2 values for As vs. Mn for South and North Matlab areas are 0.148 and 0.205, respectively (**Figure 5.10 E**). The details of total digestion results are represented in the **Appendix - 4.**

Sequential Extraction Analyses

Sequential extractions were performed for both North and South Matlab sediments. Results from sequential extractions of this core showed relative proportions in which As, Mn, and Fe are partitioned in various fractions in the sediments (**Figure 4.11**): non-specifically sorbed, specifically sorbed, amorphous and poorly crystalline hydrous oxides of Fe and Al, well crystallized hydrous oxides of Fe and Al, organicaly sorbed and residual minerals (e.g. quartz and feldspar). Comparison of leachates analyzed both immediately following each step and the next day using the same standards revealed nearly identical results for Mn and Fe, while there were a few variations with As values, especially for phases using $NH_4H_2PO_4$ and NH_4^+ -oxalate buffer. It was concluded that for low concentration elements like As, specific sequential extraction steps should be dealt with using extra precaution and validation. For interpretation purposes, only the values measured immediately following completion of each step are reported here. (**Data appendix -5**)

In the South Matlab and North Matlab sediments, a small amount (< 5%) of specifically sorbed As was detected. A significant portion of As was associated with Fe hydroxides: ~40% for amorphous and poorly crystalline phases and ~30% for well-crystallized phases, while nearly ~5% was in the residual phase. Approximately 3-5% As is associate with organic matter.

Extraction of As in this sequential extraction did not show any relation with sediment color or grain size. In general sequential As extraction showed the concentration varied in the following order: amorphous and poorly crystalline hydrous oxides of Fe and Al > well crystallized hydrous oxides of Fe and Al > specifically sorbed > organic phase > residual phases (**Figure 5.11A**).

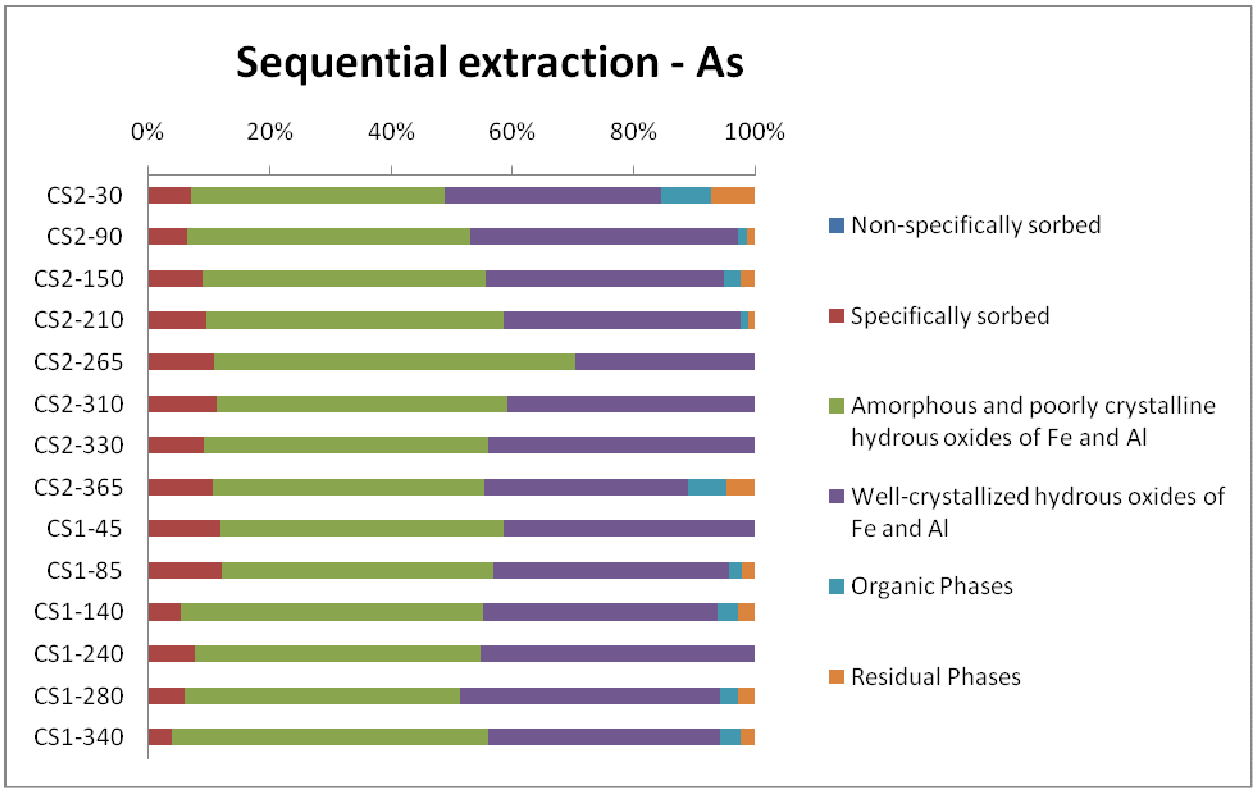

Figure 5.11A Sequentialy extracted fractionations of As as expressed as percetange. Both cores are represented here, CS1 and CS2. Depthwise sediment sequential extraction data are represented.

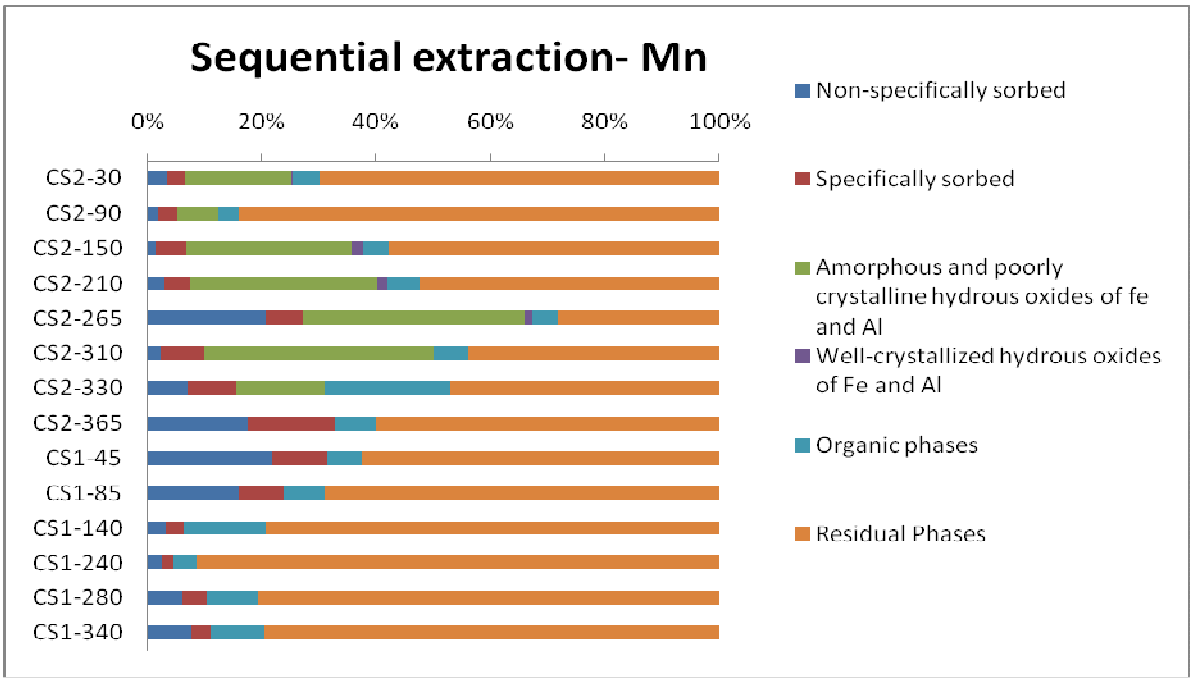

Figure 5.11B: Sequentialy extracted fractionations of Mn as expressed as percetange. Both cores are represented here, CS1 and CS2. Depthwise sediment sequential extraction data are represented.

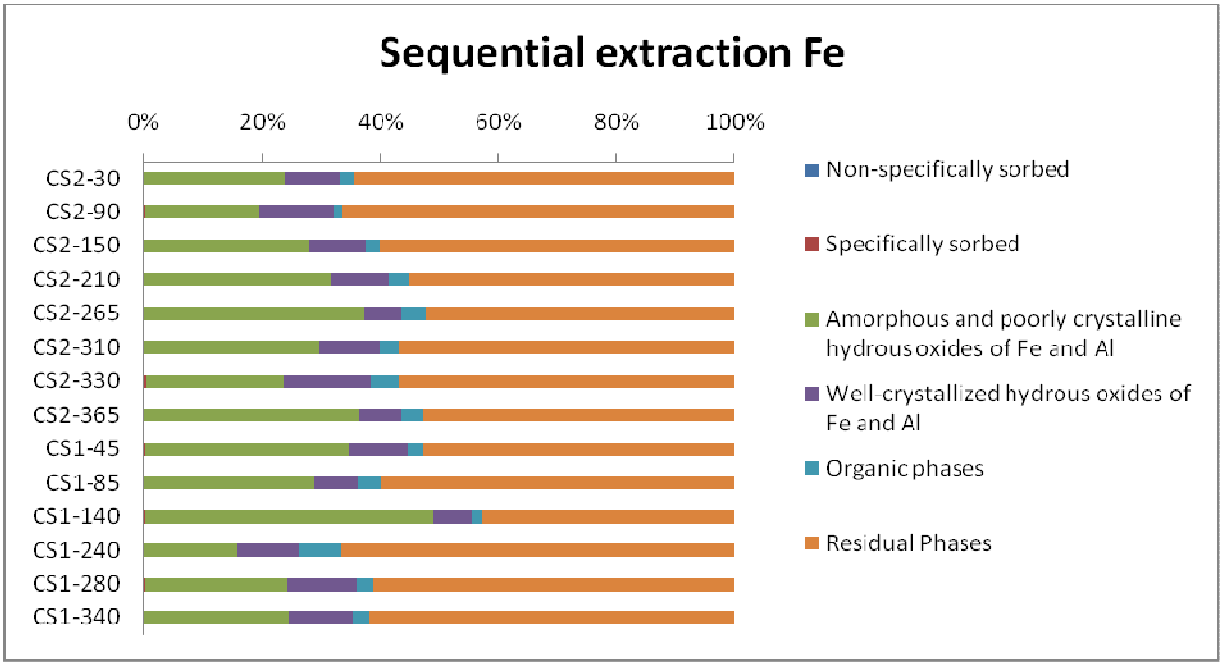

Figure 5.11C: Sequentialy extracted fractionations of Fe as expressed as percetange. Both cores are represented here, CS1 and CS2. Depthwise sediment sequential extraction data are represented.

Mn was extractable by non-specifically sorbed phase which was almost 2-5%, where As and Fe did not come out in this phase. A significant portion of Mn was associated with residual phase ~40-80%. All other phase contained the rest of the portion.

The amorphous and poorly-crystalline Fe hydroxide phase contains between ~20-25%of the Fe in the sampes. No Fe was detected in either of the sorbed phases, while 10% and 5% of the total Fe was in the well-crystalline phase and the organic phase, respectively. The remaining 60% of Fe was in the residual phase.

For Mn sequential extraction, we observed thatthe South Mmatlab samples, 10-20% of the Mn was extracted from amorphous and poorly crystalline hydrous oxides of Fe and Al phase, but North Matlab did not show Mn extraction from this phase. In general sequential Mn extraction showed residual phases > amorphous and poorly crystalline hydrous oxides of Fe and Al > non-specifically sorbed > specifically sorbed > organic phase > well crystallized hydrous oxides of Fe and Al (**Figure 5.11 B**).

Light grey sediment from the intermediate depth showed the majority of the total As was in the P-extractable (~10%) and amorphous/poorly-crystalline Fe hydroxides (50%), while 20% was in the well-crystallized Fe hydroxides. The majority of Mn was in the residual phase (70%), ~10% was P-extractable, and the Fe hydroxide phases combined for 23% of total Mn. Fe was not detected in the sorbed phases. The amorphous/poorly-crystalline Fe hydroxide phase accounted for 30% total Fe, and the well-crystalline phase housed 10% of the total Fe concentration. In general Fe extraction showed residual phases > amorphous and poorly crystalline hydrous oxides of Fe and Al > well crystallized hydrous oxides of Fe and Al > organic phase (**Figure 5.11C**). The total As concentrations for the sum of As concentrations from each of the six sequential extraction steps were all in good agreement with total As concentrations measured by ICP-OES from digestion by aqua regia.

Total Organic Carbon Extraction

The depth distribution of Total Organic Carbon (TOC %) in South Matlab and North Matlab showed similar trends (Figure 4.12) as that of As concentration with depth in the same core samples. Maximum TOC (0.98%) in South Matlab core (CS-2) was found at shallow to intermediate depths (64m).

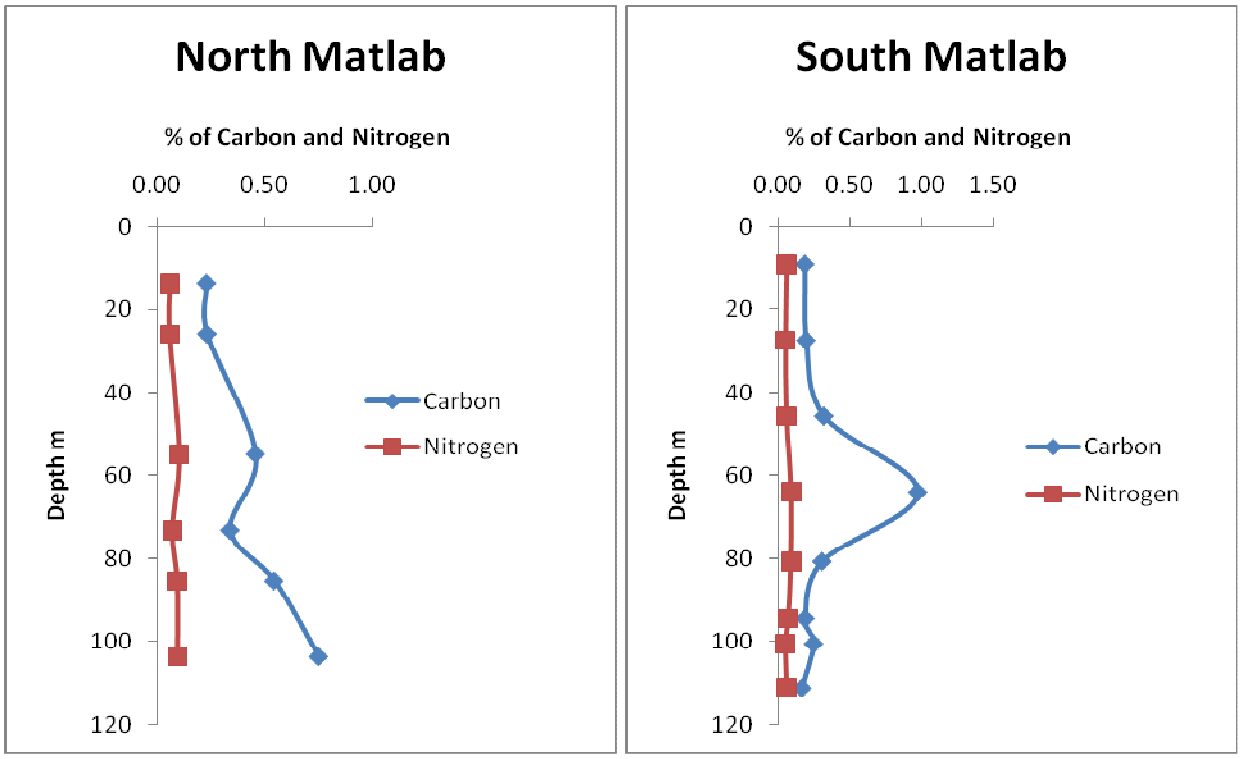

Figure 5.12: Change in concentrations of TOC % and TN% with depth for South and North Matlab cores.

The minimum TOC % of 0.17% was observed at 111m depth and the concentration of As at this depth was a minimum as well (i.e. below detection limits for the methods used here). Surprisingly, the TOC was low (0.19-0.32%) at shallow depths, down to about 32m depth, whereas the As concentration increased to 400 µg/L over this same depth range. The concentration of total nitrogen (TN) follows a similar in trend (shallow and intermediate) in South Matlab. Maximum concentrations of TN of 0.095% is observed at a depth of 64 m. Elsewhere, the concentration of TN was within 0.054 to 0.095 % (**Figure 5.12**).

Maximum TOC (0.75%) in North Matlab core (CS-1) was found at intermediate depths (104m), where the sediments are dark grey colored clay. The minimum TOC % of 0.23% was observed at shallow depths, 14m, where the concentration of As was higher than deeper light grey sediments, i.e. ~350µg/L. TOC showed little variation throught the core, i.e 023-0.75%. The concentration of TN followed a similar wt% trend and concentration with depth (shallow and intermediate) in North Matlab. Maximum concentration of TN (0.102%) was observed at 55 m. The concentration of TN was within 0.061 to 0.102% (**Figure 5.12**). The detailed results are presented in the **Appendix-6.**

Water Chemistry

Field Analyses

Water samples collected from both South and North Matlab had pH values at or near neutral range in both grey and dark grey sediments (6.7 to 7.3) and light grey sediments (6.9 to 7.6). (**Figures 5.13 A & B**). (**Appendix-7**)

Conductivity of grey and dark grey sediments bearing waters in Matlab ranged from 240 to 978μS/cm. Low-As contaminated waters from light grey aquifers in Matlab have much higher conductivity (506 to 1214 μS/cm) than grey and dark grey sediment aquifers (**Figures 5.13 E & F**).

Resistivity of grey and dark grey sediments bearing waters in Matlab ranged from 1.32E+02 to 2.07E+03 Ω·m. Low-As contaminated waters from light grey aquifer in Matlab demonstrated resistivity much higher (9.52E+01 to 1.84E+03 Ω·m) than grey and dark grey sediment aquifer waters.

Total Dissolved Solids (TDS) values for grey and dark grey sediment waters range from 243 to 532 mg/l and for light grey sediments from 252 to 526 mg/l . Dissolved oxygen (DO) for grey and dark grey colored sediments' associated waters ranged from 1.37 to 5.75 mg/l. DO values for light grey colored aquifer waters were in the range of 1.4 to 4.5 mg mg/l.

Redox potential varied widely in Matlab, grey and dark grey color sediment shows Eh as -131.4 to 96.3 mV whereas light grey color sediments' associated waters show Eh is -125 to 90.6 mV (**Figures 5.13 C & D**).

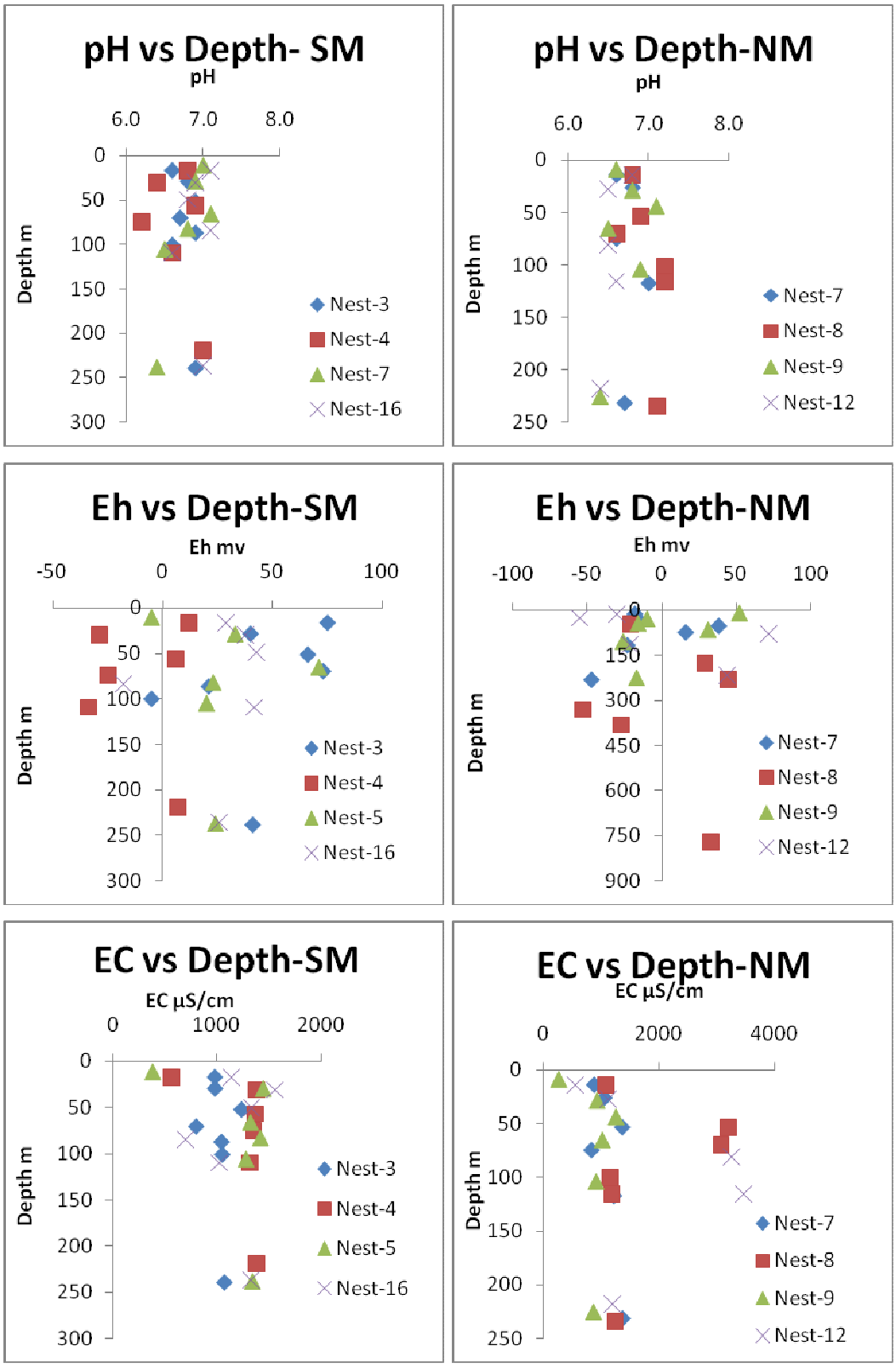

Figure 5.13 Depthwise pH, Eh and EC variations in groundwaters from selected piezometers from North and South Matlab. Piezometers selected from NM are 7, 8, 9 , 12 and 3, 4, 5, 16 from SM.

In-situ Water Chemistry (Test Kit Results)

In Matlab groundwaters, HACH® Arsenic Field Test Kit showed variation with sediment color. Most of the shallow (10 – 95m) depth grey and dark grey color sediment contain highly dissolved As concentration (50 – 1000 ppb). Within the depth range of 60-80m there were some zones of reddish brown color sediment which contain low As contaminated water. In our study seven wells fall in this zone and have As concentrations that range from 0-25ppb. The test for other wells which were within the ligh grey sediment aquifer on intermediate and deeper depth yielded low or no As concentration (eighteen well shows <10 ppb and four well shows 10-25 ppb As concentration) (**Figure 5.14 A & B**). (**Appendix-8**)

Waters with high conetrations of dissolved As (from grey and dark grey sediments), were relatively higher in HCO_3^- concentration (205 to 1050 mg/l). Lower HCO_3^- (110 to 320 mg/l) was observed in low As waters (<10ug/l) which are mainly from light grey sediments. Waters from red brow sediment (installed by SASMIT) colored sediments had low As concentrations and relatively high HCO_3^- values (400 to 900 mg/l) (**Figures 5.14 C & D**).

Ammonium (NH_4^+) values for groundwaters were higher in grey and dark grey sediments with high dissolved As than light grey colored aquifer waters. Grey and dark grey colored sediments' associated waters had NH_4^+ concentrations of 0.5 to 10.3 mg/l (with exception of seven wells within 10-25m in which no NH_4^+ was detected), and waters from light grey colored sediments ranged from 0.04 to 4.65 mg/l of NH_4^+. No NH_4^+ was detected in three of the wells sampled(nest-3 210m, nest-13 105m and nest-16 100m) in light grey colord intermediate and deep sediment (**Figures 5.14 E & F**).

In North and South Matlab, Total Fe (Fe_t) ranges from 0 to 6.98 mg/l (~7mg/l), as measured using UV-VIS spectophotometer. In shallow depths groundwaters associated with grey and dark grey sediments Fe2+ varied more (0 to 6.98 mg/l). Light grey sediments bearing waters showed 0 to 4.03 mg/l of Fe_t. For Fe^{2+} value range within 0 to 6.78 mg/l with in Matlab.

In grey and dark colored sediment, Fe^{2+} value is in the range of 0 to 6.78 mg/l; light grey colored sedimentashowed similar values of 0 to 6.48 mg/l. There weren't any difference between this two sediment colors. In South and North Matlab phosphate (PO_4^{3-}) values for groundwater are very low, less then 0.10 mg/l in most cases, and there weren't significant differences with sediment color. The field test yielded very low concentrations of SO_4^{2-} both South and North Matlab groundwater which is difficult to identify by field kit.

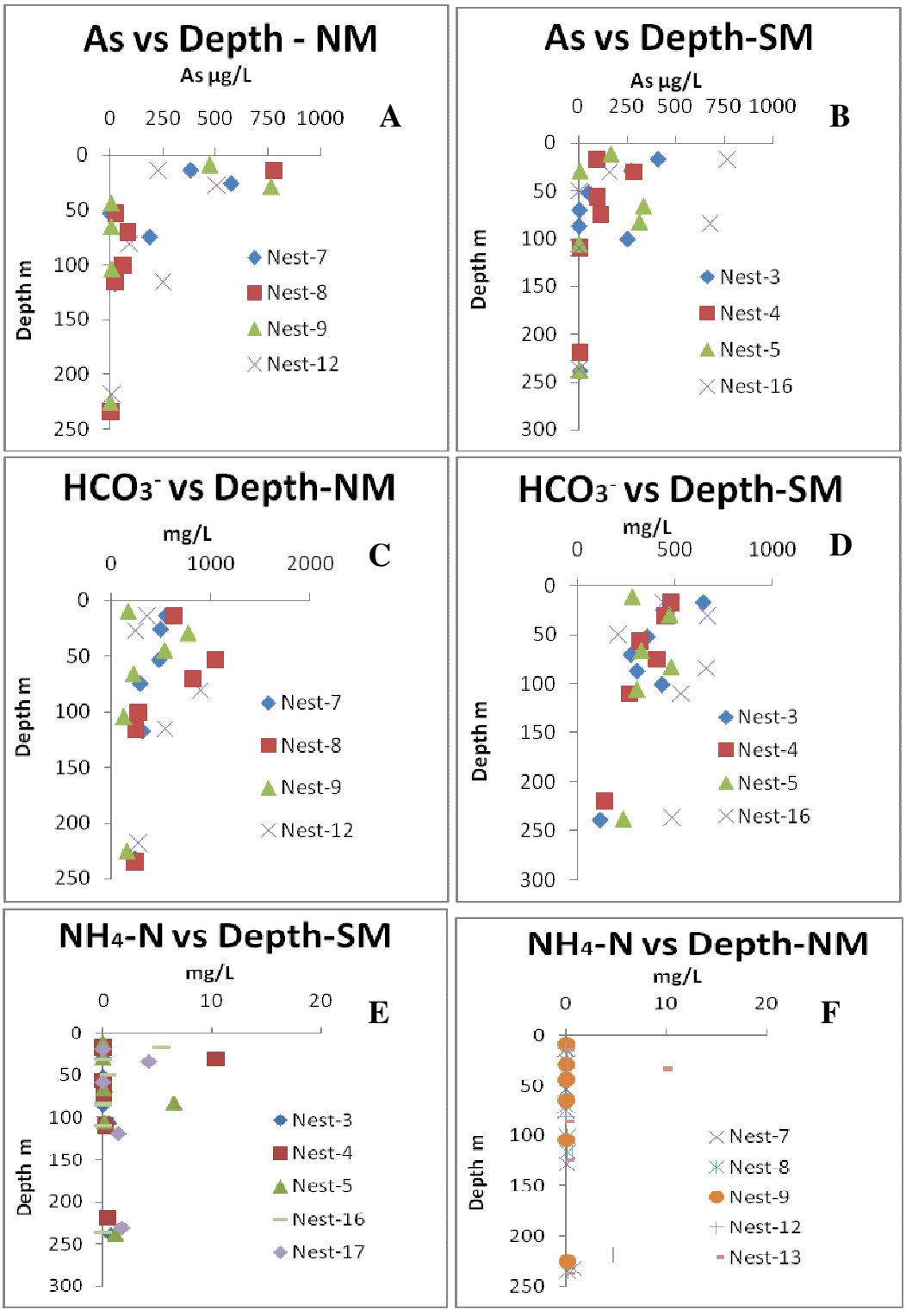

Figure 5.14 Depthwise As, HCO3- and NH4-N variations in groundwaters from selected piezometers from North and South Matlab. Piezometers selected from NM are 7, 8, 9, 12, 13 and 3 , 4, 5, 16, 17 from SM.

Total Manganese and Arsenic Analyses

Dissolved arsenic concentrations ranged from 1.13 µg/l to 11.25µg/l for most of the light grey intermediate and deeper aquifer (n=16). However, at a depth of 115m in North Matlab (nest-12, pizometer-6), a dissolved As concentration of 245 µg/l was measured, which contrasts markedly with the much lower values elsewhere. We compared this result with the SAAMIT project data base, which showed that the As level was 43 µg/l in 2012. Therefore,this high concentration may be an analytical error of the field test. Another well from North Matlab (nest-8, pizometer-4), which depth is 100m showed a moderately high dissolved As concentration of 84.5 µg/l (**Figures 5.15 A & B**). (**Appendix -9**)

Shallow (< 90 m) groundwaters contained a wide range of dissolved As concentrations, which was highly variable with depth and color. In Matlab, groundwater As levels from different wells screened within <90m depth in the aquifer varied from 5.09 to 781 µg/l within North and South Matlab. Only for five wells did it show 5.09 to 7.96 µg/l dissolved As concentrations for depths less than 90m. The sediment color in all five of these wells was reddish brown. All other (n=21) wells showed higher As concentrations of 54.58 to 781 µg/l for depths less than 90m. These wells were within grey and dark grey sediment aquifer (**Figures 5.15 A & B**).

Shallow (< 90 m) groundwaters contained a wide range of dissolved Mn concentrations, which were highly variable with depth and color. For both North and South Matlab, groundwater Mn levels from different wells screened for depths <90m in the aquifer varied from 0.13 to 3.93 mg/l. Most of the wells (n=17) therefore have Mn concentrations that are greater than the 0.04mg/l limit previously proposed by WHO as being of health councern (**Figures 5.15 C & D**).

Dissolved manganese (Mn) concentrations ranged from0.09mg/l to 0.25mg/l for most of the intermediate and deeper aquifer (n=16) where sediments are light grey in color. However, significantly higher values are observed at some specific locations. In South Matlab (nest=3, pizometer-6), at a depth of 95 m, dissolved Mn concentration is as high as 3.17 µg/l (**Figures 5.15 C & D**).

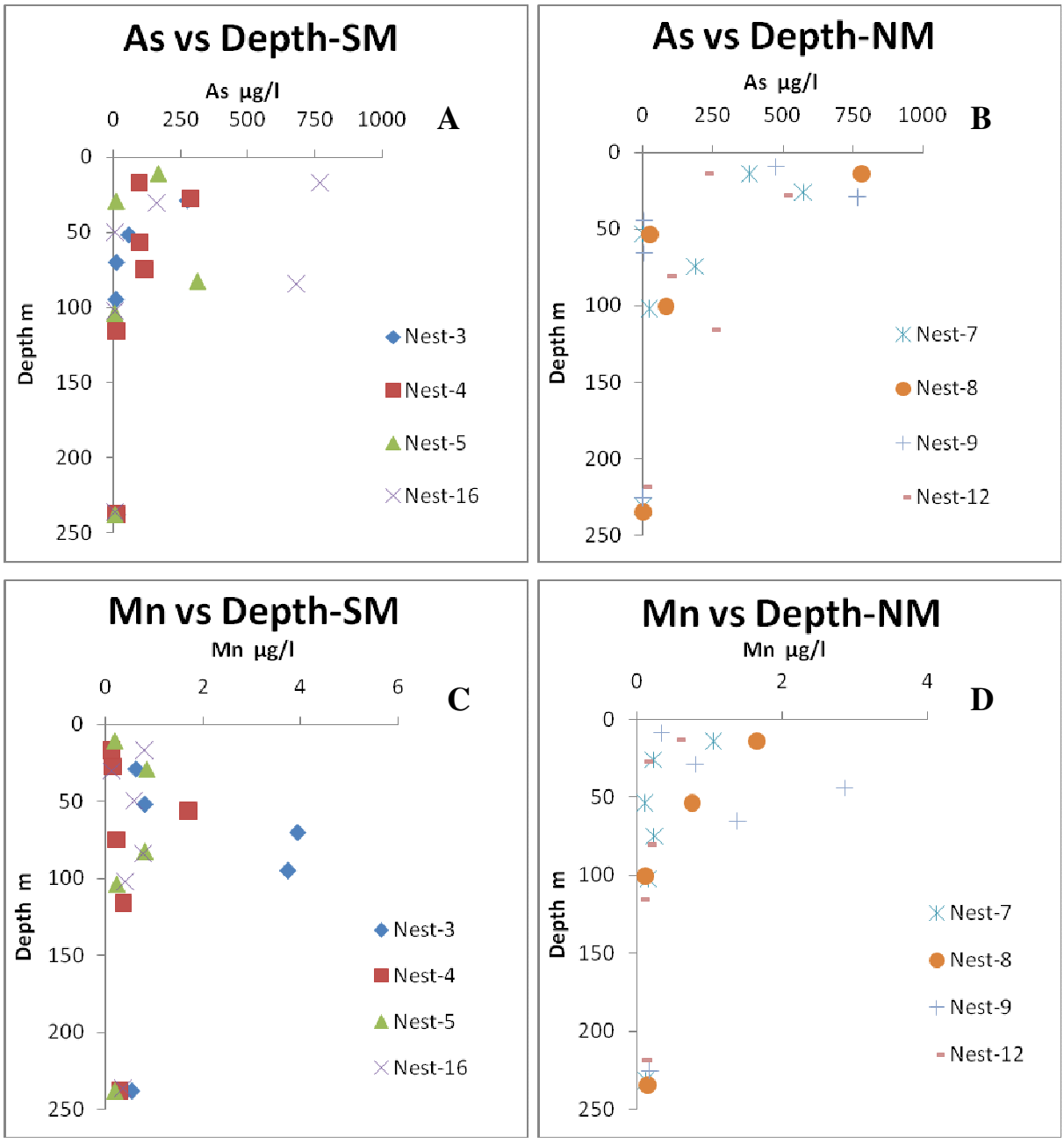

Figure 5.15 Depthwise As and Mn variation in groundwaters from selected piezometers from North and South Matlab. Piezometers selected from NM are 7, 8, 9, 12 and 3, 4, 5, 16 from SM.

Cations

Dissolved FeT was relatively similar in grey and dark grey and light grey colored sediments. In light grey colored sediment Fe ranged within 0.91 to 10.62 mg/l. Shallow aquifer grey and dark grey colored sediment showed 1.19 to 10.49 mg/l Fe level (**Figures 5.16 A & B**).

Calcium was highest in high-As bearing waters from grey and dark grey colored sediment of North Matlab (26.27 to 192mg/l). Calcium was highest in shallow aquifer from grey and dark grey colored sediment of South Matlab (37.29 to 142mg/l), which is lower than the North Matlab concentration. Intermediate and deep aquifer light grey color sediments Ca concentration was within 11.08 to 80.40 mg/l in both South and North Matlab, which is little increased in South Matlab water (**Figures 5.16 C & D**).(**Appendix-10**)

Potassium (K) concentrations in shallow aquifer had a wide range of variation. Waters in South Matlab showed a lower K concentration then North Matlab (the range of K was 0.5 to 18 mg/l and 1 to 38mg/l in South and North Matlab, respectively).In the intermediate and deep aquifers K concentrations varied between North and South Matlab. In South Matlab, K concentrations were in the range of 2 to 15 mg/l from light grey sediments. Groundwaters from South Matlab (intermediate and deep aquifers) showed K concentration within 0.5 to 5 mg/l, which was less then South Matlab K concentration in intermediate and deep aquifers (**Figures 5.17 A & B**).

Magnesium (Mg) in shallow waters from grey and dark grey sediment ranged from 8.79 to 61.68 mg/l in South Matlab. Dissolved Mg in grey and dark grey sediment on shallow aquifer were relatively higher than the shallow aquifer water from South Matlab which was 1.92 to 90.09 mg/l in North Matlab, only one well showed very high at 100m depth 146.45mg/l . In the intermediate and deep aquifer at North Matlab, Mg concentration was low, ranging from 1-10mg/l. Dissolved Mg in light grey sediment on intermediate and deeper aquifer were relatively higher than the shallow aquifer water which was 5.96 to 60.09 mg/l in South Matlab (**Figures 5.17 C & D**).

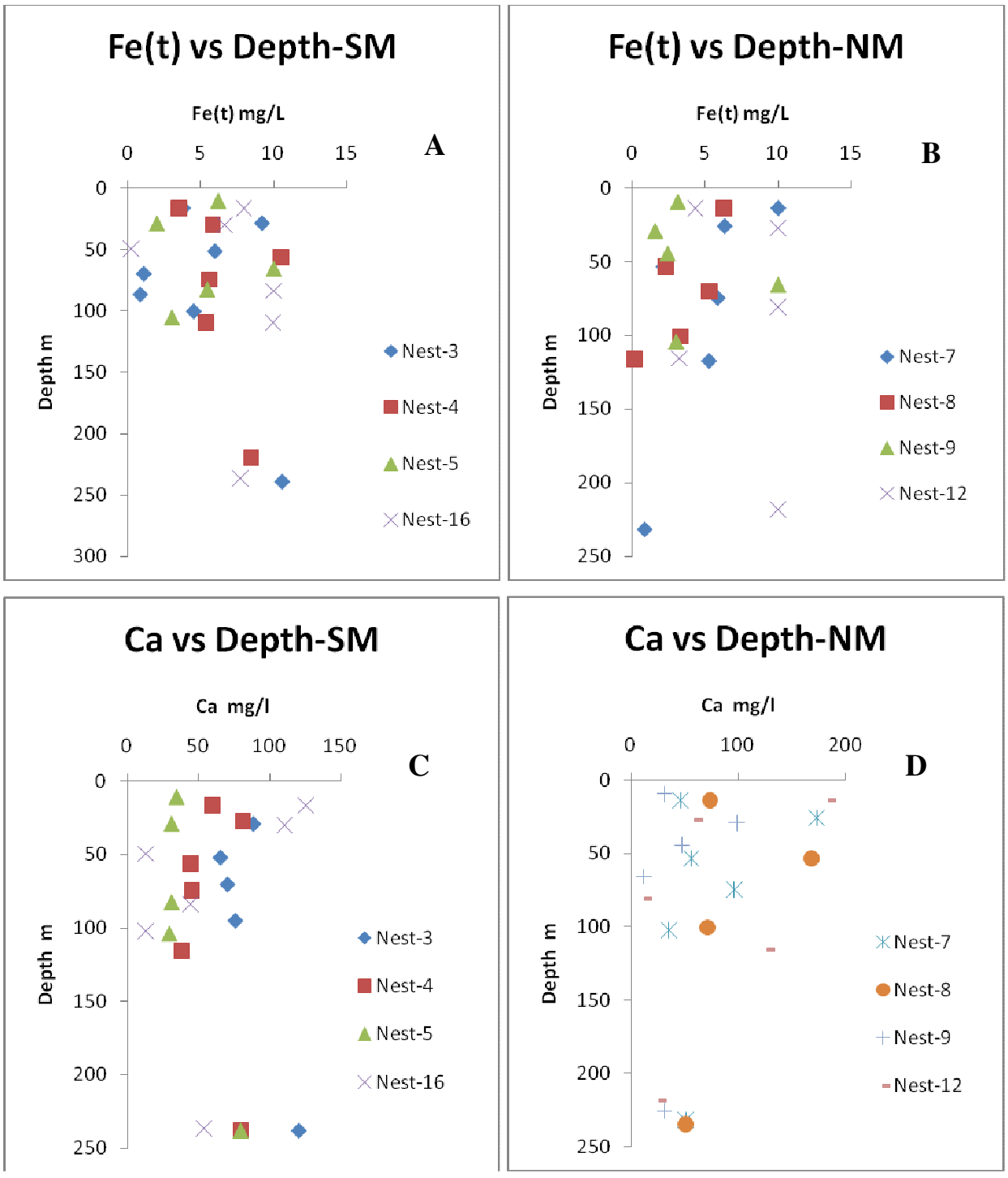

Figure 5.16 Depthwise Fe(t) and Ca variation in groundwaters from selected piezometers from North and South Matlab. Piezometers selected from NM are 7, 8, 9, 12 and 3, 4, 5, 16 from SM.

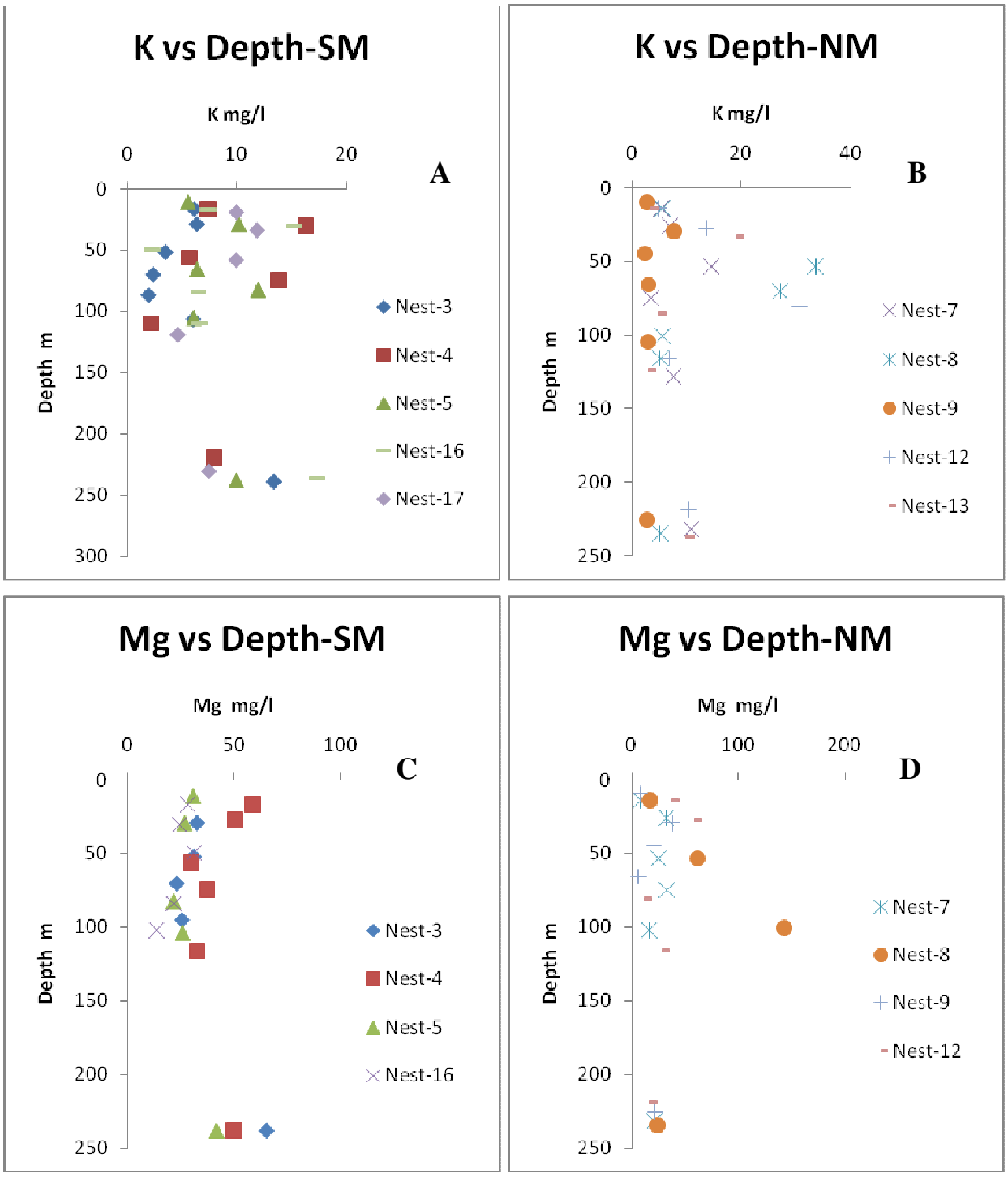

Figure 5.17 Depthwise K and Mg variation in groundwaters from selected piezometers from North and South Matlab. Piezometers selected from NM are 7, 8, 9, 12 and 3, 4, 5, 16 from SM.

Anions

Concentration of F^- for South and North Matlab water are range from 0.4 to 0.6 mg/l in shallow, intermediate and deep aquifers. Only two wells in the shallow aquifer showed higher concentration e.g., 0.9 and 1.1mg/l (**Figure 5.18**) (**Appendix-11**)

Concentration of Cl^- for shallow and intermediate aquifer water ranged from 0 to 736 mg/l in Matlab. Deeper aquifers showed 20 to 484 mg/l. (**Figure 5.18**)

Nitrate values (NO_3^{2-}) were lower in intermediate and deep aquifer waters. NO_3^{2-} was detected to be of 0 -5 mg/l in the light grey sediment water from intermediate and deep aquifers. The concentrations of nitrate were 0 to 18.6 mg/l in the shallow aquifer water which are from grey to dark grey color sediment. One well from nest-16 at 42m depth showed very high nitrate concentration 39 mg/l.(**Figure 5.18**).

Nitrite (NO_2^-) was detected in shallow and the concentration was 0.9 to 2.2 mg/l, which is higher than the intermediate and deep aquifer waters NO_2^- concentration. Less nitrite was detected in deep aquifer waters of light grey sediment from Matlab (0.5 to 0.8 mg/l) (**Figure 5.18**).

Bromide (Br^-) values were lower in shallow aquifers waters. Bromide was detected (0.4 to 4.1 mg/l) in the grey and dark grey sediment associated water in the shallow aquifers. The concentration of Br^- was slightly higher in intermediate and deep aquifers (0.5 to 6.4 mg/l) associated with light grey color sediments (**Figure 5.19**).

Phosphate (PO_4^{3-}) was detected in shallow and intermediate depth aquifer waters and were 0.8 to 23.1 mg/l in Matlab. Less phosphate was detected in deep aquifer waters of light grey sediment from Matlab (0.5 to 2.6 mg/l) (**Figure 5.19**).

Dissolved sulphate (SO_4^{2-}) was detected within the range of (1.5 to 2.1 mg/l) at shallow to intermediate depths. . In the deep aquifers, samples also showed low concentration within 0.5 to 5.8 mg/l of SO_4^{2-}. One sample from a deep aquifer showed a very high concentration of 97 mg/l (**Figure 5.19**).

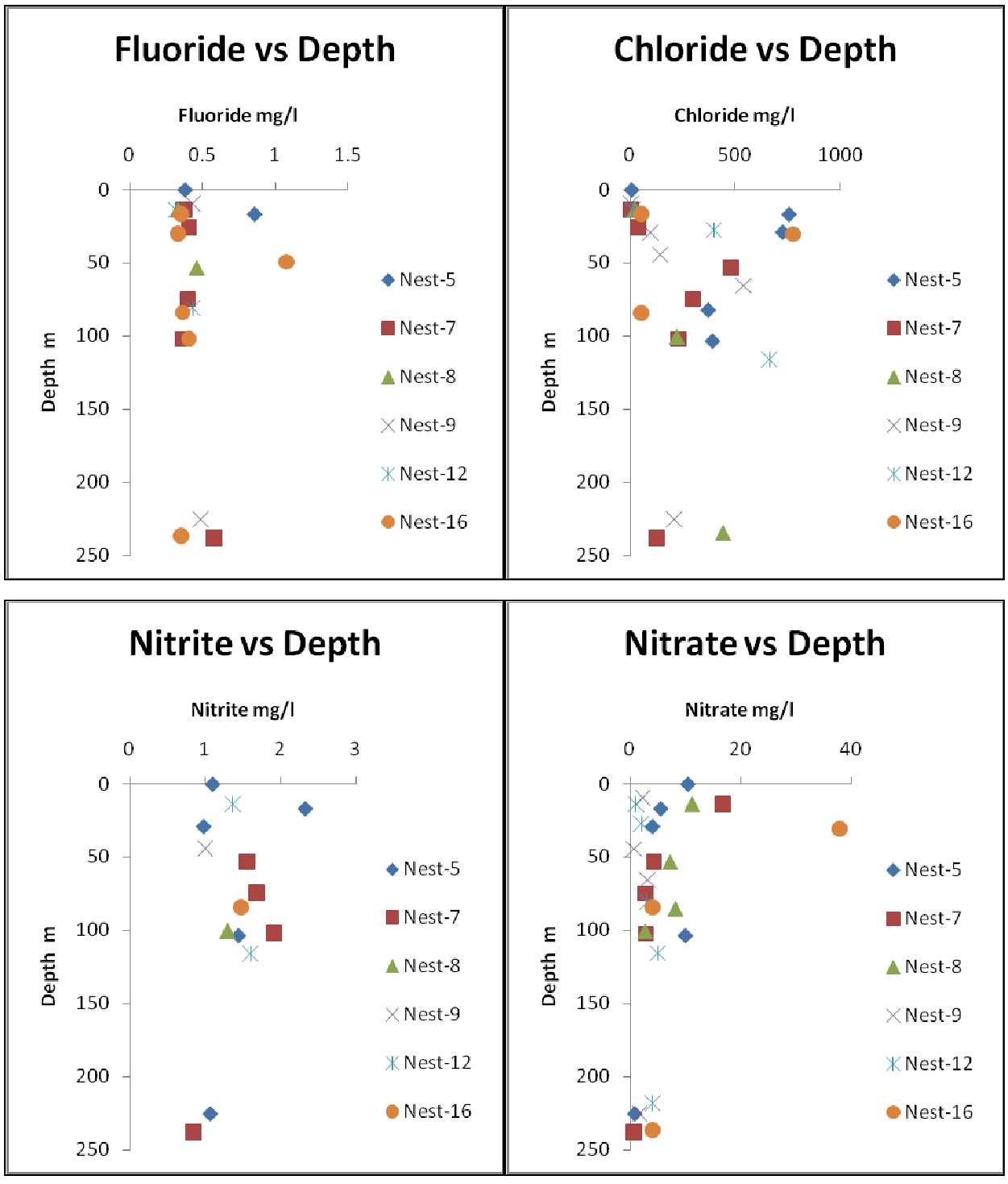

Figure 5.18 Depthwise fluoride, chloride, nitrite and nitrate variation in groundwaters from selected piezometers from North and South Matlab.(Nest 5, 7, 8, 9, 12, 16)

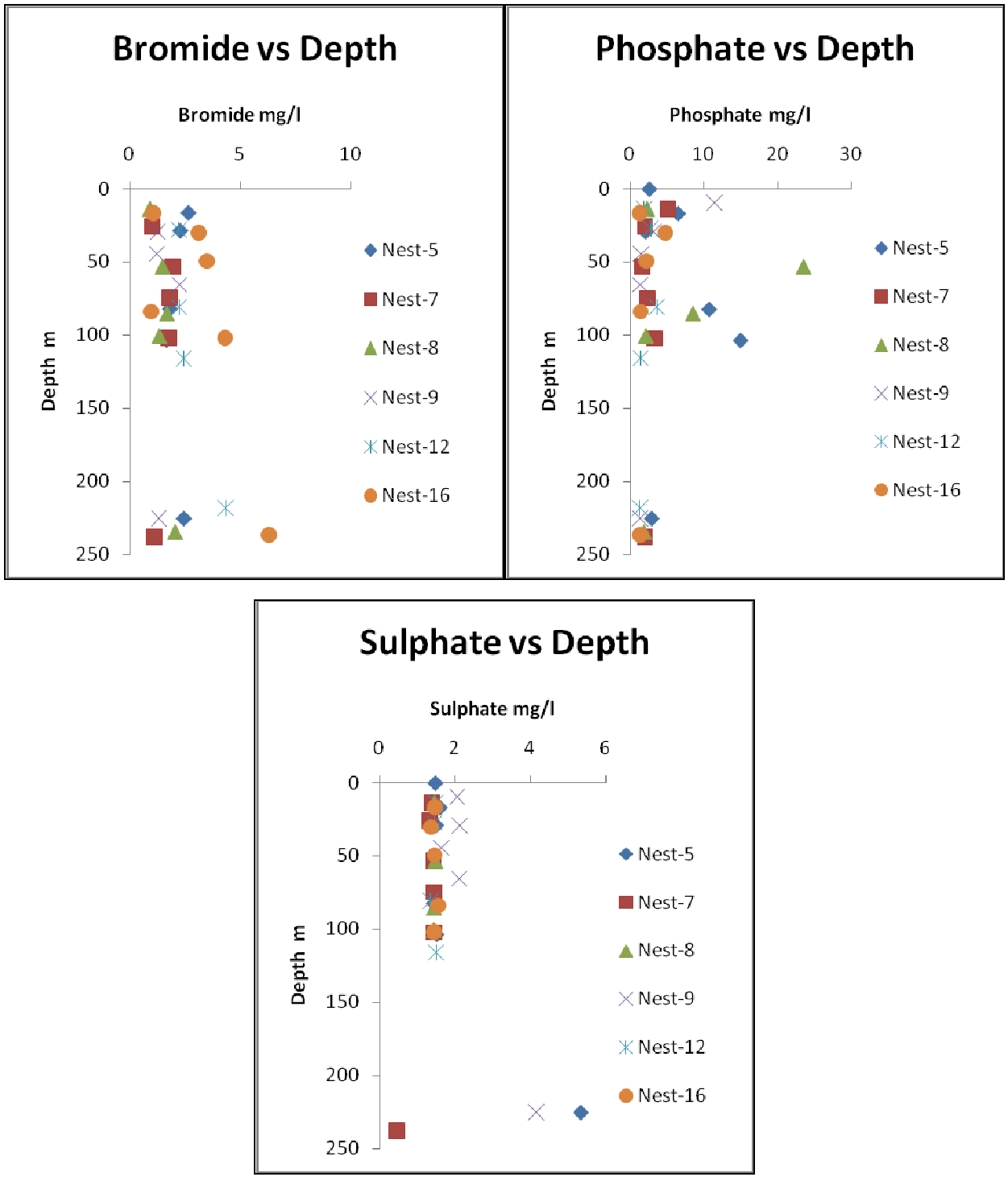

Figure 5.19 Depthwise bromide, phosphate and sulphate variations in in groundwaters from selected piezometers from North and South Matlab.(Nest 5, 7, 8, 9, 12, 16)

Ionic Correlations with Sediment Color

The concentrations of dissolve Fe, SO_4^{2-}, Mn, HCO_3^- and pH from light grey sediments have do not correlate with dissolved As (r^2=0.013, p>0.05 for Fe; r^2=0.017, p>0.05 for SO_4^{2-}; r^2=0.077, p>0.05 for Mn; r^2=0.031, p>0.05 for HCO_3^- and r^2=0.052, p>0.05 for pH). Dissolve SO_4^{2-} from light grey sediments, however, show a weak correlation with dissolve Fe (r^2=0.192, p<0.05 in **Figure 5.19**). DOC from light grey sediments also shows a weak correlation with dissolved As (r^2=0.177, p<0.05 in **Figure 5.20**)

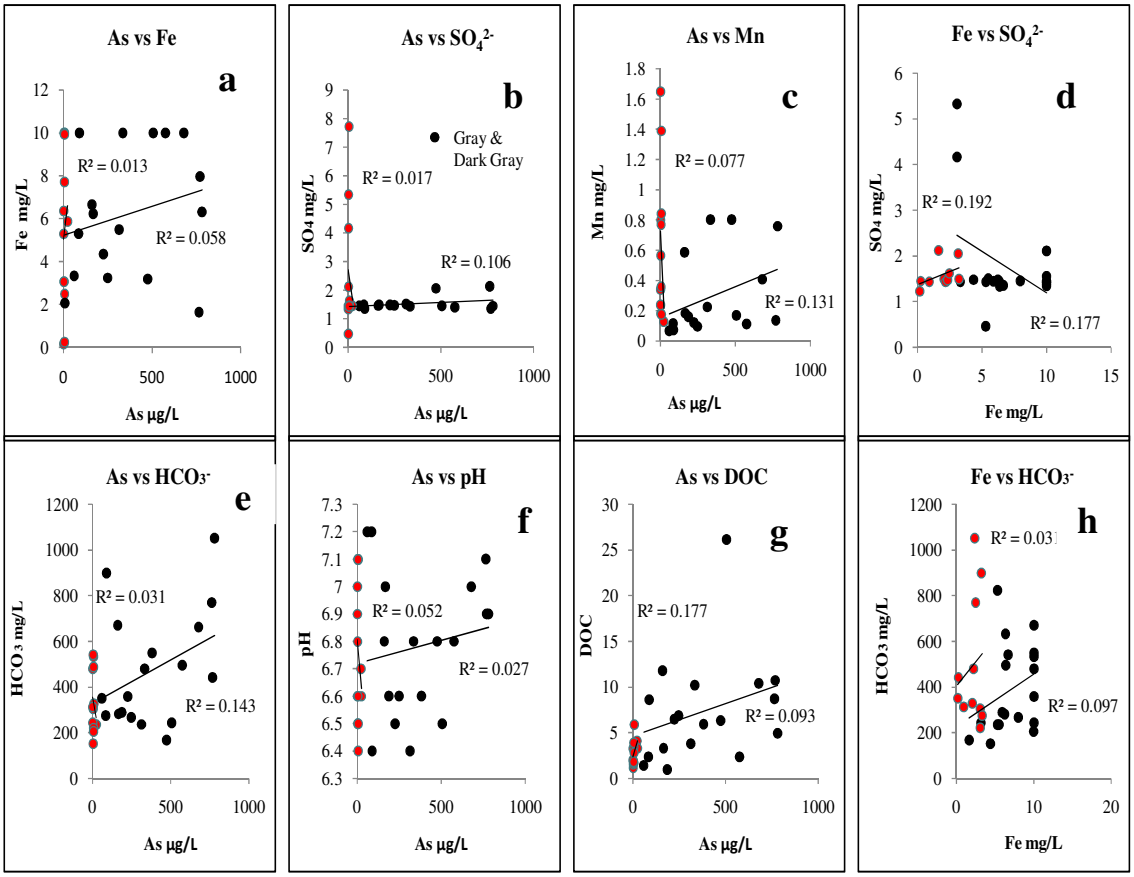

Figure 5.20 Correlation for a) As vs Fe; b) As vs SO_4^{2-}; c) As vs Mn; d) Fe vs SO_4^{2-}; e) As vs HCO_3^- ; f) As vs pH; g) As vs DOC and h) Fe vs HCO_3^- (red dots for light grey sediments and black dots for grey and dark grey color sediments)

The concentration of dissolve Mn, SO_4^{2-} and $HCO3^-$ grey and dark grey sediments have significant correlation with dissolve As (r^2=0.131, p<0.05 for Mn; r^2=0.106, p<0.05 for SO_4^{2-} and r^2=0.143, p<0.05 for HCO_3^- in **Figure 5.20**). Dissolve Fe, DOC and pH from grey and dark grey sediments have no significant correlation with dissolve As (r^2=0.058, p>0.05 for Fe; r^2=0.093, p<0.05 for DOC and r^2=0.027, p<0.05 for pH in **Figure 5.20**). Fe from grey and dark grey sediments have good correlation with SO_4^{2-} (r^2=0.177, p<0.05 in **Figure 5.20**)

Chloride/Bromide molar ratio

Cl^-/ Br^- molar ratio was calculated to study the effect of anthropogenic waste sources like pit latrines, septic tanks, highly contaminated ponds by various anthropogenic waste materials on shallow depth tube wells (McArthur et al., 2012, Xie et al., 2011) which is the major drinking water source in the Matlab. To calculate the ratio (Cl/Br) the [Cl^-] and [Br^-] were converted to molar ratios. At first the concentrations in mg/l of both Cl^- and Br^- were converted from mg/l to moles per liter by dividing the concentration of element by molecular mass and 1000 to convert it in to moles per liter. Then the moles per liter value for both Cl^- and Br^- are converted to milli moles per litter by multiplying it with 1000. Then in the final step the Cl^- concentration in milli moles per liter is divided by Br^- concentration in milli-moles per liter to get the Cl^-/Br^- molar ratio. (**Appendix -12**)

Cl^-/Br^- ratio has been calculated for piezometer nests tubewells from shallow, intermediate and deep depth from South and North Matlab. For the shallow aquifer the water Cl^-/Br^- mass ratio were in the range of 287 to 419. Cl^-/Br^- mass ratio was 231 to 425 in the intermediate and deep aquifer water. Cl^-/Br^- molar ratio for the shallow aquifer was 647 to 946 in Matlab. In the intermediate and deep aquifer this Cl^-/Br^- molar ratio was 521 to 960(**Figure 5.21**).

Cl^-/Br^- mass ratio and molar ratio for shallow, intermediate and deep aquifer water were plotted vs. As concentration and depth (**Figure 5.21**) to study the effect of anthropogenic contaminants in these drinking waters. The tubewells are mainly used for Cl^-/Br^- ratio studies because they were the main drinking water sources in Matlab. The data used for Cl^-/Br^- ratio calculations were from IC (ion chromatograph) data.

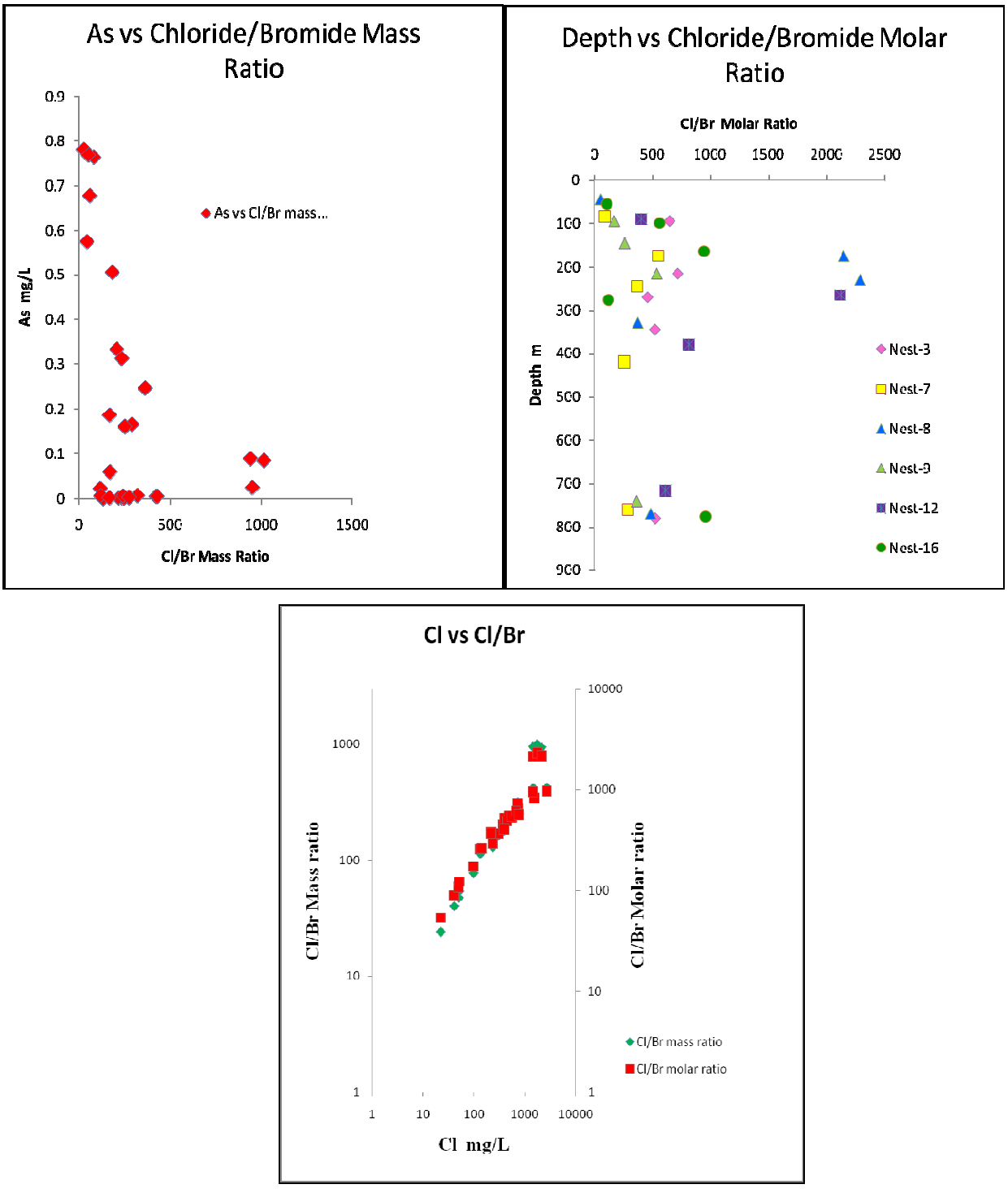

Figure 5.21 Plots showing (A) Cl/Br mass ratio variation with As concentrations in North and South Matlab groundwaters. (B) Plots showing Cl/Br molar ratio with depth in the 7 piezometer nests of North and South Matlab. (C) Plots showing Cl vs Cl/Br molar and mass ratio in Matlab tubewells.

$\delta^{18}O$ and δD results

Stable isotope values were measured for groundwater tubewells (shallow, intermediate and deep) in Matlab at the Department of Biology. Biology Global meteoric water line; GMWL ($\delta D = 8\delta^{18}O + 10$) has been plotted using the data from (Craig 1961) and the local meteoric water line, LMWL ($\delta D = 7.2\ \delta^{18}O + 7.7$) was calculated from Mukherjee et al., 2007 to study the isotopic compositions of Matlab waters for the year 2013. Values for δD and $\delta^{18}O$ for local wet season precipitation were -49‰, -64‰, and -46‰ for δD and -7.3‰, -9.3‰, and -6.7‰ for $\delta^{18}O$ in Bengal Basin (Mukherjee et al., 2007). Local dry season precipitation values for δD and $\delta^{18}O$ were: -32‰, -31‰, -36‰ and -31‰ for δD and -5.1‰, -5.1‰, -4.7‰, and -4.7‰ for $\delta^{18}O$ in Bengal Basin (Mukherjee et al., 2007). For the current study previously installed nest tubewells (shallow, intermediate & deep) wells were selected from South and North Matlab for understanding the fluctuations of stable isotope values. (**Appendix -13**)

δD values (Y-axis) were plotted against the $\delta^{18}O$ values (X-axis) for tubewell waters and detailed ranges and values are represented in the **Appendix-13.** Majority (~60%) of the tubewells (shallow and intermediate) are fall close/on the LMWL. Deep aquifer waters fall close to the GMWL. The overall isotopic composition of shallow depth tube wells are more enriched in heavier isotopes in terms of $\delta^{18}O$. Data sets for all tubewell derived groundwaters are showing parallel trend but not overlapping (**Figure 5.23**).

Figure 5.23 was produced by plotting isotopic data for tubewells reclassifying based on the As concentrations. The classification basis is: <50 µg/L As, 50-200 µg/L As, 200-500 µg/L As and >500 µg/L As to study the relation between recharge mechanisms and As distribution in Matlab waters.

Plots prepared for the comparative studies were done by plotting them together and also plotting by classifying each sample by their nests and sampling areas (**Figure 5.22**). The details of isotopic data for all samples are represented in **Appendix-13.**

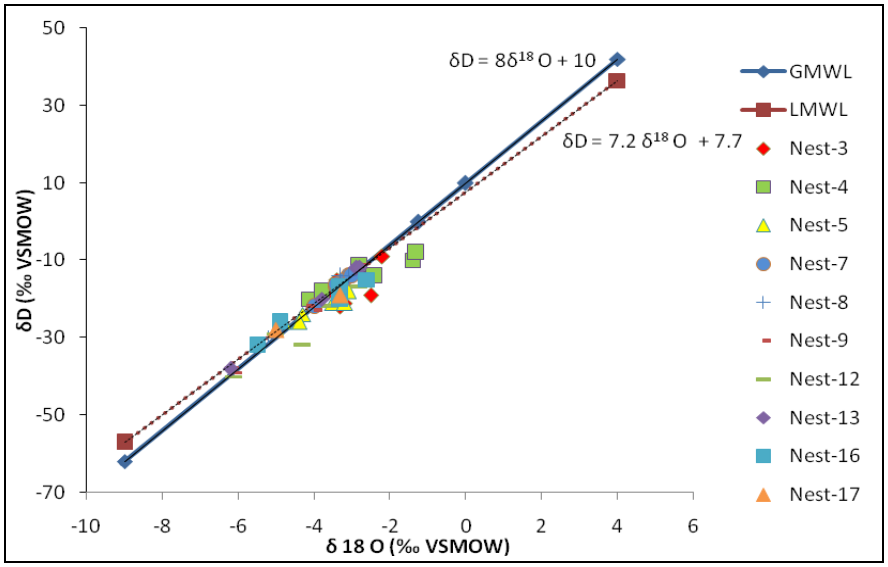

Figure 5:22 Stable isotope plots for δD and $\delta^{18}O$ demonstrating variation with classifications of nest.

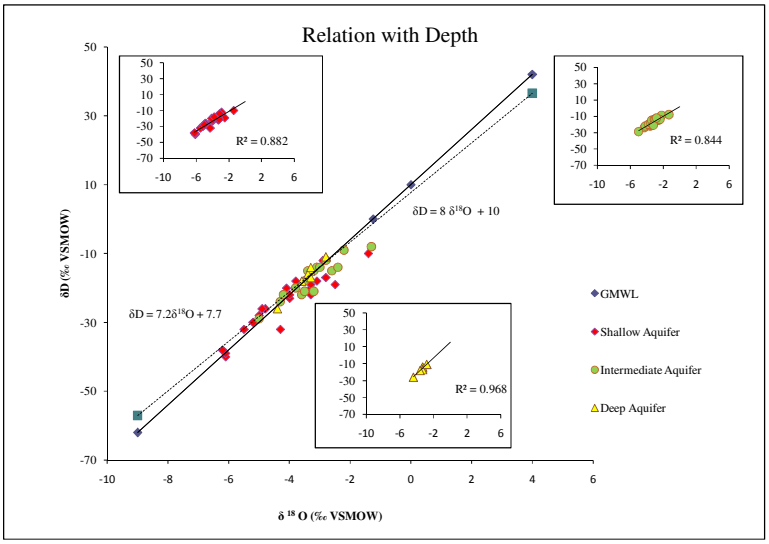

Figure 5:23 Stable isotope plots for δD and $\delta^{18}O$ calibrated to (Vienna-Standard Mean Ocean Water (V-SMOW) for tubewell waters (shallow depth 10-80m, intermediate depth

80-120m and deeper depth >200m). Global Meteoric Water Line (GMWL) and Local Meteoric Water Line (LMWL) are shown with their slope-intercept equations.

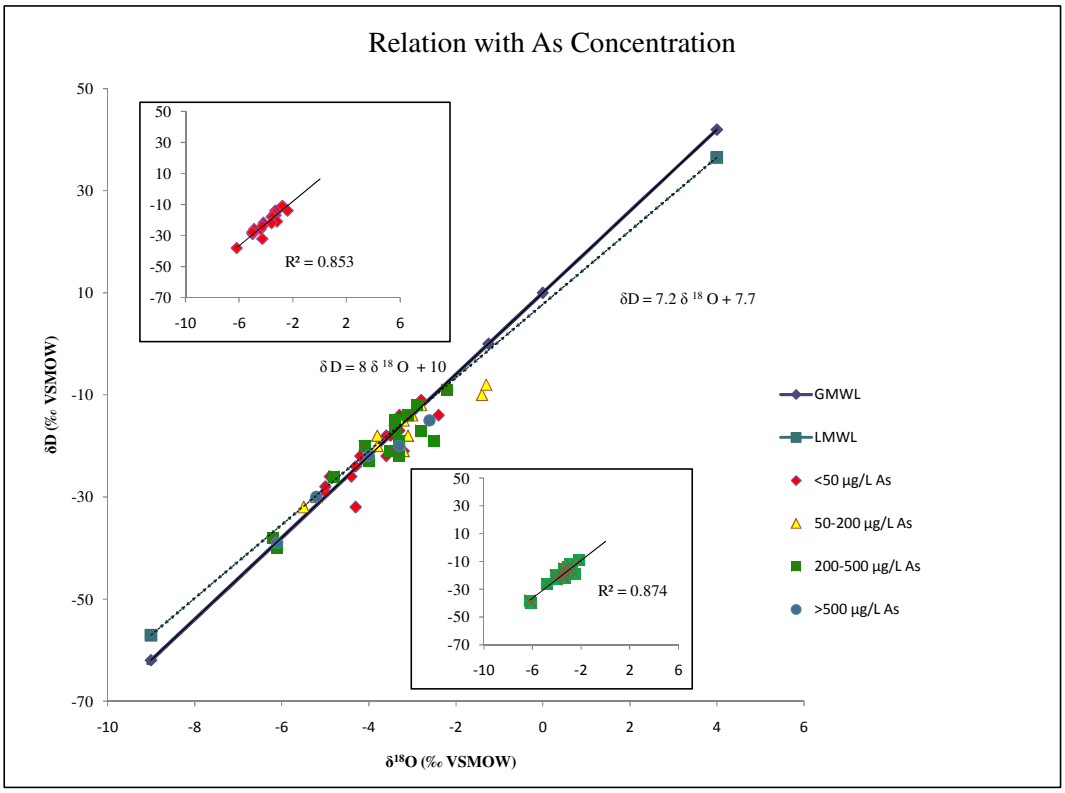

Figure 5.24 Stable isotope plots for δD and $\delta^{18}O$ calibrated to (Vienna-Standard Mean Ocean Water (V-SMOW) for tubewell waters vs dissolved As concentrations (<50 µg/l, 50-200 µg/l, 200-500 µg/l and >500 µg/l. Global Meteoric Water Line (GMWL) and Local Meteoric Water Line (LMWL) are shown with their slope-intercept equations.

Dissolved Organic Carbon

Dissolved organic carbon (DOC) concentrations were measured for South and North Matlab waters. In the intermediate and deep aquifers DOC concentration was 1.1 to 3.4 mg/l from light grey colored aquifer waters. One well from nest 14 at 110 m depth have showed DOC concentration 6.9 mg/l. In the shallow aquifers some samples showed low (0.9 to 2.7 mg/l) concentration of DOC which were from reddish brown colored layers. I DOC was higher in grey and dark grey colored shallow aquifer waters. A value (range) of DOC in this shallow aquifer

was 3.11 to 15.26 mg/l. In the nest numbers 4, 12 and 17 almost at similar 25-30m depth have very high DOC 26.6 to 27.9 mg/l (**Figure 5.25**), which is yet to be accounted for or explained. This might explain a need for repeatation of analyses for these specific samples, as they are outliers from any data that we have seen in the Bengal aquifer. Previous research in Matlab showed that other researchers found DOC concentration below 10 mg/l from the same study area. Von Bromssen et al (2007) showed that they got DOC values within 1-6 mg/l. Similarly Robinson et al. (2011) also found that the average DOC concentration within the Matlab was 1 to 5.5 mg/l.

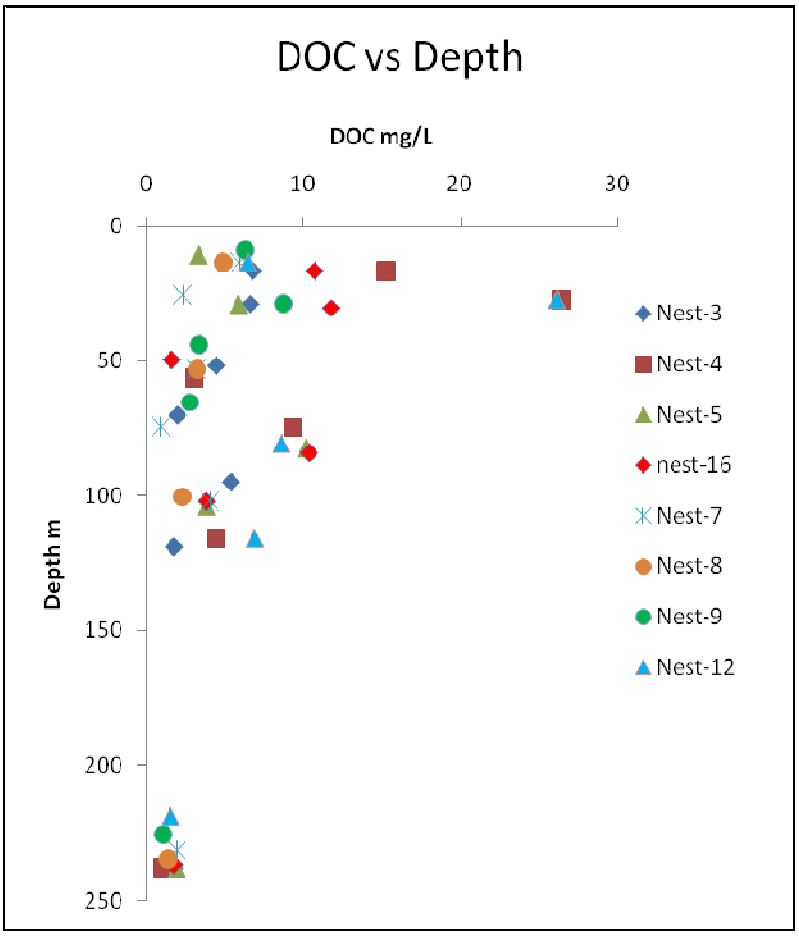

Figure 5.25 Variations of DOC concentrations in the well waters from selected piezometers from North and South Matlab.(Nests 3, 4, 5, 7, 8, 9, 12, 16)

Summary of Water Chemistry

Overall, the groundwaters from the whole study area showed a pH in the range of 6.5 to 7.5 and was predominately Ca-Mg-HCO_3^- or Na-Cl-HCO_3^- types or mixture of both two (**Figure 5.26**) depending upon depths and colors of the sediments. Groundwaters extracted from grey and dark grey sediments in shallow aquifer showed Ca-Mg-HCO_3 type waters. Intermediate and deeper depths contain light grey sediments and mostly Na^+ and Cl^- types. Intermediate depth waters had a mixture of Ca-Mg-HCO_3 and Na-Cl-HCO_3 types of waters. Deeper depth aquifers showed Na-Ca-Cl type waters. SO_4^{2-} concentrations were very low in Matlab andwithin 0 to 3 mg/l range.

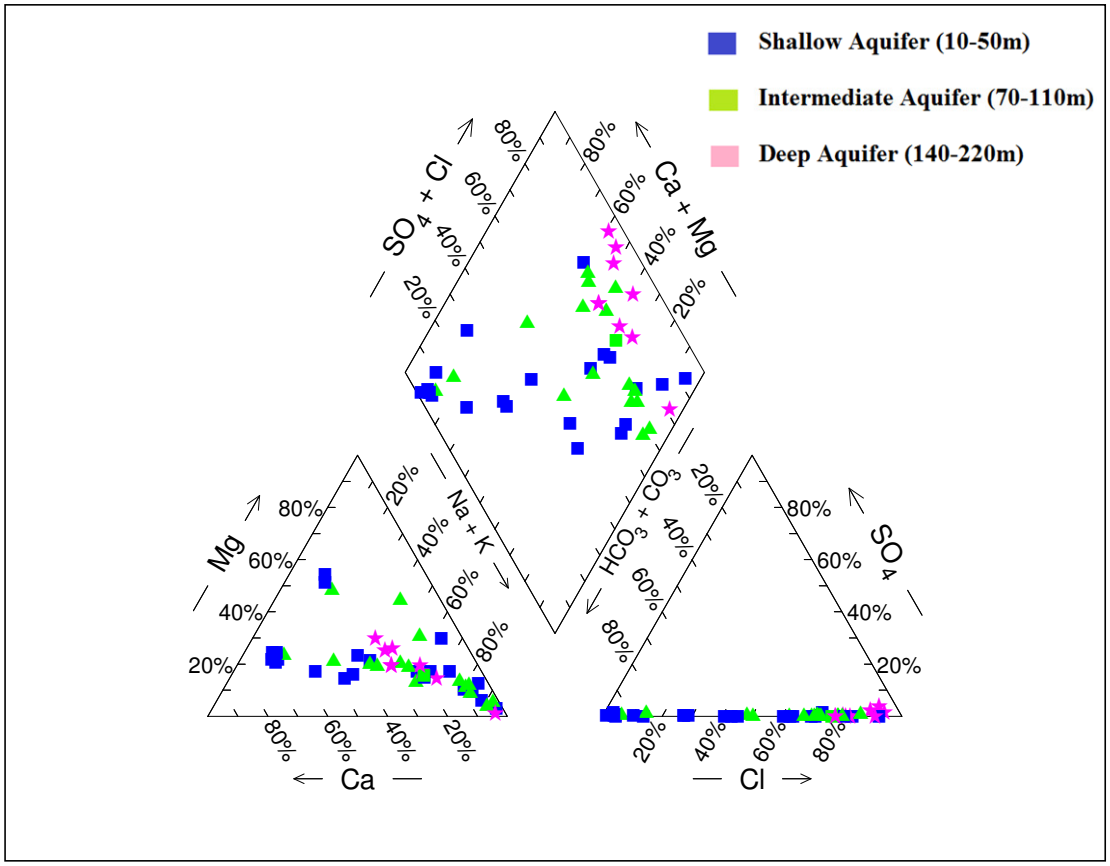

Figure 5.26 Major ion composition of the groundwater samples plotted on a Piper diagram as varying with depths.

Microbial Community Analyses

The community richness of bacteria in the sediment was estimated using Mothur v.1.1.0 (Schloss et al., 2009). 16S rRNA gene sequences were clustered into operational taxonomic units (OTUs) based on an average nucleotide similarity at fixed cutoff 0.03. Sequences with an average nucleotide similarity of 97% were binned together into single OTUs. (**Appendix-14**)

After getting the sequencing data, those data were analyzed using Mothur OpenSource Software for delineating bacterial communities and their statistical significance. For improveing our dataset we removed the sequencing errors from sequences, those sequences were taken which had average length of more than 200. For more clear sequencing dataset we removed chimeras and those sequences that classified as "Chloroplast", "Mitochondria", or "unknown" as well as archea and eukaryotic 16S rRNAs, those are not realted with present work. When the dataset were prepared, they were run for different OTU based analyses (statistical analyses) (alpha and beta diversity analyses) and pylogenetic tree. The methods in detailed are described in **Appendix-14).**

As a result of the analyses, total of 101 different bacterial families were recognized by Mothur. But only main 7-8 bacterical families constitute almost 70-90% of total percentage of bacterial group present. Main bacterial groups as within different depth sediment samples were *Bacterionvoraceae, Burkholderiaceae, Comamonadacee, Erysipelotrichaceae, Oxalobacteraceae, Moraxellaceae, Pseudomonadaceae, Rhodocyclaceae, Streptomycetaceae, Xanthomonadaceae etc* (**Figure 5.27**). Some OTUs were classified as bacterial families, which contain species known to be capable of dissimilatory iron reduction. Those bacterial groups are *Acetobacteraceae, Aeromonadaceae, Enterobacteriaceae and Rhodocyclaceae* (as in **Figure 5.28**).

Rarefaction analyses demonstrated that there was a large variation in the total number of OTUs between the samples. Shallow depths 10 and 27m had highest number of OTUs whereas 65m depth samples had lowest OTUs. It appeared that the alpha diversity of samples was related to the sediment depth: the number of OTUs per sample was highest at sediment depth 10 m and lowest at sediment depth 65 m. Although 101 bacterial families were present in the 8 specific depth samples, less than six families comprised more than 5% of the community in most of the samples (**Figure 5.27**).

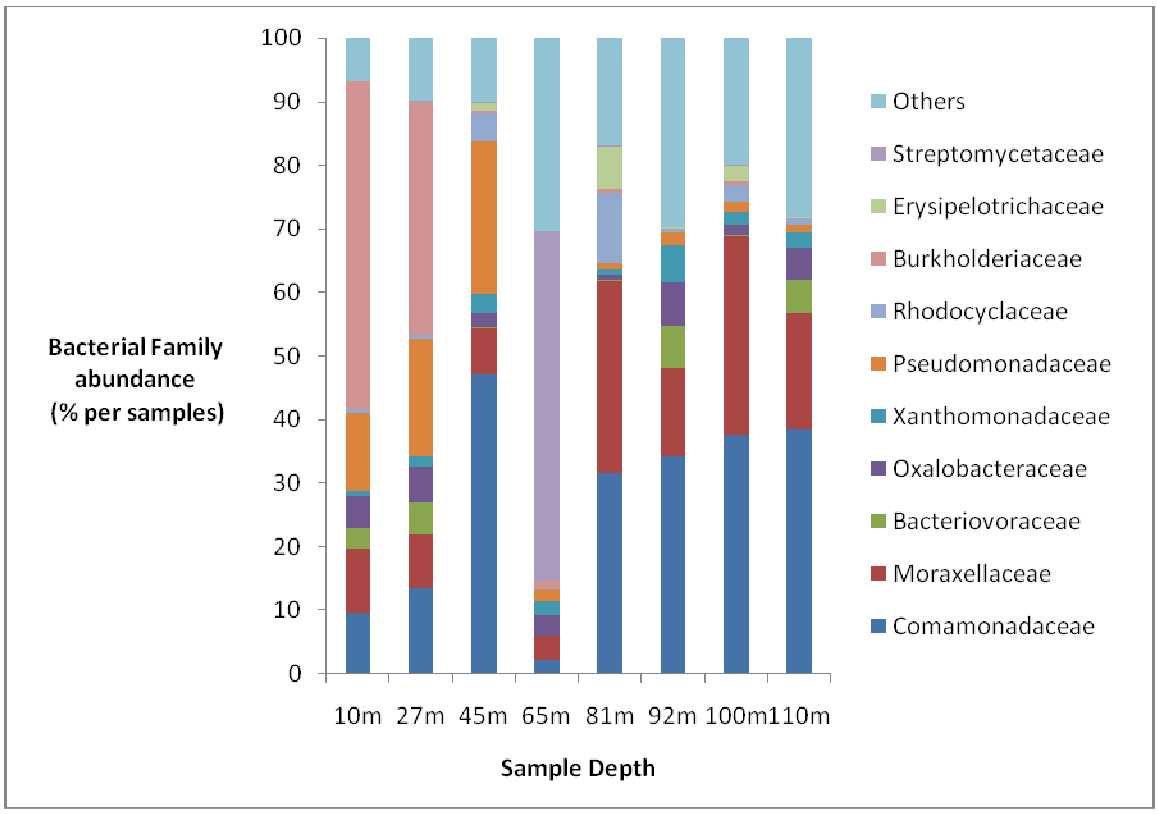

Figure 5.27 Taxonomic distribution of sequences grouped within the bacterial families as present in different depth samples from Core 2 of Nest 5 of South Matlab(groups with at least 5% average relative abundance).

Comamonadaceae and *Moraxellaceae* were more within (81m to 110m) samples in the core. But their percentanges were different in different depth samples. Most of the smaples have common bacterial family with different percentage. Some samples also have other different distinguishable bacterial families. Samples collected from 10m, 27m and 45m depths showed common bacterial families were *Comamonadaceae, Moraxellaceae* and *Pseudomonadaceae*, whereas in 10m and 27m samples one other one major predominant bacterial community *Burkholderiaceae* was present. This *Burkholderiaceae* family contains some pathogenic bacterial species (Briggs et al. 1988; Sutton et al., 2009). Some but not all species of *Burkholderiacea* are pathogens. If the sequences classified as *Burkholderiaceae* in our samples are from pathogenic species, then their presence suggests that human sewage is infiltrating the shallow portions of the aquifer. However, we have no confirmation that the sequences classified as *Burkholderiacea* were actually from pathogens. These 10m and 27m samples were from fine-sand size aquifer with gray color (black) sediments. 45m samples were from very fine size grain aquifer and those

were also gray color (black color). 65m sample showed difference than any other samples in their bacterial community. *Streptomycetaceae* was the predominant family for 65m samples. The 65m sample was dark gray in color and mainly composed by very-fine sand, silt and clay. 50% of 81m, 92m, 100m and 110m samples were composed of *Comamonadaceae* and *Moraxellaceae* (**Figure 5.27**).

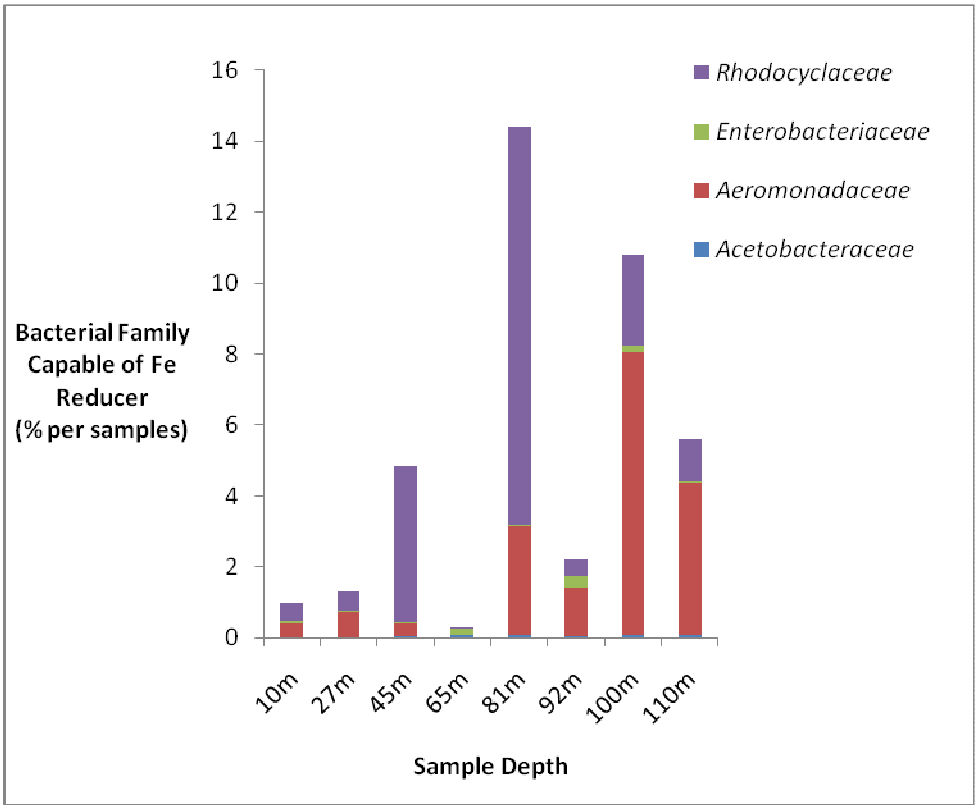

Figure 5.28 Taxonomic distribution of sequences within the family which may be capable to work as Fe reducing at different depths in core.

We separated those bacterial families which may be capable to work as Fe reducing bacteria from the other bacterial communities present in our core. We found that in our samples *Rhodocyclaceae, Enterobacteriaceae, Aeromonadaceae* and *Acetobacteraceae* were the families capable of Fe and other metal reducers. We found less percent of Fe reducing bacterial families in the samples of depths 10m, 27m, 65m and 92m. Percentages of total Fe reducers were less than 2% in these four samples. 10m, 27m and 65m samples were gray to dark gray in color and 92m sample was light gray color (tending to white).

45m and 110m samples had 6% capable of metal reducing bacteria. 81m and 100m samples had more metal reducing bacterial families than any other samples. That consituted almost 12% metal reducer bacterial families. The 81m and 100m samples were very fine sand, silt and clay mixed and dark gray in color.

We measured the similarity of the members and structures found in the various samples and visualize those similarities using the *Jaccard* and *Thetayc* coefficients. We use two non-parametric estimators to see what the predicted minimum number of overlapping OTUs is for the same samples using the summary-shared command. Later we generate a dendrogram to describe the similarity of the samples to each other. We created a dendrogram using the *jclass* and *thetayc* calculators within the *tree.shared* command. This command generates two newick-formatted tree files *final.an.thetayc.0.03.ave.tre* and *final.an.jclass.0.03.ave.tre* – which are the result of sub sampling. These tree files were visualized in software like TreeView and FigTree. Inspection of the both trees shows that individual communities cluster with themselves to the exclusion of the others (**Figure 5.29**). These analysed data postulated that different depth samples were related with their color, grain size, and bacterial community and dissolved arsenic concentrations. In the tree map 92m and 110m sediment samples were in same group which indicates they having similar kind of microbial community in addition to having medium to coarse grain sand size and light gray color (white). At these depths dissolved As concentration was less (<10 ug/L). Another microbial community group was made by 10m and 27 m depth sediment samples. Those two depths have more mica percentage (~5-10%) and they were fine sand size and gray in color (tending to black in color). Arsenic concentrations in this aquifer were 150-230 µg/L. The third group was made by 45m, 65m, 81m and 100m samples. All these samples were dark gray in color (black colored) and sediment size was mainly clay-silt. Dissolved As concentration of these samples were within 350-650 µg/L.This study enumerates significant relationships between bacterial community structure, percentage of clay fraction and sediment C, Mn, and Fe concentrations for each of these samples which suggest correlations with levels of As contamination. The statistical measure that was used to calculate similarity was *thetayc*. The statistics were performed on OTU's defined at 97% similarity (**Figure 5.29**).

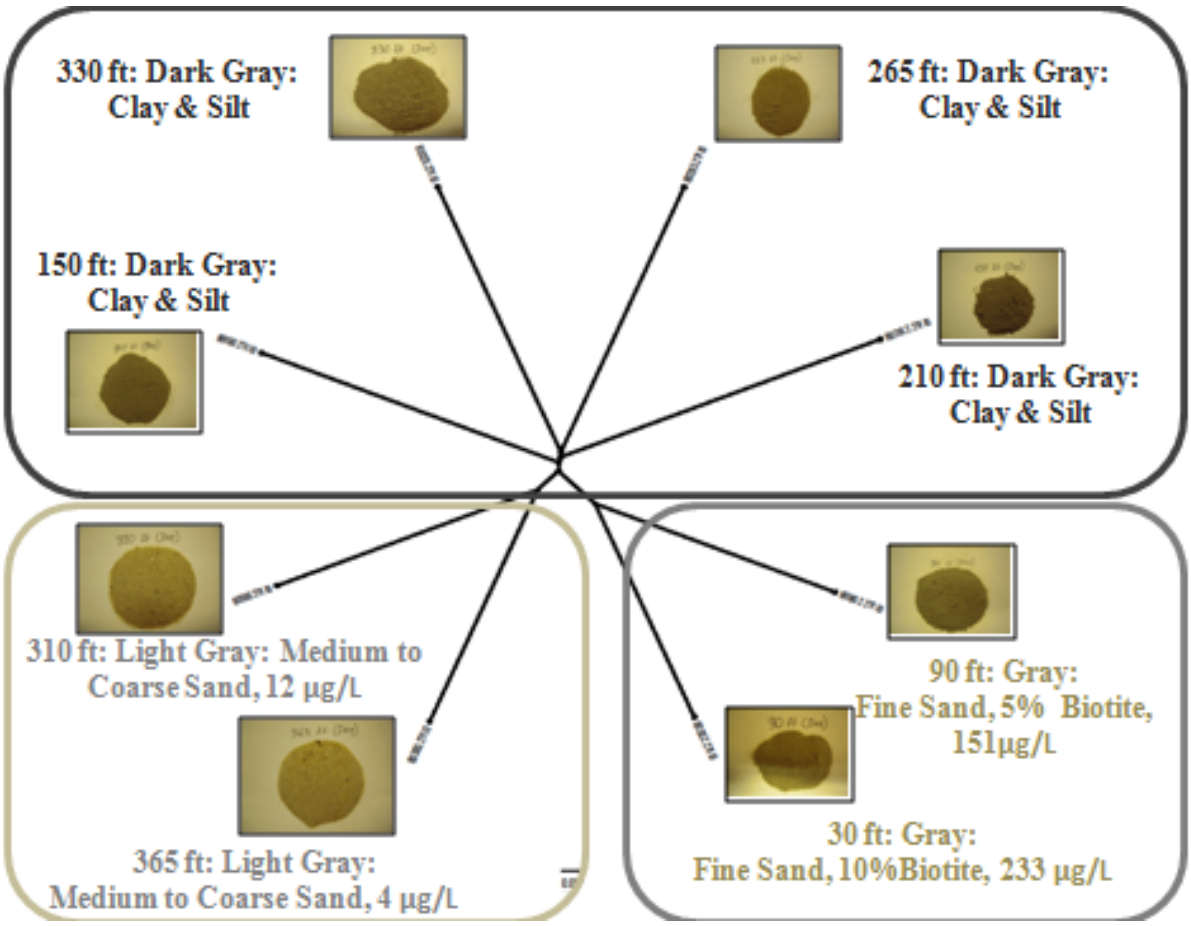

Figure 5.29 Relation of bacterical community, grain size and sediment color within the Core-2 South Matlab.

label	group	method	nseqs	coverage	sobs	invsimpson	Invsimpson-lci	invsimpson_hci	chao	chao_lci	chao_hci
0.03	10m	ave	2080	0.96	149.43	4.81	4.45	5.24	330.11	247.03	484.13
0.03	27m	ave	2080	0.95	177.98	7.98	7.34	8.74	350.51	276.33	480.78
0.03	45m	ave	2080	0.91	291.60	7.26	6.74	7.86	761.32	598.37	1010.98
0.03	65m	ave	2080	0.98	198.00	38.32	35.19	42.07	234.03	215.81	270.89
0.03	81m	ave	2080	0.88	344.16	10.03	9.29	10.90	997.28	785.86	1310.06
0.03	92m	ave	2080	0.91	315.72	28.03	25.70	30.81	675.88	551.65	865.60
0.03	100m	ave	2080	0.88	339.89	10.50	9.62	11.55	1091.51	841.11	1467.25

Table 5.1: Statistical results when calculating subsamples each to the number of sequences in the sample with the fewest 2080 nseqs (65m)

The number of sequences was different in different samples. Sequence number was highest in 10m sample which was 7409. Lowest number of sequence was in the 65m samples: 2080. In the mother, samples run with their lowest number of sequence as 2080 for sub-grouping and statistical analyses. At 0.03 OUT cutoff average coverage (community difersity) of the samples were 92% where highest coverage was in 65m samples and lowest were in 81 and 100m samples 88%. Sobs (observed community richness) shows the observed community richness in a group. Statistical data showed that sobs in light grey was 149 to 291, dark grey was 339 to 344 and light grey was 236 to 315. The parameter inverse-simpson is preferred to measure alpha-diversity because it is an indication of the richness in a community with uniform evenness that would have the same level of diversity. Same type of colored sediments showed similar values for inverse-simpson index. Inverse-Simpson for Grey colored shallow sediments' microbial communities was 4.45 to 7.34, 9.29 to 9.62 for dark grey colored sediments and 15.93 to 25.70 for light grey colored sediments (**Table 5.1**). Chao (Chao1 estimate of Community Richness) calculation is richness estimation for an OTU definition. Chao calculation gives the idea of microbial group's community richness. In the shallow grey colored sediment it is 330 to 765, for dark grey sediments microbial community it is highest 997 to 1037 and for light grey sediment the community richness is moderate respect to other colored groups which is 517 to 675.

T-test was used to see how different major bacterical communities were related with the sediment color variations. In most of the cases P values for grey/dark grey and light grey samples showed higher than 0.05. Only for major bacterical family e.g. *Pseudomonadaceae* shows P value 0.03 for grey and dark grey samples, which means grey and dark grey samples have significant diffferences with this bacterical family. For other major bacterial communities higher P value more than 0.1 were noted (**Figure 5.31**).

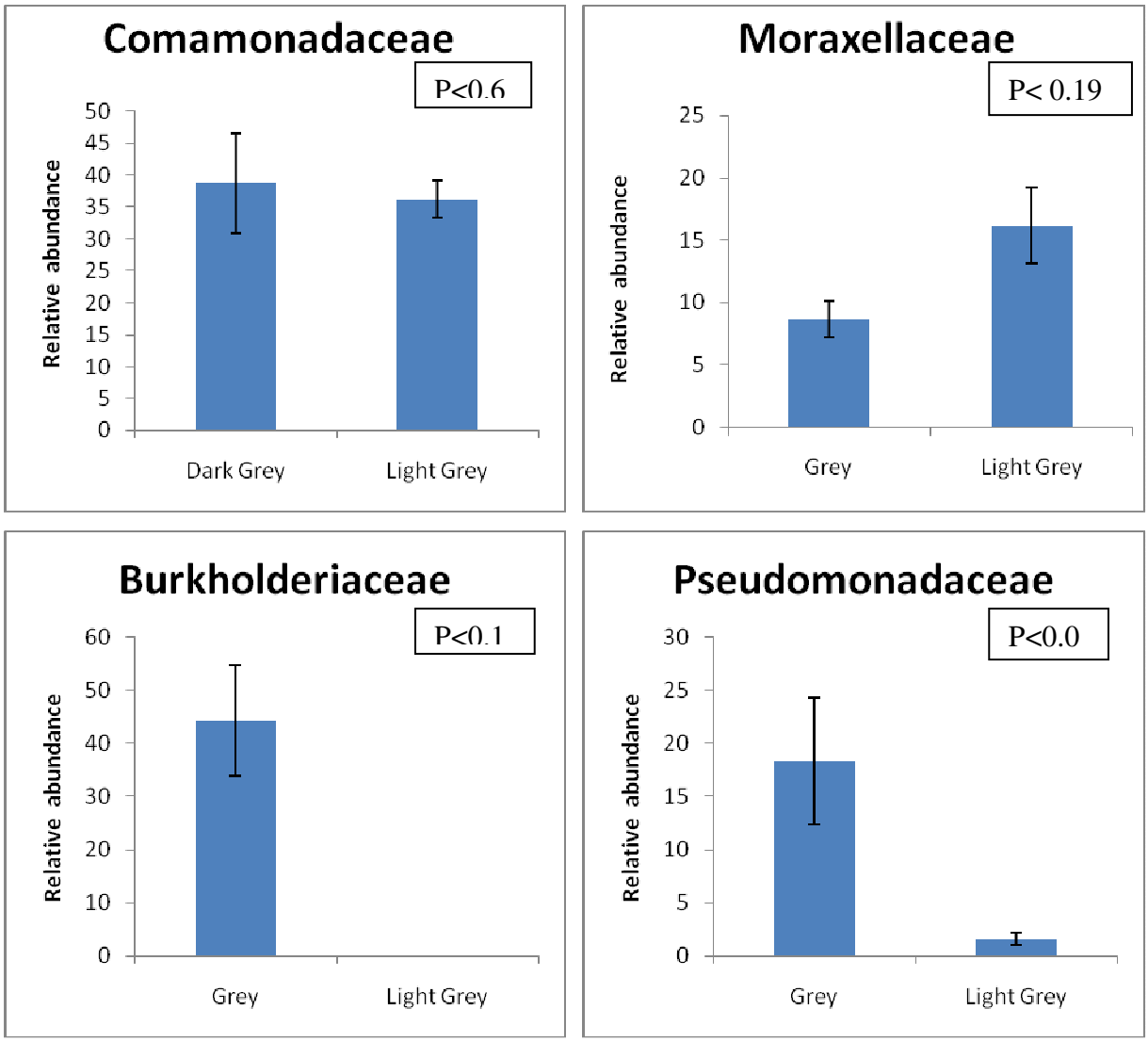

Figure 5.30 T-test results for common bacterical families present within different colored sediments. Here for the simplitcity we have charcaterised the two groups of colours of sediments- Grey (with higher dissolved As) and Light grey (with lower dissolved As).

T-test for capable of Fe reducer families also showed no correlation or significance for different colored sediment. In all samples P value is very high which is more than 0.2(**Figure 5.31**).

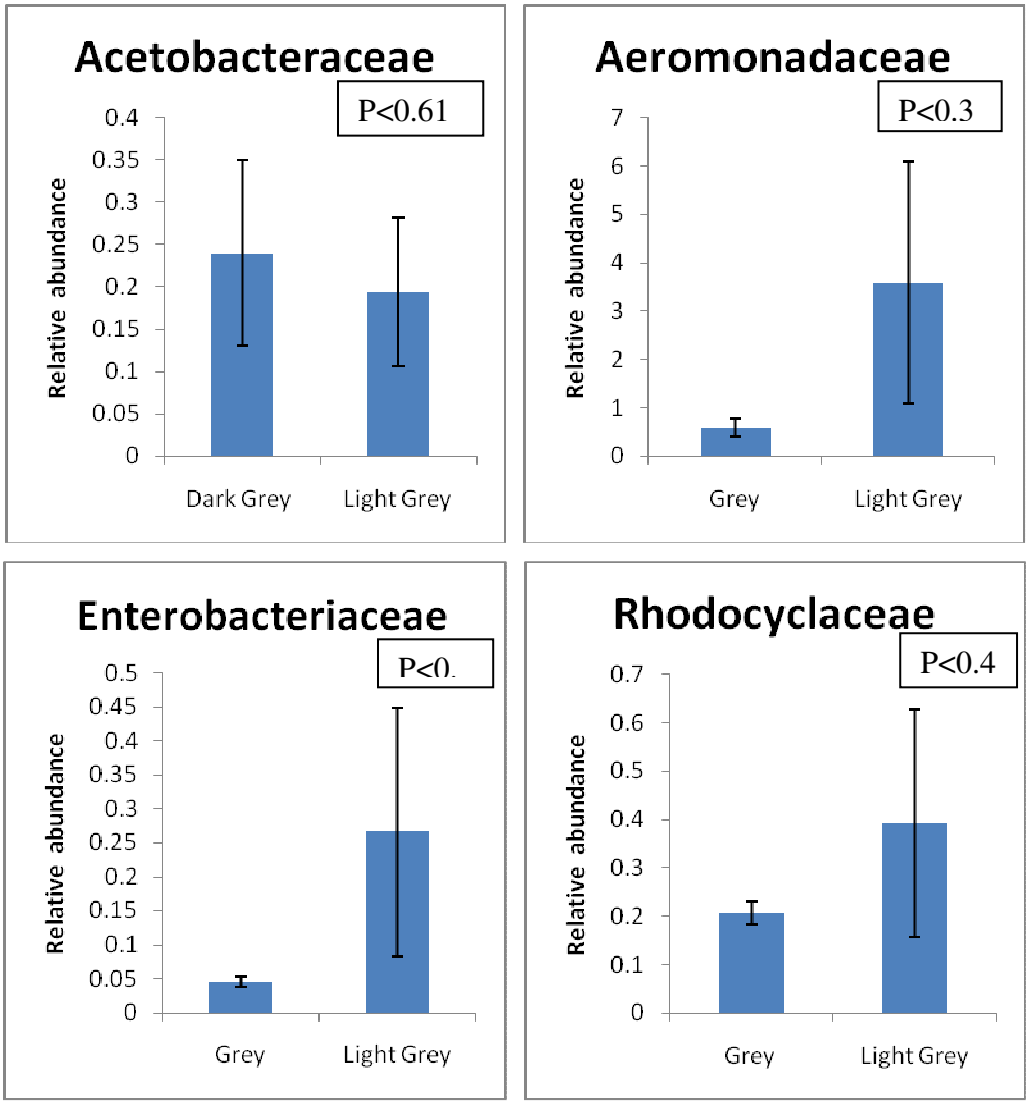

Figure 5.31 T-test results for bacterical families which are capable to reduce Fe in different color. Here for the simplitcity we have charcaterised the two groups of colours of sediments- Grey (with higher dissolved As) and Light grey (with lower dissolved As).

Chapter 6 - Discussion

We will discuss here under several subheadings our major findings from this work but we categorized four important questions that are answered.

1. How geology, geomorphology and lithology control the release of As from grey-dark grey and light grey sediments into Matlab groundwaters?

The most important differences between sediments within shallow depths are having grey or dark grey color versus sediments in intermediate depth with light grey color. These two different sediment types are important for their bulk As concentrations. From this study we found that grey and dark grey sediments contain higher As enriched water but light grey sediments show much lower or trace amounts of dissolved As. Mineralogy between grey and dark grey and light grey sediments show significant differences. It is known that certain minerals can house a suite of trace elements, including As. Grey and dark grey sediments showed ~30-40% weathered feldspar, biotite, muscovite and clay agglomerates. In contrast, light grey sediments are composed by ~80-85% quartz, with the remainder of the grains being Fe-oxides, micas and weathered feldspar.

Grey and dark grey sediments contained highly weathered minerals where As can be associated with metal oxides (particularly Fe and Mn) (Ahmed et al., 2004), since they have high specific surface areas and thus show high adsorption capacity (Zahid et al., 2009), sulfides (Polizzotto et al., 2006; Saunders et al., 2008 and references therein) and it can be absorbed on the surfaces of other minerals like carbonates (Smedley and Kinniburgh, 2002) and clays like illite (Lin and Puls, 2000, 2003; Pal et al., 2002), kaolinite (Raymahashay et al., 2003; Mukherjee et al., 2009b and references therein), and sometimes associated with chlorite (Pal et al., 2002). These types of minerals (with the exception of sulfides which are yet to be studied) were all found within the aquifer sediments in the study areas of North and South Matlab, and could be potential sources and/or sinks for As, depending upon redox conditions of aquifer sediment-water interfaces, nature of organic matter, and sediment texture(s) (Tareq et al., 2003).

Sediment particle size is also a relevant factor with regard to arsenic mobility. This may be a reflection of the grain sizes of the aquifer particles, generally fine to medium sand, in which As is less likely to associate except when it is present within an Fe-rich coating on the sand. These

types of light grey sediment aquifers probably contain little to no dissolved As for several reasons. If As was previously present in these aquifers, it could have been flushed from the aquifer during the mid-late Pleistocene Glacial Maximum when hydraulic gradients were steeper than they are today. This may be a reasonable explanation if recent deposition of this light grey sediment was relatively arsenic-free. Another plausible scenario is As could be stored in the ubiquitous Fe-rich coatings (or Fe-rich phases) found on many aquifer particles (Imam et al., 1997) which have been shown to contain more than 2000 mg/kg As in some cases (Ravenscroft et al., 2005 and references therein). Arsenic could also be sequestered in the Fe(III) oxyhydroxides due to the oxidizing nature of the sandy aquifers.

Shallow sediments in Matlab show high concentrations of As, Fe and Mn were observed, along with prominent lath-shaped biotite grains. Biotite has been shown to sorb As on its surface (Seddique et al., 2008; Hasan et al., 2009; Nath et al., 2009). High amounts of As correlating with high Ca, Mg, Fe, K, and Al in the deeper sediments could also result from presence of biotite (Mg, Fe, K, and Al) which was observed in significant amounts in thin sections. In the shallow depths of the sediment core (~60m), weathering of biotites (Seddique et al., 2008; Hasan et al., 2009) and Fe-oxides (Swartz et al., 2004), and possibly carbonates (Smedley and Kinniburgh, 2002) may be responsible for releasing As into the groundwater.

The highest amounts of As were identified in the shallow grey and dark grey sediments in Matlab within the silt/very fine sand fractions. Other high concentrations of As in sediments were found in some of the intermediate depths in the grey, very fine and fine size sand. The high proportion of bulk Fe(t) in the shallow core sediments, may indicate a strongly reducing environment. A weak correlation of aqua regia-extractable Fe and As may be related to differences in mineralogy between the high and low As sediments, a major portion of Fe being retained in more refractory minerals (possibly accompanied by a significant redistribution of As to a mobilizable phase on the surface of aquifer particles (Horneman et al., 2004)), or it may just be due to heterogeneity of the sediments. The slight correlation of As with Mn relates that As might be associated with Mn-oxides or clay minerals.

The SEM-EDX analyses showed that the elements Fe and Mn are in close association in most cases. The SEM mapping by superposing total Fe over Mn also indicates coexistence in both elements. The single elemental maps of As also showed that As is distributed throughout the sediments even if it is in very minute concentration.

Overall analyses revealed that As concentration is more in clay-rich sediments than in the sandy sediments. Fe and Mn concentrations within sediments vary similarly with As. The total digestion results thus indicate that mineralogically similar fractions of the sediments house the As, but favorable subsurface redox conditions only favor the release of As from the grey and dark grey sediments. In both North and South Matlab wherever there is a change in concentration of As, Mn and Fe(t) concentration will also change. As and Fe(t) and Fe(t) and Mn are positively correlated both in high As and low As sediments. This could be due to the adsorption of As within Fe and Mn oxyhydroxides (Rüde et al., 1997; Harvey et al., 2002; Sahai et al., 2007; Gasparatos, 2013).

Selective As extraction studies showed two major sinks for As: amorphous Fe(III) oxide (35% ± 10% of total extracted As) and well crystallized Fe and Al oxides (25% ± 10% of total extracted As), both of which are reasonable fractions on which As can be adsorbed and co-precipitated. Some ions works as dominating ion in aquifer like HCO_3^- and PO_4^{3-} which compete with As species for adsorption sites on mineral surfaces, thus releasing As into groundwater. In shallow sediments from North and South Matlab, 1.2 mg/kg (~8% of total As) was in the easily exchangeable phase, which indicates that it could be easily displaced from the sediment and mobilized into the groundwater. Silicates, sulfides, and organic matter are not affected in this phase, and Fe and Mn oxides should not be significantly solubilized (Tessier, et al., 1979). Also in the shallow sediments, 8.2 mg/kg (~50% of total As) was in the specifically sorbed (to mineral surfaces (e.g. goethite (Keon et al., 2001)) phase. Approximately 3.4 mg/kg (~27% of total As) was associated with amorphous and poorly-crystalline hydrous Fe oxides, which are thermodynamically unstable under anoxic conditions (Tessier et al., 1979). Manganese concentrations in the Matlab sediments were 14 and 33 mg/kg (14% and 32% of total Mn) was found in the same respective fractions. Sediment was grey in color at this depth, indicating enough reducing conditions that the Fe- (and Mn) oxyhydroxides could be dissolved over time, thus releasing structurally bound/co-precipitated arsenic.

Bulk XANES results showed most of the sediments have As^{3+} which means that sediments were deposited in reducing hence probably sulfidic environment and still they are retained in reducing condition. Some sediments show coexistence of both As^{3+} and As^{5+} by showing a broad peak covering 11871eV for As^{3+} and 11874for As^{5+} as also shown in Polizzotto et al., 2006. The dissociation of Fe^{3+} oxyhydroxides (FeOOH) reduction by anaerobic bacteria in

the presence of organic matter can cause the reduction of FeOOH bound As^{5+} to As $^{3+}$, which is more mobile and can get into the circulating groundwater system, thus causing arsenic toxicity (Nickson et al., 2000; Smedley and Kinniburgh 2002; Goldberg, 2002; van Geen et al., 2004; McArthur et al., 2004; Lloyd and Oremland, 2006).

Several distinct differences were found among sediments from light grey (intermediate and deeper depth) and grey and dark grey (shallow depth) and within the sediment cores CS 1 and 2 themselves. First and foremost, the color of sediments was light grey (sometime orange-brown to reddish-brown) in the low-As bearing aquifers in deeper depth, which is indicative of high proportions of Fe(III) and mixed Fe(II)/Fe(III) phases (i.e. redox conditions). In shallow depth aquifer, sediment colors were chiefly grey and dark grey in the high-As bearing aquifer sediment. The reason for this link between color and As concentration is that dissolved As concentrations are high (> 50 μg/l) where there is complete reduction of FeOOH, such that the FeOOH has released all its sorbed As into solution. That is, as FeOOH disappears, the aquifer becomes grey in color as also proposed by McArthur et al., 2004. A depositional environment rich in organic matter facilitates the complete reduction of FeOOH (McArthur et al., 2004, Van geen et al., 2009). When sorbed As is released by Mn oxides, it does not remain in solution if FeOOH reduction is incomplete, rather the As sorbs to FeOOH, and the sediments tend to be brown in color.

High Fe(II) values corresponded with (relatively) low phosphate concentrations in the sediments (and vice versa) in Matlab, for which competitive ion-exchange (upon reductive dissolution of Fe-oxyhydroxides) seems to be a plausible explanation. Also, the biotite and apatite in grey and dark grey sediments may be due to weathering to release As from the sediments, which is evidenced by sequential extraction results of As being predominantly present in the specifically-sorbed phase and associated with amorphous and poorly-crystalline hydrous oxides of Fe (and Al and Mn), as well as a significant amount of As in the residual phases in some instances. Another point to be made here is that results from total digestions and sequential extractions and results from SEM are correlated for most of these cores.

2. Controls of redox mechanisms and groundwater chemistry in release of As from grey-dark grey and light grey aquifers

Presence of lower dissolved ionic concentrations occurred in water as a result of extensive flushing from the higher elevation Pleistocene aquifers showed low condutivity**.** Dissolved oxygen (DO) and oxidation reduction potential (ORP) in high As contaminated waters in South and North Matlab were slightly higher than that would be expected for high-As waters, but were still in the upper range of anoxic or sub-oxic conditions for most samples. These higher values may have resulted from rapid partial oxidation during sampling, while DO and ORP values for low-As waters were matching for generally highly oxidized aquifers.

Aqueous speciation and spatial variability of Arsenic associated with light grey colored-aquifer waters in Matlab with low concentrations of dissolved As most likely is due to a combination of the following reasons: amount of As (< 10-12 mg/kg) were detected in the solid phase; anoxic conditions are not prevalent (waters were high in SO_4^{2-}concentrations) in the Pleistocene aquifers in this study area that can facilitate reduction of Fe-oxyhydroxides; and presence of extremely low concentrations (or complete absence in some wells) of phosphate (PO_4^{3-}) and low HCO_3^- concentrations (light grey sediment aquifer waters) that, if present, possibly could compete with arsenate (As^{5+}) for adsorption sites on mineral surfaces.

Groundwaters associated with grey to dark grey sediments from Matlab contained elevated concentrations of dissolved As, and close to 700 µg/l levels in some wells. A probable cause for significantly elevated levels of dissolved As in the groundwaters here is the reducing condition in the aquifers, which is enhanced when coupled with microbial oxidation of natural organic matter (BGS and DPHE, 2001; Harvey et al., 2005 and references therein). In Matlab, As concentrations are mostly related with color variations in sediments in the study area to demonstrate grey and dark grey colors containing elevated As concentration and light grey colored sediment containing much less of dissolved As. This could be due to local variations in groundwater flow paths caused by well pumping, or a redox front (Nickson et al., 1998; Nath et al., 2005, Von bromssen et al., 2008). McArthur et al. 2008, 2012 attributed this type of spatial variation to microbial weathering of As-rich lenses associated with paleomeanders comprising pockets of As-bearing minerals on the flanks of a buried paleochannels or oxbow lakes.

In Matlab, high groundwater As concentrations were vertically distributed over a range of 20 m that could result from As release in the shallow subsurface and later transport to depth in

the highly permeable sandy aquifers, as also the case cited by Polizzotto et al., 2006 (as shown in Munshiganj, Bangladesh 15 km away from Matlab). It can also be due to a wide zone of As bearing minerals undergoing reductive dissolution in these grey and dark grey sediments, or possibly a combination of both scenarios.

In light grey colored sediments from South and North Matlab, deeper groundwaters (> 100 m) are slightly contaminated (some well showed As at 20-25µg/l), which may be explained by very low As concentrations in the sediments or possibly from As-bearing waters from above making their way along narrow flow paths into deeper parts of the aquifers. The majority of the total As being As(III) in which As speciation was done is a reflection of the redox conditions of the aquifers, whether it is widespread or localized only in some areas. As(III) is more mobile in the subsurface (Polizzotto et al., 2006). Polizzotto et al. 2006 also states that in the presence of strongly reducing conditions in the subsurface, As(III) remains stable as As(V) is continuously reduced to As(III). Thus, accumulation of As(III) around certain well screens, coupled with possible microbial reduction of ferric iron and As(V).

High HCO_3^- concentrations may correlate with weathering of carbonates and degradation of organic matter under local reducing conditions coupled with Fe-(oxy)(hydr)oxide dissolution (Mukherjee-Goswami et al., 2008 and references therein). The presence of high ratios of Fe(II):FeT in Matlab indicate reducing conditions(Robinson et al., 2011) that, upon dissolution of the Fe-bearing hydrous oxides, could release HCO_3^- into the groundwater, along with phosphate and arsenic. Dissolved phosphate and As concentrations both show positive correlation with HCO_3^- concentrations. Low concentrations of HCO_3^- and relatively high oxygen content in waters with low dissolved As may indicate unfavorable conditions for both carbonate dissolution or reduction and subsequent dissolution of Fe oxyhydroxides (von bromssen et al., 2007., Robenson et al., 2011).

Nitrate and nitrite values were low simply due to the reducing condition of the aquifers in high-As areas. A reason sulfate values are less in water with high As may be due to a negligible amount of sulfide minerals present in the sediment; in XANES data it was shown that only negligible amount of sulfer bearing mineral (as sulfides) was present in our sediments. It would be expected under these reducing conditions that S-bearing minerals would not undergo complete or possibly not even partial dissolution. The low amounts of sulfate detected may have

been dissolved in the shallow subsurface where more oxidizing conditions existed and then transported to depth via groundwater flow (Polizzotto et al., 2006).

In tubewell waters where cations were measured, dissolved Fe was generally lower in light grey sediments than in other grey and dark grey sediments. Overall, concentrations of dissolved Mg and Ca were relatively similar, owing possibly to weathering of mafic and felsic minerals. Shallow (10 to 80 m) groundwaters mostly plotted along with the lines of the GMW and LMW. Intermediate depths (85 to 120 m) were mainly clustered along the GMWL and LMWL between -30‰ and -17‰ for δ^2H and from -5‰ and -4‰ for $\delta^{18}O$, mostly owing to non-evaporative waters. The deepest (130-220 m) tubewells sampled were more depleted than all the other tubewells, suggesting a paleo-recharge‘during a different climatic period (Mukherjee et al., 2007b) and possibly a separation from the shallower aquifer from which most of the other well water samples were collected. When values for δ^2H and $\delta^{18}O$ are viewed on the local scales, several more trends become apparent. All tubewell waters in the light grey sediment aquifer of Matlab plotted on or below the LMWL and the GMWL, which is significantly different from grey and dark grey colored sediment aquifer. δ^2H and $\delta^{18}O$ values for precipitation (Mukherjee et al., 2007b) and groundwaters (both shallow, intermediate and deep tubewell waters) all plotted on or just below the GMWL and the LMWL, had groundwaters plotted close with the GMWL and LMWL, there may had been evidence of some degree of mixing between pond water and precipitation and/or river water (Datta et al., 2011). Lighter values for $\delta^{18}O$ in deeper wells may result from older water that was recharged from similar precipitation further from the area and has followed a longer flow path for a long period of time and may have been subjected to some evaporation. This is just speculation since groundwater dating was not done in this study.

Concentrations of dissolved constituents in waters, points to reducing conditions (high Fe, DOC, HCO_3^-, PO_4^{3-}, NH_4^+, and elevated AsT; with low NO_3^-, NO_2^-, Cl^- and SO_4^{2-}) in high-As bearing grey and dark grey sediment aquifers. Stable isotope values for δ^2H and $\delta^{18}O$ indicate precipitation as predominant source of recharge to the aquifers. The spatial variability of dissolved As concentrations is complex and may be the result of multiple factors including spatially and temporally variable flow paths induced by flooding conditions and well-pumping. Deeper groundwaters though show very low dissolved As, but they can be sustainable as As-safe zones in the long run. Light grey sediment water consisted of low Fe, DOC, HCO^{3-}, PO_4^{3-}, NH_4^+, and high Cl^- and SO_4^{2-}.

3. Controls of sediment bacterial community in facilitating release of As from grey-dark grey sediments to groundwater

Bacterial community structures South Matlab cores are significantly related to various parameters we studied: tubewell locations, sediment grain size, and chemical differences in groundwater associated with these sediments, including percent silt and sediment C, total As, total Mn and total Fe concentrations. Families of different bacterial groups were abundant with their sediment color and grain size. It's showed that similar grain size with similar color contain almost same amount of total As, Mn, Fe, TOC in sediment also they have silimar type of bacterial families in there sediments.

In this present study, we found that shifts in bacterial community structures were related to changes in the sediment grain size distribution and changes in sediment C, As, Mn and Fe. Here it is shown that bacterial community structures are significantly related to sediment grain size is supported by other works that have shown that sediment grain size influences bacterial community structure. Silts and clay typically have higher concentrations of organic matter. Sandy sediments, characterized by grain sizes larger than 150μm, usually contain lower organic carbon and metal concentrations because they are mainly fromed by quartz grain (Legg et al.,2012). In other works it showed that heavy metal concentrations have been shown to correlate with bacterial community structures and function in both soil and groundwater environments (Stefanowicz et al., 2008)

In our study it showed that bacterial community structure is closely related with their color and As concentration in water. Dark gray sediments have similar type of bacterical community and theose sediments also showed similar percentage of higer level of As contamination which is close to 700μg/l. Gray colored sediment have also higher concentration of As and all grey sediments have similar type of bacterial community. This are showed that release of As from the sediments is related with bacterial community present in the sediments. This represent that bacterial community structure is significantly correlated to sediment characteristics, such as percentage of silt, sediment C, and sediment metal concentrations, which are related to groundwater As concentrations. Thus, the relationship between the proportion of different common bacterial community in our sediments and percent of clay and concentrations of C and Fe in the aquifer sediments may have important implications for understanding how the native microbial community influences groundwater As mobility at South Matlab. Sediment extraction

showed that significant fraction of total solid phase As could be bioavailable incorporated into non-amorphous mineral phases.

The phylogenetic analyses of the bacterial community in the 110m light grey sediment showed that it shared limited amount of common OTUs with the bacterial community in the grey and dark grey sediments. This finding indicates that contrasting bacterial communities inhabit light grey and grey-dark grey sediments, and that these communities may have different potentials for substrate utilization and As(III) mobilization. Moreover, little amount of known Fe(III)- or As(V)- reducing bacteria (metal reducing bacteria) were initially detected in the light grey sediment. This present study sediment microbes haven't seen any sulfate reducing bacteria, which also represent a higher As contaminated environment.

4. Different processes that lead to more As release among grey-dark grey sediments than light grey sediments from Matlab, Bangladesh

Groundwaters are Ca–Mg–HCO_3^- types in shallow aquifers which are grey and dark grey colored, Mg-HCO_3^- in the intermediate depths which are light grey color and Na-K-Cl rich in the deeper aquifers which are light grey colored. DOC concentration is higher (26.4 mg/L) in the shallow aquifer waters but groundwater DOC concentration decreases with the depth and it is very low (~1 mg/L) in the deep aquifers. These variations correlate with the concentration of As with depth in these same groundwaters. Dissolved As concentration is high (~781µg/l) in shallow grey and dark grey sediments whereas light grey sediments at intermediate depth contain lower As (<10 µg/l, only two samples showing 27 and 52 µg/L). While correlating the sediment colors to the ionic constituents of respective associated groundwaters shows that for the dark grey togrey sediments (with high As), dissolved Mn, SO_4^{2-} and HCO_3^- show significant positive correlations with As concentrations while in the case of light grey sediments (showing <10ug/L of As) demonstrate significant positive correlation with DOC. Dissolved Fe_T on other hand in both sediments (light grey and grey) show good correlation with dissolved SO_4^{2-}.

Bulk extraction of sediments showed that shallow grey and dark grey sediments have the higher As concentration (~31 mg/kg) and light grey sediments have comparatively less As (~11mg/kg). Sequential extractions for sediment fractionations showed that most of the As was bound to amorphous and poorly crystalline hydrous oxides of Fe and Al phases. Synchrotron aided bulk-XANES studies conducted on solid state sediments revealed As and S speciation in

the core samples at different depths indicating the occurrences of hotspots of As distributed randomly in light grey and grey sediments. As^{5+} is the dominating species in both South and North Matlab sediments and only shallow 14m samples from North Matlab showed As^{3+}. Sediment S species - SO_4^{2-} and S^{2-} both are present in shallow 11m sediments from South Matlab and only SO_4^{2-} was present in North Matlab shallow 14m sediments. Core sediments from both North and South Matlab show a mineral assemblage as quartz, feldspar and clay minerals with various forms of mica, kaolinite and chlorites. Secondary Fe mineral assemblages are also dominant in the high As areas where the groundwater Fe^{+2} is high. This study though does not indicate direct associations of S and As phases within minerals, but it can be inferred that reduced S^{2-} phases can only occur in highly reducing environments.

More than 101 bacterial families were identified among the eight sediment samples from the South Matlab core and out of them fewer than six families comprised more than ~5% each of the community. *Comamonadaceae* and *Moraxellaceae* were commonly detected, but their abundances varied considerably with depth. Some of the sequences from each sample were grouped in families that contain species capable of metal reductions including *Rhodocyclaceae, Enterobacteriaceae, Aeromonadaceae and Acetobacteraceae* (families capable of reducing Fe and other metals too). Our results indicate significant relationships between bacterial community structure, grain size fractionation, dissolved As concentration and sediment C, Mn, and Fe concentrations for these samples from Matlab. Groundwater abstracted from these oxidized red brown and light grey sediments in contrast to reduced greyish sediments contain significantly lower amount of dissolved As and can be a source of safe water for the future.

Chapter 7 - Conclusions

Bangladesh and other neighboring regions characterized by deltaic system are facing a crisis of As-tainted drinking waters in their local to regional aquifers. The purpose of this study has been to identify a practical approach, based on sediment color, to identification of aquifers that can provide safe drinking water. The fitness of this pragmatic tool is supported by a geochemical analysis of the geological and biological mechanisms that control the mobilization of As and Mn in the aquifers of Matlab.

Sediment groups were distinguished on the basis of color into three groups: grey, dark grey and light grey sediments. Grey and dark grey sediments are composed mainly of very fine sand, silt and clay sized feldspar, mica, clay agglomerates and quartz grains. Light grey sediments are composed mainly of medium to coarse-grained quartz and feldspar sands. SEM-EDX analysis shows that the grey and dark grey sediments have higher As contents (0.43 wt%) than light grey sediments (0.11wt%), consistent with the results of bulk sediment extraction experiments (i.e. As concentrations of 22 to 31 mg/kg and 11 to 13.5 mg/kg in light and dark grey sediments, respectively). Sequential fractionations demonstrate that most of the As is sited within amorphous and poorly crystalline hydrous oxides of Fe and Al. Organic phases also show significant As associations. Both S^{2-} and SO_4^{2-} - are present, but the dominant arsenic species is As^{3+}.Although much attention has been given to As in recent years, the risk to human health from dissolved Mn needs further research, as Mn is a known neurotoxin (Merglar 1999; Wasserman et al., 2006). This study contributes to that much-needed body of knowledge. Our results show that almost 55-60% of the wells sampled in Matlab have Mn higher than WHO MCL guidelines of 0.4 mg/L. Grey and dark grey sediments from shallow depths (~90 m) have higher bulk sediment Mn, and sequential extraction experiments demonstrate that this Mn is associated with bioavailable amorphous phases. In contrast, at intermediate depths Mn appears to be associated with less bioavailable residual phases.

Microbial community distribution within the sediments is related to sediment grain size, color and bulk As concentrations. From our analyses we found 101 bacterial families. Ten bacterial groups form almost ~95% of the sample at each depth. Within these bacterial families there are four bacterial groups found capable of reducing As and other metals. Sulfate-reducing bacteria were not found within our core samples.

Stable isotope data show that precipitation is likely to be the main source of groundwater recharge for the shallow aquifer (< 60 m) of South and North Matlab, where dissolved As concentrations are significantly elevated. The presence of reducing conditions within the high-As aquifers is evident from a number of lines of evidence: high Fe(II):Fe_t in sediments, high As(III):As_T in the groundwaters, and elevated levels of dissolved Fe, HCO_3^-, PO_4^{3-}, NH_4^+, and low NO_3^-, NO_2^-, Cl^-, and SO_4^{2-}. These observations suggest that key geochemical processes in operation within the aquifer include reductive dissolution of hydrous Fe-oxides and weathering of As-bearing clays and biotite. We have shown that reduction of Fe-oxyhydroxides and concomitant release and mobilization of phosphate into solution may result in competitive ion exchange with arsenate (or possibly arsenite) sorbed onto other minerals. Indeed, for each mg/kg of P-extractable As in sediments in Matlab, ~350 μg/l of dissolved As were found in pore waters. Hence, both reductive dissolution and competitive ion exchange processes are likely to be involved in the release mechanisms of geogenic arsenic from solid phases into groundwaters.

Higher bacterial activity (indicated by presence of higher percentage Fe-reducing bacteria) is observed in medium to fine-grained, grey to dark grey sediments that are rich in organic matter, which facilitates faster reduction of FeOOH grain coatings. This is reflected in the higher As groundwater in South and North Matlab shallow aquifer compared to the oxidizing aquifers with light grey sediment at intermediate depths. Most of the Mn observed is associated with bioavailable amorphous phases, whereas As is mostly associated with specifically sorbed sediment phases. The release of As into groundwater can therefore be attributed to bacterially mediated reducing processes. High Cl/Br molar ratios (>2241, nest-8, 40m) indicate that external sewage influx near tubewells, or the presence of pit latrines, may be a source of anthropogenic contamination of the shallow aquifer in some of the tubewells. However, high Cl/ Br molar ratios can suppress the As release mechanism in this region (McArthur et al., 2012).

In summary, this study has shown that aquifers in North and South Matlab that have light grey colored sediments provide comparatively safe drinking water, having As and Mn concentrations that are below WHO limits. Because the light grey aquifer occurs at intermediate depths, it is also economically viable for drilling with local technology and for installing water wells. A longer term issue is how to manage this aquifer for safe drinking waters for a sustainable future. Over extraction of waters may lead to contamination of the aquifer over time, by drawdown of arsenic-laden waters from shallower aquifers.

References

Acharyya, S.K., Chakraborty, P., Lahiri, S., Raymahashay, B.C., Guha, S., Bhowmik, A. 1999. Arsenic poisoning in the Ganges delta. Nature. 401, 545.

Acharyya, S.K. and B.A. Shah. 2007. Groundwater arsenic contamination affecting different geologic domains in India – a review: influence of geologic setting, fluvial geomorphology and Quaternary stratigraphy. J. Env. Sci. Health. 42, 1795-1805.

Ahmed, K.M., Bhattacharya, P., Hasan, M.A., Akhter, S.H., Alam, S.M.M., Bhuyian,M.A.H., Imam, M.B., Khan, A.A., Sracek, O. 2004. Arsenic enrichment in groundwater of the alluvial aquifers in Bangladesh: an overview. App. Geochem. 19, 181-200.

Alam, M.G.M., Tokunaga, S., Maekawa, T. 2001. Extraction of arsenic in a synthetic arsenic-contaminated soil using phosphate. Chemosphere. 43, 1035-1041.

Andrade, S., Ulbrich, H.H., Janasi, V.A., Navarro, M.S. 2009. The determination of total hydrogen, carbon, nitrogen and sulfur in silicates, silicate rocks, soils and sediments. Geostandards and Geoanalytical Research. 33, 337-345.

Appelo, C.A.J. and D. Postma. 1996. Geochemistry, Groundwater and Pollution. Rotterdam: Balkema. Armienta, M.A. and N. Segovia. Arsenic and fluoride in the groundwater of Mexico. Environ. Geochem. Health. 30, 345-353.

Baig, J.A., Kazi, T.G., Shah, A.Q., Kandhro, G.A., Afridi, H.I., Arain, M.B., Jamali, M.K., Jalbani, N. 2010. Speciation and evaluation of Arsenic in surface water and groundwater samples: A multivariate case study. Ecotoxic. And Environ. Safety. 73, 914-923.

Bakr, M.A.: Quaternary geomorphic evolution of Brahmanbaria area, Comilla and Noakhali districts, Bangladesh. – Records of Geological Survey of Bangladesh. Vol. 1, part 2, 148pp., Dhaka 1976

BGS and DPHE (British Geological Survey and Department of Public Health and Engineering), 2001. Arsenic contamination of groundwater in Bangladesh. *In*: Kinniburgh, D.G., Smedley, P.L. (Eds.), British Geological Survey (Technical Report, WC/00/19. 4 Volumes) British Geological Survey, Keyworth.

Bostick, B.C. and S. Fendorf. 2003. Arsenite sorption on troilite (FeS) and pyrite (FeS2). Geochem. Cosmochim. Acta. 67, 909-921.

Bundschuh, J., Farias, B., Martin, R., Storniolo, A., Bhattacharya, P., Cortes, J., Bonorino, G., Albouy, R. 2004. Groundwater arsenic in the Chaco-Pampean Plain, Argentina: Case study from Robles County, Santiago del Estero Province. App. Geochem. 19, 231-243.

Bundschuh, J., Perez-Cerrera, A., Litter, M.I. 2008. Distribucion del arsenico en las regones Iberica e Iberoamericana. Ed. Prog. Iberoamericano de Ciencia y Technol. para el Desarrollo, Buenos Aires, Argentina.

Bundschuh, J., Armineta, M.A., Birkle, P., Bhattacharya, P., Matschullat, J., Mukherjee, A.B. 2009. Natural Arsenic in Groundwater of Latin America. *In*: Bundschuh, J. and P. Bhattacharya (series eds): Arsenic in the environment, Volume 1. CRC Press/Balkema Publisher, Leiden, The Netherlands.

Burgess, W.G., Hoque, M.A., Michael, H.A., Voss, C.I., Breit, G.N., Ahmed, K.M. 2010. Vulnerability of deep groundwater in the Bengal Aquifer System to contamination by arsenic. Nat. Geosci. 3, 83-87.

Burnol, A. and L. Charlet. 2010. Fe(II)—Fe(III)-bearing phases as a mineralogical control on the heterogeneity of arsenic in Southeast Asian groundwater. Environ. Sci. Technol. 44, 7541-7547.

Charlet, L. and Polya D.A. 2006. Arsenic in shallow, reducing groundwaters in southern Asia: An environmental health disaster. Elements. 2, 91-96.

Charlet, L., Chakraborty, S., Appelo, C.A.J., Roman-Ross, G., Nath, B., Ansari, A.A., Lanson, M., Chatterjee, D., Mallik, S.B., 2007. Chemodynamics of an arsenic ―hotspot‖ in a West Bengal aquifer: A field and reactive transport modeling study. App. Geochem. 22, 1273-1292.

Chappelle, F.H. 2001. Ground-water microbiology and geochemistry, John Wiley & Sons Ltd, New York.

Chen, Y., Parvez, F., Gamble, M., Islam, T., Ahmed, A., Argos, M., Graziano, J.H., Ahsan, H. 2009. Arsenic exposure at low-to-moderate levels and skin lesions, arsenic metabolism, neurological functions, and biomarkers for respiratory and cardiovascular diseases: Review of recent findings from the Health Effects of Arsenic Longitudinal Study (HEALS) in Bangladesh. Toxicol. Appl. Pharmacol. 239, 184-192.

Cheng, Z., Zheng, Y., Mortlock, R., van Geen, A., 2004. Rapid multielement analyses of groundwater by high-resolution inductively coupled plasma mass spectrometry. Anal. and Bioanal. Chem. 379, 513-518.

Clauer, N., and Chaudhuri, S. 1995. Clays in Crustal Environments (Isotope dating and Tracing). Springer, 359 p.

Coplen, T.B. 1994. Reporting of stable hydrogen, carbon, and oxygen isotope abundances. Pure & Appl. Chem. 66, 273-276.

Craig, H., 1961. Isotopic Variations in Meteoric Waters. Science. 133, 1702-1703.

Cullen, W.R. and K.J. Reimer. 1989. Arsenic speciation in the environment. Chemical Reviews. 89, 713-764.

Das, D., Basu, G., Chowdhury, T.R., Chakraborty, D. 1995. Bore-hole soil-sediment analyses of some As affected areas. *In*: Proc. Int. Conf. on Arsenic in groundwater: cause, effect and remedy.

Datta, S., Mailloux, B., Jung, H.B., Hoque, M.A., Stute, M., Ahmed, K.M., Zheng, Y., 2009. Redox trapping of arsenic during groundwater discharge in sediments from the Meghna riverbank in Bangladesh. Proc. Natl. Acad. Sci. 106, 16930-16935.

Datta,S., Neal, A., Johannesson, K., Haug, J., Sarkar, D., Sur,P., Purkait, B. 2010a. Geochemical and mineralogical contrasts between low and very high arsenic affected areas in North and South Matlab district, West Bengal, India. Arsenic in Geosphere and Human Diseases. Eds. Jean, J.S., Bundschuh, J., Bhattacharya, p. 110-111.

Datta, S., Johannesson, K., Neal, A., Haug, J., Socki, R., Ocheltree, T. 2010b. Stable isotopic evaluation of arsenic hotspots and grey and dark grey aquifers in North and South Matlab, West Bengal, India. GSA AbsTracts with Programs, Vol. 42, No. 5, p. 551. Abstract # 181534. National meeting, Denver, CO.

Dhar, R.K., Biswas, B.K., Samanta, G., Mandal, B.K., Chakraborti, D., Roy, S., Jafar, A., Islam, A., Ara, G., Kabir, S., Khan, A.W., Ahmed, S.A., Hadi, S.A., 1997. Groundwater arsenic calamity in Bangladesh. Current Science. 73, 48-59.

Dhar, R. K., Y. Zheng, P. Rubenstone, van Geen, A. 2004. A rapid colorimetric method for measuring arsenic concentration in groundwater. Analytica Chimica Acta. 526, 203-209.

Dhar, R.K., Zheng, Y., Stute, M., van Geen, A., Cheng, Z., Shanewaz, M., Shamsudduha, M., Hoque, M.A., Rahman, M.W., Ahmed, K.M., 2008. Temporal variability of groundwater

chemistry in shallow and deep aquifers of Araihazar, Bangladesh. J. Cont. Hydrol. 99, 97-111.

Dickens, G. R., Koelling, M., Smith, D. C., & Schnieders, L. (2007). Rhizon sampling of pore waters on scientific drilling expeditions: an example from the IODP Expedition 302, Arctic Coring Expedition (ACEX). Scientific Drilling, 4(4), 1-4.

Dowling, C.B., Poreda, R.J., Basu, A.R., Peters, S.L. 2002. Geochemical study of arsenic release mechanisms in the Bengal Basin groundwater. Water Resour. Res. 38, 1173.

Dzombak D.A. and F.M.M. Morel. 1990. Surface Complexation Modeling- Hydrous Ferric Oxide. John Wiley, New York.

Ficklin, W.H. 1983. Separation of As(III) and As(V) in ground waters by ion-exchange. Talanta. 30, 371-373.

Fendorf, S., Michael, H.A., van Geen, A. 2010. Spatial and temporal variations of groundwater arsenic in South and Southeast Asia. Science. 328, 1123-1127.

Garai, R., Chakraborty, A.K., Dey, S.B., Saha, K.C. 1984. Chronic arsenic poisoning from tube-well water. J. Indian Med. Assoc. 82, 34-35.

Garcia, M.E. and J. Bundschuh. 2006. Control mechanisms of seasonal variation of dissolved arsenic and heavy metal concentrations in surface waters of Lake Poopo basin, Bolivia. GSA Annual Meeting, Philadelphia, 22-25 Oct, 2006. 38(7):320.

Garzanti, E., Ando, S., France-Lanord, C., Vezzoli, G., Censi, P., Galy, V., Najman, Y. 2010. Mineralogical and chemical variability of fluvial sediments 1. Bedload sand (Ganga-Brahmaputra, Bangladesh). Earth Plan. Sci. Letters. 299, 368-381.

Ghosh, A.K., Sarkar, D., Bhattacharyya, P., Maurya, U.K., Nayak, D.C. 2006. Mineralogical study of some arsenic contaminated soils of West Bengal, India. Geoderma. 136, 300-309.

Goodbred, S.L., Kuehl, S.A., Steckler, M.S., Sarker, M.H. 2003. Controls on facies distribution and stratigraphic preservation in the Ganges-Brahmaputra delta sequence. Sed. Geol. 155, 301-316.

Guha Mazumder, D.N., Haque, R., Ghosh, N., Binay, K.D., Santra, A., Chakraborty, D., Smith, A.H. 1998. Arsenic levels in drinking water and the prevalence of skin lesions in West Bengal, India. Int. J. Epidemiol. 21, 871-877.

Hamon, R.E., McLaughlin, M.J., Gilkes, R.J., Rate, A.W., Zarcinas, B., Robertson, A., Cozens, G., Radford, N., Bettenay, L. 2004. Geochemical indices allow estimation of heavy metal background concentrations in soils. Global Biogeochemical Cycles. 18, GB1014.

Haque, S.E., Johannesson, K.H. 2006. Arsenic concentrations and speciation along a groundwater flow path: The Carrizo Sand aquifer, Texas, USA. Chem. Geol. 228, 57-71.

Haque, S., Junfeng, J., Johannesson, K.H. 2008. Evaluation mobilization and transport of arsenic in sediments and groundwaters of Aquia aquifer, Maryland, USA. J. Cont. Hydrol. 99, 68-84.

Harvey, C.F., Swartz, C.H., Badruzzaman, A.B.M., Keon-Blute, N., Yu, W., Ali, M.A., Jay, J., Beckie, R., Niedan, V., Brabander, D., Oates, P.M., Ashfaque, K.N., Islam, S., Hemond, H.F., Ahmed, M.F., 2002. Arsenic mobility and groundwater extraction in Bangladesh. Science. 298, 1602-1606.

Harvey, C.F., Swartz, C.H., Badruzzaman, A.B.M., Keon-Blute, N., Yu, W., Ali, M.A., Jay, J., Beckie, R., Niedan, V., Brabander, D., Oates, P.M., Ashfaque, K.N., Islam, S., Hemond, H.F., Ahmed, M.F., 2005. Groundwater arsenic contamination on the Ganges Delta: biogeochemistry, hydrology, human perturbations, and human suffering on a large scale. C.R. Geoscience. 337, 285-296.

Harvey, C.F., Ashfaque, K.N., Yu, W., Badruzzaman, A.B.M., Ali, M.A., Oates, P.M., Michael, H.A., Neumann, R.B., Beckie, R., Islam, S., Ahmed, M.F. 2006. Groundwater dynamics and arsenic contamination in Bangladesh. Chem. Geol. 228, 112-136.

Hasan, M.A., von Brömssen, M., Bhattacharya, P., Ahmed, K.M., Siker, A.M., Jacks, G., Sracek, O., 2009. Geochemistry and mineralogy of shallow alluvial aquifers in DaudMatlab upazila in the Meghna flood plain, Bangladesh. Environ. Geol. 57, 499-511.

He, Y.T., Fitzmaurice, A.G., Bilgin, A., Choi, S., O'Day, P., Horst, J., Harrington, J., Reisinger, H.J., Burris, D.R., Hering, J.G. 2010. Geochemical processes controlling arsenic mobility in groundwater: A case study of arsenic mobilization and natural attenuation. App. Geochem. 25, 69-80.

Héry, Marina, Athanasios Rizoulis, Hervé Sanguin, David A. Cooke, Richard D. Pancost, David A. Polya, and Jonathan R. Lloyd. "Microbial ecology of arsenic-mobilizing Cambodian sediments: lithological controls uncovered by stable-isotope probing." Environmental microbiology (2014).

Hopenhayn, C. 2006. Arsenic in drinking water: impact on human health. Elements. 2, 103-107.

Hoque, M.A., Khan, A.A., Shamsudduha, M., Hossain, M.S., Islam, T., Chowdhury, S.H. 2009. Near surface lithology and spatial variation of arsenic in the shallow groundwater: southeastern Bangladesh. Environ. Geol. 56, 1687-1695.

Horneman, A., van Geen, A., Kent, D., Mathe, P. E., Zheng, Y., Dhar, R. K., O'Connell, S., Hoque, M.A., Aziz, Z., Shamsudduha, M., Seddique, A., Ahmed, K. M. 2004. Decoupling of arsenic and iron release to Bangladesh groundwater under reducing conditions. Part I: Evidence from sediment profiles. Geochim. Cosmochim. Acta. *68*, 3459-3473.

Imam, B., Alam, M., Akhter, S.H., Choudhury, S.Q., Hasan, M.A., Ahmed, K.M. 1997. Sedimentological and mineralogical studies on arsenic contaminated aquifers in Bangladesh. Department of Geology, Dhaka University, for Bangladesh Water Development Board.

Itai, T., Takahashi, Y., Seddique, A.A., Maruoka, T., Mitamura, M. 2010. Variations in the redox state of As and Fe measured by X-ray absorption spectroscopy in aquifers of Bangladesh and their effect on As adsorption. App. Geochem. 25, 34-47.

Jakariya, M., Vahter, M., Rahman, M., Wahed, M.A., Hore, S.K., Bhattacharya, P., Jacks, G., Persson, L.A. 2007. Screening of arsenic in tubewell water with field test kits: evaluation of the method from public health perspective. Sci. Total Environ. 379, 167-175.

Jung, H.B., Zheng, Y. 2006. Enhanced recovery of arsenite sorbed onto synthetic oxides by L-ascorbic acid addition to phosphate solution: calibrating a sequential leaching method for the speciation analyses of arsenic in natural samples. Water Res. 40, 2168-2180.

Kane, J.S., Arbogast, B.F., Leventhal, J.S. 1990. Characterization of Devonian Ohio Shale SDO-1 as a USGS geochemical reference sample. Geostandards Newsletter. 14, 169-196.

Keon, N.E., Swartz, C., Brabander, D.J., Harvey, C., Hemond, H.F. 2001. Validation of an arsenic sequential extraction method for evaluation mobility in sediments. Env. Sci. Technol. 35, 2778-2784.

Kocar, B.D., Herbel, M.J., Tufano, K.J., Fendorf, S. 2006. Contrasting effects of dissimilatory iron(III) and arsenic(V) reduction on arsenic retention and transport. Environ. Sci. Technol. 40, 6715-6721.

Kuznetsova, A.I., Rusakova, Y.A., Zarubina, O.V. 1999. Quality tests for determination of trace elements in mineral samples. J. Anal. Chem. 54, 898-902.

Langmuir, D. 1997. Aqueous environmental geochemistry. Upper Saddle River, New Jersey, Prentice Hall, 600 p.

Lawson, M., Ballentine, C.J., Polya, D.A., Boyce, A.J., Mondal, D., Chatterjee, D., Majumder, S., Biswas, A. 2008. The geochemical and isotopic composition of ground waters in West Bengal: tracing ground-surface water interaction and its role in arsenic release. Mineralogical Magazine. 72, 441-444.

Legg, Teresa M., Yan Zheng, Bailey Simone, Kathleen A. Radloff, Natalie Mladenov, Antonio González, Dan Knights et al. "Carbon, metals, and grain size correlate with bacterial community structure in sediments of a high arsenic aquifer." Frontiers in microbiology 3 (2012).

Lin, Z. and Puls, R.W. 2000. Adsorption, desorption and oxidation of arsenic affected by clay minerals and aging process. Environ. Geol. 39, 753-759.

Lin, N.F., Tang, J., Bian, J.M. 2002. Characteristics of environmental geochemistry in the arseniasis area of the Inner Mongolia of China. Environ. Geochem. Health. 24, 249-259.

Lin, Z. and Puls, R.W. 2003. Potential indicators for the assessment of arsenic natural attenuation in the subsurface. Adv. Environ. Res. 7, 825-834.

Loeppert, R.H., Jain, A., Abd El-Haleem, M.A., Biswas, B.K. 2003. Quantity and speciation of arsenic in soils by chemical extraction. *In*: Biogeochemistry of environmentally important trace elements. 42-56.

Lozano, R. and J.P. Bernal. 2005. Characterization of a new set of eight geochemical reference materials for XRF major and trace element analyses. Revista Mexicana de Ciencias Geologicas. 22, 329-344.

Luo, Z.D., Zhang, Y.M., Ma, L. 1997. Chronic arsenicism and cancer in inner Mongolia – consequences of well-water arsenic level greater than 50 mg/l . *In*: Arsenic Exposure and Health Effects (eds C.O. Abernathy, R.L. Calderon and W.R. Chappell), Chapman and Hall, London.

Magrisso, S., Belkin, S., Erel, Y. 2009. Lead bioavailability in soil and soil components. Water Air and Soil Pollution. 202, 315-323.

Mailloux, B.J., Alexandrova, E., Keimowitz, A.R., Wovkulich, K., Freyer, G.A., Herron, M., Stolz, J.F., Kenna, T.C., Pichler, T., Polizzotto, M.L., Dong, H., Bishop, M., Knappett

P.S.K., 2009. Microbial mineral weathering for nutrient acquisition releases arsenic. App. Env. Microbiol. 75, 2558-2565.

Manning, B.A, and Goldberg, S. 1996. Modeling competitive adsorption of arsenate with phosphate and molybdate on oxide minerals. Soil Sci. Soc. Am. J. 60, 121-131.

Mason, B. and L.G. Berry. 1978. Elements of Mineralogy. New York. Freeman.

McArthur, J.M., Ravenscroft, P., Safiulla, S., Thirlwall, M.F., 2001. Arsenic in groundwater: Testing pollution mechanisms for sedimentary aquifers in Bangladesh. Water Resour. Res. 37, 109-117.

McArthur, J.M., Banerjee, D.M., Hudson-Edwards, K.A., Mishra, R., Purohit, R., Ravenscroft, P., Cronin, A., Howarth, R.J., Chatterjee, A., Talukder, T., Lowry, D., Houghton, S., Chadha, D.K., 2004. Natural organic matter in sedimentary basins and its relation to arsenic in anoxic ground water: the example of West Bengal and its worldwide implications. App. Geochem, 19, 1255-1293.

McArthur, J.M., Ravenscroft, P., Banerjee, D.M., Milsom, J., Hudson-Edwards, K.A., Sengupta, S., Bristow, C., Sarkar, A., Tonkin, S., Purohit, R., 2008. How paleosols influence groundwater flow and arsenic pollution: A model from the Bengal Basin and its worldwide implication. Water Resour. Res. 44, W11411.

McArthur, J.M., Banerjee, D.M., Sengupta, S., Ravenscroft, P., Klump, S., Sarkar, A., Disch, B., Kipfer, R. 2010. Migraton of As, and 3He/3H ages, in groundwater from West Bengal: Implications for monitoring. Water Res. 44, 4171-4185.

Mergler, Donna. "Neurotoxic effects of low level exposure to manganese in human populations." *Environmental Research* 80, no. 2 (1999): 99-102.

Meng, X.G., Bang, S., Korfiatis, G.P. 2000. Effects of silicate, sulfate, and carbonate on arsenic removal by ferric chloride. Water Res. 34, 1255-1261.

Michael, H.A. and C. Voss. 2009. Controls on groundwater flow in the Bengal Basin of India and Bangladesh: regional modeling analyses. Hydrogeol. J. 17, 1561-1577.

Mirza, B. S., Muruganandam, S., Meng, X., Sorensen, D. L., Dupont, R. R., & McLean, J. E. (2014). Arsenic (V) Reduction in Relation to Iron (III) Transformation and Molecular Characterization of the Structural and Functional Microbial Community in Sediments of a Basin-Fill Aquifer in Northern Utah. *Applied and environmental microbiology*, *80*(10), 3198-3208.

Hossain, Mohammed, Prosun Bhattacharya, Shaun K. Frape, Gunnar Jacks, M. Mainul Islam, M. Moklesur Rahman, Mattias von Brömssen, M. Aziz Hasan, and Kazi Matin Ahmed. "Sediment color tool for targeting arsenic-safe aquifers for the installation of shallow drinking water tubewells." *Science of The Total Environment* 493 (2014): 615-625.

Morgan, J.P. and W.G. McIntire. 1959. Quaternary geology of Bengal Basin, East Pakistan, and India. GSA Bulletin. 70, 319-342

Mumford, A. C., Barringer, J. L., Benzel, W. M., Reilly, P. A., & Young, L. Y. (2012). Microbial transformations of arsenic: mobilization from glauconitic sediments to water. *Water research*, *46*(9), 2859-2868.

Mukherjee, A., Fryar, A.E., Howell, P.D. 2007a. Regional hydrostratigraphy and groundwater flow modeling in the arsenic-affected areas of the western Bengal basin, West Bengal, India. Hydrogeol. J. 15, 1397-1418.

Mukherjee, A., Fryar, A.E., Rowe, H. D., 2007b. Regional scale stable isotopic signatures of recharge and deep groundwater in the arsenic affected areas of West Bengal, India. 334, 151-161.

Mukherjee, A., von Brömssen, M., Scanlon, B., Bhattacharya, P., Fryar, A.E., Hasan, M.A., Ahmed, K.M., Chatterjee, D., Jacks, G., Sracek, O., 2008. Hydrogeochemical comparison and effects of overlapping redox zones on groundwater arsenic near the Western (Meghna sub-basin, India) and Eastern (Meghna sub-basin, Bangladesh) margins of the Bengal Basin. J. Cont. Hydrol. 99, 31-48.

Mukherjee, A., Fryar, A.E., Thomas, W.A., 2009a. Geologic, geomorphic and hydrologic framework and evolution of the Bengal basin, India and Bangladesh. J. Asian Earth. Sci. 34, 227-244.

Mukherjee, A., Fryar, A.E., O'Shea, B.M. 2009b. Major occurrences of elevated arsenic in groundwater and other natural waters. *In*: Arsenic: environmental chemistry, health threats and waste treatment. John Wiley & Sons Ltd, New York.

Mukherjee, A., Fryar, A.E., Bhattacharya, P. 2010. Regional to local-scale extent and controls on existence of deeper groundwater arsenic in western parts of Bengal Basin. GSA Program with AbsTracts. 42, 550.

Mukherjee-Goswami, A., Nath, B., Jana, J., Sahu, S.J., Sarkar, M.J., Jacks, G., Bhattacharya, P., Mukherjee, A., Polya, D.A., Jean, J., Chatterjee, D., 2008. Hydrogeochemical behavior of

arsenic-enriched groundwater in the deltaic environment: Comparison between two study sites in West Bengal, India. J. Cont. Hydro. 99, 22-30.

Naidu, R., Smith, E., Owens, G., Bhattacharya, P., Nadebaum, P. 2006. Managing arsenic in the environment from soil to human health. Australia: CSIRO Publishing, 656 p.

Naidu, R., Smith, E., Huq, S.M.I, Owens, G., 2009. Sorption and bioavailability of arsenic in selected Bangladesh soils. Environ. Geochem. Health. 31, 61-68.

Nath, B., Berner, Z., Basu Mallik, S., Chatterjee, D., Charlet, L., Stuben, D., 2005. Characterization of aquifers conducting groundwaters with low and high arsenic concentrations: a comparative case study from West Bengal, India. Mineral Magazine. 69, 841-853.

Nath, B., Sahu, S.J., Jana, J., Mukherjee-Goswami, A.; Roy, S., Sarkar, M.J., Chatterjee, D. 2008. Hydrochemistry of arsenic-enriched aquifer from rural West Bengal, India: A study of the arsenic exposure and mitigation option. Water Air Soil Pollut. 190, 95-113.

Nath, B., Chakraborty, S., Burnol, A., Stuben, D., Chatterjee, D., Charlet, L. 2009. Mobility of arsenic in the sub-surface environment: An integrated hydrogeochemical study and sorption model of the sandy aquifer materials. J. Hydrol. 364, 236-248.

Neumann, R.B., Ashfaque, K.N., Badruzzaman, A.B.M., Ali, M.A., Shoemaker, J.K., Harvey, C.F., 2010. Anthropogenic influences on groundwater arsenic concentrations in Bangladesh. Nat. Geosci. 3, 46-52.

Nicolli, H.B., Suriano, J.M., Peal, M.A.G., Ferpozzi, L.H., Baleani, O.A. 1989. Groundwater contamination with arsenic and other trace-elements in an area of the Pampa, province of Cordoba, Argentina. Environ. Geol. Water Sci. 14, 3-16.

Nickson, R., McArthur, J.M., Burgess, W.G., Ahmed, K.M., Ravenscroft, P. Rahman, M., 1998. Arsenic poisoning in Bangladesh groundwater. Nature. 395, 338.

Nickson, R., McArthur, J.M., Ravenscroft, P., Burgess, W.G., Ahmed, K.M. 2000. Mechanism of arsenic release to groundwater, Bangladesh and West Bengal. App. Geochem. 15, 403-413.

Nordstrom, D.K. 2000. An overview of arsenic mass poisoning in Bangladesh and West Bengal India. *In*: Young, C. (Ed.), Minor Elements 2000. Processing and Environmental Aspects of As, Sb, Se, Te, and Bi. Society for Mining, Metallurgy and Exploration, p. 21-30.

Nordstrom, D.K. 2002. Public health – worldwide concerns of arsenic in groundwater. Science. 296, 2143-2145.

O'Shea, B.M. 2006. Delineating the source, geochemical sinks and aqueous mobilization processes of naturally occurring arsenic in a coastal sandy aquifer, Stuarts Point, New South Wales, Australia. Ph.D. thesis. University of New South Wales, Sydney.

Pal, T., Mukherjee, P.K., Sengupta, S., Bhattacharya, A.K., Shome, S. 2002. Arsenic pollution in groundwater of West Bengal, India – An insight into the problem by subsurface sediment analyses. Gondwana Res. 5, 501-512.

Parvez, F., Chen, Y., Brandt-Rauf, P.W., Slavkovich, V., Islam, T., Ahmed, A., Argos, M., Hassan, R., Yunus, M., Haque, S.E., Balac, O., Graziano, J.H., Ahsan, H. 2010. A prospective study of respiratory symptoms associated with chronic arsenic exposure in Bangladesh: findings from the Health Effects of Arsenic Longitudinal Study (HEALS). Thorax. 65, 528-533.

PHED (Public Health Engineering Department). 1991. Arsenic pollution in groundwater in West Bengal. Report of arsenic investigation project to the National Drinking Water Mission, Delhi, India.

Plant, J.A., Kinniburgh, D.G., Smedley, P.L., Fordyce, F.M., Klinck, B.A. 2003. Arsenic and Selenium. British Geological Survey, Keyworth, Nottingham, UK. 50 p.

Polizzotto, M.L., Harvey, C.F., Sutton, S.R., Fendorf, S., 2005. Processes conducive to the release and transport of arsenic into aquifers of Bangladesh. Proc. Natl. Acad. Sci. 102, 18819-18823.

Polizzotto, M.L., Harvey, C.F., Li, G., Badruzzman, B., Ali, A., Newville, M., Sutton, S., Fendorf, S., 2006. Solid-phases and desorption processes of arsenic within Bangladesh sediments. Chem. Geology. 228, 97-111.

Polizzotto, M.L., Kocar, B.D., Benner, S.G., Sampson, M., Fendorf, S. 2008. Near-surface wetland sediments as a source of arsenic release to ground water in Asia. Nature. 454, 505-U5.

Radloff, K.A., Cheng, Z.Q., Rahman, M.W., Ahmed, K.M., Mailloux, B.J., Juhl, A.R., Schlosser, P., van Geen, A. 2007. Mobilization of arsenic during one-year incubations of grey aquifer sands from Araihazar, Bangladesh. Environ. Sci. Technol. 41, 3639-3645.

Rahman, M.M., Naidu, R., Bhattacharya, P. 2009. Arsenic contamination in groundwater in the Southeast Asia region. Environ. Geochem. Health. 31, 9-21.

Ravenscroft, P. 2003. Overview of the hydrogeology of Bangladesh. *In*: Rahman, A.A., Ravenscroft, P. (eds.) Groundwater resources development in Bangladesh. The University Press, Dhaka 43-86.

Ravenscroft, P., Burgess, W.G., Ahmed, K.M., Burren, M., Perrin, J., 2005. Arsenic in groundwater of the Bengal Basin, Bangladesh: Distribution, field relations, and hydrogeological setting. Hydrogeo. J. 13, 727-751

Raymahashay, B.C., Khare, A.S. 2003. The arsenic cycle in Late Quaternary fluvial sediments: mineralogical considerations. Current Science. 84, 1102-1104.

Reza, A.H.M.S., Jean, J-S., Yang, H-J., Lee, M-K., Woodall, B., Liu, C-C., Lee, J-F., Luo, S-D. 2010. Occurrence of arsenic in core sediments and groundwater in the Chapai-Nawabganj District, northwestern Bangladesh. Water Res. 44, 2010-2037.

Robinson, Clare, Mattias von Brömssen, Prosun Bhattacharya, Sara Häller, Annelie Bivén, Mohammed Hossain, Gunnar Jacks, Kazi Matin Ahmed, M. Aziz Hasan, and Roger Thunvik. "Dynamics of arsenic adsorption in the targeted arsenic-safe aquifers in Matlab, south-eastern Bangladesh: Insight from experimental studies." *Applied Geochemistry* 26, no. 4 (2011): 624-635.

Saha, A.K. and C. Chakrabarti. 1995. Geological and geochemical background of the As bearing groundwater occurrences of West Bengal. *In*: Proc. Int. Conf. on Arsenic in groundwater: cause, effect and remedy.

Shamsudduha, M., Hoque, M.A., Ahmed, K.M. 2005. Geochemical and hydrogeological contrasts between shallow and deeper aquifers in two villages of Araihazar, Bangladesh: Implications for deeper aquifers as drinking water sources. Geochim. Cosmochim. Acta. 69, 5203-5218.

Sankararamakrishnan, K., Chauhan, D., Nickson, R.T., Tripathi, R.M., Iyengar, L. 2008. Evaluation of two commercial field test kits used for screening of groundwater for As in northern India. Sci. Total Environ. 401, 162-167.

Saunders, J.A., Mohammad, S., Korte, N.E., Lee, M.K., Fayek, M., Castle, D., Barnet., M.O. 2005. Groundwater geochemistry, microbiology, and mineralogy in two arsenic-bearing Holocene alluvial aquifers from the United States. Advances in arsenic research -

integration of experimental and observational: studies and implications for mitigation. ACS Symposium Series. 915, 191-205.

Saunders, J.A., Lee, M.K., Shamsudduha, M., Dhakal, P., Uddin, A., Chowdhury, M.T., Ahmed, K.M. 2008. Geochemistry and mineralogy of arsenic in (natural) anaerobic groundwaters. App. Geochem. 23, 3205-3214.

Seddique, A.A., Masuda, H., Mitamura, M., Shinoda, K., Yamanaka, T., Itai, T., Maruoka, T., Uesugi, K., Ahmed, K.M., Biswas, D.K. 2008. Arsenic release from biotite into a Holocene aquifer in Bangladesh. App. Geochem. 23, 2236-2248.

Seeberg-Elverfeldt, J., Schlüter, M., Feseker, T., & Kölling, M. (2005). Rhizon sampling of pore waters near the sediment/water interface of aquatic systems. Limnology and oceanography: Methods, 3, 361-371.

Sengupta, S., McArthur, J.M., Sarkar, A., Leng, M.J., Ravenscroft, P., Howarth, R.J., Banerjee, D.M. 2008. Do ponds cause arsenic-pollution of groundwater in the Bengal Basin? An answer from West Bengal. Environ. Sci Technol. 42, 5156-5164.

Shotbolt, L. (2010). Pore water sampling from lake and estuary sediments using Rhizon samplers. Journal of Paleolimnology, 44(2), 695-700.

Sikdar, P.K. and P. Sahu. 2009. Understanding wetland sub-surface hydrology using geologic and isotopic signatures. Hydrol. Earth Syst. Sci. 13, 1313-1323.

Sinha, R., Kettanah, Y., Gibling, M.R., Tandon, S.K., Jain, M., Bhattacharjee, P.S., Dasgupta, A.S., Ghazanfari, P. 2009. Craton-derived alluvium as a major sediment source in the Himalayan Foreland Basin of India. GSA Bulletin. 121, 1596-1610.

Smedley, P.L. and D.G. Kinniburgh, 2002. A review of the source, behavior, and distribution of arsenic in natural waters. App. Geochem. 17, 517-568.

Smedley, P.L., Nicolli, H.B., Macdonald, D.M.J., Barros, A.J., Tullio, J.O. 2002. Hydrogeochemistry of arsenic and other inorganic constituents in groundwaters from La Pampa, Argentina. App. Geochem. 17, 259-284.

Smedley, P.L., Kinniburgh, D.G., Macdonald, D.M.J., Nicolli, H.B., Barros, A.J., Tullio, J.O., Pearce, J.M., Alonso, M.S. 2005. Arsenic associations in sediments from the loess aquifer of La Pampa, Argentina. App. Geochem. 20, 989-1016.

Smith, A.H., Lingas, E.O., Rahman, M. 2000. Contamination of drinking-water by arsenic in Bangladesh: a public health emergency. Bulletin of the World Health Organziation. 78, 1093-1103.

Smith, A.H., Steinmaus, C.M. 2009. Health effects of arsenic and chromium in drinking water: recent human findings. Annual Review of Public Health. 30, 107-122.

Somenahally, A. C., Hollister, E. B., Loeppert, R. H., Yan, W., & Gentry, T. J. (2011). Microbial communities in rice rhizosphere altered by intermittent and continuous flooding in fields with long-term arsenic application. *Soil Biology and Biochemistry*, *43*(6), 1220-1228.

Stüben, D., Berner, Z., Chandrasekharam, D., Karmakar, J., 2003. Arsenic enrichment in groundwater of West Bengal, India: geochemical evidence for mobilization of As under reducing conditions. App. Geochem. 18, 1417-1434.

Stute, M., Zheng, Y., Schlosser, P., Horneman, A., Dhar, R.K., Datta, S., Hoque, M.A., Seddique, A.A., Shamsudduha, M., Ahmed, K.M., van Geen, A., 2007. Hydrological control of As concentrations in Bangladesh groundwater. Water Resour. Res. 43, W09417.

Subramanian, V. 1996. The sediment load of India – an update. Erosion and Sediment Yield: Global and Regional Perspectives (Proceedings of the Exeter Symposium). IAHS Publ. 236.

Sutton, N. B., van der Kraan, G. M., van Loosdrecht, M., Muyzer, G., Bruining, J., & Schotting, R. J. (2009). Characterization of geochemical constituents and bacterial populations associated with As mobilization in deep and shallow tube wells in Bangladesh. *water research*, *43*(6), 1720-1730.

Swartz, C.H., Keon-Blute, N., Badruzzaman, B., Ali, A., Brabander, D., Jay, J., Bensancon, J., Islam, S., Hemond, H.F., Harvey, C.F. 2004. Mobility of arsenic in a Bangladesh aquifer: inferences from geochemical profiles, leaching data, and mineralogical characterization. Geochim. Cosmochim. Acta. 68, 4539-4557.

Tareq, S.M., Safiullah, S., Anawar, H.M., Rahman, M.M., Ishizuka, T. 2003. Arsenic pollution in groundwater: a self-organizing complex geochemical process in the deltaic sedimentary environment, Bangladesh. Sci. Total Environ. 313, 213-226.

Tessier, A., Campbell, P.G.C., Bisson, M. 1979. Sequential extraction procedure for the speciation of particulate trace metals. Anal. Chem. 51, no. 7.

van Geen, A., Zheng, Y., Versteeg, R., Stute, M., Horneman, A., Dhar, R., Steckler, M., Gelman, A., Small, C., Ahsan, H., Graziano, J.H., Hussain, I., Ahmed, K.M., 2003. Spatial variability of arsenic in 6000 tube wells in a 25 km2 area of Bangladesh. Water Resour. Res. 39, 1140.

van Geen, A., Protus, T., Cheng, Z., Horneman, A. 2004. Testing groundwater for arsenic in Bangladesh before installing a well. Environ. Sci. Technol. 38, 6783-6789.

van Geen, A., Cheng, Z., Seddique, A.A., Hoque, M.A., Gelman, A., Graziano, J.H., Ahsan, H., Parvez, F., Ahmed, K.M. 2005a. Reliability of a commercial kit to test groundwater for arsenic in Bangladesh. Environ. Sci. Technol. 39, 299-303.

van Geen, A., Cheng, Z., Seddique, A.A., Hoque, M.A., Gelman, A., Graziano, J.H., Ahsan, H., Parvez, F., Ahmed, K.M. 2005b. Response to comment on ―Reliability of a commercial kit to test groundwater for arsenic in Bangladesh‖. Environ. Sci. Technol. 39, 5503-5504.

van Geen, A., Zheng, Y., Cheng, Z., Aziz, Z., Hornmean, A., Dhar, R.K., Mailloux, B., Stute, M., Weinman, B., Goodbred, S., Seddique, A.A., Hoque, M.A., Ahmed, K.M. 2006. A transect of groundwater and sediment properties in Araihazar, Bangladesh: Further evidence of decoupling between As and Fe mobilization. Chem. Geol. 228, 85-96.

van Geen, A., Zheng, Y., Goodbred, S., Horneman, A., Aziz, Z., Cheng, Z., Stute, M., Mailloux, B., Weinman, B., Hoque, M.A., Seddique, M.A., Hossain, M.S., Chowdhury, S.H., Ahmed, K.M. 2008a. Flushing history as a hydrogeological control on the regional distribution of arsenic in shallow groundwater of the Bengal Basin. Environ. Sci. Technol. 42, 2283-2288.

van Geen, A., Radloff, K., Aziz, Z., Cheng, Z., Huq, M.R., Ahmed, K.M., Weinman, B., Goodbred, S., Jung, H.B., Zheng, Y., Charlet, L., Metral, J., Chakraborty, S., Gajurel, A.P., Upreti, B.N. 2008b. Comparison of arsenic concentrations in simultaneously-collected groundwater and aquifer particles from Bangladesh, India, Vietnam, and Nepal. App. Geochem. 23, 3244-3251.

van Geen, A. 2008c. Environmental science – Arsenic meets dense populations. Nat. Geosci. 1, 494-496.

Viollier, E., Inglett, P.W., Hunter, K., Roychoudhury, A.N., Cappellan, P. 2000. The ferrozine method revisited: Fe(II)/Fe(III) determination in natural waters. App. Geochem. 15, 785-790.

von Brömssen, M., Larsson, S.H., Bhattacharya, P., Hasan, M.Z., Ahmed, K.M., Jakariya, M., Sikder, M.A., Sracek, O., Biven, A., Dousova, B., Patriarca, C., Thunvik, R., Jacks, G. 2008. J. Cont. Hydro. 99, 137-149.

Wasserman, G.A., Liu, X.H., Parvez, F., Ahsan, H., Factor-Litvak, P., van Geen, A., Slavkovich, V., Lolacono, N.J., Cheng, Z.Q., Hussain, L., Momotaj, H., Graziano, J.H. 2004. Water arsenic exposure and children's intellectual function in Araihazar, Bangladesh. Environ. Health Perspect. 112, 1329-1333.

Weinman, B., Goodbred, S.L., Zheng, Y., Aziz, Z., Steckler, M., van Geen, A., Singhvi, A.K., Nagar, Y.C. 2008. Contributions of floodplain stratigraphy and evolution to the spatial patterns of groundwater arsenic in Araihazar, Bangladesh. GSA Bulletin. 120, 1567-1580.

Welch, A.H., Lico, M.S., Hughes, J.L. 1988. Arsenic in ground water of the western United States. Ground Water. 26, 333-347.

Wenzel, W.W., Kirchbaumer, N., Prohaska, T., Stingeder, G., Lombi, E., Adriano, D.C. 2001. Arsenic fractionation in soils using improved sequential extraction procedure. Anal. Chem. Acta. 436, 309-323.

Wilkie, J.A and J.G. Hering 1998. Rapid oxidation of geothermal As(III) in streamwaters of the eastern Sierra Nevada. Environ. Sci. Technol. 32, 657-662.

Yilmaz, Pelin, Laura Wegener Parfrey, Pablo Yarza, Jan Gerken, Elmar Pruesse, Christian Quast, Timmy Schweer, Jörg Peplies, Wolfgang Ludwig, and Frank Oliver Glöckner. "The SILVA and “All-species Living Tree Project (LTP)” taxonomic frameworks." *Nucleic acids research* (2013)

Yu, W.H., Harvey, C.M., Harvey, C.F. 2003. Arsenic in groundwater in Bangladesh: A geostatistical and epidemiological frame work for evaluating health effects and potential remedies. Water. Resour. Res. 39, 1146.

Zahid, A., Hassan, M.Q., Breit, G.N., Balke, K.D., Flegr, M. 2009. Accumulation of iron and arsenic in the Chandina alluvium of the lower delta plain, Southeastern Bangladesh. Env. Geochem. Health. 31, 69-84.

Zarcinas, B.A., McLaughlin, M.J., Smart, M.K. 1996. The effect of acid digestion technique on the performance of nebulization systems used in inductively coupled plasma spectrometry. Commun. Soil Sci. Plant Anal. 27, 1331-1354.

Zarcinas, B.A., Pongsakul, P., McLaughlin, M.J., Cozens, C.G. 2004. Heavy metals in soils and crops in southeast Asia. 2. Thailand. Environ. Geochem. Health. 26, 359-371.

Zheng, Y., Stute, M., van Geen, A., Gavrieli, I., Dhar, R., Simpson, H.J., Schlosser, P., Ahmed, K.M., 2004. Redox control of arsenic mobilization in Bangladesh groundwater. App. Geochem. 19, 201-214.

Appendix A - Detailed Analytical Field Measurement Technique

Field test kits for water chemistry

1. Nitrate CHEMetrics® test kit (Cat.No. K-6909D): CHEMetrics nitrate test kit was used to find the nitrate concentration of groundwater samples in the field. . Fill 1.5ml of water sample to be tested in the reaction tube (cat. no. A-0187). Then dilute the sample by adding distilled water to 15ml mark of the reaction tube. Add the contents of one cadmium foil pack (cat. no. 7440-43-9) to the reaction tube containing water sample. Cap the reaction tube firmly and shake it for three minutes then keep it undisturbed for 2 minutes. Transfer 10ml of processed sample to the sample cup (cat. no. A-0013) while doing this transfer makes sure that no cadmium particles are going in to the sample cap. Then place the CHEMetrics ampoule (cat. no.R-6904) to the sample cup containing processed sample. Snap the tip then the ampoule will fill itself leaving a bubble for mixing. Mix the ampoule several times and during this process the bubble should travel from end to end. Keep the ampoule undisturbed for 10 minutes for the color development. After the color development compare the ampoule with nitrate color standard (cat. no. C-6909 D) until best color match is found.

2. HACH® Sulfate Test kit (Model SF-1, Cat.No: 2251-00): Sulfate concentration of ground waters were measured using HACH sulfate test kit. Experiment starts with filling 25ml of water sample to be analyzed into the sample mixing bottle (24102-00). Add the contents of one Sulfa Ver® powder pillow (cat. no. 12065-66) to the sample mixing bottle containing the water sample. Fix the cap of the sample mixing bottle tightly and shake the bottle for 15 seconds and make sure that the powder is dissolved. If sulfate is present in the water sample a white turbidity would appear. Then keep the sample undisturbed for five minutes. Then invert the bottle to mix if there is any solid left behind on the bottom. Then remove the cap and pour the contents to a clean 25ml graduate cylinder (cat. no. 2172-40). Hold the graduate cylinder in a vertical position. While looking straight down in to the graduated cylinder containing water sample insert the sulfate measure dipstick (cat. no.46814-00) in to the graduated cylinder until the black dot disappears completely. While holding the dipstick at the same position where the back dot disappears and read value (number on the dipstick scale that meets with the surface of the sample) on the dipstick through the non-graduated portion of the cylinder. This number corresponds to mg/l of sulfate in the sample. If the black dot on the dipstick disappear before the

first test mark (200mg/l) then the concentration of sulfate is greater than 200mg/l . If the black dot does not disappear after the dipstick is inserted to the cylinder bottom, the sulfate concentration is less than 50mg/l. Once the experiment is done wash the cylinder and bottle properly with water. Then wash again properly with distilled water. Then rinse the bottles and tubes with distilled water at least 3 times and then wipe with chemwipes. Store the prepared sample in the waste collection bottle.

3. HACH® Orthophosphate Test kit (Model PO-19, Cat.No: 2251-00): There are 3 different types of tests for Phosphate (PO_4^{3-}) they are a). Low range phosphate concentration (0-1mg/l) test procedure. b) . Midrange phosphate concentration (0-5 mg/l) test procedure c). High range phosphate concentration (0-50 mg/l) test procedure. Spectrophotometer test for phosphate concentration was conducted to determine the concentration of phosphate. Then based on concentration of phosphate measured from spectrophotometer, the test kit procedure was decided (low, mid or high range) to reconfirm the concentration. Phosphate values were determined for all 63 samples using a HACH® Phosphate, Ortho Test Kit (0-50 mg/l Model PO-19; Cat. No. 2248-00), via colorimetric method. This procedure began by filling the two tubes in the kit to the first (5 ml) line with sample water and inserting one of the tubes into the left opening of the comparator. One PhosVer® 3 Phosphate Reagent Powder Pillow (C6H8O6, K2S2O7, Na2MoO4•2H2O) (Cat. No. 2209-99) was added to the second tube and swirled to mix. The second tube was then inserted into the right opening of the comparator. The comparator was held so that bright sunlight was directly behind the tubes. The color disc was rotated until the colors in the front windows matched. The reading in the scale window was divided by 10 to obtain mg/l phosphate. As with the other field kit procedures, the water was discarded and the tubes rinsed 3 times with de-ionized water and then 3 times again with the next sample before analyses.

4. HACH® Alkalinity test kit (Model AL-DT; Cat. No. 20637-00) Phenolphthalein and Total Alkalinity Method 8203 was used to measure alkalinity of the groundwater samples. Alkalinity was measured for each of the 63 samples using a HACH® Alkalinity Test Kit (10-4000 mg/l , Model AL-DT; Cat. No. 20637-00) digital titration method. For each sample, ~20 ml of water sample was used. The 20 ml sample was added to a 100 ml graduated cylinder, and one Phenolphthalein Indicator Powder Pillow (Cat. No. 942-99) was added to the sample, swirling the cylinder to mix the contents. The solution did not turn pink for any of the samples, so it was concluded that no value for CaCO3-P alkalinity was important for these samples. Then a

Bromcresol Green-methyl Red Indicator Powder Pillow (Cat. No. 943-99) was added to the sample and swirled to mix. A digital titration cartridge of 1.6 N H2SO4 (Cat. No. 14389-01) with a delivery tube was attached to the HACH® digital titrator and inserted in the 20 ml water sample. Titration of the sulfuric acid into the sample proceeded until a light greenish blue-grey (pH 5.1) a light violet-grey (pH 4.8) or a light pink (pH 4.5) color (depending on composition) was achieved. The total number of digits displayed on the titrator was recorded and multiplied by 5 (the respective digit multiplier for a 20 ml sample) to obtain the amount (mg/l) as HCO3-- Total Alkalinity. The resulting liquid was discarded. Before the next sample was analyzed for alkalinity, the graduated cylinder and the delivery tube were rinsed 3 times with de-ionized water and 3 times with water from the next sample to be analyzed to maintain precision and consistency.

Appendix B - Total Extraction and Sequential Extraction

Total digestion of sediment samples

Total digestion did for l sediments samples. We took 14 sediemnt samples; 3 duplicates, 3 triplicate and 1 standard reference materials (Montana Soil-I).

Total digestion by reflux tube soil digestion (Zarcinas et al., 1996)

1. Reagents require concentrated hydrochloric acid (trace grade); concentrated nitric acid (trace grade).
2. Weight out 1g of <2mm soil in to very clean restricted neck digestion tubes. If the soil was >2mm in grain size then it has to be pulverized using agate mortar and piston.
3. Aquaregia (HNO_3: HCl; 1:3) have to be prepared
4. Approximately 1 g of soil predigest with 0.5 ml of 30% H_2O_2 for 10min at room temperature
5. 2.5 ml of H_2O_2 added and allow to react for 12 h at room temperature, after that the tubes are heated on a digestion block at 90°C until the volume was reduced to ~1ml
6. 5mL of this prepared aquaregia are adding to each of the digestion tubes containing samples.
7. Digestion tubes are arranged over sample rack and left overnight inside running fume hood.
8. Next morning each digestion tube is gently swirled to make sure that there is no soil stuck on the bottom of the tubes.
9 Small glass funnels are placed in each of the digestion tubes for refluxing.
10. Digestion blocks are set to slowly ram up to 140°C and hold for 2 hrs.
11. Tubes are checked every 15-20 minutes to make sure that the soils haven't bubbled up in the tubes. If soil has started bubbling up in the tubes, then remove the tubes from the block and wash the sides of the tube down with a small amount of 0.1% nitric acid. After this procedure the tubes are return to the block and then watch for more bubbling.
12. After 2 hrs of reflux period the tubes are remove from the block and let it cool.
13. Then made up to 25 ml mark of the tubes with distilled water, mixed well with vortex and placed in the walk in refrigerator overnight covered with parafilm.

14. Next morning the solution is filter through filter papers in to pH cups.

15. Then this solution will pour to ICP vials for finding the concentration of As, Mn and Fe in ICP-OES in Dept of Agronomy at Kansas State University.

For ICP-OES analyses one blank and 4 multielement standards containing As, Mn and Fe in aquaregia matrix were prepared. They include very low range standard (As=0.5mg/l ; Mn=5 mg/l ; Fe=25 mg/l);low range standard (As=2mg/l ; Mn=10 mg/l ; Fe=50 mg/l); medium range standard (As=5 mg/l ; Mn=25 mg/l ; Fe=100 mg/l); high range standard (As=15 mg/l ; Mn=50 mg/l ; Fe=300 mg/l) and a very high range standard (As=35 mg/l ; Mn=50 mg/l ; Fe=500 mg/l).

Sequential extraction of Core Sediments

5-step method of He et al., 2010 is most relevant and therefore use for this study to find out concentration of As, Mn and Fe at various soil phases. Aquifer samples from each location are select for the study. A total of 14 samples, 3 duplicates, 2 triplicate and one standard reference material (Montana II 2711, www.nist.gov/srm ; national institute of standards and technology US department of commerce NIST) use for the experiment.

Sample preparation started by measuring of ~1 g subsamples of the wet samples were placed in previously weighed (to 0.001 g precision) plastic 50 mL centrifuge tubes in a N_2 glove box for a few days for drying

Step-1 Procedure; for Non-specifically sorbed As, Mn and Fe

(a) Prepare 0.05 M $(NH_4)_2SO_4$, was made by adding 6.574 g of $(NH_4)_2SO_4$ powder to 1L of de-ionized water.

(b) Once samples dried then weigh to nearest 0.001 g

c) 25 mL of the 0.05 M $(NH_4)_2SO_4$ added to the samples via pipette

d) Place the Samples over the shaker for 4 hours to react with the ammonium sulfate.

e) Prepare 7 multi-element standards (As, Mn, Fe) were prepared in the 0.05 M $(NH_4)_2SO_4$ matrix near expected concentrations.

f) After 4 hours of shaking, samples were removed and centrifuged at ~2100 rpm for 10 minutes

g) The solution decants into a disposable syringe and passed through a 0.45 µm filter into a 13 mm x 90 mm plastic vial for analyses by ICP-OES.

h) Preserve the remaining solution by filtering into small Evergreen vials for future analyses (by GFAAS).

i) 3 wash step with 15 mL of de-ionized water do at ~2100 rpm for 10 minutes. The remaining solution was decanted and saved in 50 mL centrifuge tubes. Centrifuge tubes with sample were weighed to account for contribution from this step onto the following step.

j) 4 multi-element standards prepared (low range Standard, As=0.5 mg/l , Mn=0.5 mg/l , Fe=2 mg/l ; medium range standard, As=1 mg/l , Mn=1 mg/l , Fe=4 mg/l , high range standard, As=2 mg/l , Mn=2 mg/l , Fe=8 mg/l ; very high range standard, As=3 mg/l , Mn=5 mg/l and Fe=10 mg/l) and one blank(As=0, Mn=0, Fe=0) were prepared for As, Mn, and Fe using the 0.05 M $(NH_4)_2SO_4$ as the matrix

Step-2 procedure: for specifically sorbed as, Mn and Fe

The extraction of the specifically sorbed ions using 0.05 M $NH_4H_2PO_4$. $NH_4H_2PO_4$ was used because As and P have similar electron configurations and form triprotic acids with similar dissociation constants (Wenzel, et al., 2001), and at equal concentrations phosphate outcompetes arsenate for adsorption sites in soils (Swartz et al., 2004) because of smaller size and higher charge density of phosphates (Manning et al., 1996).

a) 0.05 M strength was prepared by adding 5.746g of $NH_4H_2PO_4$ granules to 1L of de-ionized water.

b) 25 ml of 0.05 M $NH_4H_2PO_4$ solution was added via pipette to each 50 mL centrifuge tube and placed on the shaker overnight for 16 hours

C) Run the standards and samples with dilution factor 25 from Step 1 (during shaking for the second step) on ICP-OES using wavelengths of 193.76, 257.61, 259.94 nm for As, Mn and Fe, respectively.

d) After 16 hours of shaking, samples were centrifuged at ~2100 rpm for 10 minutes

e) Decant and filter the solution (using and Evergreen vials into a disposable syringe and passed through a 0.45 µm filter) into a 13 mm x 90 mm plastic vial for analyses by ICP-OES

f) 3 wash step with 15 ml of de-ionized water was done at ~2100 rpm for 10 minutes each. The remaining solution was decanted to 50ml centrifuge tubes and saved. Then Centrifuge tubes (with sample) were weighed to account for contribution from this step onto the following step.

g) 4 multi-element standards were prepared (low range standard As=0.5 mg/l , Mn=0.5 mg/l , Fe=2 mg/l ; medium range standard, As=1 mg/l , Mn=1 mg/l , Fe=4 mg/l , high range

standard, As=2 mg/l , Mn=2 mg/l , Fe=8 mg/l ; very high range standard, As=3 mg/l , Mn=5 mg/l and Fe=10 mg/l) and one blank (As=0, Mn=0, Fe=0)were prepared for As, Mn, and Fe using the 0.05 M $NH_4H_2PO_4$ as the matrix

Step-3 procedure: to find the concentration of as, Mn and Fe present in amorphous and poorly crystalline hydrous oxides of Fe and Al

This step starts with the preparation of a 0.2 M NH_4^+-oxalate buffer at pH 3.25 in the dark.

a) 0.2 M NH_4^+-oxalate buffer strength was achieved by adding 28.422g of NH_4^+-oxalate buffer granules to ~500 mL of de-ionized water, adjusting pH to 3.25 by adding ~16mL of concentrated HCl (trace metal grade). De-ionized water was added to bring the final volume of solution up to 1L to make the 0.2 M NH_4^+-oxalate buffer. Then wrap the beaker with aluminum foil to create darkness.

b) 25 mL of 0.2 M NH_4^+-oxalate buffer at pH 3.25 was added to each centrifuge tube with a pipette and placed in a rack in a cardboard box and covered with aluminum foil (for darkness) then placed on a shaker for 4 hours

c) Standards and samples were ran with dilution factor 25 from Step 2 on ICP-OES

d) 4 multi-element standards were prepared (low range Standard, As=0.5 mg/l , Mn=0.5 mg/l , Fe=5 mg/l ; medium range standard, As=1 mg/l , Mn=1 mg/l , Fe=25 mg/l , high range standard, As=2 mg/l , Mn=2 mg/l , Fe=50 mg/l ; very high range standard, As=3 mg/l , Mn=5 mg/l and Fe=100 mg/l) and a blank (As-0, Mn=0, Fe=0) for As, Mn, and Fe using the 0.2 M NH_4^+-oxalate buffer at pH 3.25 as the matrix .

e) After 4 hours of shaking, samples were centrifuged at ~2100 rpm for 10 minutes.

f) Decant and filter the solution (using and evergreen vials into a disposable syringe and passed through a 0.45 µm filter) into a 13 mm x 90 mm plastic vial for analyses by ICP-OES

g) 3 wash step with 15 ml of de-ionized water was done at ~2100 rpm for 10 minutes each. The remaining solution was decanted to 50 mL centrifuge tubes and saved. Centrifuge tubes (with sample) were weighed to account for contribution from this step onto the following step.

Step-4 procedure: to target well crystalline hydrous oxides of Fe and Al.(e.g. goethite, hematite)

a) Prepare the extractant by adding 28.422 g of 0.2 M NH_4^+-oxalate granules and 17.648 g of ascorbic acid to ~500 mL of de-ionized water. Solution pH was adjusted to 3.25 by adding

~13 ml of HCl (trace metal grade) and bringing the volume up to 1L ml with de-ionized water to achieve proper strength

b) 25 mL of the extractant solution was added carefully via pipette to each centrifuge tube with sample

c) Placed the centrifuge tubes in a rack in a water bath and heated at 90°C ± 5°C for 30 minutes

d) Prepare 4 standards(low range Standard, As=0.5 mg/l , Mn=0.5mg/l , Fe=5 mg/l ; medium range standard, As=1 mg/l , Mn=1mg/l , Fe=25 mg/l , high range standard, As=2 mg/l , Mn=2 mg/l , Fe=50 mg/l ; very high range standard, As=3 mg/l , Mn=5 mg/l and Fe=100 mg/l) and one blank (As=0, Mn=0, Fe=0) using the 0.2 M NH_4^+-oxalate solution adjusted to pH 3.25 as the matrix prepared for step 4.

e) Run the standards and samples with dilution factor 25 from Step 3 on ICP-OES

f) Centrifuged the samples two times at ~2100 rpm (10 minutes first time and 15 minutes time)

g) Decant and filter the solution (using and Evergreen vials into a disposable syringe and passed through a 0.45 µm filter) into a 13 mm x 90 mm plastic vial for analyses by ICP-OES)

h) 3 wash step with 15 ml of de-ionized water was done at ~2100 rpm for 10 minutes each. The remaining solution was decanted to 50ml centrifuge tubes and saved. Centrifuge tubes (with sample) were weighed to account for contribution from this step onto the following step.

Step-5: *organic matter phase*:

The sediment remaining after the P-4 extraction was rinsed with distilled deionized water

a) Dissolve 44.6 g of sodium pyrophosphate in a one liter volumetric flask with DI Water. Make an adequate quantity of solution to run all the samples.

b) Adjust the pH of the solution to pH 10 using dilute NaOH or HCl. Sodium pyrophosphate should be made every 3-4 weeks

c) Then the organic fraction was determined by a 12-h extraction with 5ml 0.1 M sodium pyrophosphate at pH 10. Sodium pyrophosphate mixed with sediment was heated on a hotplate.

d)1M Ammonium Acetate (NH4C2H3O2), Dissolve 77.1g ammonium acetate (m.w. = 77.1 g/mole) in DI H2O, Make final volume of 1 L with H2O, Sterilize by filtration and store at room temperature

e) Dissolved into 1 M ammonium acetate to make the final volume of 20 ml.

f) Prepare 4 standards(low range Standard, As=0.5 mg/l , Mn=0.5mg/l , Fe=5 mg/l ; medium range standard, As=1 mg/l , Mn=1mg/l , Fe=25 mg/l , high range standard, As=2 mg/l , Mn=2 mg/l , Fe=50 mg/l ; very high range standard, As=3 mg/l , Mn=5 mg/l and Fe=100 mg/l) and one blank (As=0, Mn=0, Fe=0) using same type of matrix.

Step-6 procedure: Residual phases excluding silicates

a) 10 mL of 1:1 HNO_3 (5 ml HNO_3:5 ml de-ionized water) was added to each centrifuge tube.

b) Cover the centrifuge tube with a watch glass and placed in a water bath at ~90°C for 15 min

c) After the 15 minutes samples were removed for cooling

d) 5 mL of concentrated HNO_3 was added to each sample, watch glasses were replaced, and samples were returned to water batch to reflux for 30 minutes

e) Keep the samples in water bath at 90°C ± 6°C for ~2 hours to evaporate (No brown fumes were observed)

f) The Standards and samples were analyzed with dilution factor 25 from Step 4 on ICP-OES under same conditions as earlier steps.

g) Remove the samples from water bath after 2 hours and let it cool

h) Add 2 mL of de-ionized water to the samples, followed by 3 ml of 30% H_2O_2 to react

i) Return the samples to water bath and heated at 90°C ± 5°C for two hours. During the first hour, a total of 13 mL of H_2O_2 was added in 1mL aliquots to each sample due to continued effervescence of the samples.

j) After two hours, samples were removed from water bath and centrifuged, decanted and filtered as done in the previous steps (using and Evergreen vials into a disposable syringe and passed through a 0.45 µm filter) into a 13 mm x 90 mm plastic vial for analyses by ICP-OES)

k) Final weights of samples were recorded, and samples were stored in refrigerator.

l) 4 multi element standards were prepared (low range Standard, As=0.5 mg/l , Mn=0.5mg/l , Fe=5 mg/l ; medium range standard, As=1mg/l , Mn=1mg/l , Fe=25 mg/l , high range standard, As=2 mg/l , Mn=2 mg/l , Fe=50 mg/l ; very high range standard, As=3 mg/l , Mn=5 mg/l and Fe=100 mg/l) were made using same concentrations as other steps in a 10:13:7 HNO_3:H_2O_2:de-ionized water matrix and one blank (As=0, Mn=0 , Fe=0) run along with samples with dilution factor 25 in the ICP-OES

Appendix C - DNA extracted from sediment using the Mo Bio PowerSoil™ DNA isolation kit

DNA was extracted from undisturbed sediment samples using the Mo Bio PowerSoil™ DNA isolation kit following the manufacturer's directed protocol (Mo Bio Laboratories, Inc., Carlsbad, CA, USA). For extracting DNA of microbes from the sediment this detailed Protocol used. For better performance it was mandatory to wear gloves at all times.

1. In a PowerBead we added 0.25 grams of soil sample.

What's happening: After my sample has been loaded into the PowerBead Tube, the next step was a homogenization and lysis procedure. The PowerBead Tube contains a buffer that (a) helped disperse the soil particles. (b) Began to dissolve humic acids and (c) protected nucleic acids from degradation.

2. Then Gently vortex to mix. What's happening: Gentle vortexing mixes the components in the PowerBead Tube and begins to disperse the sample in the PowerBead Solution.

3. We checked solution C1. If solution C1 was precipitated, heat the solution to 60'C until the precipitate has dissolved before use. What's happening: Solution C1 contains SDS and other disruption agents required for complete cell lysis. In addition to aiding in cell lysis, SDS is an anionic detergent that breaks down fatty ecids and lipids associated with the can membrane of several organisms. If it gets cold, it will form a white precipitate in the battle. Heating to 6O'C will dissolve the SDS and will not harm the SDS or the other disruption agents. Solution C1 can be used while it is still warm.

4. Add 60 µ1 of Solution C1 and invert several times or vortex briefly.

5. Secure PowerBead Tubes horizontally using the MO BIO Vortex Adapter tube hofder for the vortex (MO BIO Catalog# 13000-V 1) or secure tubes horizontally on a flat-bed vortex pad with tape. Vortex at maximum speed for 10 minutes.

What'S happening. The MO BIO vortex adapter is designed to be a simple platform to facilitate keeptng the tubes tightly attached to the vortex. It should be noted thet although you can attach tubes with tape, often the tape becomes loose and not all tubes will sheke evenly or efflcientty. This may lead to inconsistent results or lower yields. Therefore, the use of the MO BIO vortex adapter is a highlly recommended and cost effective way to obtain maximum DNA yields.

6. Make sure the PowerBead Tubes rotate freely in your cenltrifuge without rubbing. Centrifuge tubes at10.000 x g for 30 seconds at room temperature. CAUTION: Be sure not to exceed 10.000 x g or tubes may break.
7. Transfer the supernatant to a clean 2 ml CoIlection Tube.
8. Add 250 µ1 of Solution C2 and vortex for 5 seconds. Incubate at 4°C for 5 minutes.
What's happening: Solution C2 is patented Inhibitor Removal Technology@) (IRT). It contains a reagent to precipitate non-DNA organic and inorganic material including humic substances, cell debris, and proteins. It is imporlant to remove contaminating organic and inorganic matter that may reduce DNA purity and inhibit downstream DNA applications.
9. Centrifuge the tubes at room temperature for 1 minute at 10,000 x g.
10. Avoiding the pellet, transfer up to 600 µ1 of supernatant to a clean 2 ml Collection Tube (provided). What's happening: The pellet at this point contains non-DNA organic and inorganic material including humic acid, cell debris, and proteins. For the best DNA yields, and quality, avoid transferring any of the pellets.
11. Add 200 µ 1of Solution C3 and vortex briefly. Incubate at 4°C for 5 minutes.
What's happening: Solution C3 is patented Inhibitor Removal Technology@) (IRT) and is a second reagent to precipitate additionat non-DNA organic and inorganic material including humic acid, cell debris, and proteins. It is important to remove contaminating organic and inorganic matter that may reduce DNA purity and inhibit downstream DNA applications.
12. Centrifuge the tubes at room temperature for 1 minute at 10,000 x g.
13. Transfer up to 750 µ1 of supernatant to a clean 2 ml Collection Tube (provided) . What's happening: The pellet at this point contains additional non-DNA organic and inorganic material induding humic acid, celt debris, and proteins. For the best DNA yields, and quality, avoid transferring any of the pellets.
14. Shake to mix Solution C4 before use. Add 1.2 ml of Solution C4 to the supernalant (be careful solution doesn't exceed rim of tube) and vortex for 5 seconds. What's happening: Solution C4 is a high concentration seit solution. Since DNA binds tightly to silica at high salt concentrations, this will adjust the DNA solution salt concentrations to allow binding of DNA. but not non- DNA organic and inorganic material that may still be present at low levels, to the Spin filters.

15. Load approximately 675µ1 onto a Spin Filter and centrifuge at 10,000 x g for 1 minute at room temperature. Discard the flow through and add an additional 675µ1 of supernatant to the Spin Fliter and centrifuge at 10,000 x 9 for 1 minute at room temperature. Load the remaining supematant onto the spin filter and centrifuge at 10,000 x g for 1 minute at room temperature. What's happening: DNA is selectively bound to the silica membrane in the Spin Filter device in high salt solution. Contaminants pass through the filter membrane, leaving only DNA bound to the membrane.

16. Add 500 µl of Solution C5 and centrituge at room temperature for 30 seconds at 10,000 x g. What's happening: Sollution C5 is an ethanol based wash solution used to wither clean /he DNA that is bound to the silica filter membnme in the spin filter. This wash solution removes residual salt, humic acid and other contaminants while allowing the DNA to stay bound to the silica membrane.

17. Discard the flow through from the 2ml collection tube.

18. Centrifuge at room temperature for 1 minute at 10000 x g

19. Carefully place spin filter in a clean 2ml collection tube. We avoid splashing any solution C5 onto the spin filter.

20. We added 100 µl of solution C6 to the center of the white filter membren.

21. Then we centrifuge it at roomtemperature for 30 seconds at 10000 x g.

22. Then we dicard the spin filter. This was the last process, now it can use for sequencing.

Appendix C.1- Field In situ Water Geochemical Parameters (Fe_t, Fe^{2+} and NH_4-N)

This section contains general field insitu kit tests for Fe_t, Fe^{2+} and NH_4-N from South and North Matlab (Field trip in Jan 2013).

Nest	Well ID	Thana	Village	Latitude(N)	Longitude(E)	Depth m	Fe_t (mg/l)	Fe^{2+} (mg/l)	NH_3-N (mg/l)
Nest-3	N-3 P-1	Matlab Dakshin	Dighaldi	23.32567	90.70171	17			
	N-3 P-2	Matlab Dakshin	Dighaldi	23.32567	90.70171	29	6.68	0	0.11
	N-3 P-3	Matlab Dakshin	Dighaldi	23.32567	90.70171	52	5.52	5.33	
	N-3 P-4	Matlab Dakshin	Dighaldi	23.32567	90.70171	70	2.02	1.93	0.12
	N-3 P-6	Matlab Dakshin	Dighaldi	23.32567	90.70171	95	3.58	3.76	0.75
	N-3 P-7	Matlab Dakshin	Dighaldi	23.32567	90.70171	119	6.92	6.78	0.54
	N-3 P-5	Matlab Dakshin	Dighaldi	23.32567	90.70171	238	2.08	2.05	
Nest-4	N-4 P-1	Matlab Dakshin	Nandikhola	23.42652	90.77570	17	0.01	0.01	
	N-4 P-2	Matlab Dakshin	Nandikhola	23.42652	90.77570	27	0	0	10.32
	N-4 P-3	Matlab Dakshin	Nandikhola	23.42652	90.77570	56	0	6.49	
	N-4 P-4	Matlab Dakshin	Nandikhola	23.42652	90.77570	75	0.03	0	0.07
	N-4 P-6	Matlab Dakshin	Nandikhola	23.42652	90.77570	116			0.43
	N-4 P-5	Matlab Dakshin	Nandikhola	23.42652	90.77570	238	0	0	0.26
Nest-5	N-5 P-1	Matlab Dakshin	Narayanpur	23.36834	90.76748	11	6.98	6.50	
	N-5 P-2	Matlab Dakshin	Narayanpur	23.36834	90.76748	29	3.67	3.22	0.06
	N-5 P-4	Matlab Dakshin	Narayanpur	23.36834	90.76748	82	2.61	2.25	6.48
	N-5 P-6	Matlab Dakshin	Narayanpur	23.36834	90.76748	104	2.56	2.53	0.15
	N-5 P-5	Matlab Dakshin	Narayanpur	23.36834	90.76748	238	5.45	5.05	1.14
Nest-16	N-16 P-1	Matlab Dakshin	Dingavanga	23.3201	90.7378	17	3.5	0.15	5.38
	N-16 P-2	Matlab Dakshin	Dingavanga	23.3201	90.7378	30	6.53	0.01	
	N-16 P-3	Matlab Dakshin	Dingavanga	23.3201	90.7378	50	0.01	0.02	0.49
	N-16 P-4	Matlab Dakshin	Dingavanga	23.3201	90.7378	84	0.01	0.04	
	N-16 P-6	Matlab Dakshin	Dingavanga	23.3201	90.7378	102	6.52	5.63	0.00
	N-16 P-5	Matlab Dakshin	Dingavanga	23.3201	90.7378	237	0.01	0.03	0.00
	N-17 P-1	Matlab Dakshin	Kashimpur	23.33148	90.80419	19	0.04	0.03	

Nest-17	N-17 P-2	Matlab Dakshin	Kashimpur	23.33148	90.80419	34	0	0	4.23
	N-17 P-3	Matlab Dakshin	Kashimpur	23.33148	90.80419	58	0.01	0	
	N-17 P-6	Matlab Dakshin	Kashimpur	23.33148	90.80419	104	4.03	0	1.43
	N-17 P-5	Matlab Dakshin	Kashimpur	23.33148	90.80419	230	0.1	0	1.76
Nest-7	N-7 P-1	Matlab Uttar	Hapania	23.48756	90.66227	14	>3.5	3.26	2.23
	N-7 P-2	Matlab Uttar	Hapania	23.48756	90.66227	26	>3.5	3.26	2.02
	N-7 P-3	Matlab Uttar	Hapania	23.48756	90.66227	53	>3.5	5.37	>3.3
	N-7 P-4	Matlab Uttar	Hapania	23.48756	90.66227	75	3.12	2.98	>3.8
	N-7 P-6	Matlab Uttar	Hapania	23.48756	90.66227	102	2.35	2.03	0.08
	N-7 P-5	Matlab Uttar	Hapania	23.48756	90.66227	232	3.87	3.12	1.26
Nest-8	N-8 P-1	Matlab Uttar	Thakurchar	23.43483	90.63064	14			0.05
	N-8 p-2	Matlab Uttar	Thakurchar	23.43483	90.63064	53			0.11
	N-8 P-4	Matlab Uttar	Thakurchar	23.43483	90.63064	101			0.10
	N-8 P-5	Matlab Uttar	Thakurchar	23.43483	90.63064	235			0.13
Nest-9	N-9 P-1	Matlab Uttar	Tatua	23.40918	90.73529	9	2.15	0	0.00
	N-9 P-2	Matlab Uttar	Tatua	23.40918	90.73529	29	0.03	0.00	0.00
	N-9 P-3	Matlab Uttar	Tatua	23.40918	90.73529	44	0.03	0	
	N-9 P-4	Matlab Uttar	Tatua	23.40918	90.73529	66	0	0.07	0.16
	N-9 P-5	Matlab Uttar	Tatua	23.40918	90.73529	226	0.2	0.05	0.04
Nest-12	N-12 P-1	Matlab Uttar	Brahmanchalk	23.43352	90.67261	14	>3.5	0.28	
	N-12 P-2	Matlab Uttar	Brahmanchalk	23.43352	90.67261	27	2.71	0.08	0.14
	N-12 P-3	Matlab Uttar	Brahmanchalk	23.43352	90.67261	81	0.25	0.05	
	N-12 P-6	Matlab Uttar	Brahmanchalk	23.43352	90.67261	116	0	0.05	0.65
	N-12 P-5	Matlab Uttar	Brahmanchalk	23.43352	90.67261	219	2	0.50	4.65
Nest-13	N-13 P-1	Matlab Uttar	Purba Lalpur	23.47562	90.60495	14	2.65	2.23	2.89
	N-13 P-2	Matlab Uttar	Purba Lalpur	23.47562	90.60495	33	6.37	6.23	9.78
	N-13 P-3	Matlab Uttar	Purba Lalpur	23.47562	90.60495	85			2.05
	N-13 P-6	Matlab Uttar	Purba Lalpur	23.47562	90.60495	111			0.00
	N-13 P-5	Matlab Uttar	Purba Lalpur	23.47562	90.60495	237	>DL	>DL	0.06

Appendix C.2- Grain Size Analyses

Following Data shows Grain Size Analysis for South Matlab Sediments (Core-2)

South Matlab (Core -2 Samples) Grain Size					
10m			**80m**		
Coarse Sand	0.5 mm	0	Medium Sand	0.25mm	9.21
Medium Sand	0.25mm	1.32	fine sand	0.125mm	16.42
fine sand	0.125mm	35.82	very fine sand	0.0625mm	18.21
very fine sand	0.0625mm	8.67	silt & clay	<0.0625mm	6.04
silt & clay	<0.0625mm	4.09	**95m**		
27m			Coarse Sand	0.5 mm	5.06
Coarse Sand	0.5 mm	0	Medium Sand	0.25mm	26.13
Medium Sand	0.25mm	12.85	fine sand	0.125mm	15.86
fine sand	0.125mm	21.92	very fine sand	0.0625mm	2.51
very fine sand	0.0625mm	11.17	silt & clay	<0.0625mm	0.291
silt & clay	<0.0625mm	3.72	**100m**		
45m			Coarse Sand	0.5 mm	0
Coarse Sand	0.5 mm	0	Medium Sand	0.25mm	0
Medium Sand	0.25mm	5.63	fine sand	0.125mm	0
fine sand	0.125mm	14.75	very fine sand	0.0625mm	35.67
very fine sand	0.0625mm	24.1	silt & clay	<0.0625mm	14.02
silt & clay	<0.0625mm	5.41	**112m**		
65m			Coarse Sand	0.5 mm	5.43
Coarse Sand	0.5 mm	0	Medium Sand	0.25mm	25.41
Medium Sand	0.25mm	0	fine sand	0.125mm	15.63
fine sand	0.125mm	15.15	very fine sand	0.0625mm	2.67
very fine sand	0.0625mm	24.22	silt & clay	<0.0625mm	0.37
silt & clay	<0.0625mm	10.59			

Appendix C.3- Scanning Microscope Analyses

Scanning Electron Microscopy (SEM)

SEM analysis was performed to find out the concentration of various trace elements in the aquifers sediments. 6 samples (aquifer sediments) were chosen (South Matlab Core-2) for the study. Samples are taken from various depths in the aquifer (10m, 24m, 45m, 64m, 80m and 95m). Each sample was mounted on a separate aluminum SEM stub with a carbon coating. Then once the samples were magnified the area of interest was chosen and analysis was performed to find out the concentration of various elements especially As, Mn, Fe, Ca, C etc. Then grains of interest were also chosen and mapped to find concentration of various elements present in that particular grain. The concentration of elements was measured using intensity of peak in the spectrum. It depends on a number of factors, but primarily, on the probability of X-ray generation as a result of a given transition. The relative probability of generating X-rays at the various ionization energies from a given element depends on the value of the incident energy and the excitation cross section for the relevant shell. The intensity of a given line will depend on the ratio between the incident beam energy and the critical ionization energy for that line or transition. The detection is done by the secondary electrons emitted by atoms of various elements which have been excited by incident electron beam. In X-ray microanalysis it refers to the shell or level closest to the nucleus as the K shell. Electrons fill this level first. The next closest level is the L shell and then the M and then N shell etc. Since the K shell is closest to the nucleus, it requires the most energy to remove an electron from this shell. Therefore if a spectrum from an element contains K, L and M line, the K will be the highest in energy i.e. furthest towards the right of the spectrum if the scale is defined in units of energy.

Selected SEM Analyses Data

Spectrum processing: **CS-2-30(10m) grey sediments**

No peaks omitted

Processing option: All elements analyzed (Normalised)

Standard:

C CaCO3 1-Jun-1999 12:00 AM

O SiO2 1-Jun-1999 12:00 AM

Na Albite 1-Jun-1999 12:00 AM

Mg MgO 1-Jun-1999 12:00 AM

Al Al2O3 1-Jun-1999 12:00 AM

Si SiO2 1-Jun-1999 12:00 AM

K MAD-10 Feldspar 1-Jun-1999 12:00 AM

Ca Wollastonite 1-Jun-1999 12:00 AM

Ti Ti 1-Jun-1999 12:00 AM

Mn Mn 1-Jun-1999 12:00 AM

Fe Fe 1-Jun-1999 12:00 AM

As InAs 1-Jun-1999 12:00 AM

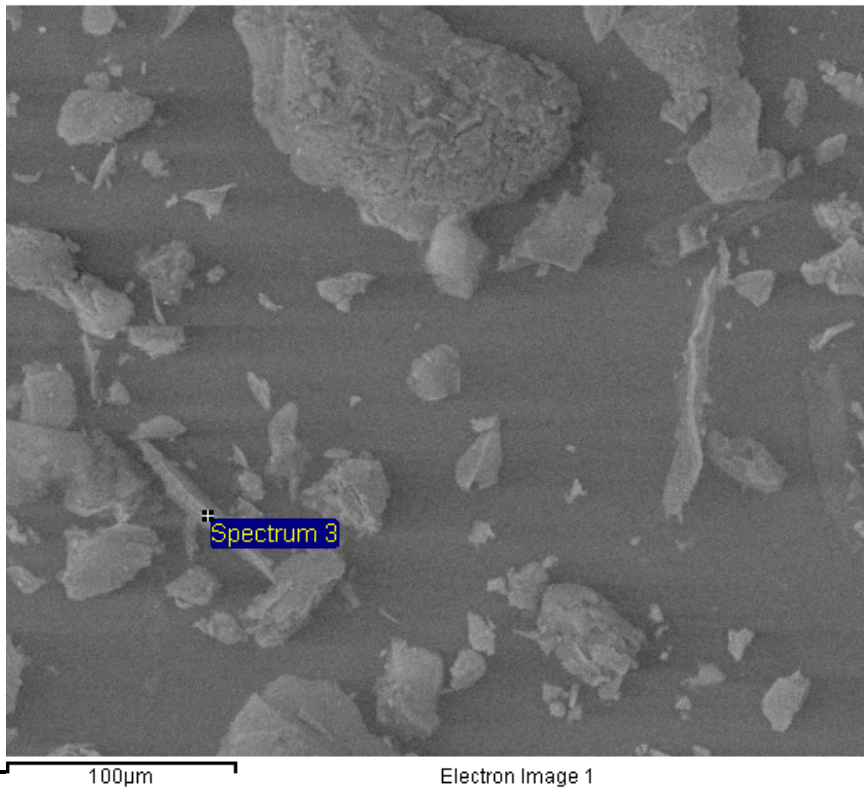

Element	Weigh%	Atomi%
C K	24.18	35.34
O K	42.07	46.15
Na K	0.60	0.46
Mg K	3.64	2.63
Al K	3.51	2.28
Si K	14.14	8.83
K K	0.37	0.17
Ca K	4.36	1.91
Ti K	0.12	0.04
Mn K	0.10	0.03
Fe K	6.79	2.13
As L	0.13	0.03
Totals	100.00	

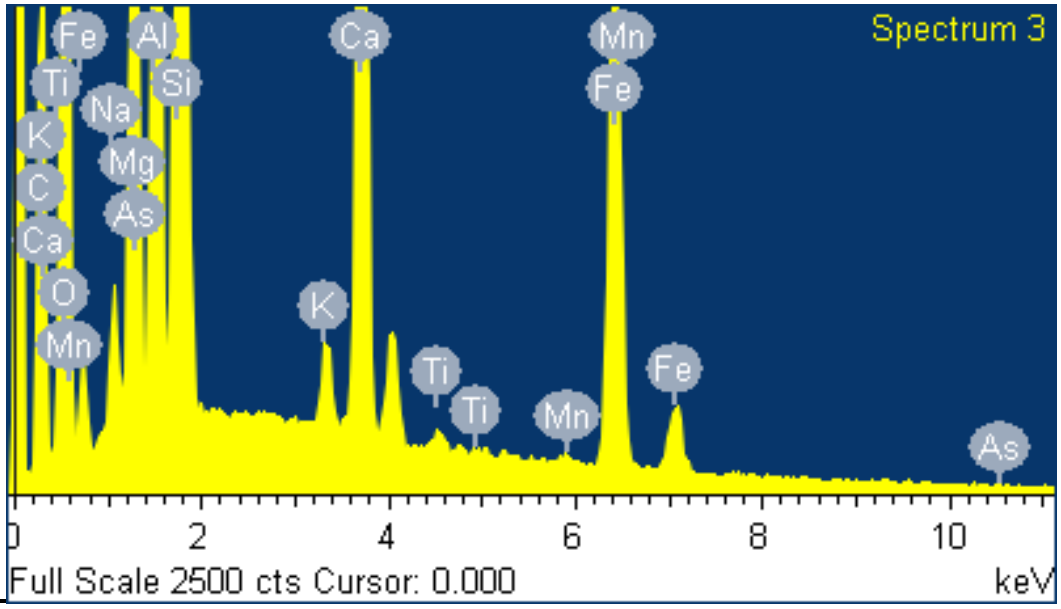

Selected SEM Analyses Data

Spectrum processing: **CS-2-90ft (28m)-grey sediments**

No peaks omitted

Processing option : All elements analyzed (Normalised)

Number of iterations = 6

Standard:

C CaCO3 1-Jun-1999 12:00 AM

O SiO2 1-Jun-1999 12:00 AM

Na Albite 1-Jun-1999 12:00 AM

Mg MgO 1-Jun-1999 12:00 AM

Al Al2O3 1-Jun-1999 12:00 AM

Si SiO2 1-Jun-1999 12:00 AM

K MAD-10 Feldspar 1-Jun-1999 12:00 AM

Ca Wollastonite 1-Jun-1999 12:00 AM

Ti Ti 1-Jun-1999 12:00 AM

Mn Mn 1-Jun-1999 12:00 AM

Fe Fe 1-Jun-1999 12:00 AM

As InAs 1-Jun-1999 12:00 AM

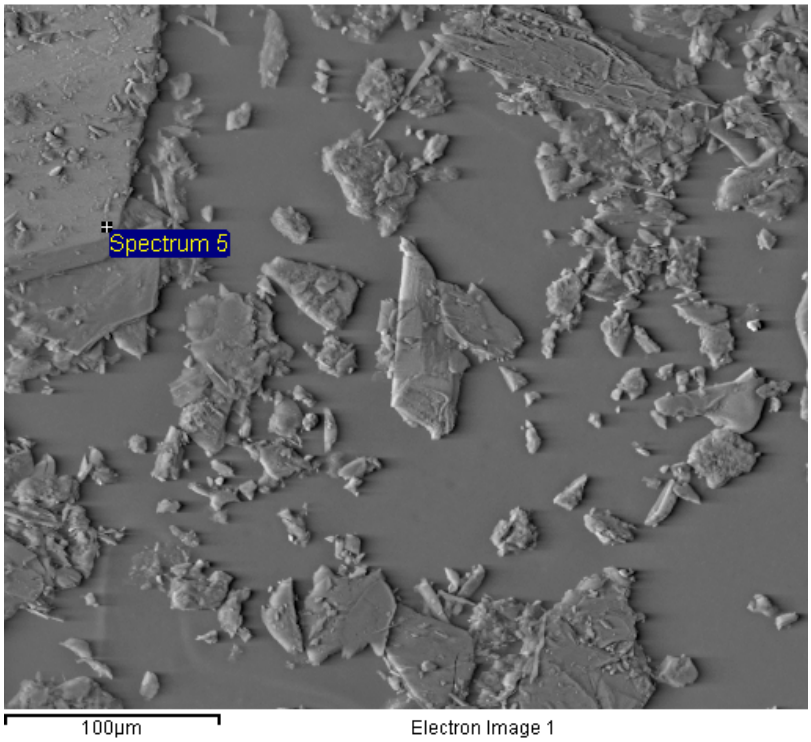

Element	Weight %	Atomic %
C K	7.54	11.72
O K	56.04	65.44
Na K	1.02	0.83
Mg K	3.17	2.44
Al K	11.96	8.28
Si K	13.33	8.87
K K	0.36	0.17
Ca K	0.22	0.10
Ti K	0.44	0.17
Mn K	0.03	0.01
Fe K	5.79	1.94
As L	0.09	0.02
Totals	100.00	

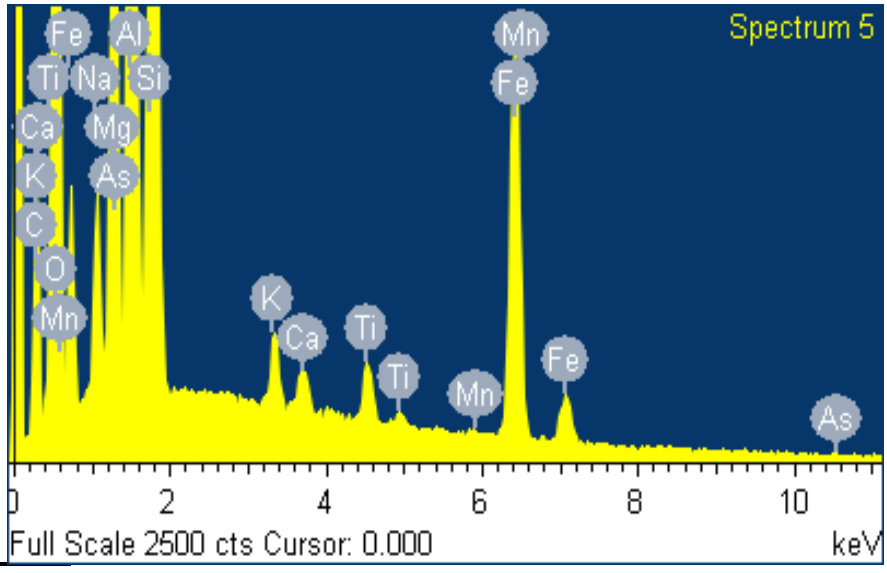

Selected SEM Analyses Data

Spectrum processing: **CS-12-150ft (45m)- dark grey sediments**

Peak possibly omitted: 8.600 keV

Processing option : All elements analyzed (Normalised)

Number of iterations = 3

Standard:

C CaCO3 1-Jun-1999 12:00 AM

O SiO2 1-Jun-1999 12:00 AM

Na Albite 1-Jun-1999 12:00 AM

Mg MgO 1-Jun-1999 12:00 AM

Al Al2O3 1-Jun-1999 12:00 AM

Si SiO2 1-Jun-1999 12:00 AM

K MAD-10 Feldspar 1-Jun-1999 12:00 AM

Ca Wollastonite 1-Jun-1999 12:00 AM

Ti Ti 1-Jun-1999 12:00 AM

Mn Mn 1-Jun-1999 12:00 AM

Fe Fe 1-Jun-1999 12:00 AM

As InAs 1-Jun-1999 12:00 AM

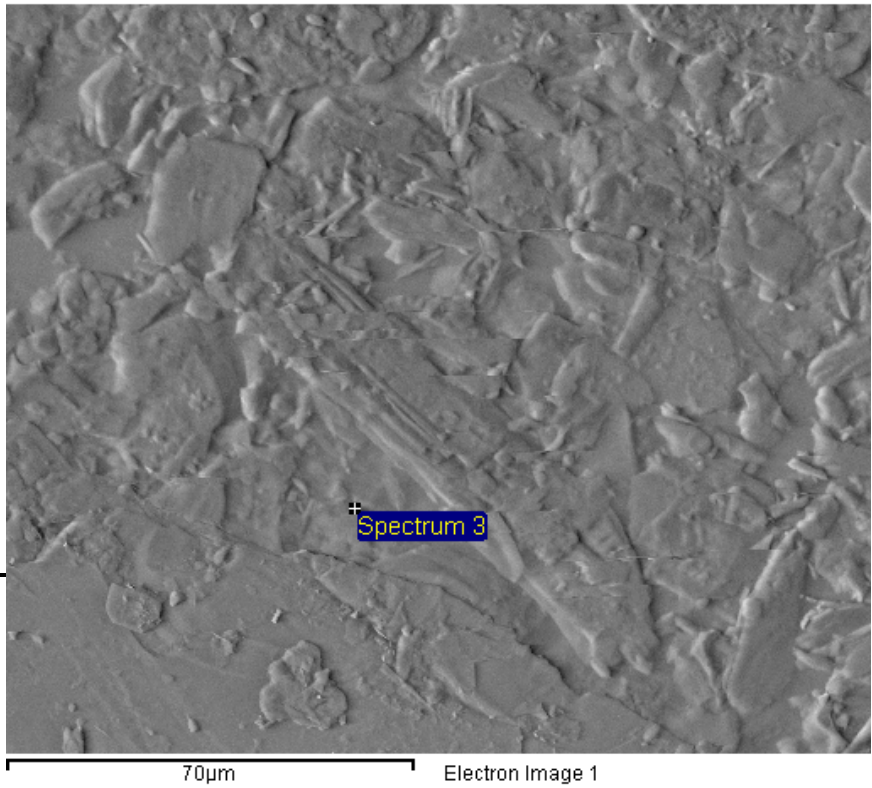

Element	Weight%	Atomic%
C K	0.80	1.48
O K	47.30	65.75
Na K	0.85	0.82
Mg K	1.38	1.26
Al K	4.98	4.10
Si K	20.73	16.42
K K	1.80	1.02
Ca K	0.82	0.46
Ti K	3.16	1.47
Mn K	0.05	0.02
Fe K	17.96	7.15
As L	0.18	0.05

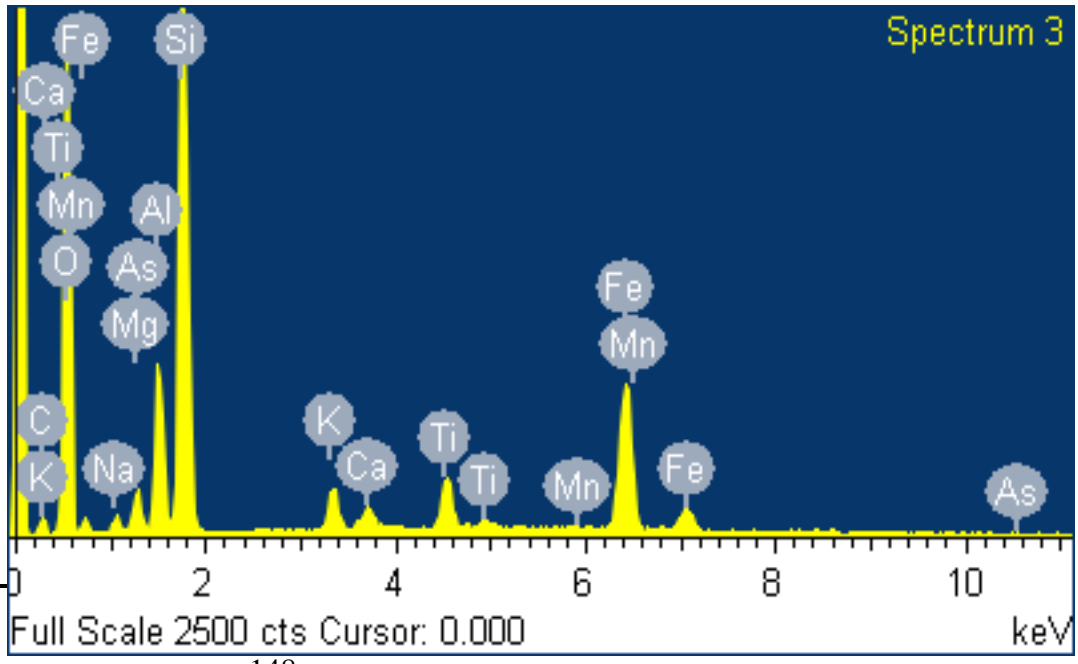

Totals	100.00

Selected SEM Analysis Data

Spectrum processing: **CS-2-210ft (64m)- grey sediments**

No peaks omitted

Processing option: All elements analyzed (Normalised)

Number of iterations = 5

Standard:

C CaCO3 1-Jun-1999 12:00 AM

O SiO2 1-Jun-1999 12:00 AM

Na Albite 1-Jun-1999 12:00 AM

Mg MgO 1-Jun-1999 12:00 AM

Al Al2O3 1-Jun-1999 12:00 AM

Si SiO2 1-Jun-1999 12:00 AM

S FeS2 1-Jun-1999 12:00 AM

K MAD-10 Feldspar 1-Jun-1999 12:00 AM

Ca Wollastonite 1-Jun-1999 12:00 AM

Ti Ti 1-Jun-1999 12:00 AM

Mn Mn 1-Jun-1999 12:00 AM

Fe Fe 1-Jun-1999 12:00 AM

As InAs 1-Jun-1999 12:00 AM

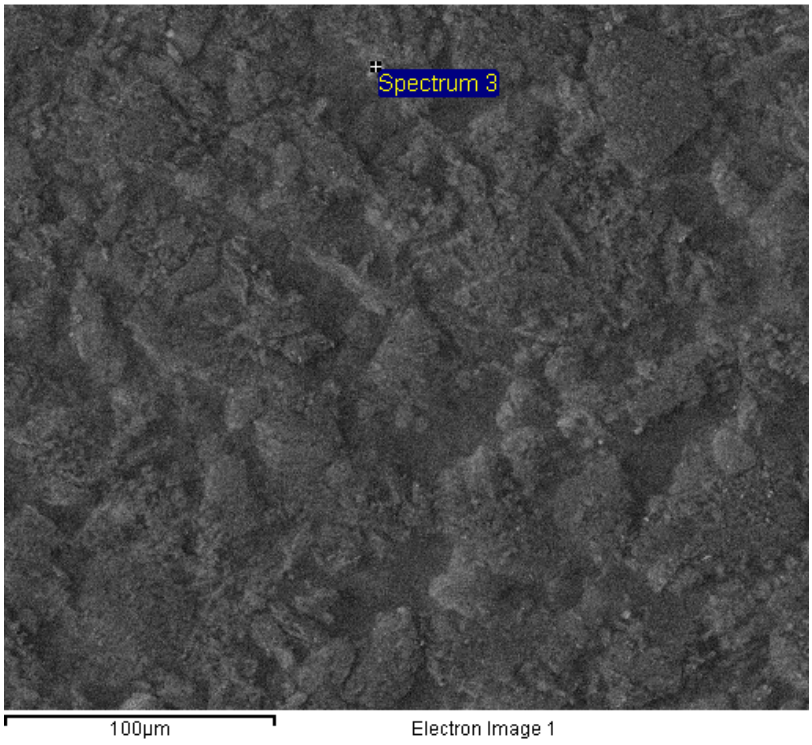

Element	Weight%	Atomic%
C K	6.35	11.96
O K	41.61	58.87
Na K	0.35	0.34
Mg K	0.55	0.52
Al K	2.89	2.42
Si K	7.32	5.90
S K	10.97	7.74
K K	0.44	0.25
Ca K	0.15	0.08
Ti K	0.14	0.06
Mn K	0.17	0.07
Fe K	28.97	11.74
As L	0.10	0.03
Totals	100.00	

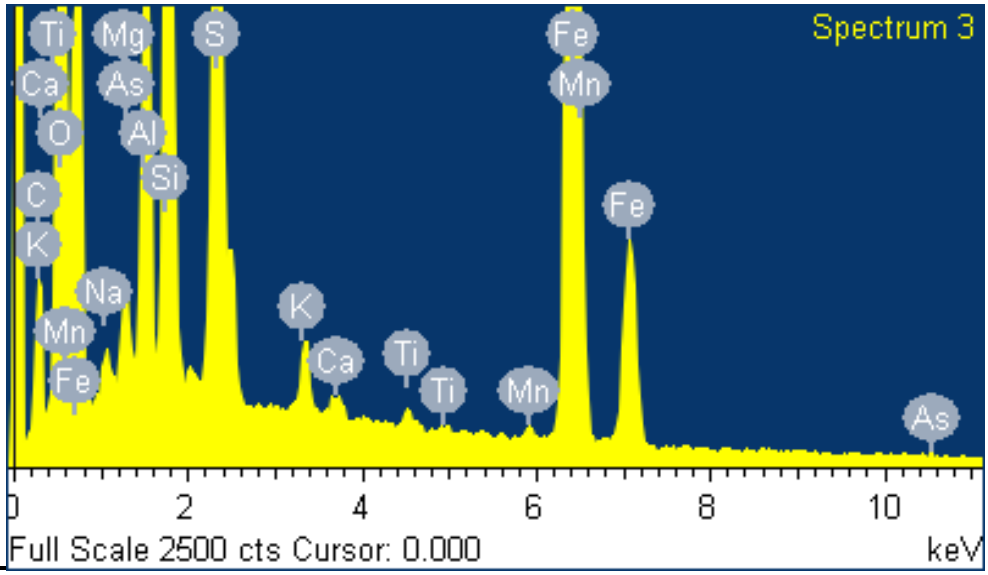

Selected SEM Analyses Data

Spectrum processing: **CS2-265 (80m) - dark grey sediment**

No peaks omitted

Processing option: All elements analyzed (Normalised)

Number of iterations = 4

Standard:

C CaCO3 1-Jun-1999 12:00 AM

O SiO2 1-Jun-1999 12:00 AM

Al Al2O3 1-Jun-1999 12:00 AM

Si SiO2 1-Jun-1999 12:00 AM

K MAD-10 Feldspar 1-Jun-1999 12:00 AM

Mn Mn 1-Jun-1999 12:00 AM

Fe Fe 1-Jun-1999 12:00 AM

As InAs 1-Jun-1999 12:00 AM

Element	Weight%	Atomic%
C K	9.88	15.29
O K	55.39	64.34
Al K	4.76	3.28
Si K	21.29	14.09
K K	1.11	0.53
Mn K	-0.16	-0.06
Fe K	7.31	2.43
As L	0.43	0.11
Totals	100.00	

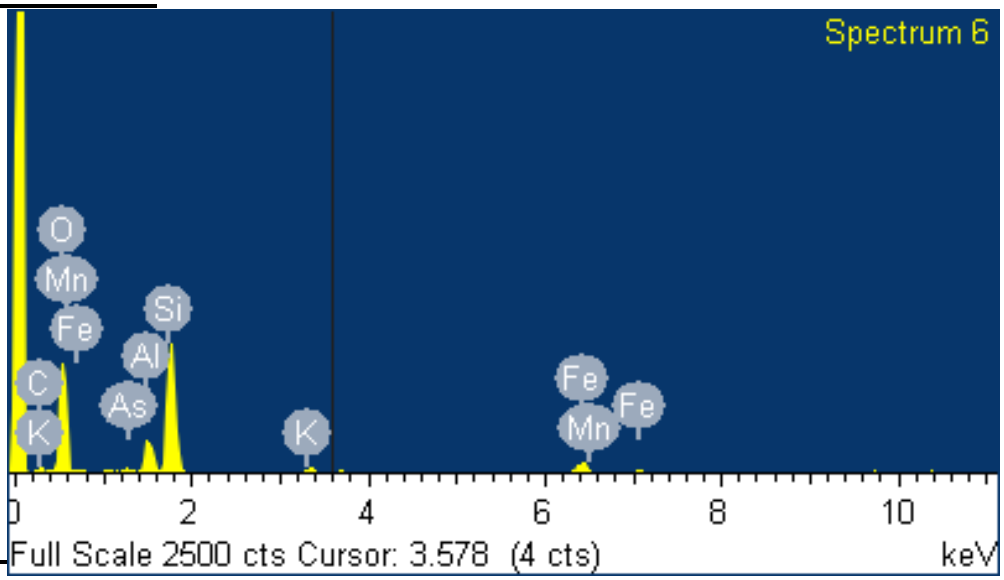

Selected SEM Analysis Data

Spectrum processing: **CS-2-310 (95m) - light grey sediments**

No peaks omitted

Processing option: All elements analyzed (Normalised)

Number of iterations = 5

Standard:

C CaCO3 1-Jun-1999 12:00 AM

O SiO2 1-Jun-1999 12:00 AM

Na Albite 1-Jun-1999 12:00 AM

Al Al2O3 1-Jun-1999 12:00 AM

Si SiO2 1-Jun-1999 12:00 AM

K MAD-10 Feldspar 1-Jun-1999 12:00 AM

Ca Wollastonite 1-Jun-1999 12:00 AM

Mn Mn 1-Jun-1999 12:00 AM

Fe Fe 1-Jun-1999 12:00 AM

As InAs 1-Jun-1999 12:00 AM

Element	Weight%	Atom%
C K	8.05	13.19
O K	42.77	52.66
Na K	0.69	0.59
Al K	1.58	1.15
Si K	45.23	31.72
K K	0.22	0.11
Ca K	0.46	0.22
Mn K	-0.07	-0.02
Fe K	0.95	0.33
As L	0.13	0.04
C K	8.05	13.19
Totals	100.00	

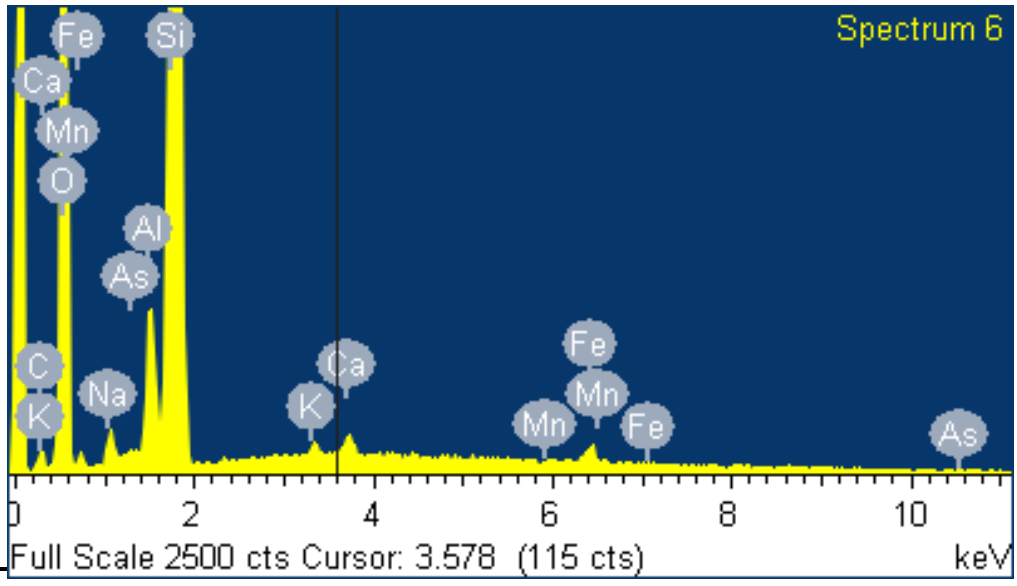

Synchrotron beam line studies of Aquifer Sediments (XANES and EXAFS)

X11A beam is mainly used for As XANES and EXAFS of aquifer sediments. Beam line X11A is a typical x-ray absorption spectroscopy beam line with a double-crystal monochromator. Set-up includes three ion-chambers to measure the transmission of the sample and a reference foil, but it is also possible to measure the fluorescence with a 13-element Ge detector to separate contributions from different elements. Beam line uses double crystal monochromator using a Huber goneometer, Si (111) or Si (311) crystals as optical system. The experimental apparatus includes solid state detector with digital electronics, 13-element Ge detector and radiation hutch. This beam line is controlled by using Mac OS 9, XDAC spectroscopy data acquisition software. Before the analysis the samples are dried (in a nitrogen glow bag) and pulverized to a fine powder using an agate motor. Latter the samples are fixed in steel sample holder and covered with polyethylene tapes on either opening. The standard operation procedure includes 1. Close the beam. 2. Fix the sample inside the radiation hutch; 3. Place the filter in front of the sample; 4. Close the hutch; 5. Start the beam .6 start the analysis (configuration for beam is attached in appendix-2). Before starting the analysis for As, the beam line was normalized for As using a gold foil. A total of 14 samples were analyzed using this beam (South Matlab (Core-2)-8 samples and North Matlab(Core-1)-6 samples).

X 15B beam: X15 B beam line is used to do sulfur speciation of samples and was optimized for spatially for energy x-ray absorption spectroscopy (XANES, EXAFS). Optics scheme was windowless (UHV) with adjustable-pitch collimating/harmonic-rejection mirror, double-crystal fixed-exit monochromator, toroidal focusing mirror. Accessible energy range was 1.2-8 keV, but optimized for 1.7-5 keV. Spatial resolution at the sample position was 0.2 mm to 1.0 mm. Sample environment inside the radiation hutch include He and UHV. Detection schemes include transmission (ion chambers and foils/grids) and fluorescence (Canberra ultra-low-energy Ge). The instrumentation of this beam line includes, Mirror 1: Cylindrical platinum coated Glidcop; 1m long; cooled; vertically collimating; incidence angle can be adjusted (0.2 deg. to 2.0 deg. range) to discriminate against harmonics; located 8 meters from the source. Monochromator: Double flat crystal UHV monochromator with fixed-exit geometry; first crystal is cooled; Bragg angle range from 10 deg. to 80 deg.; located 10 meters from the source. Crystal pairs include Si(111), Ge(111), Si(311), InSb, Beryl. Energy resolution is determined by crystals. Energy repeatability is within 0.1 eV scan-to-scan and over 24+ hours. Mirror 2: 1:1 focusing

platinum coated ULE (silica) toroid; 0.4 degree incidence angle; 1m long. Experimental apparatus includes a small hutch Box with He atmosphere and is equipped with a Ge fluorescence detector, ion chambers, and sample stage. Operating range is 1.2-8 keV. Whole system is operated by Windows MS-DOS operating system. Samples are at first pulverized to a fine powder using an agate mortar and packed inside a polyethylene cover. The operating procedure of the beam is 1. Shut the beam or shutters (by pressing the red button in the control box); 2.Undo the interlock and open the hutch; 3. Place the sample carefully inside the mounting plate inside the hutch using clips and polyethylene tapes (while doing this process fix the delicate door of the shutter to a clamp to avoid breakage and make sure that no dust go inside the hutch); 4. Lock the hutch; 4.Swetch on n the beam (by pressing green button in the control box); 5.Purge Helium gas (by rotating the control knob and make sure that the once the pointer reaches 0.5 rotate 2.5 times and stop) ; 6. Waite till I0 (in the left top monitor) is below 0.4 (ideally it should be below 0.25) and close the valve of gas chamber; 7. Target the samples with the beam using a standard fluorescence reference material; 8. Check the I(t) if it is 0.0003 (if it is 0.0003 then the beam is on the sample); 9. Check the fluorescence; 10. start the analysis. A total of 14 number of samples were analyzed in this beam (South Matlab(Core-2)-8 samples and North Matlab(Core-1)-6 samples). Only shallow samples showed good peak for interpretation.

Appendix C.4- Total Digestion of Sediments

Values presented here (mg/kg) are from Total Digestions of select sediment samples by Aqua Regia, measured by ICP-OES.

Core -1 North Matlab (N 23.487556 E 90.66227)

Sample ID	Depth(m)	As mg/Kg	Mn mg/Kg	Fe mg/Kg
CS1-45	14	31.34	123.53	11650.87
CS1-85	26	15.07	242.97	14783.32
CS1-140	43	14.65	513.24	18219.47
CS1-240	73	13.52	212.97	13588.75
CS1-280	85	16.32	830.77	21546.40
CS1-340	104	13.93	611.95	20792.61

Core-2 South Matlab (N 23.36834 E 90.76748)

Sample ID	Depth(m)	As mg/Kg	Mn mg/Kg	Fe mg/Kg
CS2-30	9	30.32	71.41	10878.50
CS2-90	27	20.91	44.01	11052.55
CS2-150	46	22.88	386.09	16829.08
CS2-210	64	27.48	876.33	21306.67
CS2-265	81	17.26	290.73	15584.25
CS2-310	95	13.86	87.97	3815.78
CS2-330	101	15.52	336.10	14871.79
CS2-365	111	12.88	63.65	4384.76

Appendix C.5 Sequential Extraction Results of Samples

Appendix C.5A

Values presented here (mg/kg) are from sequential extractions, measured by ICP-OES.

Core 1 -Arsenic

Sample ID	Depth(m)	Step-1	Step-2	Step-3	Step-4	Step-5	Step-6	Total
CS1-45	14	0	1.07	6.70	6.42	0.00	0.36	14.56
CS1-85	26	0	0.88	6.66	6.26	0.44	0.24	14.48
CS1-140	43	0	0.96	8.03	5.96	0.20	2.48	17.63
CS1-240	73	0	1.86	7.14	6.14	0.48	0.77	16.39
CS1-280	85	0	1.22	6.86	6.12	0.06	2.36	16.62
CS1-340	104	0	0.70	7.77	6.28	0.06	1.54	16.35

Core 2- Arsenic

Sample ID	Depth(m)	Step-1	Step-2	Step-3	Step-4	Step-5	Step-6	Total
CS2-30	9	0	1.22	7.28	6.22	1.45	0.19	16.35
CS2-90	27	0	0.92	6.82	6.46	0.21	0.47	14.87
CS2-150	46	0	1.47	7.63	6.44	0.45	1.93	17.91
CS2-210	64	0	2.25	12.29	6.10	0.42	5.99	27.05
CS2-265	81	0	1.73	7.40	6.27	0.00	1.41	16.82
CS2-310	95	0	1.26	6.47	6.05	0.00	1.47	15.25
CS2-330	101	0	2.13	9.11	6.81	1.28	4.17	23.50
CS2-365	111	0	0.84	7.86	6.08	0.54	0.78	16.10

Appendix C.5B

Values presented here (mg/kg) are from sequential extractions, measured by ICP-OES.

Core 1-Manganese

SampleID	Depth(m)	Step-1	Step-2	Step-3	Step-4	Step-5	Step-6	Total
CS1-45	14	4.13	3.13	0.00	0.00	6.68	151.56	165.50
CS1-85	26	8.38	5.60	27.06	0.00	12.16	109.86	163.07
CS1-140	43	20.52	20.77	213.45	5.22	29.17	325.19	614.32
CS1-240	73	16.25	22.11	0.00	20.03	25.00	231.72	315.11
CS1-280	85	13.09	5.09	0.00	15.83	11.33	600.69	646.03
CS1-340	104	10.18	10.06	0.00	28.01	18.30	505.14	571.68

Core 2-Manganese

SampleID	Depth(m)	Step-1	Step-2	Step-3	Step-4	Step-5	Step-6	Total
CS2-30	9	7.79	6.82	42.74	0.24	10.75	159.59	227.91
CS2-90	27	2.60	4.58	10.01	0.00	5.02	117.03	139.23
CS2-150	46	6.69	25.64	138.33	9.79	21.56	276.57	478.58
CS2-210	64	167.98	54.68	317.05	9.92	36.38	231.55	817.56
CS2-265	81	9.44	30.83	164.52	8.44	24.87	180.35	418.45
CS2-310	95	3.89	4.95	8.70	0.00	12.44	26.75	56.73
CS2-330	101	62.27	54.41	386.66	9.77	25.47	214.14	752.73
CS2-365	111	2.33	2.31	0.00	0.00	10.59	58.56	73.79

Appendix C.5C

Values presented here (mg/kg) are from sequential extractions, measured by ICP-OES.

Core 1-Iron

SampleID	Depth(m)	Step-1	Step-2	Step-3	Step-4	Step-5	Step-6	Total
CS1-45	14	0	12.83	1945.29	1260.89	873.27	8176.76	12269.04
CS1-85	26	0	15.31	3177.44	1536.81	374.37	8068.69	13172.62
CS1-140	43	0	7.56	7223.60	2059.68	917.52	17366.27	27574.63
CS1-240	73	0	5.98	7588.47	3190.54	977.47	14561.33	26323.79
CS1-280	85	0	20.28	14391.50	3531.43	1288.40	20405.63	39637.23
CS1-340	104	0	23.79	12031.64	4158.24	1491.42	21257.66	38962.75

Core 2-Iron

SampleID	Depth(m)	Step-1	Step-2	Step-3	Step-4	Step-5	Step-6	Total
CS2-30	9	0	14.12	3701.89	1476.77	381.32	10075.87	15649.96
CS2-90	27	0	15.60	2263.44	1446.50	215.44	7761.37	11702.35
CS2-150	46	0	8.00	7308.88	2458.78	626.15	15738.72	26140.53
CS2-210	64	0	29.69	13308.78	2247.00	1438.54	18762.39	35786.40
CS2-265	81	0	20.00	6948.63	2386.71	820.79	13421.73	23597.86
CS2-310	95	0	17.08	914.58	590.71	189.64	2267.03	3979.05
CS2-330	101	0	15.79	11464.61	2252.46	1123.08	16709.13	31565.07
CS2-365	111	0	14.54	3503.58	458.64	125.40	3070.55	7172.70

Appendix C.6-Total Carbon and Total Nitrogen of Sediment Samples

Table: (% of) Total Carbon and Total Nitrogen in sediments done in Soils Lab, K-State.

North Matlab (Core-1)		
Depth m	**Total Nitrogen**	**Total Carbon**
14	0.062	0.23
26	0.061	0.24
55	0.102	0.46
73	0.072	0.34
85	0.094	0.55
104	0.095	0.75
South Matlab (Core-2)		
9	0.064	0.19
27	0.055	0.20
46	0.061	0.32
64	0.095	0.98
81	0.094	0.31
94	0.073	0.19
101	0.054	0.25
111	0.062	0.17

Appendix C.7- Field Analyses (Hydrolab® Results)

Field Analyses: HACH® Hydrolab® Results

Nest	Well	Latitude (N)	Longitude (E)	Depth m	T(C)	pH	TDS	DO	EC (µS/c)	Resistivity	Eh (mV)
Nest-3	N-3 P-1	23.32567	90.70171	29	26	7.06	278	2.45	556	1.80E+03	-51.3
	N-3 P-2	23.32567	90.70171	29	26	7.06	278	2.45	556	1.80E+03	-51.3
	N-3 P-3	23.32567	90.70171	52	25.6	7.09	279	2.13	561	1.79E+03	40
	N-3 P-4	23.32567	90.70171	70	25.8	6.92	282	2.3	588	1.77E+03	-12.5
	N-3 P-6	23.32567	90.70171	95	25.9	6.96	254	2.5	507	1.97E+03	-20.9
	N-3 P-5	23.32567	90.70171	238	25.8	7.09	278	2.3	557	1.79E+03	8.8
Nest-4	N-4 P-1	23.42652	90.77570	17	26	7.14	286	2.56	518	1.73E+03	-46
	N-4 P-2	23.42652	90.77570	27	26.2	7.09	290	4.2	586	1.73E+03	-110.5
	N-4 P-3	23.42652	90.77570	56	27.1	6.93	285	5.75	569	1.76E+03	-75
	N-4 P-4	23.42652	90.77570	75	26.6	7.16	290	4.56	578	1.73E+03	-91.8
	N-4 P-6	23.42652	90.77570	116	26.4	7.23	274	3	546	1.83E+03	-125
	N-4 P-5	23.42652	90.77570	238	26.6	7.16	281	1.5	560	1.78E+03	-31.6
Nest-5	N-5 P-1	23.36834	90.76748	11	26	7.17	261	3.25	523	1.91E+03	-70.8
	N-5 P-2	23.36834	90.76748	29	25.8	6.9	293	3.05	596	1.71E+03	-89.6
	N-5 P-4	23.36834	90.76748	82	25.7	7.03	285	1.85	576	1.75E+03	-19.6
	N-5 P-6	23.36834	90.76748	104	25.7	7.14	271	2.95	542	1.84E+03	15
	N-5 P-5	23.36834	90.76748	238	26.1	6.92	283	2.06	569	1.76E+03	90.6
Nest-16	N-16 P-1	23.3201	90.7378	17	25.4	6.92	274	215	527	1.83E+03	-49.1
	N-16 P-2	23.3201	90.7378	30	25.9	7.06	287	2.02	583	1.74E+03	-45.1
	N-16 P-3	23.3201	90.7378	50	26	6.96	290	2.2	585	1.73E+03	4.8
	N-16 P-4	23.3201	90.7378	84	26.6	7.05	268	2.2	538	1.86E+03	-62
	N-16 P-6	23.3201	90.7378	102	26.4	7.03	288	2.25	964	1.77E+03	42
	N-16 P-5	23.3201	90.7378	237	26	7.14	291	1.96	590	1.72E+03	71.1
Nest-17	N-17 P-1	23.33148	90.80419	19	26	7.06	269	2.05	538	1.86E+03	-60.8
	N-17 P-2	23.33148	90.80419	34	26.1	7.07	283	2.04	566	1.77E+03	-58.8

	N-17 P-3	23.33148	90.80419	58	25.8	6.96	293	1.37	590	1.71E+03	22.5
	N-17 P-6	23.33148	90.80419	104	26.2	7.03	526	1.5	1047	9.52E+01	40.1
	N-17 P-5	23.33148	90.80419	230	26	7.12	286	1.4	630	1.70E+03	53.7
Nest-7	N-7 P-1	23.48756	90.66227	14	25.6	7.1	248	2.67	647	1.32E+02	34.6
	N-7 P-2	23.48756	90.66227	26	26.1	7.29	272	3.02	545	1.83E+03	-18.5
	N-7 P-3	23.48756	90.66227	53	24.5	6.7	302	3.52	602	1.66E+03	-4.2
	N-7 P-4	23.48756	90.66227	75	25.3	7.16	283	2.48	573	1.78E+03	-99.5
	N-7 P-6	23.48756	90.66227	102	26.1	7.06	289	2.58	599	1.64E+03	-78.5
	N-7 P-5	23.48756	90.66227	232	26.24	6.95	252	2.94	1214	4.77 E+03	65.6
Nest-8	N-8 P-1	23.43483	90.63064	14	25.3	7.35	335	3	620	1.80E+03	60.2
	N-8 p-2	23.43483	90.63064	53	25.5	7.14	308	3.5	800	1.67E+03	96.3
	N-8 P-4	23.43483	90.63064	101	25.5	7.12	285	3.2	588	1.79E+03	-47.4
	N-8 P-5	23.43483	90.63064	235	26.5	7.07	282	3.17	563	1.77E+03	45
Nest-9	N-9 P-1	23.40918	90.73529	9	25.6	6.95	243	1.5	485	2.07E+03	-13.4
	N-9 P-2	23.40918	90.73529	29	25.6	7.09	285	4.2	580	1.75E+03	-25.8
	N-9 P-3	23.40918	90.73529	44	24.7	6.9	532	1.5	240	9.58E+02	-33.1
	N-9 P-4	23.40918	90.73529	66	24.9	7.09	651	4.5	1294	1.71E+03	-69.3
	N-9 P-5	23.40918	90.73529	226	24	7.2	286	2.5	820	1.75E+03	-47.9
Nest-12	N-12 P-1	23.43352	90.67261	14	25.3	7.28	276	2.45	563	1.81E+03	-63
	N-12 P-2	23.43352	90.67261	27	25.6	7.17	297	2.45	640	1.72E+03	-69.6
	N-12 P-3	23.43352	90.67261	81	24.9	7.17	305	2.1	634	1.63E+03	-78.1
	N-12 P-6	23.43352	90.67261	116	25.5	7.28	292	4.5	740	1.71E+03	-85.3
	N-12 P-5	23.43352	90.67261	219	25.4	6.94	292	2.42	710	1.70E+03	56.4
Nest-13	N-13 P-1	23.47562	90.60495	14	24.9	7.35	250	2.61	580	2.01E+03	-124.9
	N-13 P-2	23.47562	90.60495	33	25.3	7.23	291	2.26	592	1.72E+03	-131.4
	N-13 P-3	23.47562	90.60495	85	24.5	7.08	298	2.24	610	1.68E+03	-54.4
	N-13 P-6	23.47562	90.60495	111	24.7	7.65	252	2.45	506	1.98E+03	-84.8
	N-13 P-5	23.47562	90.60495	237	25.3	7.54	282	2.2	565	1.78E+03	56.2

Appendix C.8- Field TEST KIT Analyses (WATER)

Field Kit Test

Nest	Well	Latitude (N)	Longitude (E)	Depth m	Alkalinity (mg/l)	NH+	As (ppb)	NO_3^- (mg/l)	Fe_t (mg/l)	Fe^{2+} (mg/l)	HCO_3^-(mg/l)	SO_4^{2-} (mg/l)
Nest-3	N-3 P-1	23.32567	90.70171	29		0.11					648	
	N-3 P-2	23.32567	90.70171	29	450	0.12	250	0	6.68	0	458	0
	N-3 P-3	23.32567	90.70171	52	350	0.75	50	0	5.52	5.33	358	0
	N-3 P-4	23.32567	90.70171	70	270	0.54	5	0	2.02	1.93	275	
	N-3 P-6	23.32567	90.70171	95	300		10	0	3.58	3.76	305	
	N-3 P-5	23.32567	90.70171	238	435		250	0	6.92	6.78	114	
Nest-4	N-4 P-1	23.42652	90.77570	17	110	10.32	10	0	2.08	2.05		
	N-4 P-2	23.42652	90.77570	27	480		100		0.01	0.01	480	
	N-4 P-3	23.42652	90.77570	56	450	0.07	300	0	0	0	450	
	N-4 P-4	23.42652	90.77570	75	320	0.43	100		0	6.49	320	
	N-4 P-6	23.42652	90.77570	116	405	0.26	150	0	0.03	0	404	
	N-4 P-5	23.42652	90.77570	238	265		10				267	
Nest-5	N-5 P-1	23.36834	90.76748	11	130	0.06	5	0	0	0	137	
	N-5 P-2	23.36834	90.76748	29	280	6.48	200	2	6.98	6.50		0
	N-5 P-4	23.36834	90.76748	82	470	0.15	10	0	3.67	3.22	282	0
	N-5 P-6	23.36834	90.76748	104	480	1.14	400		2.61	2.25	473	
	N-5 P-5	23.36834	90.76748	238	305	5.38	0	2	2.56	2.53	480	2
Nest-16	N-16 P-1	23.3201	90.7378	17	235		0	1	5.45	5.05	305	2
	N-16 P-2	23.3201	90.7378	30	440	0.49	1000		3.5	0.15	236	
	N-16 P-3	23.3201	90.7378	50	670		150		6.53	0.01		
	N-16 P-4	23.3201	90.7378	84	205	0.00	10	0	0.01	0.02	442	
	N-16 P-6	23.3201	90.7378	102	660	0.00	750	0	0.01	0.04	671	
	N-16 P-5	23.3201	90.7378	237	530		5		6.52	5.63	206	
Nest-17	N-17 P-1	23.33148	90.80419	19	485	4.23	5	0	0.01	0.03	663	
	N-17 P-2	23.33148	90.80419	34	540		300.00		0.04	0.03	534	

	N-17 P-3	23.33148	90.80419	58	540	1.43	350.00	0	0	0	488	
	N-17 P-6	23.33148	90.80419	104	420	1.76	50.00		0.01	0		
	N-17 P-5	23.33148	90.80419	230	320	2.23	0.00	0	4.03	0		
Nest-7	N-7 P-1	23.48756	90.66227	14	310	2.02	0.00	0	0.1	0		
	N-7 P-2	23.48756	90.66227	26	550	>3.3	400	0	>3.5	3.26		2
	N-7 P-3	23.48756	90.66227	53	500	>3.8	500	0	>3.5	3.26		2
	N-7 P-4	23.48756	90.66227	75	480	0.08	0	1	>3.5	5.37		1
	N-7 P-6	23.48756	90.66227	102	290	1.26	200	0	3.12	2.98		1
	N-7 P-5	23.48756	90.66227	232	310	0.05	25	0	2.35	2.03	549	0
Nest-8	N-8 P-1	23.43483	90.63064	14	235	0.11	0	2	3.87	3.12	496	1
	N-8 p-2	23.43483	90.63064	53	630	0.10	750				480	
	N-8 P-4	23.43483	90.63064	101	1050	0.13	25				290	
	N-8 P-5	23.43483	90.63064	235	275	0.00	75				313	
Nest-9	N-9 P-1	23.40918	90.73529	9	235	0.00	0				236	
	N-9 P-2	23.40918	90.73529	29	265		500		2.15	0		
	N-9 P-3	23.40918	90.73529	44	770	0.16	750	0	0.03	0.00	633	
	N-9 P-4	23.40918	90.73529	66	235	0.04	10	0	0.03	0	1052	
	N-9 P-5	23.40918	90.73529	226	220		5	0	0	0.07	275	
Nest-12	N-12 P-1	23.43352	90.67261	14	120	0.14	0	0	0.2	0.05	236	
	N-12 P-2	23.43352	90.67261	27	355		250	0	>3.5	0.28		
	N-12 P-3	23.43352	90.67261	81	240	0.65	500		2.71	0.08	168	
	N-12 P-6	23.43352	90.67261	116	900	4.65	100	0	0.25	0.05	770	
	N-12 P-5	23.43352	90.67261	219	540	2.89	250	0	0	0.05	534	
Nest-13	N-13 P-1	23.47562	90.60495	14	265	9.78	0		2	0.50	221	
	N-13 P-2	23.47562	90.60495	33	500	2.05	200.00	0	2.65	2.23	122	1
	N-13 P-3	23.47562	90.60495	85	540	0.00	450.00		6.37	6.23		
	N-13 P-6	23.47562	90.60495	111	320	0.06	75.00				358	
	N-13 P-5	23.47562	90.60495	237	210	0.11	0.00				244	

Appendix C.9- Water Analyses for Arsenic and Manganese (ICP-MS)

Nest	Well ID	Thana	Village	Latitude(N)	Longitude(E)	Depth m	Mn(mg/l)	As(µg/l)
Nest-3	N-3 P-1	Matlab Dakshin	Dighaldi	23.32567	90.70171	17	1.21	410.65
	N-3 P-2	Matlab Dakshin	Dighaldi	23.32567	90.70171	29	0.62	274.09
	N-3 P-3	Matlab Dakshin	Dighaldi	23.32567	90.70171	52	0.80	54.58
	N-3 P-4	Matlab Dakshin	Dighaldi	23.32567	90.70171	70	3.95	7.96
	N-3 P-6	Matlab Dakshin	Dighaldi	23.32567	90.70171	95	3.75	6.26
	N-3 P-5	Matlab Dakshin	Dighaldi	23.32567	90.70171	238	0.53	11.25
Nest-4	N-4 P-1	Matlab Dakshin	Nandikhola	23.42652	90.77570	17	0.13	95.41
	N-4 P-2	Matlab Dakshin	Nandikhola	23.42652	90.77570	27	0.15	286.49
	N-4 P-3	Matlab Dakshin	Nandikhola	23.42652	90.77570	56	1.71	98.33
	N-4 P-4	Matlab Dakshin	Nandikhola	23.42652	90.77570	75	0.22	115.15
	N-4 P-6	Matlab Dakshin	Nandikhola	23.42652	90.77570	116	0.37	9.30
	N-4 P-5	Matlab Dakshin	Nandikhola	23.42652	90.77570	238	0.30	9.24
Nest-5	N-5 P-1	Matlab Dakshin	Narayanpur	23.36834	90.76748	11	0.183	166
	N-5 P-2	Matlab Dakshin	Narayanpur	23.36834	90.76748	29	0.842	6.98
	N-5 P-4	Matlab Dakshin	Narayanpur	23.36834	90.76748	82	0.802	313
	N-5 P-6	Matlab Dakshin	Narayanpur	23.36834	90.76748	104	0.225	2.11
	N-5 P-5	Matlab Dakshin	Narayanpur	23.36834	90.76748	238	0.184	3.2
Nest-16	N-16 P-1	Matlab Dakshin	Dingavanga	23.3201	90.7378	17	0.801	769
	N-16 P-2	Matlab Dakshin	Dingavanga	23.3201	90.7378	30	0.135	161
	N-16 P-3	Matlab Dakshin	Dingavanga	23.3201	90.7378	50	0.586	5.09
	N-16 P-4	Matlab Dakshin	Dingavanga	23.3201	90.7378	84	0.771	679
	N-16 P-6	Matlab Dakshin	Dingavanga	23.3201	90.7378	102	0.408	5.13
	N-16 P-5	Matlab Dakshin	Dingavanga	23.3201	90.7378	237	0.359	4.15
Nest-7	N-7 P-1	Matlab Uttar	Hapania	23.48756	90.66227	14	1.06	382
	N-7 P-2	Matlab Uttar	Hapania	23.48756	90.66227	26	0.228	575
	N-7 P-3	Matlab Uttar	Hapania	23.48756	90.66227	53	0.112	1.12

	N-7 P-4	Matlab Uttar	Hapania	23.48756	90.66227	75	0.239	187
	N-7 P-6	Matlab Uttar	Hapania	23.48756	90.66227	102	0.159	22.9
	N-7 P-5	Matlab Uttar	Hapania	23.48756	90.66227	232	0.128	0.44
Nest-8	N-8 P-1	Matlab Uttar	Thakurchar	23.43483	90.63064	14	1.65	781
	N-8 p-2	Matlab Uttar	Thakurchar	23.43483	90.63064	53	0.759	25.3
	N-8 P-4	Matlab Uttar	Thakurchar	23.43483	90.63064	101	0.115	84.5
	N-8 P-5	Matlab Uttar	Thakurchar	23.43483	90.63064	235	0.145	1.15
Nest-9	N-9 P-1	Matlab Uttar	Tatua	23.40918	90.73529	9	0.342	474
	N-9 P-2	Matlab Uttar	Tatua	23.40918	90.73529	29	0.803	764
	N-9 P-3	Matlab Uttar	Tatua	23.40918	90.73529	44	2.87	6.12
	N-9 P-4	Matlab Uttar	Tatua	23.40918	90.73529	66	1.39	6.03
	N-9 P-5	Matlab Uttar	Tatua	23.40918	90.73529	226	0.177	1.81
Nest-12	N-12 P-1	Matlab Uttar	Brahmanchalk	23.43352	90.67261	14	0.566	225
	N-12 P-2	Matlab Uttar	Brahmanchalk	23.43352	90.67261	27	0.121	506
	N-12 P-3	Matlab Uttar	Brahmanchalk	23.43352	90.67261	81	0.169	88.6
	N-12 P-6	Matlab Uttar	Brahmanchalk	23.43352	90.67261	116	0.0735	248
	N-12 P-5	Matlab Uttar	Brahmanchalk	23.43352	90.67261	219	0.0955	2.49

Appendix C.10- Water Cation Analyses (Fe_t, Ca, Mg and K) by ICP-OES

Nest	Well ID	Latitude(N)	Longitude(E)	Depth m	Ca (mg/l)	Mg(mg/l)	Fe(t) (mg/l)	K (mg/l)
Nest-3	N-3 P-1	23.32567	90.70171	17	159.51	29.67	3.86	6.15
	N-3 P-2	23.32567	90.70171	29	88.63	32.67	9.25	6.37
	N-3 P-3	23.32567	90.70171	52	65.40	31.17	6.03	3.51
	N-3 P-4	23.32567	90.70171	70	70.36	23.15	1.17	2.39
	N-3 P-6	23.32567	90.70171	95	75.86	25.63	0.93	1.98
	N-3 P-5	23.32567	90.70171	238	120.56	65.22	10.62	6.05
Nest-4	N-4 P-1	23.42652	90.77570	17	59.79	58.67	3.56	
	N-4 P-2	23.42652	90.77570	27	81.58	50.33	5.86	7.40
	N-4 P-3	23.42652	90.77570	56	44.27	30.12	10.49	16.29
	N-4 P-4	23.42652	90.77570	75	45.68	37.71	5.61	5.67
	N-4 P-6	23.42652	90.77570	116	38.27	32.81	5.40	13.82
	N-4 P-5	23.42652	90.77570	238	80.28	50.00	8.47	2.18
Nest-5	N-5 P-1	23.36834	90.76748	11	34.63	30.88	6.22	5.41
	N-5 P-2	23.36834	90.76748	29	31.08	26.83	2.05	4.07
	N-5 P-4	23.36834	90.76748	82	31.10	21.60	10	8.42
	N-5 P-6	23.36834	90.76748	104	29.59	25.85	5.48	4.02
	N-5 P-5	23.36834	90.76748	238	79.76	41.91	3.07	8.46
Nest-16	N-16 P-1	23.3201	90.7378	17	125.83	28.47	7.96	5.51
	N-16 P-2	23.3201	90.7378	30	110.77	24.69	6.66	14.4
	N-16 P-3	23.3201	90.7378	50	13.35	31.38	0.24	1.14
	N-16 P-4	23.3201	90.7378	84	44.67	21.89	10	5.49
	N-16 P-6	23.3201	90.7378	102	13.29	13.90	9.94	11
	N-16 P-5	23.3201	90.7378	237	54.20	29.14	7.72	4
Nest-7	N-7 P-1	23.48756	90.66227	14	46.37	8.79	10	5.06
	N-7 P-2	23.48756	90.66227	26	173.42	32.58	6.36	5.22
	N-7 P-3	23.48756	90.66227	53	56.44	25.19	2.19	4.9

	N-7 P-4	23.48756	90.66227	75	96.51	33.23	5.88	4.93
	N-7 P-6	23.48756	90.66227	102	35.48	16.92	5.29	2.04
	N-7 P-5	23.48756	90.66227	232	51.24	21.21	0.91	4.89
Nest-8	N-8 P-1	23.43483	90.63064	14	74.61	17.08	6.32	4.94
	N-8 p-2	23.43483	90.63064	53	168.88	61.68	2.33	20
	N-8 P-4	23.43483	90.63064	101	71.98	143.09	5.3	20
	N-8 P-5	23.43483	90.63064	235	51.60	24.31	0.16	5.06
Nest-9	N-9 P-1	23.40918	90.73529	9	31.20	8.53	3.17	2.84
	N-9 P-2	23.40918	90.73529	29	99.07	38.35	1.63	5.86
	N-9 P-3	23.40918	90.73529	44	47.79	21.24	2.48	1.48
	N-9 P-4	23.40918	90.73529	66	11.91	6.67	10	2.49
	N-9 P-5	23.40918	90.73529	226	31.36	22.25	3.06	1.82
Nest-12	N-12 P-1	23.43352	90.67261	14	184.08	37.52	4.35	3.71
	N-12 P-2	23.43352	90.67261	27	59.80	58.84	10	8.16
	N-12 P-3	23.43352	90.67261	81	12.94	12.27	10	20
	N-12 P-6	23.43352	90.67261	116	127.32	28.70	3.23	5.39
	N-12 P-5	23.43352	90.67261	219	26.27	17.04	10	6.64

Appendix C.11- Water Anion Analyses by Ion Chromatograph

Nest	Well ID	F(mg/l)	Cl(mg/l)	NO_2(mg/l)	Bromide(mg/l)	NO_3(mg/l)	PO_4-P(mg/l)	SO_4(mg/l)
Nest -5	P-1	0.38	6.36	1.10	n.a	10.45	2.62	1.48
	p-2	0.86	759.31	2.32	2.64	5.53	6.53	1.60
	P-3	n.a	728.35	0.99	2.29	4.02	2.04	1.50
	P-4	n.a	372.82	n.a	1.83	n.a	10.75	1.43
	P-5	n.a	n.a	1.07	2.44	0.80	2.94	5.33
	P-6	n.a	393.22	1.44	1.69	9.98	15.03	1.51
Nest-7	P-1	0.37	4.88	n.a	n.a	16.92	5.15	1.40
	P-2	0.41	41.36	n.a	1.03	n.a	2.00	1.33
	P-3	n.a	483.15	1.56	1.99	4.39	1.62	1.43
	P-4	0.40	300.67	1.68	1.83	2.85	2.36	1.45
	P-5	0.58	130.01	0.84	1.14	0.71	1.99	0.46
	P-6	0.37	232.25	1.92	1.79	2.90	3.35	1.44
Nest-8	P-1	0.33	22.03	n.a	0.91	11.28	2.35	1.45
	P-2	0.46	n.a	n.a	1.49	7.30	23.51	1.48
	P-3	n.a	n.a	n.a	1.70	8.27	8.55	1.44
	P-4	n.a	222.70	1.30	1.35	2.76	2.19	1.44
	P-5	n.a	442.29	n.a	2.06	n.a	1.95	n.a
Nest -9	P-1	0.43	3.64	n.a	n.a	2.36	11.47	2.06
	P-2	n.a	98.39	n.a	1.27	n.a	3.19	2.13
	P-3	n.a	144.02	1.00	1.23	0.71	1.51	1.62
	P-4	n.a	541.58	n.a	2.26	3.25	1.42	2.11
	P-5	0.49	212.44	n.a	1.30	1.75	1.38	4.17
Nest-12	P-1	0.32	12.07	1.37	n.a	8.96	1.87	1.48
	P-2	n.a	398.94	n.a	2.23	39.17	2.74	1.45
	P-3	0.43	n.a	n.a	2.25	4.30	3.59	1.35
	P-5	n.a	n.a	n.a	4.34	n.a	1.35	n.a
	P-6	n.a	664.63	1.60	2.45	3.27	1.43	1.50
Nest -16	P-1	0.35	50.35	n.a	1.06	n.a	1.29	1.46
	P-2	0.33	776.95	n.a	3.12	37.87	4.76	1.36
	P-3	1.08	n.a	n.a	3.48	n.a	2.17	1.46
	P-4	0.36	52.01	1.48	0.95	4.17	1.39	1.55
	P-5	0.35	n.a	n.a	6.29	4.13	1.30	97.28
	P-6	0.40	n.a	n.a	4.30	n.a	n.a	1.43

T-Test for Water Chemistry

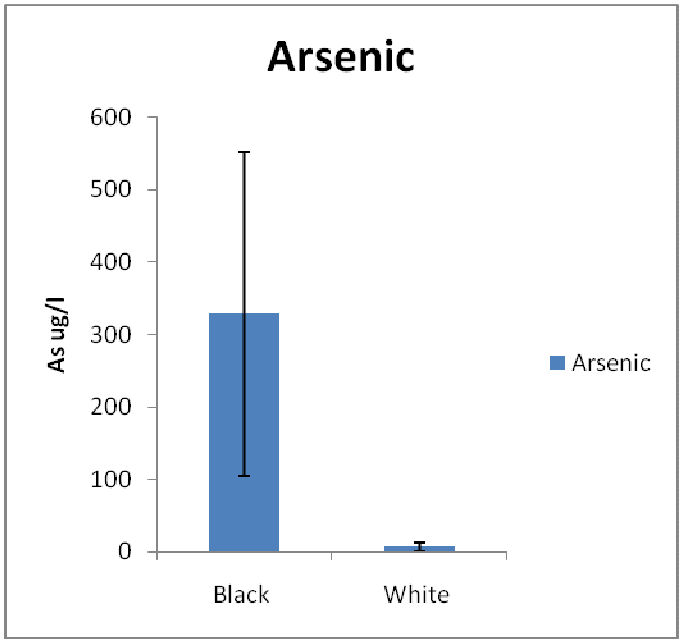

t-Test: Two-Sample Assuming Unequal Variances

	Variable 1	*Variable 2*
Mean	328.6769	6.901518
Variance	49807.96	43.77779
Observations	21	20
Hypothesized Mean Difference	0	
df	20	
t Stat	6.604087	
P(T<=t) one-tail	9.84E-07	
t Critical one-tail	1.724718	
P(T<=t) two-tail	1.97E-06	
t Critical two-tail	2.085963	

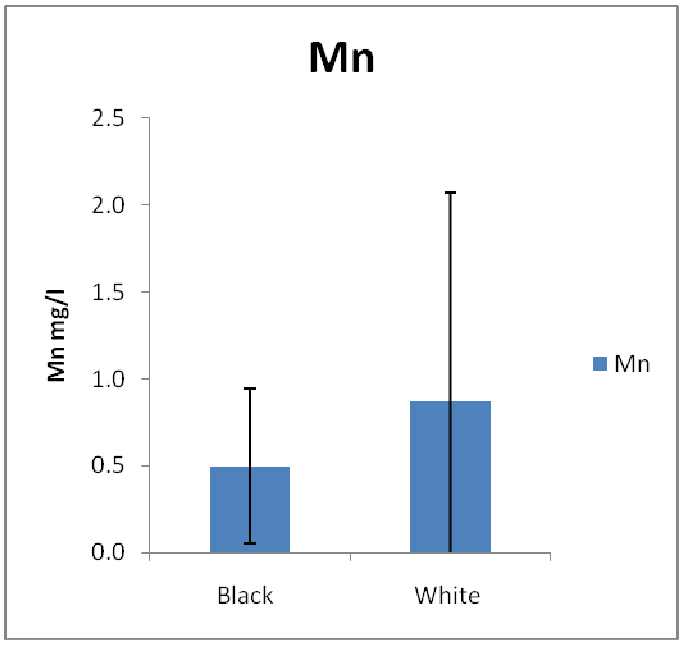

t-Test: Two-Sample Assuming Unequal Variances

	Variable 1	*Variable 2*
Mean	0.497743	0.867383
Variance	0.198188	1.444833
Observations	21	20
Hypothesized Mean Difference	0	
df	24	
t Stat	-1.29337	
P(T<=t) one-tail	0.104097	
t Critical one-tail	1.710882	
P(T<=t) two-tail	0.208194	
t Critical two-tail	2.063899	

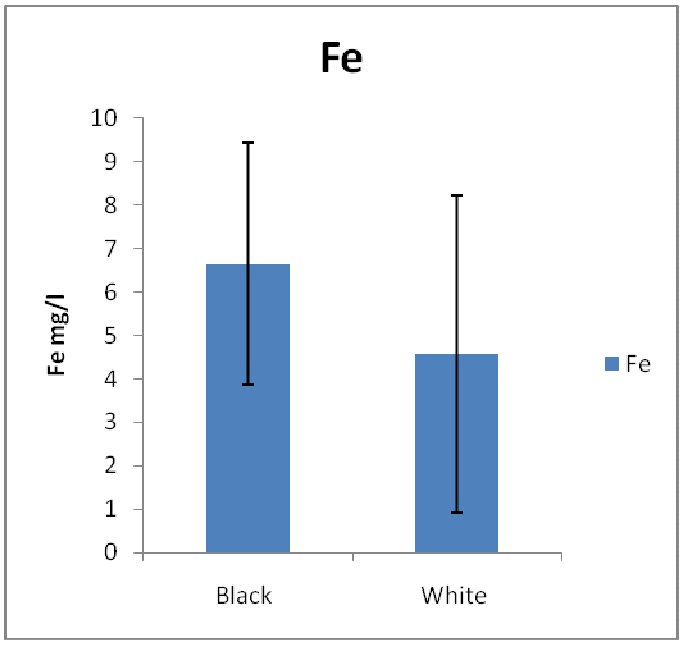

t-Test: Two-Sample Assuming Unequal Variances

	Variable 1	*Variable 2*
Mean	6.637794	4.576243
Variance	7.770285	13.36349
Observations	21	20
Hypothesized Mean Difference	0	
df	36	
t Stat	2.02328	
P(T<=t) one-tail	0.025259	
t Critical one-tail	1.688298	
P(T<=t) two-tail	0.050518	
t Critical two-tail	2.028094	

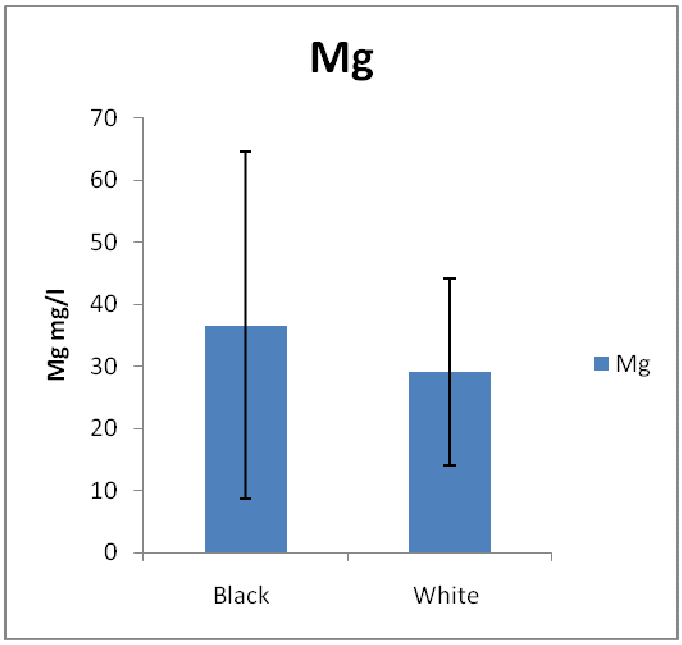

t-Test: Two-Sample Assuming Unequal Variances

	Variable 1	*Variable 2*
Mean	36.59979	29.11704
Variance	777.3085	225.6194
Observations	21	20
Hypothesized Mean Difference	0	
df	31	
t Stat	1.076731	
P(T<=t) one-tail	0.144954	
t Critical one-tail	1.695519	
P(T<=t) two-tail	0.289909	
t Critical two-tail	2.039513	

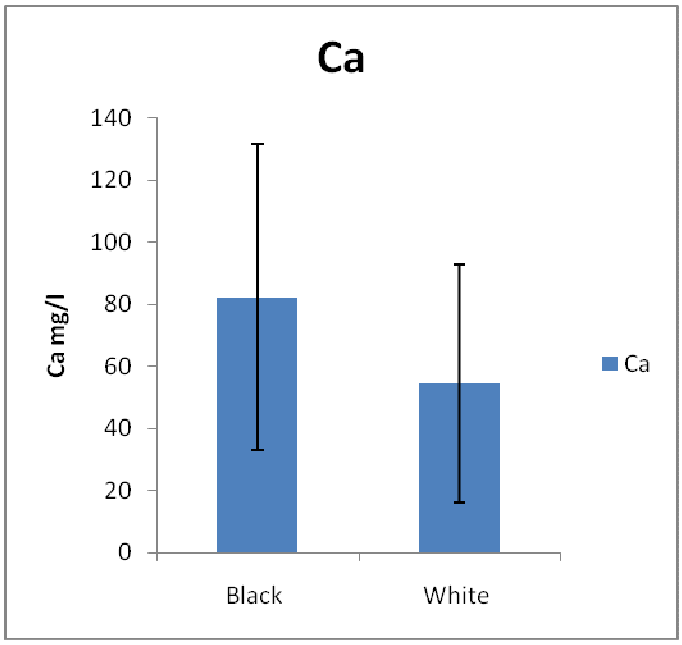

t-Test: Two-Sample Assuming Unequal Variances

	Variable 1	*Variable 2*
Mean	82.34	54.3772
Variance	2440.404	1466.13
Observations	21	20
Hypothesized Mean Difference	0	
df	37	
t Stat	2.031222	
P(T<=t) one-tail	0.024731	
t Critical one-tail	1.687094	
P(T<=t) two-tail	0.049463	
t Critical two-tail	2.026192	

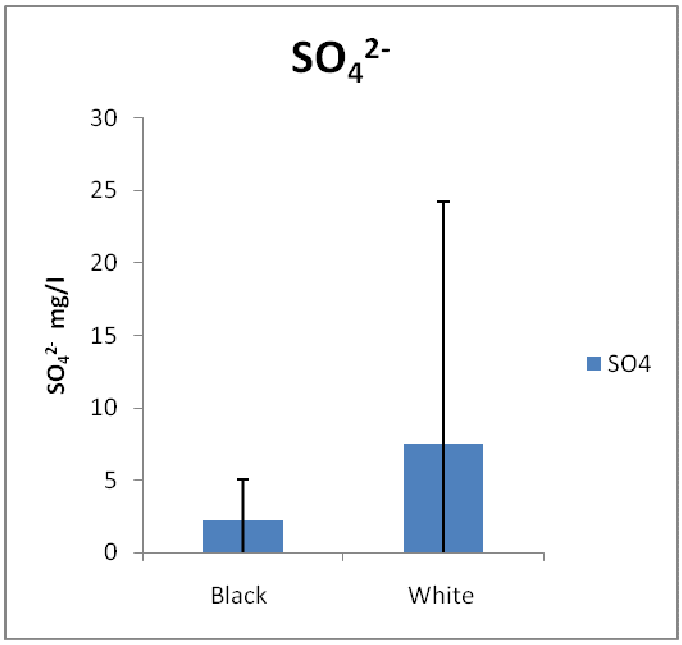

t-Test: Two-Sample Assuming Unequal Variances

	Variable 1	*Variable 2*
Mean	2.230316	7.538269
Variance	8.14211	278.2298
Observations	19	16
Hypothesized Mean Difference	0	
df	16	
t Stat	-1.25747	
P(T<=t) one-tail	0.113314	
t Critical one-tail	1.745884	
P(T<=t) two-tail	0.226627	
t Critical two-tail	2.119905	

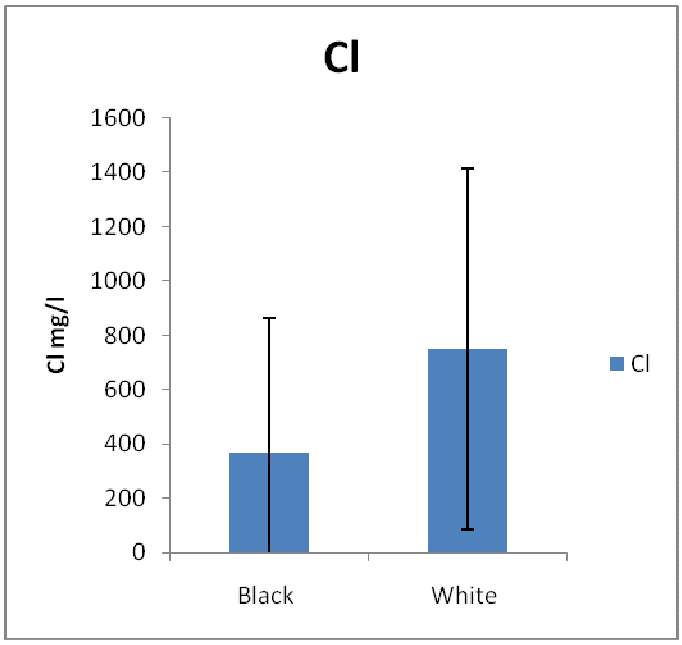

t-Test: Two-Sample Assuming Unequal Variances

	Variable 1	*Variable 2*
Mean	367.2724	750.2246
Variance	247218.4	439921.7
Observations	21	20
Hypothesized Mean Difference	0	
df	35	
t Stat	-2.08396	
P(T<=t) one-tail	0.022265	
t Critical one-tail	1.689572	
P(T<=t) two-tail	0.04453	
t Critical two-tail	2.030108	

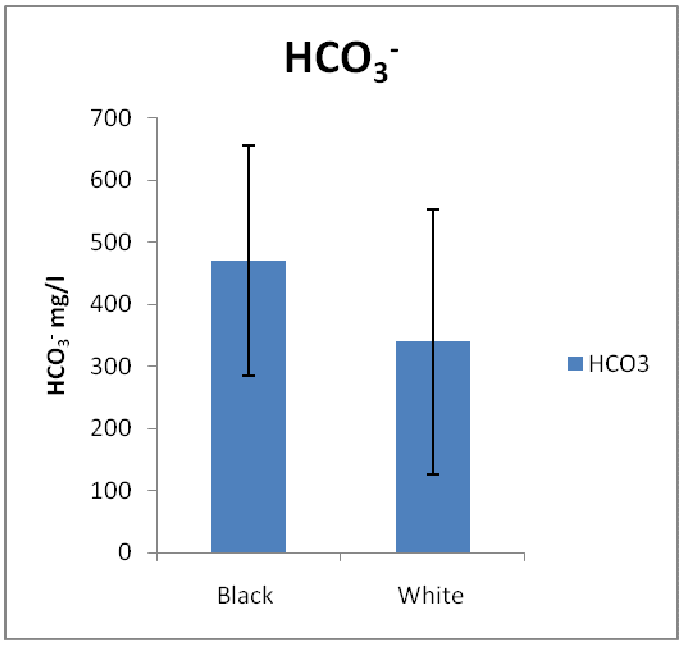

t-Test: Two-Sample Assuming Unequal Variances

	Variable 1	*Variable 2*
Mean	470.9345	340.0438
Variance	34273.34	45462.91
Observations	21	20
Hypothesized Mean Difference	0	
df	38	
t Stat	2.094531	
P(T<=t) one-tail	0.021467	
t Critical one-tail	1.685954	
P(T<=t) two-tail	0.042934	
t Critical two-tail	2.024394	

Appendix C.12- Chloride/Bromide ratio

Nest	Sample No.	Cl (ppm)	Br- (ppm)	Cl/Br Mass ratio	Cl moles/Litter	Cl milli moles /litter	Br Moles/Litter	Br millimols/Litter	Cl/Br Molar ratio
Nest-5	p-2	759.31	2.64	287.09	0.0214	21.4173	0.000033	0.0331	647.05
	P-3	728.35	2.29	318.24	0.0205	20.5441	0.000029	0.0286	717.24
	P-4	372.82	1.83	203.31	0.0105	10.5160	0.000023	0.0230	458.21
	P-5	566.00	2.44	231.57	0.0160	15.9648	0.000031	0.0306	521.91
	P-6	393.22	1.69	232.87	0.0111	11.0913	0.000021	0.0211	524.84
Nest-7	P-2	41.36	1.03	40.33	0.0012	1.1665	0.000013	0.0128	90.90
	P-3	483.15	1.99	243.28	0.0136	13.6280	0.000025	0.0249	548.30
	P-4	300.67	1.83	164.00	0.0085	8.4807	0.000023	0.0229	369.63
	P-5	130.01	1.14	113.86	0.0037	3.6672	0.000014	0.0143	256.61
	P-6	232.25	1.79	129.68	0.0066	6.5509	0.000022	0.0224	292.26
Nest-8	P-1	22.03	0.91	24.11	0.0006	0.6214	0.000011	0.0114	54.33
	P-2	1414.00	1.49	950.20	0.0399	39.8838	0.000019	0.0186	2141.57
	P-4	222.70	1.35	165.47	0.0063	6.2817	0.000017	0.0168	372.93
	P-5	442.29	2.06	214.55	0.0125	12.4754	0.000026	0.0258	483.55
Nest-9	P-2	98.39	1.27	77.75	0.0028	2.7752	0.000016	0.0158	175.24
	P-3	144.02	1.23	117.21	0.0041	4.0622	0.000015	0.0154	264.17
	P-4	541.58	2.26	239.66	0.0153	15.2759	0.000028	0.0283	540.14
	P-5	212.44	1.30	163.20	0.0060	5.9922	0.000016	0.0163	367.83
Nest-12	P-2	398.94	2.23	178.99	0.0113	11.2526	0.000028	0.0279	403.40
	P-5	1565.00	4.34	360.28	0.0441	44.1429	0.000054	0.0544	812.01
	P-6	664.63	2.45	271.17	0.0187	18.7467	0.000031	0.0307	611.15
Nest-16	P-1	50.35	1.06	47.58	0.0014	1.4203	0.000013	0.0132	107.24
	P-2	776.95	3.12	249.19	0.0219	21.9150	0.000039	0.0390	561.63
	P-3	1462.00	3.48	419.93	0.0412	41.2377	0.000044	0.0436	946.45
	P-4	52.01	0.95	54.77	0.0015	1.4671	0.000012	0.0119	123.45

Appendix C.13 – Environmental Isotope Data for Waters (δD and $\delta^{18}O$)

Nest	Well_ID	Depth (m)	dD	d18O
Nest-3	N-3 P-1	17	-19.0	-2.5
	N-3 P-2	29	-22	-3.3
	N-3 P-3	52	-21	-3.2
	N-3 P-4	87	-18	-3.5
	N-3 P-5	240	-18	-3.6
	N-3 P-6	70	-9.0	-2.2
	N-3 P-7	95	-15	-3.4
Nest-4	N-4 P-1	17	-10	-1.4
	N-4 P-2	30	-20	-4.1
	N-4 P-3	56	-18	-3.8
	N-4 P-4	75	-8	-1.3
	N-4 P-5	238	-11	-2.8
	N-4 P-6	104	-14.0	-2.4
Nest-5	N-5 P-1	11	-18	-3.1
	N-5 P-2	29	-26	-4.8
	N-5 P-3	66	-24.0	-4.3
	N-5 P-4	82	-21.0	-3.5
	N-5 P-5	238	-26	-4.4
	N-5 P-6	108	-21.0	-3.2
Nest-7	N-7 P-1	14	-17.0	-3.4
	N-7 P-2	26	-22	-4
	N-7 P-3	53	-14	-3.1
	N-7 P-4	75	-15	-3.2
	N-7 P-5	232	-16	-3.4
	N-7 p-6	102	-14	-3
Nest-8	N-8 P-1	14	-30.0	-5.2
	N-8 P-3	53	-30	-5.2
	N-8 P-4	101	-14	-3.1
	N-8 P-5	235	-14.0	-3.3
Nest-9	N-9 P-1	9	-23	-4
	N-9 P-2	29	-39	-6.1
	N-9 P-3	44	-38	-6.2
	N-9 P-4	66	-22	-4.2
	N-9 P-5	226	-11	-2.8
Nest-12	N-12 P-1	14	-17	-2.8
	N-12 P-2	27	-40	-6.1

	N-12 P-3	50	-32	-4.3
	N-12 P-4	81	-22	-3.6
	N-12 P-5	219	-15	-3.3
	N-12 P-6	116	-29	-5
Nest-13	N-13 P-1	14	-12	-2.9
	N-13 P-3	85	-20	-3.8
	N-13 P-2	33	-38	-6.2
	N-13 P-6	111	-12	-2.8
Nest-16	N-16 P-1	17	-20	-3.3
	N-16 P-2	30	-32	-5.5
	N-16 P-3	50	-26	-4.9
	N-16 P-4	84	-15	-2.6
	N-16 P-5	237	-17	-3.3
Nest-17	N-17 P-1	19	-19	-3.3
	N-17 P-3	58	-28	-5

Appendix C.14 – Microbial community Analyses

Processing 454 Pyrosequencing data with MOTHUR: For Bacteria

At first we installed MOTHUR

This protocol follows the protocol provided online by Pat Schloss, the author of MOTHUR and a professor at the University of Michigan (http://www.MOTHUR.org/wiki/454_SOP). We read the descriptions in the online protocol; they contain additional detail. Also, for each command, I follow the link in the online version to read more about what the command does and what options are available.

Secondly, to help minimize the amount of information we need to type in for each command, temporarily change the default directory MOTHUR which set for my analysis like this:

MOTHUR > set.dir(tempdefault=C:\Users\Md\Desktop\Bacteria)

Getting started

First I need to extract a fasta, qual, and flow data from the binary file (i.e., the sff file) supplied by the sequencing facility:

MOTHUR > sffinfo(sff=040213MK27F.sff, flow=t)

Why do we include flow=t? The flow parameter allows us to indicate if we would like a flowgram file generated. We can do it by default flow=true. Which is telling us the software flow=T, we are telling it that we want this command to generate a flowgram. We need this for subsequent steps.

Next, take a look at the data using the fasta file generated above. It is important that the fasta file will have the same filename as the original sff file but will have the extension .fasta.

MOTHUR > summary.seqs(fasta=040213MK27F.fasta)

Reducing sequence error using flowgrams

Before doing any analyses of pyrosequencing data, it is necessary to remove poor quality data. The Schloss SOP offers two ways of doing this; shhh.flows is the preferred method so it is what is summarized here. Before taking this step, however, we first need to separate each flowgram according to barcode and primer combination. We need to make sure our sequences have a minimum length. We select 360 as the minimum number of flows that each sequence must contain to make it into a “trim” file.

MOTHUR > trim.flows(flow=040213MK27F.flow, oligos=040213MK27F.oligos, pdiffs=2, bdiffs=1, minflows=360, processors=2)

Next we run shhh.flows to denoise our data:

MOTHUR > shhh.flows(file=040213MK27F.flow.files, processors=2)

We don't want to use all of our processors but more=better. After this is complete, we feed the shhh.fasta and shhh.names file into trim.seqs to remove barcode and primer sequences, we make sure everything is at least 200 basepairs long, remove sequences with homopolymers longer than 8 bp, and get the reverse compliment of each sequence:

MOTHUR > trim.seqs(fasta=040213MK27F.shhh.fasta, name=040213MK27F.shhh.names, oligos=040213MK27F.oligos, pdiffs=2, bdiffs=1, maxhomop=8, minlength=200, flip=t, processors=2)

Next, check out what you have left:

MOTHUR > summary.seqs(fasta=040213MK27F.shhh.trim.fasta, name=040213MK27F.shhh.trim.names)

Processing improved sequences

Next, simplify the dataset so we are only working with unique sequences. We'll still keep track of totals but we don't need to use all of the data in the calculations.

MOTHUR > unique.seqs(fasta=040213MK27F.shhh.trim.fasta, name=040213MK27F.shhh.trim.names)

Look at the data again:

MOTHUR > summary.seqs()

Next, you need to align our data to a known database. We will use one of the Silva databases, which can be accesses through the Schloss SOP. We can download it from http://www.MOTHUR.org/wiki/Silva_reference_alignment and get the database we need. Put a copy of the database fasta in the folder we are working on. Here we are working on bacteria, so we use bacteria data set. We should align to the Silva database using the following command line:

MOTHUR > align.seqs(fasta=040213MK27F.shhh.trim.unique.fasta, reference=silva.bacteria.fasta, processors=2, flip=t)

Important point: flip=t option is not listed in the Schloss SOP. Dr. Kirk includes it here because he has found it necessary when working with MR DNA data. Dr. Kirk comments "This may not

always be the case. This is a critical step. Play with the options for this command and make sure your data look good before moving on."

MOTHUR > summary.seqs()

	Start	End	NBases	Ambigs	Polymer	NumSeqs
Minimum:	1007	1106	7	0	2	1
2.5%-tile:	1044	5315	214	0	4	417
25%-tile:	1044	5693	256	0	5	4761
Median:	1044	5711	263	0	5	9521
75%-tile:	1044	6099	269	0	5	14281
97.5%-tile:	1044	6334	281	0	7	18565
Maximum:	43248	43261	303	0	8	19041
Mean:	1046.78	5830.32	260.498	0	4.90599	
total # of seqs:	19041					

We can see that pretty much all of our sequences end at position 27659 of the alignment space (the full alignment is 50,000 columns long). We also see that 97.5% of our sequences are at least 255 bp long.

To make sure that all of the sequences overlap in the same alignment space we need to remove those sequences that are outside the desired range using the screen.seqs command. There are several ways to run this command that are perfectly acceptable. The goal is to think about and then optimize the criteria so that we have as many long sequences as possible - these two factors are inversely related to each other. Our preferred approach is to set the start and end positions. These parameters indicate the position by which all sequences must start by and end after. Setting these will allow us to dictate the alignment coordinates of our sequences so that they all overlap. We prefer this to setting a minimum length because sequences (especially in the V1 region) vary in length when they cover the same region. We can do this as follows:

MOTHUR > screen.seqs(fasta=040213MK27F.shhh.trim.unique.align, name=040213MK27F.shhh.trim.unique.names,group=040213MK27F.shhh.groups, start=1044, optimize=end, criteria=95, processors=2)

Setting criteria to 95 means that the program will remove sequences that stop before 95% of the sequences do. At this point, take another look on our data:

MOTHUR > summary.seqs(fasta=040213MK27F.shhh.trim.unique.good.align, name=040213MK27F.shhh.trim.unique.good.names)

Again, this is a critical step. If we see that we are wiping out our data, then we need to re-do screen.seqs. Look at the options for that command (http://www.MOTHUR.org/wiki/Screen.seqs).

Next, we need to filter our alignment so that all of our sequences only overlap in the same region and to improve any columns in the alignment that don't contain data. We do this using the filter.seqs command.

MOTHUR > filter.seqs(fasta=040213MK27F.shhh.trim.unique.good.align, vertical=t, trump=., processors=2)

In this command," trump=." Will remove any column that has a "." character, which indicates missing data. The vertical=t option will remove any column that contains exclusively gaps. Our data is much simpler now because we have force everything into the same alignment space and eliminated overhangs. Now let's further simplify the data by using the unique.seqs command:

MOTHUR > unique.seqs(fasta=040213MK27F.shhh.trim.unique.good.filter.fasta, name=040213MK27F.shhh.trim.unique.good.names)

And now merge sequence counts that are within 2 bp of a more abundant sequence:

MOTHUR > pre.cluster(fasta=040213MK27F.shhh.trim.unique.good.filter.unique.fasta, name=040213MK27F.shhh.trim.unique.good.filter.names, group=040213MK27F.shhh.good.groups, diffs=2)

Check our data to make sure you haven't lost your sequences and that they generally fall in the range of 200-300 bp.

MOTHUR > summary.seqs(fasta=040213MK27F.shhh.trim.unique.good.filter.unique.precluster.fasta, name=040213MK27F.shhh.trim.unique.good.filter.unique.precluster.names)

Start	End	NBases	Ambigs	Polymer	NumSeqs	
Minimum:		1	681	208	0	3	1
2.5%-tile:		1	681	220	0	4	1303
25%-tile:	1	681	245	0	5	13028	
Median:	1	681	247	0	5	26055	
75%-tile:	1	681	247	0	5	39082	
97.5%-tile:		1	681	259	0	7	50856
Maximum:		7	681	272	0	8	52108
Mean:	1.009	681	244.948	0	5.00558		
# of unique seqs:		8634					
total # of seqs:		52108					

We still have the same total number of sequences, but we now have 8,634 unique sequences.

Removing Chimeras

To this point we have been concerned with removing sequencing errors. The next thing we need to do is to identify chimeras. MOTHUR has a number of methods for tools for detecting chimeras. Our preferred method is to use chimera.uchime using the sequences as their own reference:

MOTHUR >
chimera.uchime(fasta=040213MK27F.shhh.trim.unique.good.filter.unique.precluster.fasta, name=040213MK27F.shhh.trim.unique.good.filter.unique.precluster.names, group=040213MK27F.shhh.good.groups, processors=2)

MOTHUR >
remove.seqs(accnos=040213MK27F.shhh.trim.unique.good.filter.unique.precluster.uchime.accnos, fasta=040213MK27F.shhh.trim.unique.good.filter.unique.precluster.fasta, name=040213MK27F.shhh.trim.unique.good.filter.unique.precluster.names, group=040213MK27F.shhh.good.groups, dups=t)

Check out what we have left:

MOTHUR > summary.seqs (name=current)

Removing Contaminants

The command below has the taxonomy template and taxonomy used in the SOP.

MOTHUR >
classify.seqs(fasta=040213MK27F.shhh.trim.unique.good.filter.unique.precluster.pick.fasta, name=040213MK27F.shhh.trim.unique.good.filter.unique.precluster.pick.names, group=040213MK27F.shhh.good.pick.groups, template=trainset9_032012.pds.fasta, taxonomy=trainset9_032012.pds.tax, cutoff=80, processors=2)

Now let's use the remove.lineage command to remove those sequences that classified as "Chloroplast", "Mitochondria", or "unknown" (those sequences that could not be classified at the Kingdom level) as well as archaeal and eukaryotic 16S/18S rRNAs, since our primers are not designed to amplify these populations here:

MOTHUR >
remove.lineage(fasta=040213MK27F.shhh.trim.unique.good.filter.unique.precluster.pick.fasta, name=040213MK27F.shhh.trim.unique.good.filter.unique.precluster.pick.names, group=040213MK27F.shhh.good.pick.groups, taxonomy=040213MK27F.shhh.trim.unique.good.filter.unique.precluster.pick.pds.wang.taxonomy, taxon=Mitochondria-Chloroplast-Archaea-Eukaryota-unknown)

MOTHUR >
summary.seqs(fasta=040213MK27F.shhh.trim.unique.good.filter.unique.precluster.pick.pick.fasta, name=040213MK27F.shhh.trim.unique.good.filter.unique.precluster.pick.pick.names)

Preparing inputs for analysis

Don't worry about the remove.groups step (Dr. Kirk suggest). It is helpful to do the file rename part. we manually change the file name here and use the commands listed in the SOP.

Define OTUs

Option one works pretty well. We follow this step as listed in the SOP

MOTHUR > dist.seqs(fasta=040213MK27F.final.fasta, cutoff=0.15, processors=2)

The file "final.an.shared" you generate has a matrix that provides the number of sequences in each OTU (97% identity) in each sample. The file "final.an.0.03.cons.taxonomy" lists the taxonomy for each OTU and the number of sequences in each OTU. In order to link the abundance and taxonomy of each OTU in each sample, we need to combine these files. First, paste them into separate worksheets in a single excel file. Then, transpose the "final.an.shared" matrix. Lastly, use the vlookup function in excel to search the "final.an.shared" matrix for each OTU and return the number of sequences corresponding to the sample ID. Alternatively, we can bin up our sequences into phylotypes and then take a closer look at our data (Phylotype section below).

After the number of OTUs has been defined and the data is in our excel file, we need to process your data just a bit more before we can do statistical analyses that allow us to compare samples on an equal basis. First we count the number of groups in your samples:

MOTHUR > count.groups(shared=040213MK27F.final.an.shared)

From the output, we can notice that not every sample had the same number of sequences. Now sub-sample the data for each sample, selecting only the number of sequences equivalent to the number in the group with the fewest. **In our sample fewest numbers had 2080 sequences.**

MOTHUR > sub.sample(shared=040213MK27F.final.an.shared, size=2080)

This step removes some of the groups that are not that abundant. If we don't have a "final.an.shared" file in your folder, you can use the final.fasta. Now, get the taxonomic information for each group that remains:

MOTHUR > classify.otu(list=040213MK27F.final.an.list, name=040213MK27F.final.names, taxonomy=040213MK27F.final.taxonomy, label=0.03)

Phylotype

With the completion of that last step, We generally have no reason to assign sequences to phylotypes. The phylotype command goes through the taxonomy file and bins sequences together that have the same taxonomy. Here we do it to the genus level:

MOTHUR > phylotype(taxonomy=040213MK27F.final.taxonomy,
name=040213MK27F.final.names, label=1)

Like above, we want to make a shared file and standardize the number of sequences in each group:

MOTHUR > make.shared(list=040213MK27F.final.tx.list, group=040213MK27F.final.groups, label=1)
MOTHUR > sub.sample(shared=040213MK27F.final.tx.shared, size=2080)

Finally, just to keep things consistent, we get the taxonomy of each phylotype:

MOTHUR > classify.otu(list=040213MK27F.final.tx.list, name=040213MK27F.final.names, taxonomy=040213MK27F.final.taxonomy, label=1)

Phylogenetic tree

There are many ways to construct phylogenetic trees. We have ported clearcut into MOTHUR to generate neighbor joining trees. By default we do not use their heuristic, so these are real neighbor joining trees which you may or may not think are "real". First we need to subsample the sequences from each group and then construct a phylip-formatted distance matrix, which we calculate with dist.seqs:

MOTHUR > dist.seqs(fasta=040213MK27F.final.fasta, output=phylip, processors=2)

Now we call on clearcut:

MOTHUR > clearcut(phylip=040213MK27F.final.phylip.dist)

For our Sample it's too big and large which we can't present!

OTU-based analyses - Alpha-Diversity

The Schloss SOP describes how to make Chao, inverse-Simpson, and rarefaction curves for you samples. These are useful if you need to evaluate whether the number of sequences we collected for each of your samples was sufficient. In other words, it helps you answer the question, are the diversity values you calculate sensitive to your sampling effort. If values are not sensitive, you can trust your values. If they are, ideally you would collect more samples. Follow the commands listed in the protocol to perform these calculations.

Another convenient way to quantify alpha diversity and sampling coverage is with the summary.single command, which produces a file with several diversity values summarized for

each sample. The command listed in the Schloss SOP lists specific calculators (the default is a large list of calculators).

MOTHUR > summary.single(calc=nseques-coverage-sobs-invsimpson-chao, subsample=2080)

Full list of calculators here http://www.MOTHUR.org/wiki/Calculators

sobs – observed community richness

chao – the Chao1 estimate of community richness

invsimpson – the inverse Simpson index (1/D) of community diversity

hci and lci correspond to high and low confidence intervals

These data will be outputted to a table in a file called final.an.groups.ave-std.summary. **Interestingly, the sample coverages were all above 97%, indicating that we did a pretty good job of sampling the communities**

Beta Diversity Measurements

Now we'd like to compare the membership and structure of the various samples using an OTU-based approach. Let's start by generating a heatmap of the relative abundance of each OTU across the 24 samples using the heatmap.bin command and log2 scaling the relative abundance values. Because there are so many OTUs, let's just look at the top 50 OTUs:

MOTHUR > heatmap.bin(shared=040213MK27F.final.an.shared, scale=log2, numotu=50)

This will generate an SVG-formatted file that can be visualized in Safari or manipulated in graphics software such as Adobe Illustrator. Needless to say these heatmaps can be a bit of Rorshock. A legend can be found at the bottom left corner of the heat map.

Now let's calculate the similarity of the membership and structure found in the various samples and visualize those similarities in a heatmap with the Jaccard and thetayc coefficients. We will do this with the heatmap.sim command:

MOTHUR > heatmap.sim(calc=jclass-thetayc)

The output will be in two SVG-formatted files called final.an.0.03.jclass.heatmap.sim.svg and final.an.0.03.thetayc.heatmap.sim.svg**. In all of these heatmaps the red colors indicate communities that are more similar than those with black colors.**

After that we generated a dendrogram to describe the similarity of the samples to each other. We generated this dendrogram using the jclass and thetayc calculators within the tree.shared command:

MOTHUR > tree.shared(calc=thetayc-jclass, subsample=2080)

This command generates two newick-formatted tree files - final.an.thetayc.0.03.ave.tre and final.an.jclass.0.03.ave.tre - that are the result of subsampling 2080 sequences 1000 times. The trees can be visualized in software like TreeView or FigTree. Inspection of the both trees shows that individuals' communities cluster with themselves to the exclusion of the others. We can test to deterine whether the clustering within the tree is statistically significant or not using by choosing from the parsimony, unifrac.unweighted, or unifrac.weighted commands.

Another popular way of visualizing beta-diversity information is through ordination plots. We can calculate distances between samples using the dist.shared command:

MOTHUR > dist.shared(shared=040213MK27F.final.an.shared, calc=thetayc-jclass, subsample=2080)

The two resulting distance matrices (i.e. final.an.thetayc.0.03.lt.ave.dist and final.an.jclass.0.03.lt.ave.dist) can then be visualized using the pcoa or nmds plots.

2. Bacterial Families (%) within Different Samples (South Matlab, Core-2).

	30ft(10m)	90ft(27m)	150ft(45m)	210ft(65m)	265(81m)	310ft(91m)	330ft(100m)	365ft(110m)
comamonadaceae	9.564	13.403	47.096	2.163	31.513	34.111	37.692	38.315
moraxellaceae	10.179	8.474	7.268	3.906	30.480	14.001	31.223	18.332
bacteriovoraceae	3.134	4.985	0.238	0.000	0.067	6.640	0.031	5.257
oxalobacteraceae	5.060	5.616	2.126	3.215	0.684	6.726	1.721	5.078
aeromonadaceae	0.395	0.720	0.365	0.000	3.072	1.390	7.975	4.308
cystobacterineae	0.012	0.079	0.000	0.000	0.040	0.412	0.077	2.835
flavobacteriaceae	0.128	0.304	0.651	0.000	0.174	6.143	1.260	2.601
rhodospirillaceae	0.151	0.124	0.428	0.150	0.389	0.223	0.169	2.491
xanthomonadaceae	0.824	1.688	2.936	2.224	0.818	6.005	1.921	2.340
chromatiaceae	0.418	0.979	0.206	0.150	0.013	4.290	0.000	1.913
caulobacteraceae	0.174	0.428	0.111	0.811	0.121	1.287	0.092	1.885
neisseriaceae	0.139	0.158	0.127	0.000	0.054	0.669	0.415	1.803
sphingomonadaceae	0.139	0.281	0.222	0.631	0.416	1.184	0.353	1.638
pseudomonadaceae	12.326	18.557	24.151	1.863	0.953	2.008	1.690	1.266

rhodocyclaceae	0.522	0.529	4.427	0.060	11.215	0.498	2.551	1.170
rhizobiaceae	1.938	1.542	0.222	3.876	0.241	2.213	0.123	1.156
cyclobacteriaceae	0.012	0.124	0.920	0.000	0.201	0.669	0.154	0.977
methylophilaceae	0.766	0.709	0.508	0.811	0.443	2.076	1.690	0.867
sphingobacteriaceae	0.151	0.135	0.349	0.571	0.443	0.343	0.092	0.784
shewanellaceae	0.035	0.068	0.079	0.000	0.013	0.583	0.138	0.619
bradyrhizobiaceae	0.360	0.506	0.476	3.966	0.349	0.858	0.630	0.509
brucellaceae	0.058	0.135	0.079	1.863	0.027	0.669	0.092	0.427
erythrobacteraceae	0.104	0.079	0.238	1.983	0.282	1.939	0.292	0.358
alteromonadaceae	0.104	0.383	0.222	0.150	0.000	0.498	0.015	0.358
rikenellaceae	0.000	0.000	0.000	0.000	0.027	0.120	0.000	0.303
chitinophagaceae	0.162	0.135	0.603	0.841	0.885	0.275	0.384	0.275
phyllobacteriaceae	0.046	0.045	0.032	1.022	0.040	0.412	0.031	0.261
alcaligenaceae	0.093	0.056	0.048	0.180	0.094	0.377	0.092	0.206
campylobacteraceae	0.000	0.023	0.175	0.000	1.020	0.034	0.323	0.165
cytophagaceae	0.081	0.135	0.365	1.322	0.617	0.137	0.323	0.124
hyphomicrobiaceae	0.058	0.045	0.032	0.421	0.201	0.223	0.123	0.124
rhodobacteraceae	0.000	0.000	0.238	2.344	0.121	0.086	0.215	0.110
sinobacteraceae	0.371	0.731	0.698	0.000	0.349	0.377	0.154	0.096
legionellaceae	0.000	0.045	0.587	0.000	3.394	0.120	1.844	0.083
burkholderiaceae	51.636	36.856	0.317	1.142	0.456	0.154	0.569	0.069
acetobacteraceae	0.000	0.000	0.048	0.060	0.080	0.034	0.061	0.069
nocardioidaceae	0.197	0.405	0.048	0.060	0.000	0.326	0.031	0.069
bdellovibrionaceae	0.046	0.023	0.000	0.000	0.000	0.275	0.000	0.069
verrucomicrobiaceae	0.000	0.000	0.000	0.000	0.000	0.069	0.000	0.069
opitutaceae	0.035	0.090	0.063	0.000	0.000	0.000	0.000	0.069
porphyromonadaceae	0.000	0.000	0.095	0.000	0.094	0.017	0.061	0.055
nannocystineae	0.000	0.000	0.048	0.000	0.617	0.017	0.814	0.041

enterobacteriaceae	0.058	0.034	0.016	0.180	0.027	0.292	0.200	0.041
clostridiaceae	0.000	0.000	0.000	0.000	0.188	0.103	0.000	0.041
oceanospirillaceae	0.000	0.011	0.095	0.000	0.040	0.000	0.000	0.041
desulfurellaceae	0.000	0.000	0.000	0.000	0.000	0.000	0.000	0.041
erysipelotrichaceae	0.000	0.000	1.365	0.000	6.990	0.086	2.658	0.028
xanthobacteraceae	0.081	0.068	0.095	0.180	0.416	0.034	0.277	0.028
acidobacteriaceae	0.000	0.000	0.016	0.270	0.040	0.000	0.200	0.028
planctomycetaceae	0.000	0.068	0.000	0.000	0.027	0.137	0.061	0.028
micrococcaceae	0.000	0.034	0.000	0.120	0.000	0.275	0.031	0.028
beijerinckiaceae	0.000	0.000	0.048	0.000	0.134	0.017	0.015	0.028
hyphomonadaceae	0.000	0.000	0.016	0.000	0.000	0.086	0.000	0.028
sporichthyaceae	0.000	0.000	0.000	0.000	0.523	0.000	0.000	0.028
hydrogenophilaceae	0.000	0.000	0.111	0.120	0.107	0.000	0.000	0.028
rhodobiaceae	0.000	0.000	0.000	0.090	0.040	0.000	0.215	0.014
family unspecified	0.070	0.068	0.032	0.000	0.201	0.086	0.200	0.014
candidatus_chloracidobacterium	0.000	0.023	0.000	0.000	0.027	0.000	0.092	0.014
nitrosomonadaceae	0.000	0.000	0.143	0.090	0.134	0.000	0.123	0.000
nitrospiraceae	0.000	0.034	0.000	0.000	0.148	0.000	0.108	0.000
bacillaceae	0.000	0.000	0.000	0.180	0.054	0.000	0.092	0.000
micromonosporaceae	0.000	0.000	0.032	1.292	0.040	0.000	0.061	0.000
methylobacteriaceae	0.000	0.023	0.000	1.863	0.000	0.000	0.061	0.000
streptomycetaceae	0.000	0.011	0.048	54.988	0.027	0.000	0.046	0.000
gemmatimonadaceae	0.000	0.000	0.000	0.000	0.000	0.000	0.046	0.000
peptococcaceae	0.000	0.000	0.016	0.000	0.013	0.000	0.031	0.000
peptostreptococcaceae	0.000	0.000	0.016	0.000	0.295	0.000	0.015	0.000
rubrobacteriaceae	0.000	0.000	0.000	0.000	0.027	0.000	0.015	0.000
ectothiorhodospiraceae	0.000	0.000	0.143	0.000	0.000	0.000	0.015	0.000
dietziaceae	0.000	0.056	0.000	0.000	0.000	0.000	0.015	0.000

cryomorphaceae	0.000	0.000	0.079	0.000	0.054	0.206	0.000	0.000
candidatus_solibacter	0.000	0.000	0.016	0.000	0.094	0.051	0.000	0.000
caldilineaceae	0.070	0.034	0.032	0.000	0.000	0.051	0.000	0.000
sorangiineae	0.000	0.000	0.079	0.000	0.040	0.034	0.000	0.000
intrasporangiaceae	0.000	0.000	0.000	0.090	0.000	0.017	0.000	0.000
syntrophaceae	0.000	0.000	0.048	0.000	0.000	0.017	0.000	0.000
planococcaceae	0.000	0.045	0.000	0.000	0.000	0.017	0.000	0.000
anaerolineaceae	0.000	0.000	0.127	0.180	0.188	0.000	0.000	0.000
nitrospinaceae	0.000	0.000	0.016	0.000	0.040	0.000	0.000	0.000
sbr1093 (candidate division)	0.000	0.000	0.016	0.000	0.027	0.000	0.000	0.000
veillonellaceae	0.000	0.000	0.000	0.000	0.027	0.000	0.000	0.000
methylocystaceae	0.000	0.000	0.000	0.120	0.013	0.000	0.000	0.000
ruminococcaceae	0.000	0.000	0.016	0.000	0.013	0.000	0.000	0.000
nocardiaceae	0.000	0.000	0.000	0.721	0.000	0.000	0.000	0.000
corynebacteriaceae	0.000	0.023	0.000	0.631	0.000	0.000	0.000	0.000
microbacteriaceae	0.000	0.000	0.000	0.631	0.000	0.000	0.000	0.000
propionibacteriaceae	0.012	0.011	0.000	0.541	0.000	0.000	0.000	0.000
streptococcaceae	0.000	0.000	0.000	0.481	0.000	0.000	0.000	0.000
paenibacillaceae	0.000	0.000	0.000	0.421	0.000	0.000	0.000	0.000
staphylococcaceae	0.000	0.000	0.000	0.391	0.000	0.000	0.000	0.000
pseudonocardiaceae	0.000	0.000	0.000	0.210	0.000	0.000	0.000	0.000
dehalococcoidaceae	0.000	0.000	0.000	0.120	0.000	0.000	0.000	0.000
ktedonobacteraceae	0.000	0.000	0.000	0.120	0.000	0.000	0.000	0.000
mycobacteriaceae	0.000	0.000	0.000	0.090	0.000	0.000	0.000	0.000
trueperaceae	0.000	0.000	0.000	0.090	0.000	0.000	0.000	0.000
gallionellaceae	0.221	0.461	0.428	0.000	0.000	0.000	0.000	0.000
marinilabiaceae	0.000	0.000	0.063	0.000	0.000	0.000	0.000	0.000
patulibacteraceae	0.000	0.000	0.048	0.000	0.000	0.000	0.000	0.000

myxococcaceae	0.012	0.169	0.000	0.000	0.000	0.000	0.000	0.000
helicobacteraceae	0.035	0.135	0.000	0.000	0.000	0.000	0.000	0.000
candidatus_captivus	0.023	0.101	0.000	0.000	0.000	0.000	0.000	0.000

3. Statistical Results Calculated for subsamples each to the number of sequences in the sample with the fewest nseqs (65m)

label	group	method	nseqs	coverage	sobs	invsimpson	Invsimpson-lci	invsimpson_hci	chao	chao_lci	chao_hci
0.03	10m	ave	2080	0.96	149.43	4.81	4.45	5.24	330.11	247.03	484.13
0.03	27m	ave	2080	0.95	177.98	7.98	7.34	8.74	350.51	276.33	480.78
0.03	45m	ave	2080	0.91	291.60	7.26	6.74	7.86	761.32	598.37	1010.98
0.03	65m	ave	2080	0.98	198.00	38.32	35.19	42.07	234.03	215.81	270.89
0.03	81m	ave	2080	0.88	344.16	10.03	9.29	10.90	997.28	785.86	1310.06
0.03	92m	ave	2080	0.91	315.72	28.03	25.70	30.81	675.88	551.65	865.60
0.03	100m	ave	2080	0.88	339.89	10.50	9.62	11.55	1091.51	841.11	1467.25

4. T-test for important bacterial families

Comamonadaceae

t-Test: Two-Sample Assuming Unequal Variances

	Variable 1	*Variable 2*
Mean	38.76717	36.21331
Variance	61.5734	8.837878
Observations	3	2
Hypothesized Mean Difference	0	
df	3	
t Stat	0.51135	
P(T<=t) one-tail	0.322182	
t Critical one-tail	2.353363	
P(T<=t) two-tail	0.644363	
t Critical two-tail	3.182446	

Moraxellaceae

t-Test: Two-Sample Assuming Unequal Variances

	Variable 1	*Variable 2*
Mean	8.640092	16.16666
Variance	2.139465	9.376981
Observations	3	2
Hypothesized Mean Difference	0	
df	1	
t Stat	-3.23843	
P(T<=t) one-tail	0.095335	
t Critical one-tail	6.313752	
P(T<=t) two-tail	0.19067	
t Critical two-tail	12.7062	

Burkholderiaceae

t-Test: Two-Sample Assuming Unequal Variances

	Variable 1	*Variable 2*
Mean	44.24611	0.11162
Variance	109.2355	0.003665
Observations	2	2
Hypothesized Mean Difference	0	
df	1	
t Stat	5.971783	
P(T<=t) one-tail	0.052812	
t Critical one-tail	6.313752	
P(T<=t) two-tail	0.105625	
t Critical two-tail	12.7062	

Pseudomonadaceae

t-Test: Two-Sample Assuming Unequal Variances

	Variable 1	*Variable 2*
Mean	18.34475	1.63686
Variance	34.99247	0.274821
Observations	3	2
Hypothesized Mean Difference	0	
df	2	
t Stat	4.863532	
P(T<=t) one-tail	0.019886	
t Critical one-tail	2.919986	
P(T<=t) two-tail	0.039771	
t Critical two-tail	4.302653	

Acetobacteraceae

t-Test: Two-Sample Assuming Unequal Variances

	Variable 1	*Variable 2*
Mean	0.239719	0.19382
Variance	0.011957	0.007662
Observations	4	2
Hypothesized Mean Difference	0	
df	3	
t Stat	0.555795	
P(T<=t) one-tail	0.308556	
t Critical one-tail	2.353363	
P(T<=t) two-tail	0.617111	
t Critical two-tail	3.182446	

Aeromonadaceae

t-Test: Two-Sample Assuming Unequal Variances

	Variable 1	*Variable 2*
Mean	0.586574	3.591061
Variance	0.037273	6.21593
Observations	3	2
Hypothesized Mean Difference	0	
df	1	
t Stat	-1.70085	
P(T<=t) one-tail	0.169184	

t Critical one-tail	6.313752
P(T<=t) two-tail	0.338367
t Critical two-tail	12.7062

Enterobacteriaceae

t-Test: Two-Sample Assuming Unequal Variances

	Variable 1	*Variable 2*
Mean	0.045654	0.323137
Variance	5.93E-05	0.033376
Observations	3	2
Hypothesized Mean Difference	0	
df	1	
t Stat	-2.14673	
P(T<=t) one-tail	0.138762	
t Critical one-tail	6.313752	
P(T<=t) two-tail	0.277525	
t Critical two-tail	12.7062	

Rhodocyclaceae

t-Test: Two-Sample Assuming Unequal Variances

	Variable 1	Variable 2
Mean	0.206322	0.392766
Variance	0.000564	0.055516
Observations	2	2
Hypothesized Mean Difference	0	
df	1	
t Stat	-1.11342	
P(T<=t) one-tail	0.232934	
t Critical one-tail	6.313752	
P(T<=t) two-tail	0.465867	
t Critical two-tail	12.7062	